

---

**Arterial Wall Immunity in Hyperlipidemic Mice is Regulated  
by the Sympathetic Nervous System**

**Yuanfang Li**

---



München 2020



Aus dem Institut für Prophylaxe und Epidemiologie der Kreislaufkrankheiten

Institut der Ludwig-Maximilians-Universität München

Direktor: Univ.-Prof. Dr. med. Christian Weber

# **Arterial Wall Immunity in Hyperlipidemic Mice is Regulated by the Sympathetic Nervous System**



Dissertation  
zum Erwerb des Doktorgrades der Naturwissenschaften  
an der Medizinischen Fakultät der  
Ludwig-Maximilians-Universität zu München

vorgelegt von  
Yuanfang Li

aus  
Henan, VR China

2020



Mit Genehmigung der Medizinischen Fakultät  
der Universität München

**Betreuer(in): Univ.-Prof. Dr. rer. nat. Sabine Steffens**

**Zweitgutachter: PD Dr. rer. Nat. Andreas Herbst**

**Dekan: Prof. Dr. med. dent. Reinhard Hickel**

**Tag der mündlichen Prüfung: 14.01.2021**



# Eidesstattliche Versicherung

**Li, Yuanfang**

Ich erkläre hiermit an Eides statt, dass ich die vorliegende Dissertation mit dem Thema  
**Arterial Wall Immunity in Hyperlipidemic Mice is Regulated by the Sympathetic Nervous System**

selbständig verfasst, mich außer der angegebenen keiner weiteren Hilfsmittel bedient und alle Erkenntnisse, die aus dem Schrifttum ganz oder annähernd übernommen sind, als solche kenntlich gemacht und nach ihrer Herkunft unter Bezeichnung der Fundstelle einzeln nachgewiesen habe.

Ich erkläre des Weiteren, dass die hier vorgelegte Dissertation nicht in gleicher oder in ähnlicher Form bei einer anderen Stelle zur Erlangung eines akademischen Grades eingereicht wurde.

München, 25.06.2020

Ort, Datum

Yuanfang Li

Unterschrift Doktorandin/Doktorand



**Arterial Wall Immunity in Hyperlipidemic  
Mice is Regulated by the Sympathetic Nervous  
System**

# TABLE OF CONTENTS

1 INTRODUCTION .....	1
1.1 Atherosclerosis .....	1
1.2 Nervous system .....	8
1.3 Interactions of the immune system and the SNS .....	13
1.4 Interplay of the vascular system and the NS .....	14
1.5 Atherosclerosis and the SNS .....	15
1.6 Aims of the thesis .....	17
2 MATERIALS AND METHODS .....	18
2.1 Materials .....	18
2.2. Methods .....	22
3 RESULTS .....	39
3.1. NE concentrations increased during aging and atherosclerosis .....	39
3.2. TH <sup>+</sup> sympathetic axon density in the arterial adventitia of <i>ApoE</i> <sup>-/-</sup> mice .....	40
3.3 Laser capture microdissection arrays revealed the presence of SNS constituents in atherosclerotic adventitia .....	42
3.4 Chemical sympathectomy by 6-OHDA .....	48
3.5 Surgical sympathectomy by celiac ganglionectomy .....	70
4. DISCUSSION .....	79
4.1 Territoriality of the arterial SNS innervation in atherosclerosis .....	80
4.2 Site of neuronal responses in the aorta .....	82
4.3 Immunometabolic effects of SNS denervation .....	85
4.4 Sympathetic denervation prevents athero-progression .....	85
4.5 Outlook .....	86
5. SUMMARY .....	88
6. ZUSAMMENFASSUNG .....	89
7. REFERENCES .....	90
8. ACKNOWLEDGEMENTS .....	100
9. SUPPLEMENT .....	101

## ABBREVIATIONS

# ABBREVIATIONS

6-OHDA	6- hydroxydopamine
ADR	Adrenergic receptor
ANOVA	Analysis of variance
ApoE	Apolipoprotein E
ATLOs	Artery tertiary lymphoid organs
BSA	Bovine serum albumin
CG	Celiac ganglia
CGX	Celiac ganglionectomy
CMP	Common myeloid progenitor
CNS	Central NS
DAPI	4',6-diamidino-2-phenylindole
DCs	Dendritic cells
DPBS	Dulbecco's phosphate-buffered saline
EDTA	Ethylenediaminetetraacetic acid
ELISA	Enzyme-linked immunosorbent assay
FACS	Fluorescence-activated cell sorting
FDCs	Follicular dendritic cells
FITC	Fluorescein isothiocyanate
FVD	Fixable viability dyes
gAT	Gonadal adipose tissue
GRA	Granulocyte
GMP	Granulocyte-monocyte progenitor
GO	Gene ontology
H/E	Hematoxylin/eosin
HFD	High-fat diet
IL	Interleukin
i.p.	Intraperitoneal
LC	Locus coeruleus
LCM	Laser capture microdissection
LN	Lymph node
LSK	Lineage <sup>-</sup> Sca1 <sup>+</sup> c-kit <sup>+</sup>
MI	Myocardial infarction
NE	Norepinephrine / noradrenaline

## ABBREVIATIONS

NF	Neurofilament
NS	Nervous system
NSD	Nervous system development
ORO	Oil red O
PBS	Phosphate-buffered saline
PFA	Paraformaldehyde
PNS	Peripheral NS
PSNS	Parasympathetic NS
PVI	Plaque vulnerability index
ROI	Regions of interest
ROS	Reactive oxygen species
SLOs	Secondary lymphoid organs
SMA	Alpha-smooth muscle actin
SMCs	Smooth muscle cells
SNS	Sympathetic NS
TCR	T cell receptor
TH	Tyrosine hydroxylase
Th	Helper T cells
TLOs	Tertiary lymphoid organs
T <sub>reg</sub>	Regulatory T cells
t-SNE	T-distributed stochastic neighbor embedding
WT	Wild type

# 1 INTRODUCTION

## 1.1 Atherosclerosis

### 1.1.1 Atherosclerosis is an unresolvable inflammatory disease

Inflammation arises when the immune system is activated to remove harmful pathogens and/or other invading organisms or molecules<sup>1</sup>. Inflammation can be resolvable if the immune system is capable of removing the causative factors with resultant restoration of tissue homeostasis. It will, however, become unresolvable and chronic if the immune system fails to eliminate the invaders. Unresolvable inflammation is uncontrolled, progresses over time, and may cause severe tissue damage resulting in organ dysfunction, which - when not compensated - leads to clinically significant diseases and possibly death<sup>2</sup>.

The majority of chronic human diseases are caused by unresolvable inflammation initiated by immune cells (i.e., all white blood cells) infiltration of peripheral tissues. The immune system is activated when it recognizes harmful activity (“danger signals”), and it is then prompted to infiltrate peripheral tissues by exogenous or - in some instances - endogenous agents, including modified lipids or lipoproteins. Human unresolvable inflammatory diseases include atherosclerosis (the major cause of death worldwide), Alzheimer’s disease (the major cause of dementia), chronic obstructive lung disease, obesity, diabetes, cancer, multiple sclerosis (a major autoimmune disease), rheumatoid arthritis, and many more<sup>2,3</sup>.

A report by the World Health Organization demonstrates that the major mortality worldwide is caused by chronic diseases (Fig. 1). Mortalities were reported for every four years between 2002 and 2018, and are predicted for 2022 - 2030. The mortality of chronic diseases increased between 2002 and 2018. Especially deaths caused by cardiovascular diseases were expected to increase. In 2017, cardiovascular diseases related to death reached ~18 million<sup>4</sup>. At the same time, death rates of infectious diseases are predicted to decrease over time. The data indicate a major shift in distinct disease conditions, from communicable to non-communicable diseases<sup>5</sup>.

## INTRODUCTION

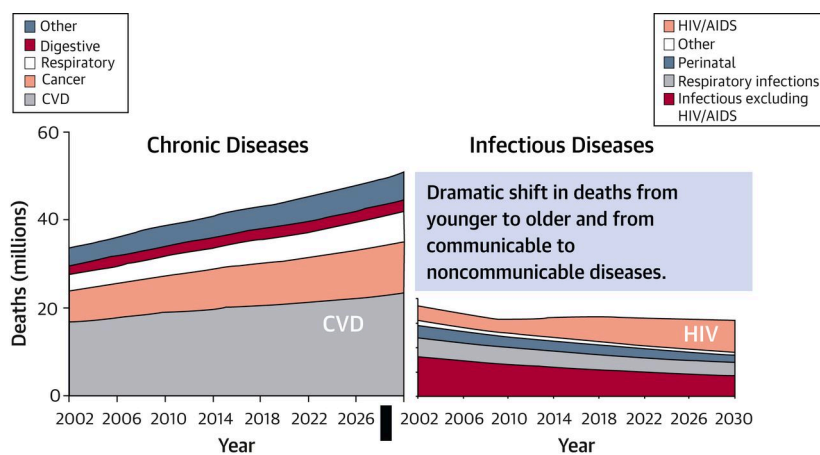


**Figure 1. Global Burden of Chronic and Infectious Diseases worldwide.** Reproduced from Valentin Fuster<sup>5</sup>. The figure demonstrates the number of deaths caused by chronic and infectious diseases between 2002 and 2018, and the predictions between 2022 and 2030 worldwide. The left side shows that mortalities of cardiovascular diseases slightly increased between 2002 and 2018, but are predicted to increase further by 2030 to become the major cause of human death globally. The right side shows the total number of deaths caused by infectious diseases, which decreased between 20002 and 2018, and are predicted to decrease further by 2030.

### 1.1.2 Development of atherosclerosis

Atherosclerosis is a chronic inflammatory disease<sup>6,7</sup> that occurs in the vessel wall of large- and medium-sized arteries, including the aorta, coronary arteries, cerebral arteries, and other beds of the arterial tree<sup>8</sup>. Several genetic and environmental risk factors are known to contribute to the development of atherosclerosis, including hyperlipidemia, aging, hypertension, obesity, diabetes mellitus, smoking, sedentary lifestyle, and high-fat diets<sup>9</sup>. Atherosclerosis is the most common cause of death worldwide<sup>10,11</sup>. Depending on organ manifestation, it may lead to myocardial infarcts, stroke, kidney dysfunction, and a large number of other diseases<sup>9,12</sup>. Atherosclerotic plaques, i.e., the ultimate cause of tissue damage, are initiated in the intima layer of the arterial wall. The intima - in normal arteries - consists of a monolayer of endothelial cells that line the internal basement membrane separating the lamina intima and the lamina media. Sub-endothelial accumulation of low-density lipoprotein in the intima is considered as one of the most important initiators for atherosclerotic plaque development. Low-density lipoprotein is thought to be oxidized in the intima followed by the expression of adhesion molecules including intercellular adhesion molecule 1, vascular cell adhesion molecule 1 on endothelial cells leading to monocyte migration into the intima, and differentiation of

## INTRODUCTION

the monocytes into macrophages and dendritic cells (DCs), which may locally proliferate in the plaque. Macrophages engulf the oxidized low-density lipoprotein and become foam cells. During atherogenesis, neutrophils, granulocytes, mast cells, and T cells accumulate in the plaque. Moreover, smooth muscle cells (SMCs) proliferate and migrate from the media into the plaque. During plaque progression, migrating SMCs and collagenous connective tissue form a fibromuscular connective tissue cap that covers the lipid-rich necrotic core of the plaque. The recent studies on SMCs in atherosclerosis demonstrated that the activated SMCs communicated with immune cells in both of the atherosclerotic plaque and adventitia, and initiated the atherosclerosis immunity and the formation of ATLOs. Moreover, calcium deposits may be observed in advanced plaques. Fully developed plaques contain a large acellular part having necrotic cores and a cellular part containing macrophages, mast cells, granulocytes, lipid-laden foam cells, DCs, T cells, and SMCs<sup>9,13,14</sup>.

### 1.1.3 Plaque vulnerability

In advanced stages, the atherosclerotic plaque can be classified into stable or unstable (vulnerable) types. Characteristics of a vulnerable plaque include: thin fibrous cap, large necrotic core, tissue proteolysis, increased lipid-rich macrophage accumulation, and reduced SMCs and collagen content. Unstable plaques are the major causes of plaque rupture and subsequent thrombosis leading to acute cardiovascular events such as stroke or myocardial infarction<sup>15,16</sup>. The term plaque vulnerability index (PVI)<sup>17</sup> is an important indicator of whether the plaque that is at higher risk of rupture leading to thrombosis and a useful parameter to evaluate the effectiveness of potential new therapies<sup>17</sup>. The higher the plaque vulnerability index, the higher the instability of the plaque. Unlike humans, apolipoprotein E knock-out (*ApoE*<sup>-/-</sup>) mice do not develop ruptured or rupture-prone plaques (no thrombus, plaque hemorrhage, etc.), and myocardial infarction – even in mice as old as 120 weeks age with heavy atherosclerosis<sup>18,19</sup>. However, some features of vulnerable plaques and myocardial infarcts have been induced in *ApoE*<sup>-/-</sup> mice under distinct experimental conditions<sup>20</sup>.

### 1.1.4 Atherosclerosis and aging

Aging is one of the most important risk factors for atherosclerosis development, but it remains the least understood of all risk factors. As a complex process, aging involves cell cycle arrest, chromatin

## INTRODUCTION

silencing, epigenetic modifications, morphology remodeling with functional impairments, changes in metabolism, senescence, and apoptosis<sup>21,22</sup>. Since several biochemical pathways and vascular alterations are common features of aging and atherosclerosis, atherosclerosis can be viewed as one form of accelerated vascular aging<sup>23</sup>. Even in the absence of atherosclerosis, vascular aging develops intimal and medial thickening and loss of elasticity, which leads to vessel wall stiffness<sup>24</sup>. In the experimental *ApoE*<sup>-/-</sup> mouse model, atherosclerotic plaque emerges in the aortic root at early age, then travels down the aorta through the aortic arch to reach the abdominal aorta at later stage of the disease over time during aging. Importantly, aging was found to be a major determinant of adventitia restructuring. Fully developed ATLOs in the abdominal aorta form during advanced stages of atherosclerosis at 78 weeks but early ATLOs form at around 52 weeks in *ApoE*<sup>-/-</sup> mice, indicating ATLO development depends on aging<sup>25,26</sup>. Aging is systemically associated with immune senescence of T cells, B cells, and in particular expansion of Regulatory T (T<sub>reg</sub>) cells locally in ATLOs<sup>25,27,28</sup>.

### 1.1.5 Mouse models of atherosclerosis

Hyperlipidemic mice have been used to investigate the molecular mechanisms underlying human atherosclerosis<sup>29</sup>. In hyperlipidemic mice, atherosclerotic plaques emerge in the aortic root within the first 32 weeks of life (this is the case for *ApoE*<sup>-/-</sup> mice). With time, plaques develop in other segments of the arterial tree, including the abdominal aorta and carotid arteries<sup>9</sup>. In the past decades, several hypotheses on the molecular mechanisms underlying atherosclerosis have been proposed. However, the details and molecular mechanisms of the initiation of atherosclerosis remain largely elusive. To study atherosclerosis, the *ApoE*<sup>-/-</sup> mouse has evolved as one of the most widely used experimental models of atherosclerosis. The *ApoE*<sup>-/-</sup> mouse is constitutively hyperlipidemic and develops atherosclerosis spontaneously<sup>29</sup>. The majority of studies have employed a high-fat cholesterol-rich diet (HFD)<sup>30</sup> to examine the structure and the cellularity of the plaques. In addition, low-density lipoprotein receptor-deficient (*LDLR*<sup>-/-</sup>) mice have also been used to study atherosclerosis. *LDLR*<sup>-/-</sup> mice develop no or mild atherosclerosis on normal chow diet. However, these mice have dramatically elevated cholesterol levels and increased lesion formation throughout the aorta on a variety of high-fat diets (HFD)<sup>31,32</sup>. More recently, new experimental models based on tamoxifen-induced conditional *ApoE* deletion in adult mice and adeno-associated virus-mediated proprotein convertase

subtilisin/kexin type 9 (PCSK9) gain-of-function in mice or hamsters have been developed to study atherosclerosis<sup>33,34</sup>.

### **1.1.6 Immune responses in atherosclerosis**

Most chronic inflammatory diseases show mixed innate and adaptive immune responses. Innate immune responses are carried out by macrophages, DCs, neutrophils, mast cells, and innate lymphoid cells<sup>35</sup>. These cells recognize non-self danger molecules such as danger-associated molecular patterns or pathogen-associated molecular patterns through broad specificity-acting receptors and then become activated to protect the body by eliminating the foreign dangers<sup>7,36</sup>. In addition, self-derived molecules may mimic cellular infection, damage, and multiple forms of stress, which can be recognized by the immune system, and initiate inflammation. Some of these molecules are recognized by danger-associated molecular patterns<sup>37</sup>. The innate immune response is, however, nonspecific, i.e., antigen epitope-independent. All pathogens, including viruses, bacteria, parasites, prions, fungi, or toxins, can be detected by innate immune cells. Innate immunity defends the body as its rapid first line, which begins within minutes to hours<sup>7,36</sup>. In contrast, adaptive immune responses are antigen-specific. They are initiated when a pathogen cannot be eliminated by innate defense mechanisms within a very short period of time. Antigen-presenting cells, including activated macrophages and DCs, present antigen to lymphocytes. T cells recognize antigens presented by antigen-presenting cells through their T cell receptor (TCR), while B cells recognize antigen through B cell receptors. Subsequently, the lymphocytes are activated and proliferate, forming distinct clones of memory cells that will become active when the antigen persists or when the antigen will invade the organisms again during a later stage in life. The adaptive responses that follow antigen exposure include direct attack by cytotoxic T lymphocytes (CD8 positive T cells), CD4 positive T cells of various sub-lineages (also termed T helper cells), and antigen-specific B cell clones to produce antibodies against the antigens. Thus, the adaptive immune response is slower than innate but more powerful and very specific<sup>7,36,38</sup>.

The immune responses in atherosclerosis include both innate and adaptive responses. In atherosclerosis, potentially harmful molecules are detected by the innate immune system<sup>7,36</sup>. Monocytes are recruited from the circulation and migrate into the intima, then they proliferate and differentiate into macrophages and dendritic cells. T cells also migrate into the intima, constituting a

## INTRODUCTION

major cell type of atherosclerosis immunity. Several adhesion molecules and chemokines, such as selectins, i.e., vascular-cell adhesion molecule 1, intercellular adhesion molecule 1, and monocyte chemoattractant protein-1 (also known as CC-type chemokine, CCL2) promote monocyte recruitment as well as the attraction of T cells. Most of the T cells in atherosclerotic plaques are CD3<sup>+</sup>CD4<sup>+</sup> T cells. Moreover, antigen-presenting cells, including macrophages and DCs, present antigens to T cells. Plaque macrophages, DCs, and T cells secrete pro-inflammatory cytokines such as interferon- $\gamma$ , interleukin-2 (IL-2), tumor necrosis factor- $\alpha$ , and - $\beta$ , as well as anti-inflammatory cytokines such as IL-10 and IL-4. These cytokines promote or dampen inflammation, and thus critically participate in cellular immunity. In addition to CD4<sup>+</sup> helper T cells (Th), atherosclerotic plaques harbor CD8<sup>+</sup> T cells<sup>36</sup>. However, the role of plaque CD8<sup>+</sup> T cells for atherosclerosis immunity has remained unclear<sup>39</sup>. T<sub>reg</sub> cells are an important component of the immune system, specialized for the suppression of both Th1 and Th2 pathogenic immune responses against self or foreign antigens. They control T cell and other immune cells' homeostasis by suppressing their activity, and few can also be observed in the diseased arterial wall<sup>40</sup>.

### 1.1.7 Artery tertiary lymphoid organ neogenesis

Lymphoid organs include primary lymphoid organs (PLOs), secondary lymphoid organs (SLOs), and tertiary lymphoid organs (TLOs). PLOs are the bone marrow and the thymus, which emerge during embryonic development. SLOs, including the spleen, lymph nodes, and Peyer's patches, also develop during embryogenesis at predetermined sites where stromal lymphoid tissue organizer cells interact with hematopoietic lymphoid tissue inducer cells<sup>41</sup>. In sharp contrast, TLOs develop at diverse locations during unresolvable or chronic inflammation as immune cell aggregates within or around the inflamed tissue in adult organisms through the involvement of lymphoid tissue organizer like cells<sup>26</sup>. Thus, TLOs function as transient organizers of adaptive immune responses in chronically inflamed tissues depending on the disease conditions, unlike SLOs.

Previously, our group has shown that immune cells infiltrate the inflamed abdominal aorta adventitia adjacent to atherosclerotic plaque in aged hyperlipidemic mice with advanced atherosclerosis and form a follicle-like structure, which we named as artery tertiary lymphoid organs (ATLOs)<sup>42,25</sup>. Meanwhile, ATLOs have been observed in human atherosclerotic tissues, including coronary arteries

## INTRODUCTION

and abdominal aorta<sup>43</sup>, indicating that ATLO is an important component of human atherosclerosis. In aged *ApoE*<sup>-/-</sup> mice, atherosclerosis activates the lymphotoxin  $\beta$  receptor on media SMCs to become lymphoid tissue organizer cells and induce the lymphorganogenic chemokines, i.e., CXC chemokine ligand 13 and CC chemokine ligand 21<sup>27,44</sup>. These chemokines, in turn, trigger the formation of ATLOs, which share functional and structural features with SLOs, including separate T cell areas and B cell follicles<sup>45</sup>. ATLO development occurs in 3 stages. Stage I is defined as a small aggregate of mixed T cells with few B cells, stage II contains larger aggregates with separated B and T cell areas but - at this stage - no follicular dendritic cells (FDCs) can be observed, whereas stage III, i.e., the advanced form of an ATLO, contains separate B cell follicles with FDCs in activated germinal centers, T cell areas contain mainly T cells, T<sub>reg</sub> cells, DCs, and macrophages, and plasma cells in the shoulder region of ATLOs<sup>45,26</sup>. Plasma cell niches are home to short- and long-lived plasma cells<sup>46</sup>. In ATLOs, angiogenesis and lymph vessel neogenesis becomes prominent together with a dense network of conduits connecting the arterial media with newly formed high endothelial venules within the T-cell areas of ATLOs<sup>25,26,45,47</sup>. This distinctive anatomy of conduits in SLOs versus ATLOs is interesting in view of the hypothesis that chemokine gradients may exist within ATLOs with possible CXCL13 derived from activated media segments adjacent to atherosclerotic plaques. ATLO transcriptomes resembled those of SLOs, yet inflammation-regulating genes were expressed at significantly higher levels in ATLOs compared to lymph nodes<sup>27,28,47</sup>.

Tissue-specific homing and education of effector memory T cells and central memory T cells are essential for long-term immunosurveillance in general and in ATLOs in particular. ATLOs have been shown to directly trigger homing of naïve CD4<sup>+</sup> and naïve CD8<sup>+</sup> T cells into the abdominal aorta adventitia, and thus, they control aorta T cell responses in aged *ApoE*<sup>-/-</sup> mice<sup>27</sup>. ATLOs promote T cell recruitment, prime CD4<sup>+</sup> T cells, and locally generate and activate CD4<sup>+</sup>, CD8<sup>+</sup>, and induced T<sub>reg</sub> cells. These events mimic many events normally carried out in SLOs, such as lymph nodes. Importantly, when the ATLO structure was disrupted by VSMC-specific deletion of the lymphotoxin  $\beta$  receptor, atherosclerosis was increased in aged *ApoE*<sup>-/-</sup> mice<sup>27</sup>. These data indicate that the immune system employs ATLOs to organize aorta T and B cell homeostasis during aging, which is consistent with the hypothesis that ATLOs protect the arterial wall from atherosclerosis via VSMC-LT $\beta$ Rs<sup>27</sup>. Since ATLOs contain both pro- and anti-inflammatory immune cells, the dichotomic nature of ATLO generate opposing immune responses that promote the generation of antigen-specific lymphocyte subsets. It is very likely that the initial purpose of ATLO neogenesis is to eliminate antigen and/or

fight against atherosclerosis inflammation.

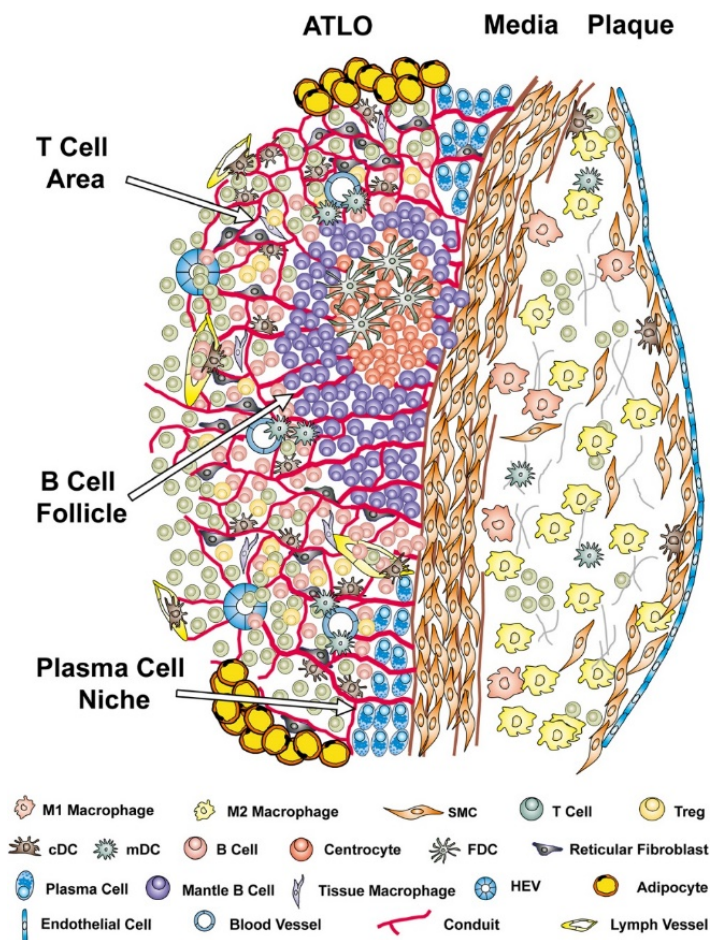


**Figure 2. The cellularity and structure of ATLOs.** Reproduced from Mohanta, S. K. et al.<sup>26</sup>. The schematic graph shows the structure and cellularity of stage III ATLOs. ATLOs stage III contains T cell areas with T cells, T<sub>reg</sub> cells, macrophages, and DCs; B cell follicles with FDCs and plasma cell niches. Moreover, ATLOs are supplied with multiple newly formed lymph vessels, blood vessels, high endothelial venules, and conduits.

## 1.2 Nervous system

The nervous system (NS) can be divided into the central NS (CNS) and the peripheral NS (PNS) (Fig. 3). The CNS in mammals consists of the brain and the spinal cord. The PNS is distributed throughout the organism, containing the autonomic NS and the sensory/somatic NS. Nerve fibers, their individual axons, and corresponding peripheral ganglia of the PNS transport electrical nerve impulses from the periphery to the CNS (afferents) or from the CNS to the target organs (efferents). The autonomic NS,

## INTRODUCTION

including the sympathetic NS (SNS) and the parasympathetic NS (PSNS) function unconsciously. The SNS serves as a so-called “fight or flight” system. On the other hand, the PSNS is known as the “rest and digest” system implicating fundamentally different and principally distinct roles in tissue homeostasis. Pre-ganglionic nerves connect ganglia and CNS, post-ganglionic nerves connect ganglia and target organs. The PNS also includes the enteric NS, which is independently regulated by multiple circumstances, including the microbiome<sup>48</sup> that are crucial for the regulation of food digestion. It should be noted, however, that the gut is also connected to the brain via the SNS and PSNS<sup>49,50</sup>.

The SNS is an important component of the autonomic nervous system. The SNS in the brain includes sympathetic neurons in the cortex, hypothalamus, midbrain, pons, and medulla. The SNS in the spinal cord includes the lateral gray column and the intermediolateral column. The SNS in the periphery originates from intermediolateral column of spinal cord segments thorax (T) T1 to segments lumbar (L) L3. It connects target organs via sympathetic chain ganglia and para-aortic ganglia. In peripheral sympathetic ganglia, acetylcholine is the neurotransmitter, whereas in the target organs, sympathetic neurons release NE and epinephrine as neurotransmitters. Peripheral sympathetic ganglia include sympathetic chain ganglia, celiac ganglia, and the superior and inferior mesenteric ganglia<sup>51</sup>.

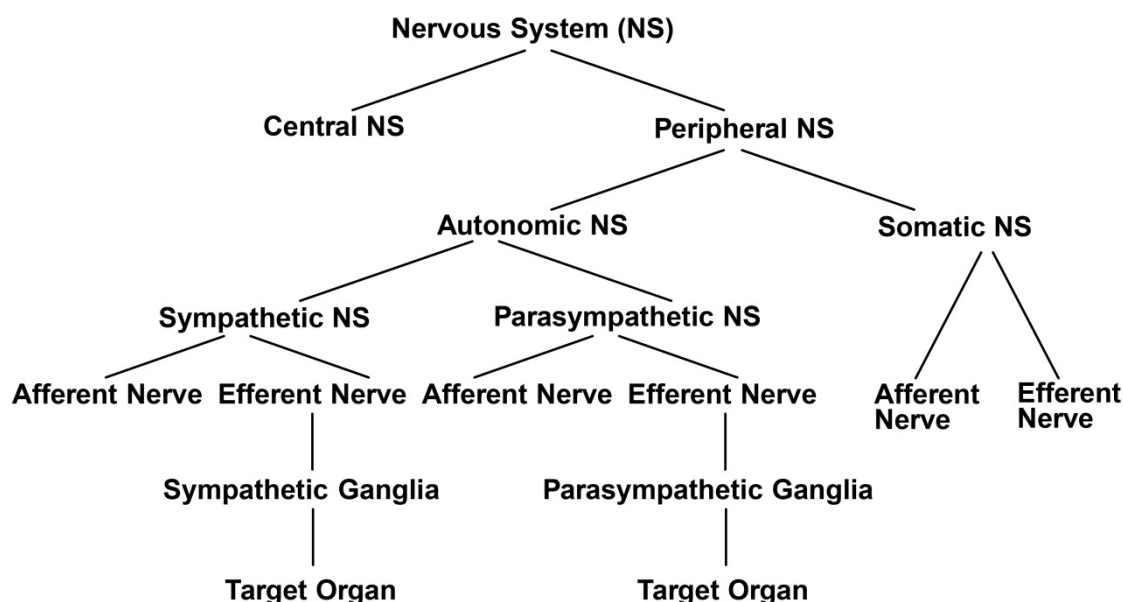


**Figure 3. Constituents of the NS.** The NS consists of the CNS and the PNS. The PNS contains the autonomic NS and the sensory/somatic NS. The autonomic NS includes the SNS and the PSNS. All three NSs consist of afferent and efferent nerves. Preganglionic neurons connect the CNS and the PNS ganglia, whereas postganglionic neurons connect the PNS ganglia and the peripheral target organs. The enteric NS is not depicted here for ease of reading.

### 1.2.1 Role of PNS in peripheral tissue homeostasis and inflammation

The NS can impact peripheral tissue homeostasis through distinct mechanisms: Afferent sensory neurons receive internal or external stimuli, including touch, pain, temperature, pressure, and chemicals. Sensory axon endings are in contact with immune cells and receive information from inflammatory mediators or cytokines through corresponding receptors<sup>52-54</sup>. In the afferent axon endings, the chemical signals of inflammation are transformed into action potentials<sup>55</sup>. The interneurons in the CNS receive and integrate these action potentials, and then relay them to the efferent neurons. Efferent neurons transduce information from the CNS to the peripheral organs. In particular, the efferent parasympathetic nerves directly release acetylcholine or instruct immune cells to produce acetylcholine at the site of inflammation, which inhibits pro-inflammatory cytokine release and thereby attenuates peripheral inflammation<sup>52</sup>. This inhibitory pathway mediated by parasympathetic vagus nerve is called as cholinergic anti-inflammatory pathway<sup>54,56</sup>. In addition, the efferent sympathetic nerves are equally important in regulating peripheral inflammation<sup>54,57-59</sup>. Interestingly, the SNS has been reported to play opposing roles in acute and chronic inflammation, e.g., the SNS is pro-inflammatory in the acute phase of collagen-induced arthritis, whereas it appears to be anti-inflammatory in chronic rheumatoid arthritis and chronic intestinal inflammation<sup>57,60,61</sup>.

It is known that both PLOs and SLOs are extensively innervated by the SNS<sup>62</sup>: The bone marrow is innervated by both the SNS<sup>63</sup> and the PSNS<sup>64,65</sup>, whereas the thymus is innervated by the PSNS and the sensory NS<sup>65,66</sup>. Moreover, the spleen receives innervation from the SNS<sup>43,67,68</sup> and the PSNS<sup>65,66,69,70</sup>. Finally, peripheral lymph nodes are innervated by the sensory NS<sup>64,71,72</sup>, and Peyer's patches are innervated by the PSNS<sup>65,73</sup>. For the SNS and PSNS, it was reported that sensory neurons could be activated by bacterial stimuli and modulate pain and inflammation<sup>74</sup>; the immune system is regulated by nociceptor sensory neurons in bacterial infection of the lung<sup>75</sup>. These data provide important evidence of a direct relation between immunity and the NS.

### 1.2.2 SNS functions in health and disease

SNS functions in the brain consist of the dopaminergic pathway, the adrenergic pathway, and the

## INTRODUCTION

cholinergic pathway<sup>67,76,77</sup>, whereas the SNS mainly consists of the adrenergic pathway in the periphery<sup>78,79</sup>. Activation of the peripheral adrenergic pathway causes constriction of blood vessels, and its inhibition causes dilatation of blood vessels. SNS activation also increases heart rate, relaxation of bronchi, vasoconstriction in the kidney, and lipolysis in adipocytes<sup>80</sup>.

In the cardiovascular system, the SNS controls heart function during stress, including heart rate variability and left ventricular output<sup>81</sup>. In the immune system, the SNS impacts both innate and adaptive immunity in health and disease<sup>82</sup>: Stress causes SNS activation-induced inhibition of pro-inflammatory cytokine (IL-1 $\beta$ , IL-6, and tumor necrosis factor- $\alpha$ ) production by splenic macrophages<sup>83</sup>. NE stimulates the generation of CD8<sup>+</sup> T cell lytic activity in cultured murine spleen cells and human peripheral blood cells<sup>62</sup>.

The effects of aging and disease conditions on sympathetic innervations of different organs have been delineated. The sympathetic neurohormone/neurotransmitter NE is increased in human plasma during aging<sup>84</sup>. A previous theory claimed that the periarterial nervous system development would stop at about two weeks after birth<sup>85</sup>, whereas more recently, this view has been revised, and studies reported that the axon network in the rat aorta undergoes restructuring in aging animals<sup>55</sup>. Furthermore, the tissue NE was determined to be increased in stress, stroke, or MI mouse models<sup>86-88</sup>.

Because of the potential importance of the SNS, several groups performed chemical sympathectomy to study the effect of sympathetic denervation on the immune system and inflammation. Sympathectomy increases Foxp3<sup>+</sup> T<sub>reg</sub> cells in the CD4<sup>+</sup> T cell population in Fas-deficient *lpr/lpr* (lymphoproliferative diseased) spleen<sup>89</sup> and affects multiple immune system-dependent diseases, including myocardial infarction<sup>88,90</sup> and collagen- and antigen-induced arthritis<sup>61,91</sup>. Sympathectomy reduces early arthritis scores in collagen-induced arthritis mouse models through increased anti-inflammatory cytokines like IL-4 and IL-10 production by lymph node (LN) cells before injection of collagen-II, whereas it increased arthritis at later stages through increased pro-inflammatory cytokines like tumor necrosis factor and interferon- $\gamma$  production by LN cells and splenocytes. However, no data on cytokine production in early arthritis were reported<sup>43,91</sup>. Atherosclerosis triggered by myocardial infarction (MI) was reported to be attenuated by chemical sympathectomy in *ApoE*<sup>-/-</sup> mice fed with HFD<sup>88</sup>. The same experiments also reduced the number of myeloid cells in plaque after MI<sup>90</sup>, whereas the infarct size was reduced by chemical sympathectomy in rats<sup>92</sup>.

## INTRODUCTION

Importantly, sympathectomy has been demonstrated to affect the immune system in normal and diseased mice. Sympathectomy decreased norepinephrine (NE) level in spleen but increased splenic T<sub>reg</sub> cell percentages in WT mice. Additionally, NE treatment induced apoptosis of CD4<sup>+</sup> T cells and CD4<sup>+</sup>Foxp3<sup>+</sup> T<sub>reg</sub> cells *in vitro*, suggesting that the SNS maintains the T<sub>reg</sub> cell population in spleen through NE secretion<sup>89</sup>. Weights of the spleen and inguinal lymph nodes (iLNs), as well as total cell numbers in iLNs, were increased after sympathectomy during arthritis<sup>93</sup>. Moreover, sympathectomy reduced myeloid cells in blood after MI in *ApoE*<sup>-/-</sup> mice<sup>90</sup>, whereas it decreased T and B cell numbers in the blood of WT mice<sup>94</sup>. In addition, surgical denervation of celiac ganglia reduced placental growth factor in spleen and lymphocytes infiltration in para-aortic tissue and kidney, thereby attenuated angiotensin-II induced hypertension<sup>68</sup>. These data indicated that the SNS can be pro- or anti-inflammatory depending on the disease conditions and that it regulates lymphocyte homeostasis in the circulation and tissues (see Table 1).

**Table.1. Effects of sympathetic denervation in health and diseases.**

Animal Model	Diet	Approach (Dose)	Effects in Health	References
C57Bl/6	Normal diet	6-OHDA (150 mg/kg)	Sympathectomy increased T <sub>reg</sub> percentages in spleen	89
C57Bl/6	Normal diet	6-OHDA (200 mg/kg)	Sympathectomy decreased T and B cell numbers in blood	94
DBA/1J	Normal diet	6-OHDA (80 mg/kg)	Sympathectomy increased total cell numbers and organ weights in iLNs and spleen	93
<b>Effects in Diseases</b>				
C57Bl/6	Normal diet	6-OHDA (150 mg/kg)	Sympathectomy reduced acute antigen-induced arthritis	95
DBA/1J	Normal diet	6-OHDA (80 mg/kg)	Early sympathectomy reduced collagen-induced arthritis, whereas late sympathectomy increased arthritis.	61
C57/Bl6	Normal diet	Celiac ganglionectomy (CGX)	CGX reduced placental growth factor in spleen and lymphocytes infiltration in periaortic tissue and kidney, thereby attenuated angiotensin-II induced hypertension.	68
<i>ApoE</i> <sup>-/-</sup>	High cholesterol diet	6-OHDA (250 mg/kg)	Sympathectomy decreased adhesion molecules expression in aortic endothelial cells and reduced myeloid cells in blood, and plaque after myocardial infarction	88,90
Rat	Normal diet	6-OHDA (100 mg/kg)	6-OHDA denervation significantly reduced the myocardial infarct size induced by physical and psychological stress.	92

Adrenergic receptors (ADRs) are a class of G protein-coupled receptors and constitute the targets of catecholamines, especially NE (noradrenaline) and epinephrine (adrenaline). ADRs include ADR $\alpha$ 1,  $\alpha$ 2,  $\beta$ 1,  $\beta$ 2, and  $\beta$ 3<sup>96</sup>. In the circulation, ADR $\beta$ 1 play an essential role in the regulation of the cardiovascular system<sup>97</sup>; activation of ADR $\beta$ 2 relaxes smooth muscle and dilates blood vessels; ADR $\beta$ 3 present in endothelium and myocardium may have specific beneficial effects in the cardiovascular system including cardioprotection<sup>98</sup>.

### 1.3 Interactions of the immune system and the SNS

Though it has been considered that the immune system and nervous systems functioned independently, it is now well-established that prominent bidirectional communication pathways exist between them<sup>99</sup>, which established the field of neuroimmunology<sup>53,56,62,100-102</sup>. The PLOs and SLOs, including bone marrow, thymus, spleen, and LNs are innervated by the SNS, but not by the parasympathetic NS<sup>62</sup>. Increasing evidence of pharmacology, electrophysiology, and molecular biology indicated that immune cells in the lymphoid microenvironment could release neurotransmitters and often express receptors for neurotransmitters<sup>103-105</sup>. The following points on the study progress of the immune system and SNS interactions should be noticed:

1) Multiple pathways (both neural and non-neural) of communication are available to transfer information between local or systemic immune status and CNS<sup>106-108</sup>. 2) Sympathetic nerves release catecholamines, including epinephrine and norepinephrine<sup>109</sup>. Immune cells can also synthesize neurotransmitters and express neuroimmune receptors. For instances, macrophages, and B cell can produce catecholamines<sup>60,110,111</sup>; and express  $\beta$ 2 adrenergic receptors (ADR $\beta$ 2)<sup>53</sup>. Moreover, T and B cells can produce acetylcholine, whereas macrophages, T cells, and B cells can express nicotinic acetylcholine receptor<sup>112-114</sup>. 3) Neuronal responses can regulate homing/recruitment, activation, migration, and maturation of immune cells in lymphoid organs. For instance, sympathetic innervations promote homing of leukocytes to bone marrow<sup>115</sup>, and activation of sympathetic NS can enhance recruitment and activation of lymphocytes, including CD4<sup>+</sup> T cells in spleen and lymph nodes<sup>116</sup>. 4) Receptors and autonomic nuclei, which present at many levels of the supraspinal neuraxis and neural-immune interactions, can occur at a huge number of sites in these distributed systems

## INTRODUCTION

(brain and selective nuclei)<sup>99,107,117-119</sup>. 5) The autonomic nervous system is highly responsive to the administration of cytokines and immune cell factors administered via a number of different routes, including; intravenous<sup>120,121</sup>, intra-arterial<sup>122</sup>, and central microinjections<sup>123,124</sup> in selected nuclei<sup>99</sup>. 6) SNS innervates the spleen and other secondary lymphoid organs, and alterations in splenic sympathetic nerve discharge can influence peripheral immune responses, including changes in splenic cytokine gene expression<sup>99,125</sup>.

In mouse models of collagen-induced arthritis, tyrosine hydroxylase (TH) positive, sympathetic nerve fibers were reduced in spleen accompanied with splenic cytokine release<sup>126</sup>. Moreover, T and B cell-deficient SCID mice show a reduced TH<sup>+</sup> sympathetic axon density in white pulp of the spleen, which becomes normal after the reconstitution of adaptively transferred T cells indicating the modulation of peripheral innervations by immune cells<sup>127</sup>. Likewise, TH<sup>+</sup> sympathetic axons were abundant in splenic red pulp of chronic arthritic rats, possibly due to the migration of activated immune cells from the white pulp<sup>128</sup>. When taken together, the distribution pattern of nerve axons in lymphoid organs, the presence of neurotransmitters and their receptors in immune cells, the neuromodulation of immune functions, and the immune regulation of the NS altogether provide the anatomical, cellular and molecular basis for bidirectional communications between the NS and the immune system<sup>53,54,129</sup>.

### **1.4 Interplay of the vascular system and the NS**

The vascular system closely interacts with the NS. Axons contribute to the branching of blood vessels and, *vice versa*, the development of axons in the vascular system requires neurotrophic proteins secreted by cellular constituents of the blood vessel<sup>130,131</sup>. For example, vascular SMCs in mesenteric and cutaneous arteries produce axon guidance protein netrin-1, and lack of netrin-1 significantly decreased TH<sup>+</sup> axons in mesenteric arteries, suggesting that netrin-1 is essential for the development of sympathetic arterial innervation in mice<sup>132</sup>. In addition, coronary artery VSMCs in the developing mouse heart during angiogenesis and branching secrete nerve growth factor and regulate axon growth to reach target cells<sup>131</sup>.

Intriguingly, peripheral nerves are essential for arterial differentiation and branching *in vivo* during embryonic vascular development<sup>131</sup>. Sensory neurons secrete vascular endothelial growth factor to regulate arteriogenesis and branching<sup>131</sup>. The autonomic innervations, which are located in the

## INTRODUCTION

adventitia of medium- and large arteries, can affect endoluminal inflammation, including atherosclerosis<sup>133</sup>. As one of the two interacting divisions of the ANS, the SNS regulates heart rate, blood pressure, vasomotor tone of the blood vessel, and myocardial contractility<sup>134-138</sup>. In contrast, parasympathetic stimulation decreases heart rate. However, arteries do not respond to parasympathetic stimulation since most of them lack parasympathetic innervation. The contractility of arteries is therefore largely regulated by sympathetic nervous system input as an increase in sympathetic stimulation leads to vasoconstriction while its decrease induces vasodilatation<sup>137</sup>.

### 1.5 Atherosclerosis and the SNS

During the past decades, increasing evidence for sympathetic and sensory innervation in peripheral inflamed tissues has been delineated<sup>65,73</sup>. Sympathetic nerves are present in and around the arterial wall adventitia<sup>65</sup>. It has been hypothesized that local nerve endings secrete neurotransmitters and may affect blood vessel homeostasis and/or adventitial immune cells directly<sup>139</sup> though evidence for this possibility has yet to be obtained. Conversely, there is ample evidence that soluble neurotransmitters affect blood vessel homeostasis, including endothelial cell homeostasis, in many ways<sup>133</sup>. In large- and medium-sized arteries, unlike arterioles, nerve axons reach only to the adventitia/media border and never innervate the outer portion of the media, and no axons are present in the intima or in atherosclerotic plaques of medium- and large arteries (unpublished data of our lab). This is in sharp contrast to arterioles, which contribute to blood pressure regulation where sympathetic NS axons innervate the VSMCs to contract.

The density of periadventitial neurofilament (NF) positive nerves appeared to be increased in human coronary arteries with increasing stages of atherosclerosis, and the NF positive axons co-localized with mast cells in human coronary adventitia<sup>140</sup>. However, axon density with increasing atherosclerosis did not reach statistical significance though there was a significant correlation of axon density and mast cell abundance. MI enhanced TH positive area in the aortic root and aortic arch NE content of HFD fed *ApoE*<sup>-/-</sup> mice<sup>88</sup>. However, as the number of axons was not determined, it was not clear whether this reflects an increase of TH per nerve axon or an increase of the nerve axon density per tissue volume. Moreover, it remained unclear whether the extent of atherosclerosis in MI-induced HFD-fed *ApoE*<sup>-/-</sup> mice correlated with the adventitial nerve axon density. Therefore, the relation

## INTRODUCTION

between axon density in the adventitia and atherosclerosis remains unknown.

## 1.6 Aims of the thesis

The overarching goal of this thesis was to investigate the pathophysiological relevance of arterial SNS innervation in atherosclerosis. Because ATLOs develop in advanced atherosclerosis, the investigation of SNS function in atherosclerosis was extended to ATLOs. Based on previous observations of ATLOs in the adventitia of aged hyperlipidemic mice and atherosclerosis-associated adventitial sympathetic innervation, we hypothesized that SNS innervation might be a consequence of atherosclerosis or *vice versa* that an increase in adventitial axons density of the NS directly affects atherosclerosis.

In particular, the aim of my experimental work was to examine the role of the SNS on atherosclerosis, the immune system, and ATLO neogenesis in young and aged *ApoE*<sup>-/-</sup> mice. To address these issues experimentally, we asked the following specific questions:

- 1) Does atherosclerosis affect aortic sympathetic innervation?
- 2) Does sympathetic denervation affect atherosclerosis and ATLOs of the diseased aorta?

## 2 MATERIALS AND METHODS

### 2.1 Materials

#### 2.1.1 Mice

WT C57BL/6J and *ApoE*<sup>-/-</sup> mice on a C57BL/6J background were purchased from Jackson Lab (USA) and Janvier lab (France) and housed in the animal facility of University Hospital of Munich. Mice were housed in a specific pathogen-free environment on a 12 hours light/dark cycle and fed standard diet and water ad libitum. To minimize variability, only male mice were used. All animal experiments were performed in strict adherence to local governmental and institutional animal care regulations (Gz.: 55.2-1-54-2532-6-2014, Regierung Oberbayern München).

#### 2.1.2 Reagents, buffers, and equipment

The following tables contain the list of reagents, buffers, and equipment.

**Table 2: List of reagents**

Reagents	Company	Catalogue No.	Storage
6-Hydroxydopamine hydrochloride	Sigma-aldrich	H4381-1G	4° C
Paraformaldehyde (PFA)	Sigma	P-6148	RT
Ethylenediaminetetraacetic acid (EDTA)	Roth	8040.1	RT
Sucrose	Sigma-Aldrich	90M003524V	RT
Oil red O	Romeis	S378	RT
Sudan IV	Sigma	198102	RT
Sucrose	Sigma	S9378	RT
Hematoxylin	Dako	S2020	RT
Giemsa	Merck	192040100	RT
10% bovine serum albumin (BSA)	Aurion	70411/1	4° C
Sirius Red	Waldeck	1A-280	RT
Picric acid	Sigma	P6744	RT under hood
Glacial acetic acid	Sigma	A-6283	RT under hood

## MATERIALS AND METHODS

Acetone	Merck	K40718714	RT under hood
Isopentane	Roth	3926.1	RT under hood
Isopropanol	Merck	K40615718	RT under hood
Methanol	Roth	Sorte420	RT under hood
Tissue Tec	Sakura	0827400006	RT
Fluoromount G	DAKO	S3023	4° C
Roti- Histokit 2	Roth	9713	RT
Faramount Aqueous Mounting Medium	DAKO	S3025	4° C
NE ELISA kit	Labor Diagnostika Nord (LDN)	BA E-5200	4° C

**Table 3: List of buffers**

Solution	Composition	Storage
PBS (1X)	137 mM NaCl, 2.7 mM KCl, 10 mM Na <sub>2</sub> HPO <sub>4</sub> , 1.76 mM KH <sub>2</sub> PO <sub>4</sub> , pH 7.4;	RT
FACS buffer	PBS with 2% fetal calf serum(FCS; Lonza)	4°C
Ammonium-Chloride-Potassium lysis buffer	0.15 mM NH <sub>4</sub> Cl, 1 mM KHCO <sub>3</sub> , 0.1 mM Na <sub>2</sub> EDTA, pH 7.2-7.4;	RT
PBS for Giemsa stain	Na <sub>2</sub> HPO <sub>4</sub> ·2H <sub>2</sub> O, KH <sub>2</sub> PO <sub>4</sub> with dist. water; 0.1M, pH 6.8	RT
PBST	PBS with 0.05% Triton-X 100	4°C
4% PFA	40 g paraformaldehyde in PBS (1000 ml final), pH 7.2-7.4	4°C
PBA	PBS with 1% BSA	Prepare fresh
Blocking solution	PBS with 1% BSA and 0.05% Triton-X 100	Prepare fresh
Oil red O stock	0.5 g Oil red O in 100 ml isopropanol	RT
Sudan IV stock	0.5 g Sudan IV in a mixture of 35 ml ethanol, 50 ml acetone, and 20 ml water	RT
Catecholamine stabilizing solution for homogenization <sup>65</sup>	0.01N HCl, 1mM EDTA, 4mM Na <sub>2</sub> S <sub>2</sub> O <sub>5</sub> , pH 7.5	4°C
Acidified water <sup>141</sup>	5ml glacial acetic acid into 1000ml d water	RT
Picro-Sirius red solution <sup>141</sup>	Sirius red powder dissolved in picric acid, the final concentration as 0.1%.	RT

**Table 4: List of equipment**

Name	Company	Model/Type
Balance	Ohaus	Analytical Plus
Centrifuge	Eppendorf	Centrifuge5415 R

## MATERIALS AND METHODS

	Thermo Scientific	Heraeus®Multifuge®3S-R
Black dissection wax	CR Scientific	C3541
Minutien Pins	Fine Scientific Tools	26002-15
Complete blood cell counter	scil Vet abc	scil animal care company GmbH
Flow cytometer	BD	Canto-II
Dissection Stereomicroscope	Leica	Stemi 2000
Light microscope	Leica	DM LB
Fluorescence microscope	Leica	DM 6000 B
Veroklav Laboratory Autoclave	Thermo Scientific	Ype:500
-80°C freezer	Miele	C7736CD
Cryostat microtome	Leica Biosystems	Leica RM2235
Microplate Reader	Tecan	Spectra Fluor Plus
NanoDrop	Thermo Scientific	ND-2000
Confocal laser scanning microscope	Leica	True Confocal Scanner (TCS)-SP8

### 2.1.3. Antibodies for immunofluorescence microscopy

The following tables contain the primary and secondary antibodies used to characterize PNS axons, immune cells, TLO structures by immunofluorescence confocal microscopy and their working dilutions, and company details.

#### 2.1.3.1. Primary antibodies

**Table 5: List of primary neuronal antibodies used to define PNS axons**

Antibody	Clone	Cells/Structure	Host	Dilution	Company
Anti-neurofilament 200 (NF200)	Polyclonal	Pan-neuronal	Rabbit	1:1000	Sigma
Anti-neurofilament M (NFM)	Polyclonal	Pan-neuronal	Chicken	1:500	Chemicon
Anti-TH Rabbit	Polyclonal	Sympathetic	Rabbit	1:500	Millipore
Anti-TH Sheep	Polyclonal	Sympathetic	Sheep	1:200	Millipore
Anti-NeuN	MAB377X	Neuronal cell body	Mouse	1:100	Millipore

**Table 6: List of primary antibodies used to characterize immune cells and TLO structures**

Antibody	Clone	Cells/Structure	Host	Dilution	Company
Anti-CD45	YW62.3	Pan-leukocyte marker	Rat	1:100	Biozol

## MATERIALS AND METHODS

Anti-CD68	FA-11	Macrophage or monocyte	Rat	1:50	Serotec
Anti-CD3e	145-2C11	Pan-T cell	A. Hamster	1:100	BD
Anti-B220	RA3-6B2	Pan-B cell	Rat	1:200	BD
Anti-Foxp3	FJK-16s	T <sub>reg</sub> cell	Rat	1:200	eBioscience
Anti-SMA-FITC	1A4	SMC	Mouse	1:400	ThermoFisher

### 2.1.3.2. Secondary antibodies

**Table 7: List of secondary antibodies**

Antibody	Host	Format	Dilution	Company
Anti-rabbit IgG	Goat	Alexa 488	1:200	Invitrogen
	Donkey	Cy3; Cy5	1:300	Dianova
	Goat	Cy3; Cy5	1:300	Dianova
Anti-rat IgG	Donkey	Alexa 488	1:100	Molecular Probes
	Donkey	Cy3; Cy5	1:300	Dianova
Anti-A. Hamster IgG	Goat	Cy3	1:300	Dianova
		Cy5	1:300	Dianova
Anti-chicken IgY	Donkey	Cy3	1:300	Dianova
Anti-sheep IgG	Donkey	Cy3	1:300	Dianova
Anti-FITC IgG	Mouse	Cy3	1:300	Dianova

### 2.1.4 Antibodies for flow cytometry

**Table 8: List of flow cytometry antibodies**

Antibody	Clone	Format	Dilution	Company
FVD	-	APC-Cy7	1:200	eBioscience
Anti-CD45	30-F11	Percp-Cy5.5	1:200	eBioscience
Anti-TCR $\beta$	H57-597	BV605	1:200	Biolegend
Anti- CD4	GK1.5	PE-Cy7	1:200	eBioscience
Anti-CD8 $\alpha$	53-6.7	V450	1:200	eBioscience
Anti-B220	RA3-6B2	V500	1:200	eBioscience
Anti-CD11b	M1/70	APC	1:200	eBioscience
Anti-CD11c	N418	FITC	1:200	eBioscience
Anti-Foxp3	FJK-16s	PE	1:200	eBioscience
Anti- CD44	IM7	APC-Cy7	1:200	eBioscience
Anti- CD62L	MEL-14	FITC	1:200	eBioscience
Anti- CD69	H1.2F3	PE	1:200	BD

## MATERIALS AND METHODS

Anti- Sca1	D7	BV605	1:500	Biologend
Anti- CD135	A2F10	APC	1:500	Biologend
Anti- CD127	A7R34	APC-Cy7	1:500	Biologend
Anti- TER-119	TER-119	Pacific Blue	1:500	Biologend
Anti-Gr-1	RB6-8C5	Pacific Blue	1:500	Biologend
Anti- B220	RA3-6B2	Pacific Blue	1:500	Biologend
Anti-CD11b	M1/70	Pacific Blue	1:500	Biologend
Anti-CD3	17A2	Pacific Blue	1:500	Biologend
Anti-CD150	TC15-12F12	PerCP/Cy5.5	1:500	Biologend
Anti-CD34	RAM34	FITC	1:500	BD
Anti- CD16/32	93	PE	1:500	Biologend
Anti- CD48	HM48-1	BV510	1:500	Biologend
Anti-c-kit	2B8	PE-Cy7	1:500	Biologend

## 2.2. Methods

### 2.2.1 Sympathetic denervation

#### 2.2.1.1 Chemical sympathectomy

Chemical sympathetic ablation was performed by injecting sympathetic neurotoxin, 6-hydroxydopamine (6-OHDA, Sigma) in 0.1% ascorbic acid in saline<sup>61,90,93</sup>. 6-OHDA was injected i.p. at a dose of 100 mg per kg body weight two days before day 0 and 250 mg per kg body weight on day 0 (after 48 hours) followed by 250 mg per kg body weight per week until 4 wks. The control group received the same amount of vehicle injection (0.1% ascorbic acid, i.p.) for the same duration of time. Animals were sacrificed one week after the last injection. Only male mice were used to minimize variability and were randomly assigned for treatments.

6-OHDA binds to dopaminergic transporter or norepinephrine transporter on the cell surface to enter the cell. It then forms free radicals or reversibly inhibits the mitochondrial respiratory chain complexes I and IV leading to increase reactive oxygen species (ROS) production and membrane permeability and decrease in ATP levels, disruption of mitochondrial membrane potential and function, and eventually cell death<sup>142</sup>.

### **2.2.1.2 Surgical sympathectomy**

Surgical transection of the coeliac ganglia (CGX) was performed in collaboration with Profs. Daniela Carnevale and Giuseppe Lembo at Department of Angiocardioneurology and Translational Medicine, IRCCS Neuromed, Pozzilli, Italy. For this purpose, 8 months old mice were anesthetized with isoflurane supplemented with oxygen (5% induction, 1.5% maintenance) as previously described<sup>68</sup>. CGX allowed removal of sympathetic splanchnic innervation, including splenic nerve and fibers, nerve and fibers innervating the abdominal aorta, and a part of the coeliac vagus nerve. For sham procedure mice underwent the same surgery for the exposure of the coeliac ganglion but without performing the removal. The animals were sacrificed 8 months post-surgery. To minimize variability, only male mice were used, and animals were randomized to denervation or sham treatments.

### **2.2.2. Blood counter measurement**

Blood was withdrawn from the heart using a 1 ml syringe with a 23-gauge needle and collected in 1.5 ml EDTA-precoated tubes. 2  $\mu$ l anticoagulated blood was used for the measurement of blood parameters using complete blood cell counter Scil Vet abc (scil animal care company GmbH). The measurement and outcomes of the blood counter were automatically recorded.

### **2.2.3. Lipid ultracentrifugation of plasma samples.**

Blood was withdrawn from the heart using a 1 ml syringe with a 23-gauge needle and collected in 1.5 ml EDTA-precoated tubes. The anticoagulated blood samples were centrifuged at 6,000 rpm for 10 min. The plasma was collected, aliquoted at 50 $\mu$ l of volume, and stored at 4°C. Plasma cholesterol and triglycerides were determined by lipid ultracentrifugation in collaboration with Prof. Daniel Teupser and Dr. Wolfgang Wilfert (Institute of Laboratory Medicine, Clinical Chemistry and Molecular Diagnostics, University Hospital of Munich).

#### 2.2.4. Tissue preparation, embedding, and sectioning

Mice were anesthetized with ketamine, intraperitoneal (i.p.), and the body weight was measured. The vasculature was perfused by left ventricular puncture with 10 ml of 0.5 mM ice-cold EDTA in phosphate-buffered saline (PBS) followed by 20 ml ice-cold PBS and 10 ml ice-cold FACS buffer by using a 10 ml syringe with a 23-gauge needle attached.

The weights of the whole spleen, liver, heart, left kidney, and iLNs (both) were measured. For the gonadal adipose tissue (gAT), the gonadal fat pads around testicles (left and right sides) were carefully isolated and weighed. The tissues from vital organs, including a lobe of the lung, a piece of liver, half of a kidney, a piece of intestine, including Payer's Patch, were embedded in Tissue Tek (Sakura Finetek). The spleen was cut into three pieces: one half for flow cytometry, about 1mm length of spleen tissue from the tip was immediately frozen in the liquid nitrogen and stored at -80°C for the NE concentration and the rest for sectioning. Renal LN, mesenteric LN, and lumbar LN were isolated to examine the immune cells by flow cytometry. To analyze the development of atherosclerotic plaque, the whole aorta was isolated and stained with Sudan IV. For the sectioning purpose, the whole aorta with adjacent adipose tissue (up to 1 mm peripheral to the aorta) was isolated under a dissecting microscope. From the level above the coronary artery near the atria onto the level below the iliac bifurcation of the abdominal aorta, the aorta was cut into four parts: thorax-I: thoracic aorta from the level of the coronary artery to the level of 5th rib that includes the short ascending aorta, aortic arch containing no branching with it. The innominate and aortic arch were embedded for the sectioning purpose, while the left common carotid and the left subclavian arteries were quickly frozen in liquid nitrogen for measuring of the NE concentrations; thorax-II: thoracic aorta from the level of 7th rib to the diaphragm level including intercostal arteries; abdomen-I: abdominal aorta below the diaphragm to the middle of the abdominal aorta including the celiac, the superior mesenteric, the right and left renal arteries; and abdomen-II: abdominal aorta from the middle of the abdominal aorta to below the level of iliac bifurcation. The common iliac arteries at the iliac bifurcation were immediately frozen for NE measurement. Different parts of the aorta were then embedded in Tissue-Tec. All tissue blocks were frozen in chilled isopentane over dry ice, and tissue blocks were stored at -80°C until cryosectioning. Serial 10 µm-thick cross-sections were prepared with a microtome cryostat at -20°C, mounted on Polysine glass slides (Thermo Scientific), and air-dried. All slides were kept in slide holders and stored at -80°C until further use.

## MATERIALS AND METHODS

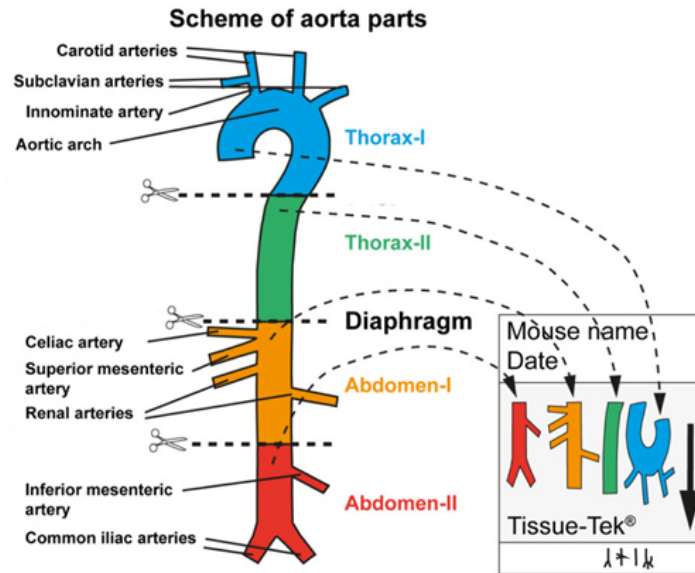


**Fig.4. Schematic graph of aorta segments and workflow.**<sup>35</sup> Reproduced from Mohanta, S. K., et al. The aorta was collected including the thorax-I (cyan) with its branches, i.e., the innominate artery including the right subclavian artery and the right common carotid artery, the left carotid artery, and the left subclavian artery; thorax-II (green); the abdomen-I (yellow) with its branches including the celiac artery, the superior mesenteric artery, the right and left renal arteries, and the abdomen-II (red) with its branches including the inferior mesenteric artery, and the common iliac arteries at the iliac bifurcation. The diaphragm delineates the border between the thorax and the abdomen. The inset below shows the four sections of the complete aorta in tissue block. Rotate thorax-I at 180° angle before embedding. Arrow indicates the direction of cutting.

For the sectioning of aortic roots, the heart was dissected and placed on wet tissue. The heart was separated from the aorta by holding the heart with the forceps and cutting with a scalpel blade at the top approximately one-third of it, as showed in Figure 5. The upper portion of the heart that contains the aortic root was placed in a cryomold and filled with Tissue-Tec. It should be positioned to be perpendicular to the bottom surface of the tissue mold and avoid the bubbles inside of the heart.

## MATERIALS AND METHODS

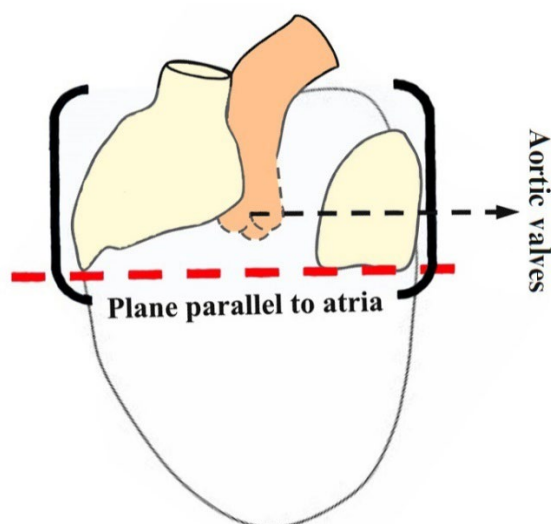


**Figure 5. Schematic for positioning of the heart for aortic root cross-sectioning.** (Adapted from “Methods in Mouse Atherosclerosis”, by Vicente Andrés and Beatriz Dorado). The cutting position of the heart for aortic root sectioning is as shown in the schematic diagram<sup>55</sup>.

### 2.2.5. En-face staining and quantification

To perform *en-face* whole-mount staining, the aorta was cleaned of all para-aortic adipose tissue under the dissecting microscope. The entire length of the isolated aorta was longitudinally split to expose the intimal surface, pinned to flat black wax plate and immersed in a 5% sucrose solution in 4% PFA, fixed overnight at 4°C. Aortae were rinsed with PBS for 3 x 10 minutes prior to 5-minutes wash in 70% ethanol. A working solution of Sudan IV was made by dissolving 500 mg of Sudan IV in a mixture of 35 ml ethanol, 50 ml acetone, and 20 ml distilled water. The whole aorta was immersed in Sudan IV working solution for 10 min, followed by two washes in 70% ethanol and a further rinsing in distilled water<sup>35</sup>.

In order to quantify the percentages of lipid deposition in the thoracic, abdominal, and entire aorta, images were taken using a digital camera (DSLR-a580, Sony) with a standard bar. The Sudan IV positive area in the aorta was quantified using Java-based image processing software Image J. The percentage area of the lesion was calculated using the Sudan IV positive area and area of the thoracic, abdominal, and total aorta. The images to be measured were opened with the software Image J. Then, the image scale was set with the standard bar on the images. After the calibration for the image, on the measurement toolbar “polygon selections” icon was used to outline and measure the area of the

## MATERIALS AND METHODS

thoracic aorta and abdominal aorta. The aorta was separated into the thoracic and abdominal aorta at the level of the diaphragm<sup>143</sup>. The Sudan IV positive lesion areas on each part were outlined and traced with “polygon selections”. Then the selected lesions were checked through the microscope. The selections were saved to the ‘ROI Manager’. The data were exported using the ‘measure’ in the ROI Manager.

The percentage of the area of the lesions in the aorta area was calculated, respectively. The sum of the thoracic aorta area and abdominal aorta area together is total aorta area. And the percentage of lesions in the total aorta was calculated with the total lesion area and the total aorta area.

### **2.2.6. Histological staining**

Frozen aortic root cryosections (10 µm) were warmed on a hot plate maintained at 37° C for 1 min, followed by air-dry for 30 min at room temperature. Every 10th serial section at 100 µm intervals was stained with Oil Red O/hematoxylin (OR/H) or with hematoxylin/eosin (H/E) staining. For OR/H staining, sections were stained with Oil Red O working solution (1: 0.66 dilutions in distilled water) for 10 min, briefly rinsed in 60% isopropanol, and stained with hematoxylin for 6 min. Then sections were thoroughly washed in tap water (pH>7) for 10 min and mounted with an aqueous Faramount Mounting Medium. For H/E staining, sections were fixed in 4% PFA for 10 min, rehydrated in PBS for 10 min, and stained with hematoxylin for 6 min, then thoroughly washed in tap water (pH>7) for 10 min. Afterward, the sections were stained with eosin working solution for 10 minutes and then washed with absolute ethanol for 30 seconds, and then air-dried and mounted in Roti-Histokit II.

Images were taken with a microscope (Leica DM6000B, Leica Microsystems) connected to a camera (Leica DFC295, Leica Microsystems). All pictures of sections were taken with 10x objective and 10x ocular lens. All sections were evaluated with Leica LAS V4.6 software (Leica, Germany) and ImageJ (NIH, USA).

### **2.2.7. Immunofluorescence staining**

Immunofluorescence staining was performed for CD68<sup>+</sup> macrophage/DC, CD3e<sup>+</sup> T cells, alpha-

## MATERIALS AND METHODS

smooth muscle actin (SMA)<sup>+</sup> SMC. 10  $\mu$ m fresh frozen tissue sections were prepared by microtome and stored at -80 °C. The frozen sections were thawed on the hotplate at 37°C for 1 minute and air dry for 30 minutes. Sections were fixed with 4% PFA for 10 minutes. Sections were rehydrated in PBS at RT for 10 min and incubated in blocking buffer (PBS containing 5% serum) for 1 hour. After blocking, sections were incubated for 2 hours or overnight with primary antibodies or cocktail of primary antibodies for neuronal and immune cell markers, as shown in Table 2.4 and 2.5, diluted at the appropriate dilution in PBS with 0.25% BSA at room temperature. For intranuclear and intracellular staining, depending on the requirements of different primary antibodies, sections were 1) incubated with 2% PFA solution for 5 minutes at room temperature, then rinsing with PBS. Before and after the fixation in 100% acetone for 2 min at 4°C, sections were submerged in 50% acetone; 2) fixed with acetone for 5 minutes, then air-dried for 30 min; or 3) fixed with 1% PFA for 10 min, permeabilized with 0.05% Triton X-100 in 1% BSA-PBS for 30 min, and incubated with primary antibody for 2 hours or overnight diluted with 0.25% BSA and 0.05% Triton X-100. After three 5-mins washes in PBS, sections were incubated 1 hour with fluorescent-labeled secondary antibodies (indicated in table 2.6) diluted with 0.25% BSA and 4',6-diamidino-2-phenylindole (DAPI) nuclear stain (1:1000 or 500 dilutions). Secondary antibodies were conjugated with Cy3, Cy5, and Alexa 488. Following three 5-mins washes, specimens were mounted in Fluoromount-G mounting media. For negative controls, primary antibodies were omitted, whereas the rest of the procedure was done exactly as described. No immunostaining was observed in negative controls. In the case of high background staining, 0.05% Triton X-100 was added with PBS for final washing to reduce the unspecific background of the specimen. Single immunostaining procedure was routinely used before double or triple immunostaining.

### 2.2.8. Fluorescence microscopy

Stained tissue sections were analyzed using a laser microscope DM 6000 B (Leica, Germany). Fluorophores were visualized by using a 488-nm excitation filter and 505/530-nm emission filter for Alexa 488, a 568-nm excitation and 575/615-nm emission filter for Cy3 and 633-nm excitation, and 650-nm emission long-pass filter for Cy5. Single 1024  $\times$  1024-pixel images or 512  $\times$  512-pixel images were captured. Images from WT and *ApoE*<sup>-/-</sup> tissue sections were acquired under identical microscope

settings using the sequential acquisition of different channels to avoid overlap between fluorophores.

### **2.2.9. Confocal microscopy**

Confocal images were acquired using a Leica TCS SP8 (Leica Microsystems, Germany) equipped with a UV laser, a white light laser, hybrid detectors, and a 20X multi-immersion objective. Each dye was excited and acquired sequentially as follows: DAPI: excitation 405nm, detection 420-470nm; FITC/Alexa Fluor 488: excitation 490nm, detection 500-550nm; Cy3: excitation 591nm, detection 600-640nm; Cy5: excitation 652nm, detection 670-720nm. Single 1024×1024-pixel images were captured. Images from WT and *ApoE*<sup>-/-</sup> tissue sections were acquired. For co-localization analysis, non-overlapping fluorophores such as Alexa 488 and Cy5 were used to avoid cross-talk and/or bleeding through. Raw images were analyzed with the Leica Application Suite X (v.3.1 Leica Microsystems, Germany).

### **2.2.10. Image analysis and processing**

ImageJ (NIH, USA) was routinely used for image processing. Only brightness and contrast were adjusted for the whole frame, and no part of a frame was enhanced or modified in any way. All images were saved as TIF files and exported to adobe illustrator CS6 (Adobe software) for figure arrangement.

### **2.2.11. Morphometry**

#### **2.2.11.1. Morphometry of TH<sup>+</sup> axon density in adventitia**

10 μm thick frozen sections were prepared. From each mouse, we obtained approximately 80 sections per aortic root, and approximately 700 sections per abdominal aorta, of which 8 - 10 serial sections were used of adventitia innervations studies. Serial tissue sections were stained with NFM and TH antibodies, and confocal images were acquired using a 20X objective of Leica TCS SP8 (Leica, Germany). 3-5 images per section were acquired, and the TH<sup>+</sup> axons of at least 5 μm length in the

## MATERIALS AND METHODS

aorta adventitia were manually counted. The adventitia axon density was determined as the number of NFM<sup>+</sup>TH<sup>+</sup> axons per mm<sup>2</sup> adventitia area.

### **2.2.11.2. Morphometry of TH<sup>+</sup> axons in spleen**

For quantification of TH<sup>+</sup> sympathetic axons in the spleen, 10 µm thick cryosections were prepared from the middle half of the spleen. 6 serial sections at every 500 µm interval were stained with NFM and TH antibodies, and confocal images were acquired with 20X objective as described above. 6-8 images per section were acquired, and the axon area was determined. Briefly, the scale was set for each image. The border of the region of interest was depicted with the “Polygon selections” tool and recorded. The “Threshold” tool was applied. The areas of NFM<sup>+</sup>TH<sup>+</sup> double-positive signals in the region of interest were recorded and measured in Excel.

### **2.2.11.3. Morphometry of plaque, and ATLO size**

To quantify plaque and ATLO sizes, every 10<sup>th</sup> serial sections were stained with Oil Red O/Hematoxylin (OR/H) staining. The OR/H images were opened with the software Image J, and the scale was set for each image. The borders of the lumen, internal elastic layer, external elastic layer, and adventitia were all depicted with the “Polygon selections” tool and saved to the “ROI Manager”. Then the data were exported using the “measure” in the ROI Manager. The difference between the areas covered by the internal elastic lamina and lumen was considered as intima area, while the difference between the areas of the external elastic lamina and internal elastic lamina was considered as media area, and the difference between the areas occupied by the adventitia and external elastic lamina was considered as adventitia area. Plaque size was determined by the ratio of intima area : media area, whereas ATLO size was determined by the ratio of adventitia area : media area. In addition, every 10<sup>th</sup> serial sections in the entire abdominal aorta were examined for counting the number of ATLOs.

#### 2.2.11.4. Quantification of necrotic core and fibrous cap thickness in plaque areas

Serial frozen aortic tissue sections (10  $\mu\text{m}$  thick) at 100  $\mu\text{m}$  intervals were stained with H/E staining for quantification of necrotic core area and fibrous cap thickness.

Stained sections were examined using an epi-fluorescence microscope DM6000B (Leica, Germany) with a bright field filter. All pictures of sections were taken with a 10x objective. To quantify the image with H/E staining, the scale was set for each image. Necrotic core areas and fibrous cap thickness in plaques were quantified in 5-8 sections per mouse in 3-5 mice per group using Image J (NIH, USA). The borders of the region of interest, i.e., atherosclerotic plaques and the acellular empty necrotic core areas, were depicted with the “Polygon selections” tool respectively and recorded. The necrotic core area was normalized to plaque area percentage. Fibrous cap thickness was averaged from 3-5 measurements in each plaque.

#### 2.2.11.5. Quantification of immune cell density in plaque and ATLO

Serial frozen aortic tissue sections (10  $\mu\text{m}$  thick) at 100  $\mu\text{m}$  intervals were stained for macrophages (CD68), SMCs (SMA), T cells (CD3e), and T<sub>reg</sub> cells (CD3e/Foxp3) with the immunofluorescence staining method above. Stained sections were examined using a confocal laser scanning microscope TCS SP8 (Leica, Germany) with appropriate excitation and emission filters. All pictures were taken with a 20X objective. Identical staining protocols, including the equal concentration of the same primary and secondary antibody and identical microscope settings (channel settings, channel, intensity, and resolution), were applied for both the control and treated tissue sections.

The CD68<sup>+</sup> macrophage, SMA<sup>+</sup> SMC, and CD3e<sup>+</sup> T cell infiltration in the plaque areas were quantified with CD68, SMA, and CD3e antibody stained pictures, whereas Foxp3<sup>+</sup>CD3e<sup>+</sup> T<sub>reg</sub> cells in ATLOs were quantified with Foxp3 and CD3e antibody stained pictures using the software ImageJ. The images were opened with the software Image J. The image scale was set with the standard bar on the images. After the calibration for the image, the intimal layer was encircled using the “polygon selections” tool. The intimal layer was defined by the internal elastic lamina and the lumen. The intima area was saved to the “ROI Manager”. Then the immunofluorescence pictures of CD68 were segmented by thresholding to create binary images<sup>144</sup>. The “area fraction” of CD68<sup>+</sup> macrophage in

## MATERIALS AND METHODS

plaque area and the plaque area can be exported with the “measure” tool in the “ROI Manager”. Macrophage density was normalized to stained area percentage in abdominal adventitia per mouse. SMA<sup>+</sup> SMC area in plaque was quantified in a similar way as macrophage area. In order to count the CD3e<sup>+</sup> T cell numbers in the plaque area, the CD3e antibody and DAPI stained images were merged, and CD3e and DAPI double-positive cells were counted as the CD3e<sup>+</sup> T cells.

For adventitia or ATLO T<sub>reg</sub> cell density, 5-8 parallel sections of the same location i.e., abdominal aorta below the renal artery were used. To count the CD3e<sup>+</sup> Foxp3<sup>+</sup> T<sub>reg</sub> cell numbers in the ATLO area, the CD3e/Foxp3 antibodies and DAPI stained images were merged, and CD3e, Foxp3 and DAPI triple-positive cells were counted as the T<sub>reg</sub> cells. The numbers of T<sub>reg</sub> cells were quantified among total T cells in each field of view (FOV) with 2-3 FOVs per ATLO section.

### **2.2.11.6. Quantification of TH<sup>+</sup> sympathetic neurons in the locus coeruleus in brain**

The serial brain cryosections (20 μm thick) with cerebellum from the posterior parts of the brain at 100 μm intervals were stained with TH and NeuN antisera with the immunofluorescence staining method above. Stained sections were examined using a confocal laser scanning microscope TCS SP8 (Leica, Germany) with appropriate excitation and emission filters, and with a 20X objective.

The locus coeruleus (LC) area below the 4<sup>th</sup> ventricle was defined using Allen mouse brain ATLAS (<https://mouse.brain-map.org/>). The TH<sup>+</sup> sympathetic neurons and NeuN<sup>+</sup> neuronal nuclei in the LC areas were quantified using the software ImageJ. Briefly, the images were opened with the software Image J. The image scale was set with the standard bar on the images. After the calibration for the image, the LC area was encircled using the “polygon selections” tool. The TH<sup>+</sup>NeuN<sup>+</sup> and NeuN<sup>+</sup> neurons were manually counted using the ‘analyze particle’ parameter. The percentage of TH/NeuN double-positive neurons among NeuN positive neurons were analyzed.

### **2.2.12. Picro-Sirius red staining for collagen area in plaque**

Picro-Sirius Red staining was used for histological analysis of collagen. The protocol was a gift from Anders & Vielhauer Research Laboratory, Munich<sup>141</sup>.

## MATERIALS AND METHODS

Cryo-sections were thawed on the hotplate at 37° C for 1 minute and air-dried for 30 minutes. 4% PFA was used to fix the air-dried sections for 5 minutes. Slides were immersed in PBS for 5 minutes and thereafter in Sirius-red solution for 1 hour. The slides were washed twice with acidified water. The water was removed, followed by three times washing with 100% Ethanol. The slides were cleared by two times washing with Xylene.

To quantify the image with Sirius Red staining, the scale was set for each image. The borders of atherosclerotic plaques were firstly depicted. The “Threshold” tool was applied, and the percentages of Sirius Red stained area in plaques were measured and recorded.

### 2.2.13. Plaque vulnerability index

To analyze the stability of the plaque, the Plaque Vulnerability Index (PVI) was calculated using the formula below<sup>15</sup>.

$$PVI = \frac{(NC \text{ area}\% + CD68 \text{ area}\%)}{(SMC \text{ area}\% + collagen \text{ area}\%)}$$

### 2.2.14. Flow cytometry

Flow cytometry (FACS) experiments were performed using the established protocols for sample preparations and measurements from our lab.

#### 2.2.14.1. Preparation of single leukocyte suspensions from blood

Blood was drawn by heart puncture using a 1 ml syringe with a 23-gauge needle and immediately mixed with 5 ml 5 mM EDTA-PBS buffer in a 15 ml Falcon tube. The blood was then centrifuged, and the red pellet was resuspended and lysed in 5 ml Ammonium-Chloride-Potassium lysis buffer for 5 min at RT. An additional 5 ml FACS buffer was added, and centrifugation was carried out. The lysis step was repeated if the pellet still contained red blood cells. The final pellet was resuspended in 2 ml of ice-cold FACS buffer and counted for cell number.

### **2.2.14.2. Preparation of single-cell suspensions from spleen and LNs**

Mouse spleen was cut into small pieces, and the lymph nodes were cut into half. The tissues were transferred to a 70  $\mu\text{m}$  cell strainer placed on a falcon tube. The cell suspension was collected in a tube by softly mashing the tissue with a syringe-piston and by intermittently adding FACS buffer. A total volume of the cell suspension was made-up to give 5 ml. The cell suspension was centrifuged, and the supernatant was carefully discarded. The pellet was re-suspended in 5 ml Ammonium-Chloride-Potassium lysis buffer and incubated for 5 minutes at RT to lyse red blood cells. This red blood cell lysis step is not necessary when working with mouse LNs. An additional 5 ml FACS buffer was added, and centrifugation was carried out at  $400 \times g$  for 5 min at  $4^\circ\text{C}$ . The pellet was resuspended in 5 ml of ice-cold FACS buffer (the volume of FACS buffer may change depending on the size of the pellet), and a single cell suspension was obtained by filtering again through a 70  $\mu\text{m}$  cell strainer. The concentrations of the cell suspensions were counted as indicated above.

### **2.2.14.3. Preparation of single-cell suspensions from bone marrows**

The mouse femurs were dissociated from the muscles and cleaned. The distal metaphysis was removed, and the femur was placed into the 1.5 ml Eppendorf tube with the cut end facing down. Bone marrow was flushed via centrifugation at 5000 rpm for 5 min at  $4^\circ\text{C}$ . The bone marrow sample in the tube was resuspended in 1ml ice-cold FACS buffer.

### **2.2.14.4. Extracellular staining for FACS**

One to three million cells were aliquoted in 96-well v-bottom plate or 1.5 ml Eppendorf tube and centrifuged. The pellet was resuspended with 50  $\mu\text{l}$  diluted antibody cocktail (up to 8 colors) in FACS buffer and incubated for 30 minutes at  $4^\circ\text{C}$  except for progenitor antibody cocktail where bone marrow cells were incubated for 60 minutes at  $4^\circ\text{C}$ . After incubation, cells were centrifuged and washed twice with FACS buffer. For biotin-labeled antibodies, the cell sample was incubated with 50

## MATERIALS AND METHODS

$\mu$ l diluted streptavidin-conjugated antibody for 20 minutes at 4°C. The sample was centrifuged and washed twice. Then it was measured on the same day or stained for intracellular protein.

Single cells from blood, spleen, and lymph nodes were stained with antibodies against CD45, CD11b, CD11c, TCRb, CD4, CD8, B220, Foxp3. Leukocyte populations were defined as follows: B cells (CD45<sup>+</sup>TCRb<sup>-</sup>B220<sup>+</sup>), CD4 T cells (CD45<sup>+</sup>TCRb<sup>+</sup>B220<sup>-</sup>CD8<sup>-</sup>CD4<sup>+</sup>), Foxp3 T<sub>reg</sub> cells (CD45<sup>+</sup>TCRb<sup>+</sup>B220<sup>-</sup>CD8<sup>-</sup>CD4<sup>+</sup>Foxp3<sup>+</sup>), CD8 T cells (CD45<sup>+</sup>TCRb<sup>+</sup>B220<sup>-</sup>CD8<sup>+</sup>CD4<sup>-</sup>), CD11b<sup>+</sup> monocytes/macrophages/neutrophils (CD45<sup>+</sup>TCRb<sup>-</sup>B220<sup>-</sup>CD11b<sup>+</sup>CD11c<sup>-</sup>), DCs (CD45<sup>+</sup>TCRb<sup>-</sup>B220<sup>-</sup>CD11b<sup>+</sup>CD11c<sup>+</sup>).

Cells from bone marrow were stained with antibodies against TER-119, Gr1, B220, CD3, CD11b, CD150, CD34, CD48, CD16/32, c-kit, Sca1. Hematopoietic cell populations were defined as follows: LSK as Lin<sup>-</sup>c-Kit<sup>+</sup>Sca-1<sup>+</sup> gate, myeloid progenitor cells (MPC) as Lin<sup>-</sup>c-kit<sup>+</sup>sca-1<sup>-</sup> gate, hematopoietic stem cells (HSC) as Lin<sup>-</sup>c-kit<sup>+</sup>Sca-1<sup>+</sup>CD48<sup>-</sup>CD150<sup>+</sup> gate, common lymphoid progenitors (CLP) as Lin<sup>-</sup>c-kit<sup>+</sup>Sca-1<sup>+</sup>CD127<sup>+</sup> gate, common myeloid progenitor (CMP) as Lin<sup>-</sup>c-kit<sup>+</sup>sca-1<sup>-</sup>CD34<sup>+</sup>CD16/32<sup>-</sup> gate, granulocyte-monocyte progenitor cells (GMP) as Lin<sup>-</sup>c-kit<sup>+</sup>Sca-1<sup>-</sup>CD34<sup>+</sup>CD16/32<sup>+</sup> gate.

### 2.2.14.5. Intracellular staining for FACS

After surface staining as described above, the cell sample was fixed and permeabilized according to the manufacturer's instruction with minor changes. The cell pellet was incubated with 200  $\mu$ l of freshly prepared fixation/permeabilization working solution (1part fixation/permeabilization concentrate buffer was mixed with 3 parts fixation/ permeabilization dilute buffer) for 50 minutes at 4°C. Then the sample was centrifuged and washed with 300  $\mu$ l of 1  $\times$  permeabilization buffer (which was prepared from 10  $\times$  permeabilization buffer dilution by sterile water). After centrifugation, the sample was re-suspended with 100  $\mu$ l 1  $\times$  permeabilization buffer and kept at 4°C for 20 minutes. Without washing, 0.4  $\mu$ l PE anti-mouse Foxp3 antibody or 2  $\mu$ l APC anti-mouse. Then the sample was centrifuged and washed twice with 300  $\mu$ l 1 $\times$  permeabilization buffer. Single cells from blood, spleen, and lymph nodes were stained with antibodies against CD45, CD11b, CD11c, TCRb, CD4, CD8, B220, and Foxp3. After the staining, the pellet was re-suspended with 200  $\mu$ l FACS buffer and

was used for FACS analysis.

#### **2.2.14.6. Analysis of cells by flow cytometry**

Flow cytometry measurements were performed using the BD FACS Canto-II. Data were analyzed using the FACS Diva v6.1 software (BD) or FlowJo software (Tree Star). The monoclonal antibodies used for flow cytometric analysis were purchased from eBiosciences and BD Biosciences (see Table 8). The fluorescence labels on the antibodies are light-sensitive. Therefore, staining was performed in the dark. Unless otherwise indicated, all centrifugations were performed at 1500 rpm for 5 minutes at 4°C.

#### **2.2.15. Flow cytometry derived t-SNE reduction maps of total leukocytes**

The t-Distributed Stochastic Neighbor Embedding (t-SNE) is a state-of-the-art dimensionality reduction algorithm for non-linear data representation that allows visualization of multi-dimensional flow cytometry data in fewer dimensions or a low dimensional distribution (map) while still maintaining the structure of the data. Living cells (singlets) were manually gated from multicolor flow cytometry data and were exported in an FCS file. The t-SNE dimensionality reduction mapping was performed on total CD45<sup>+</sup> leukocytes of spleen and lymph nodes using FlowJo (version 10)<sup>145,146</sup>.

5000 flow cytometry events from the total leukocytes were used for the t-SNE analysis. We used auto t-SNE (opt-SNE) using the following parameters: Iterations: 1200; Perplexity: 20; learning rate: 200; and KNN algorithm with Barnes-Hut approximations, and visualized different populations using t-SNE map.

#### **2.2.16. Enzyme-linked immunosorbent assay (ELISA)**

In order to obtain the NE levels in mouse serum, approximately 200 µl of mouse blood was collected into tubes and centrifuged at 10,000 rpm for 15 min. The serum samples were then collected and

## MATERIALS AND METHODS

frozen in 20  $\mu$ l aliquots in liquid nitrogen and stored at  $-80^{\circ}\text{C}$  until further use for the measurement of NE levels with ELISA as described below. In order to determine tissue NE levels, small pieces of spleen, aortic tissues were snap-frozen in liquid nitrogen and stored at  $-80^{\circ}\text{C}$  until further use. Spleen samples were homogenized in 200  $\mu$ l of the catecholamine-stabilizing solution, which contained 0.01 N HCl, 1 mM EDTA, 4 mM  $\text{Na}_2\text{S}_2\text{O}_5$ , and pH was adjusted to 7.5<sup>88</sup>. The iliac/aortic arch samples were homogenized in 50  $\mu$ l of catecholamine-stabilizing solution. The homogenized samples were centrifuged at 5000 rpm for 5 min at RT. The supernatants were collected, and the protein concentrations were measured with the “Protein 280” feature of NanoDrop (ThermoFisher).

The serum and the homogenized tissue samples were prepared for NE ELISA following the instructions provided in the manual of the ELISA kit (NE-5200, Labor Diagnostika Nord GmbH & Co.KG). All the samples were put into the 48-well extraction plate by using a cis-diol-specific affinity gel (provided in the ELISA kit) and washed several times to remove unspecific proteins or tissue fragments. The target proteins were dissolved into hydrochloric acid and transferred to 96-wells plate (both are provided in the ELISA kit) for acylation and enzymatic processing. Finally, the samples were transferred into an antigen-coated 96-well plate and kept with the anti-serum (both are provided in the ELISA kit) overnight at  $4^{\circ}\text{C}$ ; absorbance was measured using a multi-well plate reader (SpectraFluor Plus, Tecan) at 450 nm. NE concentrations of serum samples were reported as ng/ml, whereas NE levels of tissue samples were normalized to total tissue protein concentration (ng/mg)<sup>88,111</sup>, or reported as ng/ml.

### 2.2.17. Laser capture microdissection (LCM) and microarray analyses

Aorta tissue mRNA microarray analyses were performed using Affymetrix mouse whole-genome 430 A 2.0 microarrays, as previously reported<sup>45,147</sup>. Total aortas of 3 WT and 3 *ApoE*<sup>-/-</sup> mice each at 6, 32, and 78 weeks and LCM-derived arterial wall compartments at 78 weeks were extracted. Briefly, RNA was extracted from different tissues and purified using the RNeasy Micro kit (QIAGEN). cDNA and cRNA were synthesized, amplified, and purified as previously described<sup>147</sup>. The raw transcriptome data (CEL files) were mined for sympathetic nervous system-associated genes, which represents my contribution (not previously published). Signal intensities were calculated from the raw data and scaled to an array trimmed mean of 200. All further steps were performed using R and

## MATERIALS AND METHODS

Bioconductor<sup>148</sup>. Logarithmized signals were normalized across arrays of every analysis using quantile normalization<sup>149</sup>, and data were filtered before statistical analysis to remove genes with low expression or without variability between 2 groups. Probe sets were included if, in one group, a minimum of 2 arrays was called the present (detection  $P \leq 0.05$ ), and 2 or 3 arrays showed a log signal  $\geq \log_2(200)$ . Recorded genes were required to be up-regulated with a fold change of at least  $\log_2(2.0)$  between groups. The  $\log_2$  value of genes expression (normal distribution) was used for the quantification of highly expressed genes. To correct media effects in LCM experiments (error caused by nearby media tissue) on adventitia measurements, i.e., WT abdominal adventitia, *ApoE*<sup>-/-</sup> adventitia without plaque, or ATLO, a correction procedure was performed as previously described ( $RME \leq 0.666$ )<sup>147</sup>. After applying filters, the resulting list was subjected to a one-way analysis of variance (ANOVA) with Benjamini and Hochberg correction for multiple testing between several WT and *ApoE*<sup>-/-</sup> groups<sup>45</sup> or a Student's t-test ( $P \leq 0.05$ ) for comparing two WT and/or *ApoE*<sup>-/-</sup> groups<sup>147</sup>. The resulting total lists of differentially expressed probe sets ( $P \leq 0.05$ ) were used as the basis for derived lists of GO terms.

### 2.2.18. Statistical analyses

All measurements were expressed as means of N samples  $\pm$  SEM. Data were analyzed with two-sided unpaired Student's t-test to compare two groups and/or one-way analysis of variance (ANOVA) to compare multiple groups by GraphPad Prism 8 (GraphPad Software, San Diego). We used Welch's correction for the two-sided Student's t-test and Bonferroni's post-hoc correction for ANOVA. Values of  $P < 0.05$  were considered to be statistically significant.

### 3 RESULTS

#### 3.1. NE concentrations increased during aging and atherosclerosis

Norepinephrine (NE) is the key sympathetic neurotransmitter in peripheral tissues. Plasma NE concentrations were shown to increase during aging in normotensive rats and humans<sup>150,151</sup>. Moreover, the splenic NE concentration was known to be increased in angiotensin II-treated hypertensive mice<sup>68</sup>. While no literature data regarding the changes of tissue NE during aging were found, it has been reported that bone marrow NE concentrations in WT mice increased after stroke<sup>87</sup> or other types of stress<sup>86</sup>. Moreover, NE concentrations in the aortic arch of *ApoE*<sup>-/-</sup> mice were shown to be increased after MI<sup>88</sup>. However, the alteration of tissue NE concentration during aging is unknown.

To examine the effect of aging on NE levels in our model, NE levels in the blood of 9 weeks old young, 30 weeks old adult, and 78 weeks old aged mice, respectively, were determined first. Serum NE concentrations in adult mice were similar to that of young mice, whereas serum NE levels in aged mice were significantly higher than in adult or young mice (Fig.6.A). These data on increased serum NE concentrations in mice were consistent with published data in rats and humans. To examine changes in tissue NE levels, including SLOs during aging, we next measured NE concentrations in the spleen of young, adult, and aged *ApoE*<sup>-/-</sup> mice. Interestingly, adult spleen NE concentration was significantly higher vs. young spleen but lower than aged spleen, indicating an increase in spleen NE levels across their lifespan (Fig.6.B). To determine the effect of atherosclerosis on tissue NE level, we measured NE concentrations in aged WT abdominal aorta, *ApoE*<sup>-/-</sup> abdominal aorta without or with plaque. NE concentrations in *ApoE*<sup>-/-</sup> abdominal aorta without plaque were similar to those in WT abdominal aorta. However, NE levels were markedly increased in abdominal aorta with plaques vs. *ApoE*<sup>-/-</sup> abdominal aorta without plaque or WT abdominal aorta (Fig.6.C). Our data indicated that the NE concentrations increased during aging in both genotypes and that atherosclerosis was associated with enhanced aortic NE concentrations in a highly territorialized way.

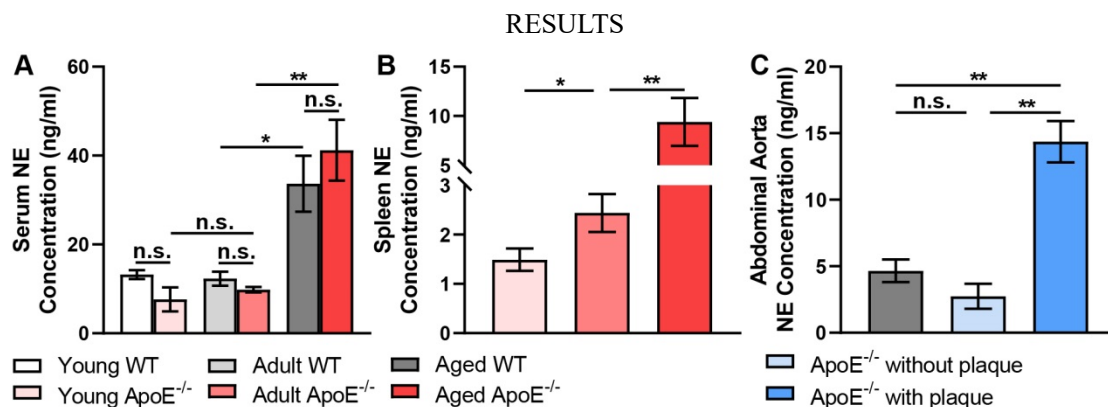


**Figure 6. NE concentrations increase during aging in *ApoE*<sup>-/-</sup> mice.** **A)** Serum NE levels in young, adult, and aged WT and *ApoE*<sup>-/-</sup> mice. Young mice were 9 weeks old, adult mice were 30 weeks old, and aged mice were 78 weeks old. N = 3 young, 27 adult and 7 aged *ApoE*<sup>-/-</sup> mice; 4 young, 4 adult, and 8 aged WT mice. **B)** Spleen NE levels in young, adult, and aged *ApoE*<sup>-/-</sup> mice. N = 10 young, 19 adult and 17 aged *ApoE*<sup>-/-</sup> mice. **C)** Tissue NE in the abdominal aorta of aged WT and *ApoE*<sup>-/-</sup> mice. NE concentrations of the lower segment of the abdominal aorta (A2) in aged WT mice, A2 segment without plaque or with plaques in aged *ApoE*<sup>-/-</sup> mice. N = 8 young, 5 adult and 4 aged *ApoE*<sup>-/-</sup> mice. Data represent means  $\pm$  SEM; two-tailed unpaired Student's t-test, \*:  $p < 0.05$ ; \*\*:  $p < 0.01$ ; n.s.: not significant.

### 3.2. TH<sup>+</sup> sympathetic axon density in the arterial adventitia of *ApoE*<sup>-/-</sup> mice

Unpublished data of our group showed that NF200<sup>+</sup> axons, including TH<sup>+</sup> sympathetic axons, innervate both the WT and *ApoE*<sup>-/-</sup> aorta adventitia (Mohanta S. K., PhD thesis, 2014; Mohanta S. K. et al. 2020, under review). Quantification of these axons demonstrated that the NF200<sup>+</sup> axon density in abdominal aorta with plaque was significantly higher than in the abdominal aorta without plaque or WT abdominal aorta. Moreover, NF200<sup>+</sup> axon density was further increased in ATLOs vs. other aorta segments (Mohanta S. K. et al. 2020, under review). These data indicated that the NS was directly affected by atherosclerosis in a highly territorialized fashion. The presence of NFM<sup>+</sup>TH<sup>+</sup> sympathetic axons in the adventitia, together with aortic NE data, raised the possibility that the increased NE levels in the diseased aorta might be due to enhanced TH (tyrosine hydroxylase, key enzyme for NE synthesis)<sup>+</sup> sympathetic axons in the atherosclerotic aorta adventitia. To confirm this hypothesis, we quantified TH<sup>+</sup> axon density in the aortic root and abdominal aorta of adult and aged WT and *ApoE*<sup>-/-</sup> mice, respectively. It is important to note that we never observed NF200-stained axons penetrate the external lamina in WT or *ApoE*<sup>-/-</sup> mice at any age.

## RESULTS

### 3.2.1 TH<sup>+</sup>NFM<sup>+</sup> sympathetic axon density increased in adult aortic roots

To determine the effect of early atherosclerosis in adventitia sympathetic innervation, we examined aortic roots of 32 weeks old adult WT or *ApoE*<sup>-/-</sup> mice. TH/NFM double-positive axons (arrow) were detected in the adventitia, but not in the media (dotted line) nor in plaque (Fig.7. A). Few TH<sup>+</sup> axons were detected in the adventitia-media border in both genotypes. Comparatively more TH/NFM double-positive axons (arrow) were detected in the adventitia adjacent to atherosclerotic plaques in adult *ApoE*<sup>-/-</sup> mice vs. the WT adventitia (Fig.7. A). Quantification TH/NFM double-positive axons per adventitia area in aortic root sections (every 10<sup>th</sup> section) demonstrated that the TH<sup>+</sup>NFM<sup>+</sup> sympathetic axon density in the adventitia of adult *ApoE*<sup>-/-</sup> mice was ~2.5 fold vs. WT mice (Fig.7. B).

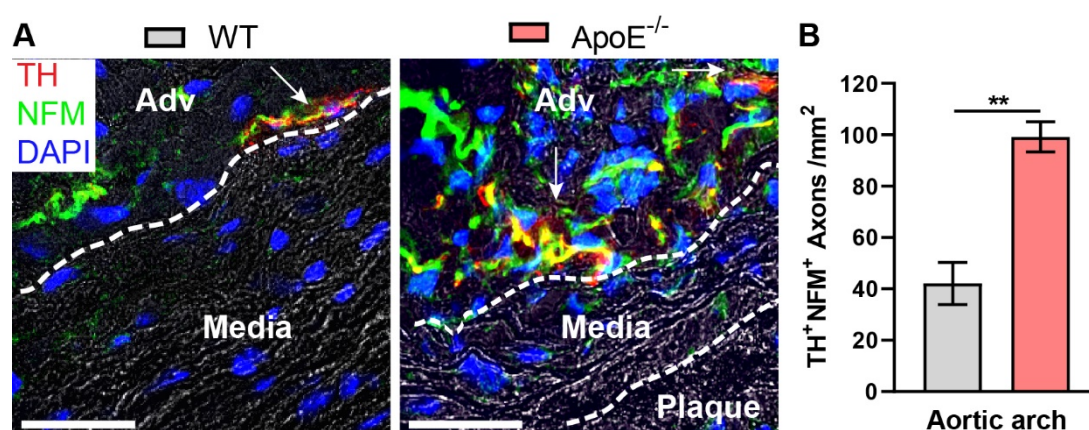


**Figure 7. Sympathetic axon density increased in adult *ApoE*<sup>-/-</sup> mice.** A) Representative images of the immunofluorescence stained aortic root in adult WT and *ApoE*<sup>-/-</sup> mice. TH was stained red; NFM was stained green; DNA was stained blue. The area between dotted lines designates the media layer. Arrows indicate TH<sup>+</sup>NFM<sup>+</sup> axons. Scale bar: 50  $\mu$ m. B) Quantification of TH<sup>+</sup>NFM<sup>+</sup> axons in aortic root sections. N = 3 adult WT and 3 adult *ApoE*<sup>-/-</sup> mice. Data represent means  $\pm$  SEM; two-tailed unpaired Student's t-test, \*\*: p < 0.01.

### 3.2.2 TH<sup>+</sup>NFM<sup>+</sup> sympathetic axon density increased in the aged aorta

To determine how advanced atherosclerosis affected adventitia sympathetic innervation, we examined the abdominal aorta of 78 weeks old aged WT or *ApoE*<sup>-/-</sup> mice. TH/NFM double-positive

## RESULTS

axons (arrow) were detected in the adventitia/ATLO, but not in the media (dotted line) nor in the plaque (Fig.8. A). Few TH<sup>+</sup> sympathetic axons were detected in the adventitia-media border in both genotypes. Comparatively more TH/NFM double-positive axons (arrow) were detected in the adventitia adjacent to atherosclerotic plaque in aged *ApoE*<sup>-/-</sup> mice vs. WT adventitia (Fig.8. A). Quantification of TH/NFM double-positive axons in WT abdominal aorta sections (every 10<sup>th</sup> section) and in *ApoE*<sup>-/-</sup> abdominal aorta sections with ATLOs (every 10<sup>th</sup> section) demonstrated that the TH<sup>+</sup>NFM<sup>+</sup> sympathetic axon density in the adventitia of aged *ApoE*<sup>-/-</sup> mice was 2 fold higher vs. WT mice (Fig.8. B).

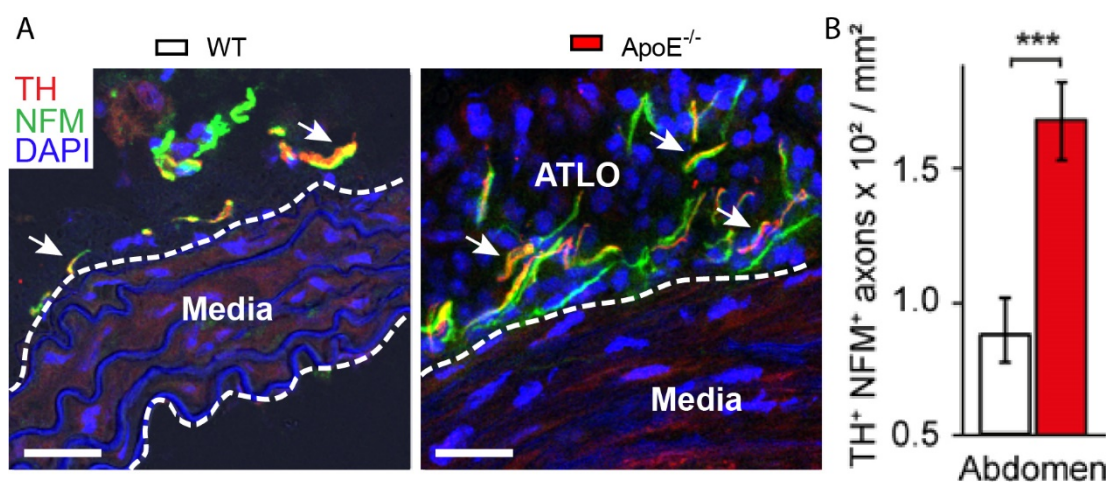


**Figure 8. Sympathetic axon density increased in aged *ApoE*<sup>-/-</sup> mice.** A) Representative images of the immunofluorescence stained abdominal aorta adventitia in aged WT and *ApoE*<sup>-/-</sup> mice. TH was stained red; NFM was stained green; DNA was stained blue. The dotted line indicates media. Arrows indicate TH<sup>+</sup>NFM<sup>+</sup> axons. Scale bar: 50µm. B) Quantification of TH<sup>+</sup>NFM<sup>+</sup> axons in WT abdominal aorta vs. ATLO. N = 5 aged WT and 4 aged *ApoE*<sup>-/-</sup> mice. Data represent means ± SEM; two-tailed unpaired Student's t-test, \*\*\*: p<0.005.

### 3.3 Laser capture microdissection arrays revealed the presence of SNS constituents in atherosclerotic adventitia

Our data demonstrated i) that NE levels in serum and spleen increased during aging and that NE concentrations increased in aorta segments afflicted with atherosclerosis; ii) that sympathetic axons innervated the aorta adventitia and ATLOs; iii) that the sympathetic innervations specifically

## RESULTS

increased in ATLOs *vs.* WT adventitia. Moreover, unpublished data from our lab provide evidence that ATLO immune cells directly interacted with innervating nerve fibers that were associated with disease severity (Mohanta S. K. *et al.* 2020, *under review*). Similar to SLOs, immune cells in ATLOs could express neurotransmitter-receptors and produce neurotransmitters. Recent data supported the hypothesis that ATLOs in atherosclerosis secreted numerous neuronal cues that were responsible for axon growth, guidance, and survival, including Semaphorin (Sema) 3A, Sema4D, and Plexin (Plxn) B2<sup>27,45,152</sup>. Interestingly, Sema3E and Sema4D were known to play roles in the regulation of infiltration and migration of macrophages in atherosclerotic plaques<sup>153,154</sup>. Our own data on ATLOs and the results of others on neuroimmune crosstalk raised important questions: i) how does atherosclerosis influence adventitia sympathetic innervations, and ii) does ATLO neogenesis promote SNS growth, development, and guidance and/or *vice versa*?

To answer these questions, we used our whole mouse genome mRNA expression arrays data bank<sup>45</sup>, to examine differential nervous system gene expression in the whole aorta, RNA extracts of WT and *ApoE*<sup>-/-</sup> mice as well as in abdominal aorta adventitia by laser capture microdissection (LCM)-based approach. To examine the effect of aging on SNS development, whole aortae RNA extracts of WT mice and *ApoE*<sup>-/-</sup> mice at 6 weeks, 32 weeks, and 78 weeks of ages were analyzed. Multiple differentially expressed genes of interest were examined by using gene ontology (GO) terms according to the National Center for Biotechnology Information (<http://www.ncbi.nlm.nih.gov/>) and the gene ontology data banks (<http://www.geneontology.org/>) such as nervous system development (GO: 0007399; 373 genes), autonomic nervous system development (GO: 0048483; 22 genes), sympathetic nervous system development (GO: 0048485; 10 genes), axon (GO: 0030424; 196 genes), regulation of axon guidance (GO: 1902667; 20 genes) in WT and *ApoE*<sup>-/-</sup> aortas (Fig.9; supplement Table S1).

The mining of differential gene expression profiles in the diseased total aorta during aging yielded important candidates of neuroimmune crosstalk including *bex1* (brain expressed X-linked 1); interleukin 6; nerve growth factor, purinergic receptor P2X ligand-gated ion channel 4 (P2X4), *Unc-5*, netrin receptor C. Each of these genes plays important roles in the PNS, and many of them are mediators of neuroimmune cardiovascular crosstalk. Heatmaps demonstrated multiple up-regulated genes such as *Sema4D*, early growth response 2 (*Egr2*), and neuropilin 2 (*Nrp2*) and down-regulated genes such as *Sema3A*, *Sema3F*, neuron navigator 2 (*Nav2*) and neurotrophin 3 (*Ntf3*) in WT *vs.*

## RESULTS

*ApoE*<sup>-/-</sup> aorta during aging (Fig.9). Semaphorins are known to play important roles in the formation and functioning of the cardiovascular and immune systems in addition to their roles in the NS development and in axonal guidance<sup>155</sup>. As the semaphorin class-3 receptor, Nrp2 guides axonal growth during the development of the nervous system<sup>156</sup>. Nav2 plays an important role in CNS development<sup>157</sup>. Ntf3 supports the survival and differentiation of neurons of the peripheral and central nervous systems and promotes growth and differentiation of new neurons and synapses<sup>158,159</sup>.

Neuronal guidance gene Sema4D was highly up-regulated in WT vs. *ApoE*<sup>-/-</sup> mice. Notably, Sema4D was also up-regulated in adult and aged *ApoE*<sup>-/-</sup> aortas vs. their young and adult counterparts, respectively. Importantly, in *ApoE*<sup>-/-</sup> aortae at 78 week multiple axonogenesis and axon repellent genes including Sema3A and Sema3F were down-regulated vs. 78 week-old WT aortas, and Sema3A and Sema3F had a tendency of down-regulation in aged *ApoE*<sup>-/-</sup> aortas vs. young and adult mice. These data revealed dramatic changes in the aortae of aged *ApoE*<sup>-/-</sup> mice at 78 weeks and indicated that age-dependent changes in axon growth and guidance factors occurred in WT and *ApoE*<sup>-/-</sup> mice (Fig.9; supplement Table S1).

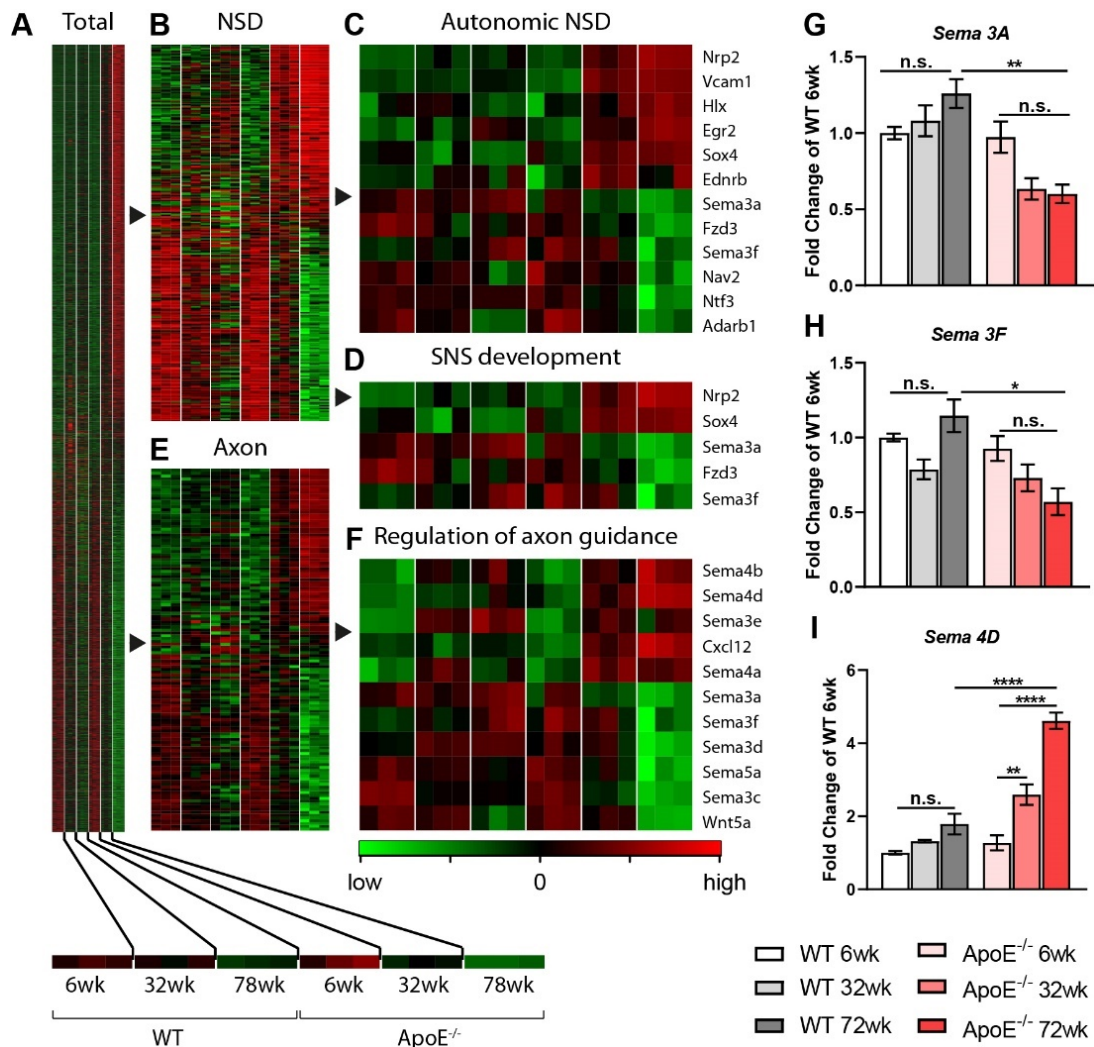
In addition, LCM-derived tissues of adventitia, adventitia without plaque, and ATLOs from WT and *ApoE*<sup>-/-</sup> mice were compared by microarray analyses<sup>147</sup>. This mRNA expression database was also used to search for neuronal growth, survival, and guidance molecules. Genes of interest including nervous system development (GO: 0007399; 136 genes), neuron projection development (GO: 0031175; 120 genes), regulation of neuron projection development (GO: 0010975; 69 genes), axon (GO: 0030424; 62 genes), and regulation of axon guidance (GO: 1902667; 5 genes), in aged WT and *ApoE*<sup>-/-</sup> abdominal adventitia were examined (Fig.10; supplement Table S2).

Heatmaps, together with the statistical analyses of each mRNA, demonstrated many up-regulated genes such as PlxnB2, PlxnC1, Sema4D, and thymus cell antigen 1 (Thy1, CD90) and down-regulated genes such as reticulon 4 (Rtn4), and Neurofibromin 1 (Nf1) in ATLOs (Fig.10). Plexins, together with semaphorins, was reported to stabilize synaptic transmission in the developing and mature NS<sup>160-162</sup>, while Thy1 is associated with neurovascular function<sup>163</sup>. By contrast, Rtn4 provides inhibitory signals for neurite outgrowth<sup>164</sup>, and loss of Nf1 led to neurotrophin-independent survival of embryonic sensory and sympathetic neurons<sup>165</sup>. Notably, neuron projection development genes, including the axon guidance-regulating gene, i.e., Sema4D and neuron projection development

## RESULTS

regulating gene *PlxnB2*, were up-regulated in ATLOs vs. aged WT and *ApoE*<sup>-/-</sup> adventitia without plaque (Fig.10G-I).

In summary, the microarrays data indicate that the nervous system development-related genes in *ApoE*<sup>-/-</sup> mice were affected by aging and atherosclerosis, and in particular, within ATLOs of diseased aorta adventitia. These findings, together with immunofluorescence and ELISA data, suggest that enhanced sympathetic NS development-related genes in *ApoE*<sup>-/-</sup> mice were possibly expressed by newly formed axons during atherosclerosis and the immune cells recruited in an inflammatory microenvironment in ATLOs. This provides strong evidence for robust atherosclerosis-SNS crosstalk and, in particular robust ATLO-SNS crosstalk, highlighting the existence of a hitherto unrecognized atherosclerosis-SNS circuit in aged hyperlipidemic mouse aortas.



## RESULTS

**Figure 9. Differential Neuronal Gene Expression in WT and *ApoE*<sup>-/-</sup> Aortas.** **A)** Heatmaps of differentially regulated genes in total aorta RNA extracts based on the reanalysis of published microarray data<sup>45</sup>. Gene expression in aortae was displayed separately from 6, 32, and 78 weeks old WT and *ApoE*<sup>-/-</sup> mice. The following GO terms were analyzed from total genes: **B)** nervous system development (GO: 0007399); **C)** autonomic nervous system development (GO: 0048483); **D)** sympathetic nervous system development (GO: 0048485); **E)** axon (GO: 0030424); **F)** regulation of axon guidance (GO: 1902667). **G,H,I)** Quantitation of aorta genes expression (log<sub>2</sub> value) for semaphrine3A, semaphrine3F, semaphrine4D in WT and *ApoE*<sup>-/-</sup> mice during aging. Data represents Means ± SEM. The statistical analyses on the raw CEL-file data. 6 groups of samples were compared using one-way ANOVA with Bonferroni's post-hoc test. \*:P<0.05, \*\*:P<0.001; 6 weeks WT (N=3); 32 weeks WT (N=3); 78 weeks WT (N=3); 6 weeks *ApoE*<sup>-/-</sup> (N=3); 32 weeks *ApoE*<sup>-/-</sup> (N=3); 78 weeks *ApoE*<sup>-/-</sup> (N=3).

RESULTS

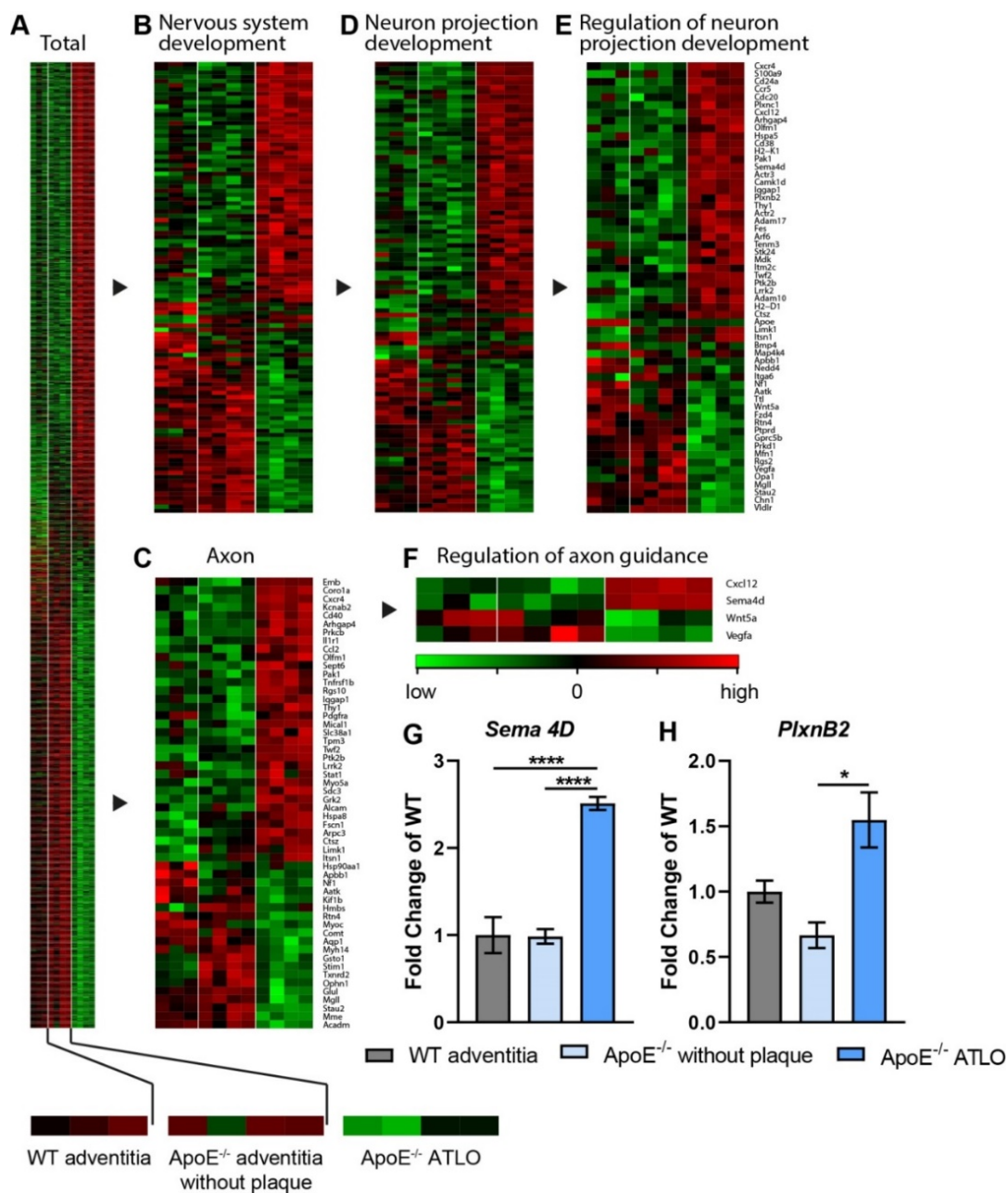


**Figure 10. Differential Neuronal Gene Expression in WT and *ApoE*<sup>-/-</sup> Abdominal Adventitia.** **A)** Heatmaps of differentially regulated genes (ANOVA; RME ≤ 0.66) in abdominal adventitia RNA extracts, based on reanalysis of published microarray data (reference). Gene expression in LCM-derived abdominal adventitia was shown from aged WT adventitia, aged *ApoE*<sup>-/-</sup> abdominal aortae without plaque and ATLO in *ApoE*<sup>-/-</sup> abdominal adventitia. The following GO terms were analyzed from total genes: **B)** nervous system development (GO: 0007399); **C)** axon (GO: 0030424); **D)** neuron projection development (GO: 0048483); **E)** regulation of neuron projection development (GO: 0048485); **F)** regulation of axon guidance (GO: 1902667). **G, H)** Quantitation of mRNA expression (log<sub>2</sub> value) for semaphorin 4D, and plexin B2 in *ApoE*<sup>-/-</sup> abdominal aortae without plaque and ATLO in *ApoE*<sup>-/-</sup> abdominal adventitia vs. WT adventitia in aged WT and *ApoE*<sup>-/-</sup> mice. Means ± SEM, \*:P<0.05, \*\*\*\*:P<0.0001; one-way ANOVA with Bonferroni's post-hoc

## RESULTS

test. 78 weeks WT (N=3); 78 weeks *ApoE*<sup>-/-</sup> adventitia without plaque (N=4); 78 weeks *ApoE*<sup>-/-</sup> adventitia with ATLO (N=4).

### 3.4 Chemical sympathectomy by 6-OHDA

Since we observed that sympathetic innervation and NE levels markedly increased during atherosclerosis in the diseased artery adventitia, we wished to examine the effect of the SNS on atherosclerosis progression. For this purpose, chemical sympathetic denervation was performed using 6-OHDA in adult and aged *ApoE*<sup>-/-</sup> mice by adapting previously described methods in mice<sup>61,90</sup>. 6-OHDA was demonstrated to deplete the sympathetic axons in peripheral tissues<sup>93</sup>.

#### 3.4.1 Effects of chemical sympathectomy in adult mice

To determine the effects of chemical sympathectomy in early atherosclerosis, *ApoE*<sup>-/-</sup> male mice at 28 weeks of age were injected with 6-OHDA for 4 weeks and sacrificed one week after the last injection according to the workflow shown below in Fig.11. Blood, spleen, LNs, kidney, liver, heart, aorta, and adipose tissue were harvested for further analyses.

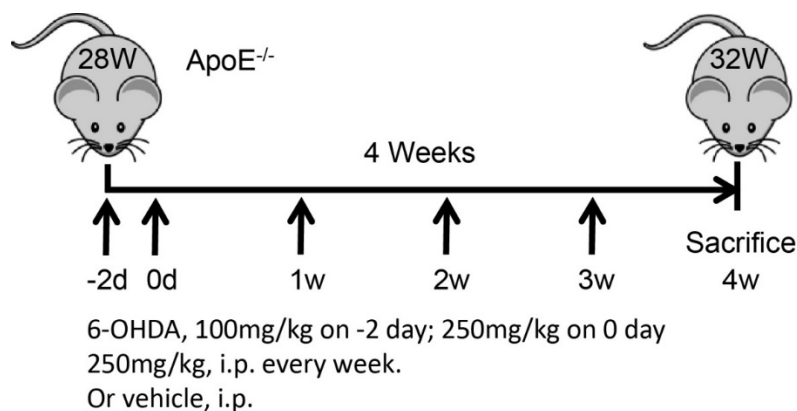


**Figure 11. Workflow for 6-OHDA treatment in adult mice.** Treatment was started at the age of 28 weeks. The treated group received a 6-OHDA injection of 100 mg/kg body weight two days before day 0. On day 0, mice received 250 mg/kg body weight. 6-OHDA was dissolved in saline containing 0.1% ascorbic acid. Thereafter, the animals were treated three more times, one injection every week. The control group received the same volume of vehicle, which is in saline

## RESULTS

containing 0.1% ascorbic acid but without 6-OHDA. Animals were fed with normal diet and sacrificed 1 week after the last injection.

### 3.4.1.1 NE concentration was reduced in treated adult mice

To determine the effectiveness of the 6-OHDA treatment, NE levels in spleen and the aorta were measured. We observed that the NE concentration in the spleen of sympathetically denervated mice was more than 90% reduced vs. vehicle-treated controls. Similarly, the NE level in the iliac artery of 6-OHDA-treated mice was about 85% reduced vs. the control mice (Fig.12.). This indicated that chemical denervation of the SNS was successful.

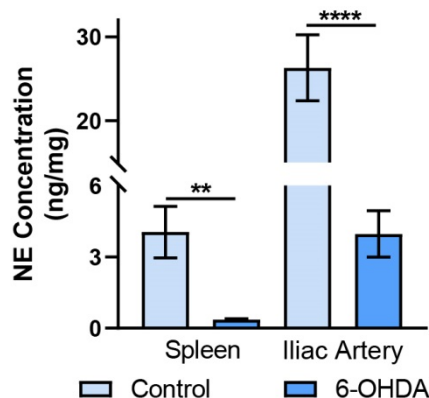


**Figure 12. Tissue NE concentrations reduced by 6-OHDA in spleen and iliac artery of adult mice in time window of 4 weeks of 6-OHDA treatment.** The figure showed the quantitative analysis of the NE concentrations in spleen and iliac artery of control and treated animals. Spleens and iliac arteries were frozen in liquid nitrogen. NE levels were measured with ELISA. N = 11 spleens from control mice, 14 spleens from 6-OHDA-treated mice, 11 iliac arteries from control mice, 14 iliac arteries from 6-OHDA-treated mice. Data represent means  $\pm$  SEM; two-tailed unpaired Student's t-test, \*\*:  $p < 0.01$ ; \*\*\*\*:  $p < 0.001$ ; n.s.: not significant.

### 3.4.1.2 Effect of chemical sympathectomy on physiological parameters in adult mice

Depletion of the peripheral SNS caused changes in various physiological parameters of the animal, including heart rate<sup>166</sup>, body temperature<sup>167</sup>, and behavior<sup>168,169</sup>. To monitor the status of the mice following treatment, body weights and plasma cholesterol were measured. The data demonstrated

## RESULTS

that the body weight of 6-OHDA-treated groups significantly declined (Fig.13.A), which was consistent with published data<sup>170</sup>. To determine the cause of the body weight reduction and to detect potential side effects of 6-OHDA, the weights of spleen, kidney, liver, heart, and iLNs were measured. Based on the body weight of the animals, the relative organ weight of individual mice was also calculated (to determine organ-specific changes), but this parameter did not show significant differences between control and treated animals (Fig.13.B). The data indicated that chemical sympathectomy moderately reduced the body weight of the animals, but did not disproportionately affect the relative weights of spleen, kidney, liver, heart, or LNs. However, we noticed that treatment led to a significant decrease of gonadal adipose tissue (gAT, circles in Fig.13.C) weight. Though 6-OHDA was applied in *in vivo* research for decades, its effect on adipose tissue weight was not yet determined. In our experiments, the weight of gAT was reduced by ~50% in 6-OHDA-treated mice vs. controls (Fig.13.D).

Since *ApoE*<sup>-/-</sup> mice were hyperlipidemic under normal chow diet, it was important to determine whether the blood lipid levels were altered after sympathetic denervation under our experimental conditions. To determine the effect of chemical sympathectomy on blood lipid, total cholesterol concentrations were measured by ultracentrifugation. Although the means of total cholesterol showed a tendency of decrease, these levels (amounting to a decrease of about 15%) did not reach statistical significance (Fig.13.E). Until today, the effect of 6-OHDA treatment on circulating cholesterol levels has not been reported to our knowledge.

## RESULTS

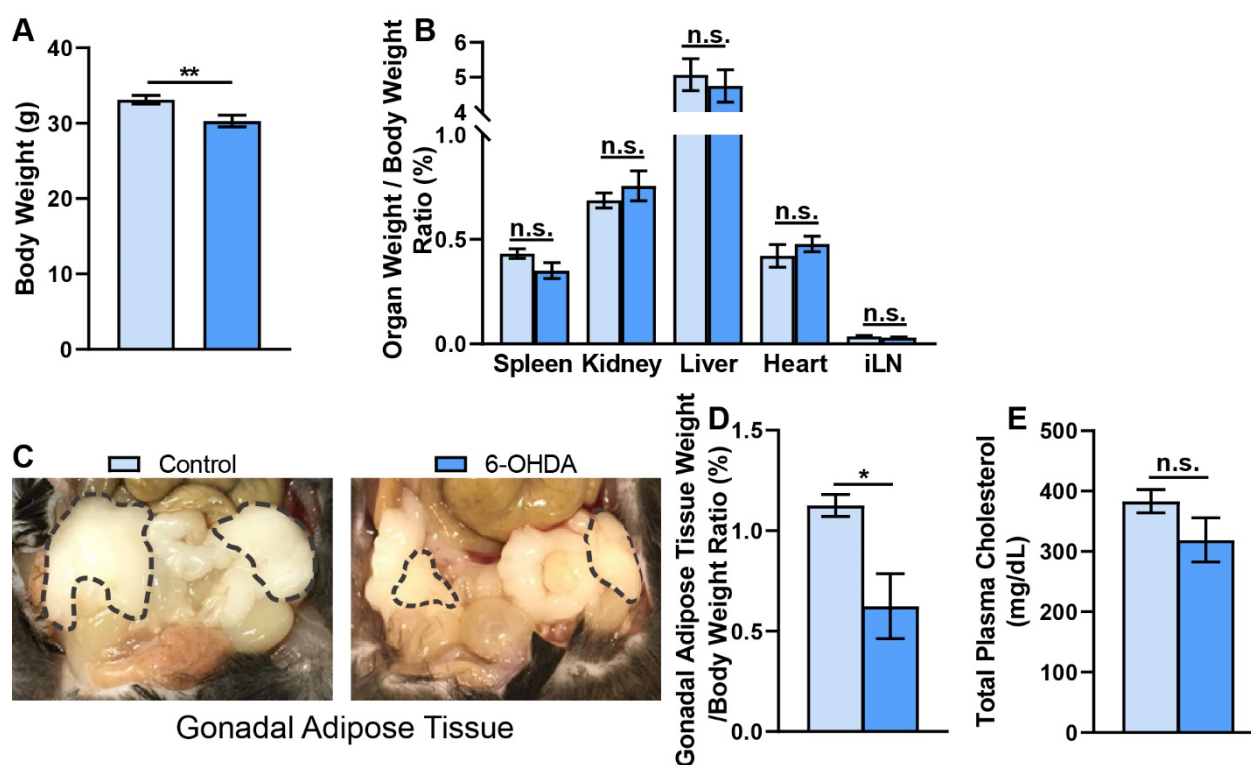


**Figure 13. Absolute and relative body weights and gonadal adipose tissue of adult mice.** **A)** Body weights of the animals were determined on the day of sacrifice. N = 13 control mice and 13 6-OHDA-treated mice. **B)** The organ weight/body weight ratio of spleen, kidney, liver, heart, and iLN. N = 10 controls and 9 treated mice. **C)** Representative images of gAT (circled) in control and 6-OHDA-treated mice. **D)** The ratio of gAT weight from body weight. N = 6 control and 5 treated mice. Data represent means  $\pm$  SEM; two-tailed unpaired Student's t-test, \*:  $p < 0.05$ ; \*\*:  $p < 0.01$ ; n.s.: not significant. **E)** Total plasma cholesterol concentrations. Plasma was collected after 4 weeks of chemical sympathectomy. N = 10 controls and 9 6-OHDA-treated.

### 3.4.1.3 Effect of chemical sympathectomy on blood parameters of adult mice

To determine the effect of chemical sympathectomy on hematological changes, the blood of 32 weeks old *ApoE*<sup>-/-</sup> mice treated with 6-OHDA for 4 weeks was analyzed. The data did not reveal changes in the total number of white blood cells or numbers of their subtypes, red blood cells, and platelets (Fig.14.A). Moreover, the other blood parameters remained unchanged (Fig.14.B), suggesting that 6-OHDA treatment did not produce major hematological alterations<sup>171</sup>.

## RESULTS

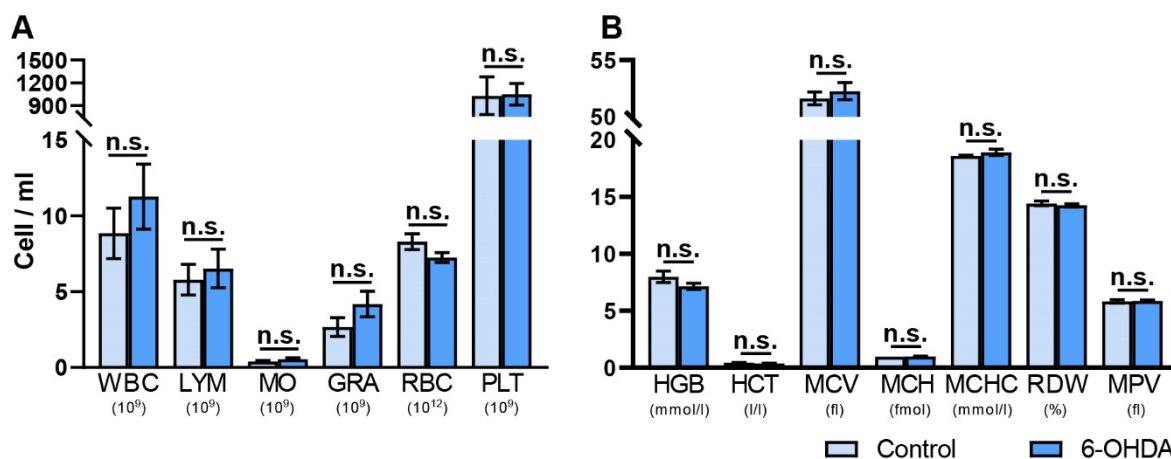


**Figure 14. No hematological alteration with 6-OHDA treatment.** A) Blood leukocyte counts. Blood samples were taken at endpoints through cardiac puncture under anesthesia. Total number of white blood cells (WBC), numbers of lymphocytes (LYM), monocytes (MO) and granulocytes (GRA), red blood cells (RBC) and platelets (PLT) were demonstrated. B) Determination of other blood components by automated blood counter. Hemoglobin (HGB), hematocrit (HCT), mean corpuscular volume (MCV), mean corpuscular hemoglobin (MCH), mean corpuscular hemoglobin concentration (MCHC), red cell distribution width (RDW) and mean platelet volume (MPV) were demonstrated. N = 10 control and 9 treated mice. Data represent means  $\pm$  SEM; two-tailed unpaired Student's t-test, n.s.: not significant.

### 3.4.1.4 Effect of chemical sympathectomy on myeloid and lymphocyte subsets in SLOs and the circulation

The lack of effect of chemical sympathectomy on blood leukocyte counts was somewhat unexpected since the immune system is known to be regulated by the SNS<sup>172,173</sup>. Acute MI had been reported to trigger the SNS in *ApoE*<sup>-/-</sup> mice, and CD11b<sup>+</sup> monocytes/macrophages/neutrophils increased after MI<sup>90</sup>. SLOs and blood were regulated by chemical sympathectomy. 6-OHDA treatment in WT mice was reported to reduce CD11b<sup>+</sup> leukocytes in blood and spleen and increased Foxp3<sup>+</sup> T<sub>reg</sub> cells in spleen<sup>174</sup>. Furthermore, 6-OHDA or apparent splenic nerve sympathectomy were reported to reduce CD11b<sup>+</sup> monocytes/macrophages/neutrophils cells in the spleen reservoir of diabetic mice<sup>175</sup>. Foxp3<sup>+</sup> T<sub>reg</sub> cells were reported to be increased 10 days after 6-OHDA treatment vs. control WT mice<sup>89</sup>. Therefore, we sought to determine the immune cell composition in lymphoid organs and the circulation in our mouse cohorts in more detail. Spleens, lymph nodes, and blood were analyzed with flow cytometry using appropriate gating strategy (Fig.15.A). FACS analyses of T cells showed that

## RESULTS

the percentage of the CD4<sup>+</sup> T helper (Th) cells among total CD45<sup>+</sup> leukocytes decreased in SLOs and blood of treated animals (Fig.15.B, C), whereas CD4<sup>+</sup> Foxp3<sup>+</sup> T<sub>reg</sub> cells among total CD45<sup>+</sup> leukocytes markedly increased in spleen, para-aortic LNs and blood in 6-OHDA-treated *vs.* controls (Fig.15.D, E). Moreover, myeloid cell analyses showed that CD11b<sup>+</sup>CD11c<sup>+</sup> DCs among total CD45<sup>+</sup> leukocytes significantly decreased in spleen and blood, but not in paraaortic LNs of treated mice compared to controls (Fig.15.F, G). Our data indicated that CD4<sup>+</sup> Th cells, Foxp3<sup>+</sup> T<sub>reg</sub> cells, and CD11b<sup>+</sup>CD11c<sup>+</sup> DCs were affected by the chemical sympathectomy. The data on increased T<sub>reg</sub> cells were consistent with previously published literature<sup>89,93,94</sup>.

## RESULTS

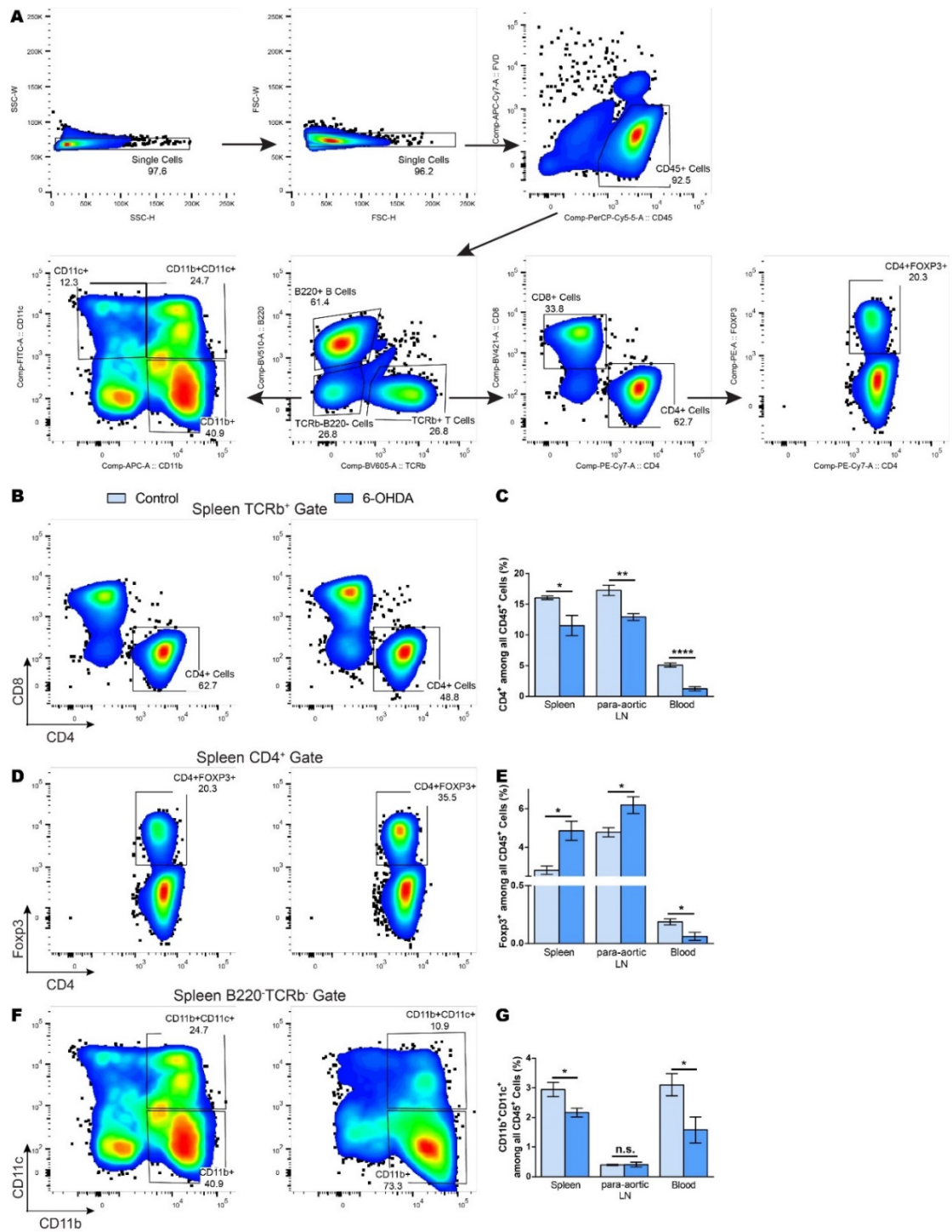


**Figure 15. CD4<sup>+</sup> Th cells and CD11b<sup>+</sup>CD11c<sup>+</sup> DCs decreased, and T<sub>reg</sub> cells increased in SLOs and the circulation of 6-OHDA-treated adult mice.** **A)** Gating strategy of FACS analysis in spleen, para-aortic LN, and blood of adult mice. **B)** Gating of CD4<sup>+</sup> T helper cells. **C)** Quantification of Th cells as percentage of CD4<sup>+</sup> among all CD45<sup>+</sup> leukocytes of SLOs and circulation. N = 8 spleens of control mice, 5 spleens of 6-OHDA-treated mice, 8 para-aortic LNs of control mice, 5 para-aortic LNs of treated mice, 8 blood samples of control mice and 5 blood samples of treated mice. **D)** Gating strategy of Foxp3<sup>+</sup> T<sub>reg</sub> cells. **E)** Quantification of T<sub>reg</sub> cells as percentage of Foxp3<sup>+</sup> among all CD45<sup>+</sup> leukocytes in SLOs and circulation. N = 8 spleens of control mice, 5 spleens of 6-OHDA-treated mice, 8 para-aortic LNs of control mice, 5

## RESULTS

para-aortic LNs of treated mice, 8 blood samples of control mice and 5 blood samples of treated mice. **F)** Gating strategy of CD11b<sup>+</sup> and CD11b<sup>+</sup>CD11c<sup>+</sup> myeloid cells. **G)** Quantification of CD11b<sup>+</sup>CD11c<sup>+</sup> DCs as percentage of all CD45<sup>+</sup> leukocytes in SLOs and blood. N = 8 controls and 5 treated mice. Data represent means ± SEM; two-tailed unpaired Student's t-test, \*: p<0.05; \*\*: p<0.01; \*\*\*\*: p<0.001; n.s.: not significant.

### 3.4.1.5 Correlation between NE and Treg cells in the spleen

Published data suggest that increasing T<sub>reg</sub> counts might largely be due to the reduction in NE levels<sup>89</sup>. Therefore, a possible correlation between splenic NE levels and T<sub>reg</sub> cells was analyzed. We observed that tissue NE levels dramatically decreased upon chemical sympathectomy, while the Foxp3<sup>+</sup> T<sub>reg</sub> cells sharply increased in SLOs and the circulation of 6-OHDA-treated mice. As expected, Pearson's correlation analysis of NE levels and T<sub>reg</sub> cells confirmed that spleen NE concentration was negatively correlated with T<sub>reg</sub> cell frequencies, which is in agreement with the published data (Fig.16.).

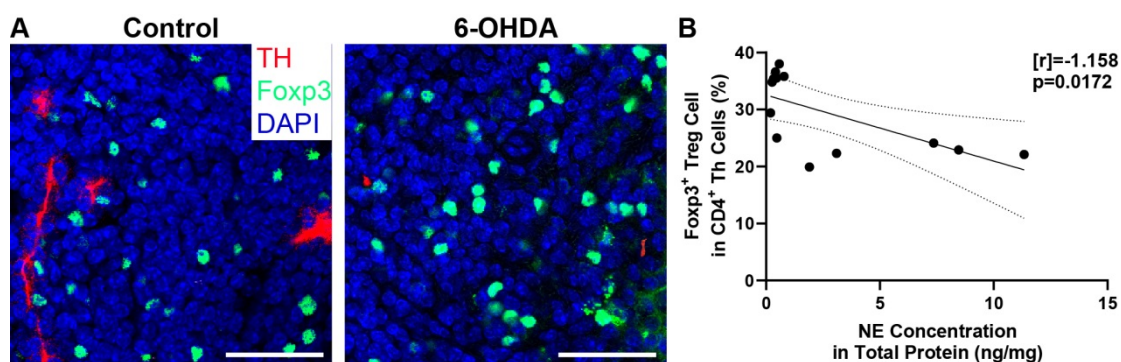


**Figure 16. Negative correlation between tissue NE and spleen T<sub>reg</sub> cells.** **A)** Representative images of TH<sup>+</sup> area and Foxp3<sup>+</sup> cells in spleens of control and sympathetically denervated mice. 10 μm fresh frozen sections of spleen were stained with TH and Foxp3 antibodies. TH was stained red; Foxp3 was stained green; DNA was stained blue. Scale bar: 100 μm. **B)** Pearson's correlation coefficient of splenic NE concentration with Foxp3 expressing cells ( $r = -1.158$ ;  $p = 0.0172$ ) indicates the relation between the percentage of T<sub>reg</sub> cells and tissue NE concentrations. T<sub>reg</sub> cells were quantified in 10 spleen sections per mouse. N = 10 serial sections per mouse in 6 controls and 7 treated mice.

## RESULTS

### 3.4.1.6 Effect of chemical sympathectomy in 32 weeks old adult mice on a chow diet

To analyze the effect of 6-OHDA on atherosclerotic plaque size during a short time window of 4 weeks treatment, aortas of 32 weeks old mice were examined. It should be noted that mice at this age and maintained on chow diet did not show significant atherosclerosis in the abdominal aorta and that atherosclerosis development at this early time point in the thoracic aorta was rather limited implicating considerable variability between individual mice. The primary purpose of these experiments, therefore, was to examine the toxicity of the drug and to examine its effect on the immune system and to compare its effects with that of surgical denervation of the SNS using CGX. No apparent major toxicity was observed (but see data on aged mice below). In addition, aortas were stained with Sudan IV to perform en-face analyses. The data revealed a moderate increase in en-face stained plaque areas in the thoracic aorta, including aortic arch and descending thoracic aorta (data not shown). Similarly, the plaque of the aortic root also seemed to show a moderate increase in size, particularly when the specific distances of the aortic root from the aortic sinus were examined (data not shown). Parameters of plaque vulnerability (macrophage content, SMC area, necrotic core area, fibrous cap thickness, and collagen content), however, remained unchanged under these experimental conditions (see below similar measurements in aged mice). However, we noticed multiple effects of the drug on the immune system, including the bone marrow, secondary lymphoid organs, and the circulation. Nevertheless, some of the short term effects are noteworthy in view of my analyses to compare the systemic effects of the drug and the surgical approach to take out the celiac ganglion followed by a longer period of 8 months thereafter (see below). When taken together, however, these data in adult mice should be interpreted with caution because a longer period of treatment would be required to definitely ascertain the effects of 6-OHDA on atherosclerosis development.

### 3.4.2 Effects of chemical sympathectomy in aged mice during a short time window of 4 weeks

To study the effect of chemical sympathectomy on advanced atherosclerosis and ATLOs, *ApoE*<sup>-/-</sup> male mice at the age of 66 weeks were treated with 6-OHDA following the workflow below (Fig.17.).

## RESULTS

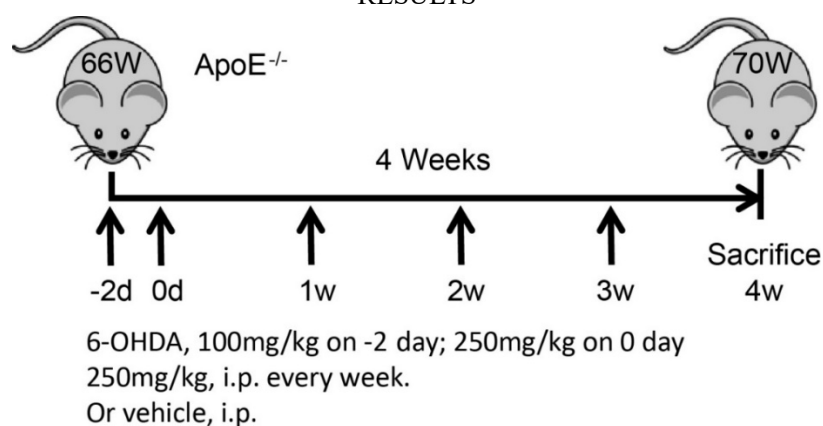


**Figure 17. Workflow of 6-OHDA treatment in aged mice.** Injection began at -2 days at the age of 66 weeks. The treated group received 6-OHDA injection of 100 mg/kg bodyweight at -2 day. On day 0, mice received 250 mg/kg body weight. Thereafter, the animals were treated three more times, one injection every 7 days. The control group received the same volume of vehicle. Animals were maintained on normal diet and sacrificed 7 days after the last injection.

### 3.4.2.1 NE concentrations and TH<sup>+</sup> areas were reduced in 6-OHDA-treated aged mice

To determine the specificity of 6-OHDA treatment, NE levels in spleen and aorta were measured with ELISA. The spleen was sectioned and stained with TH antibody. Tissue NE concentrations of the spleen were reduced ~70% (Fig.18.A), and it decreased ~90% in iliac arteries (Fig.18.B) upon treatment. Our data demonstrated that TH<sup>+</sup> sympathetic axons in spleen decreased ~90% upon treatment (Fig.18.C&D). The data indicated that our treatment protocol was effective.

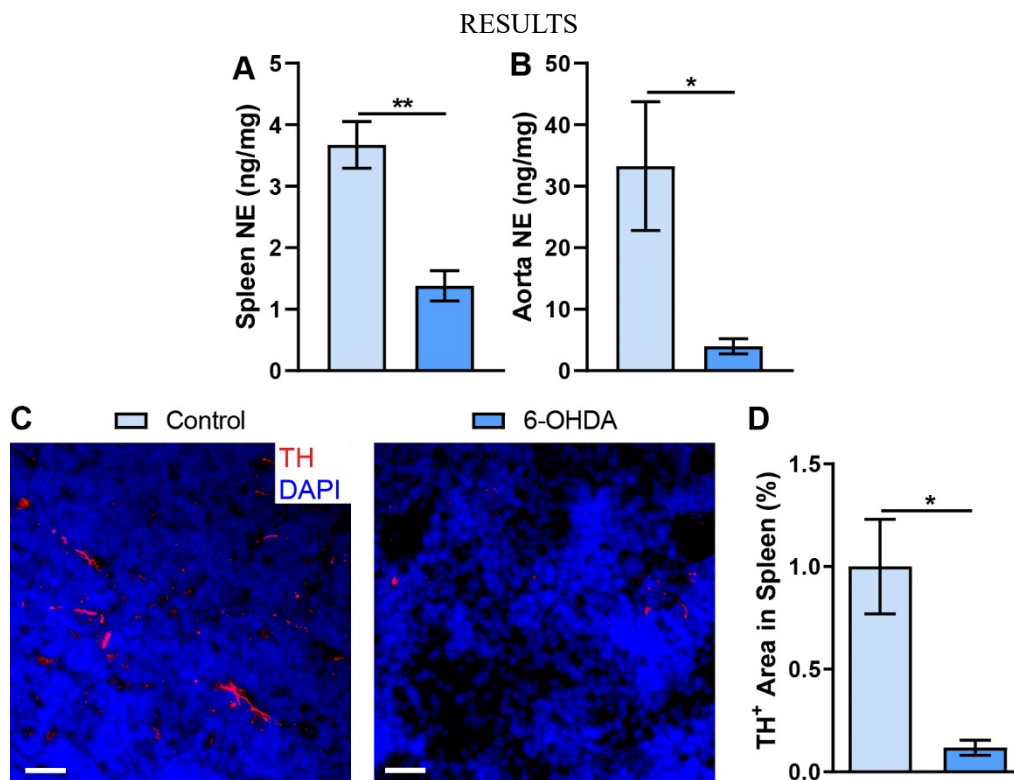


**Figure 18. NE concentrations reduced in spleen and iliac artery; the TH<sup>+</sup> area reduced in spleen.** **A)** Quantification of splenic NE concentrations in control and treated animals. N = 4 control mice and 7 6-OHDA-treated mice. **B)** Quantification of tissue NE concentrations in iliac aorta of control and treated animals. N = 3 control mice and 4 treated mice. **C)** Representative images of TH<sup>+</sup> area in the spleen of control and treated mice, showing the sympathetic axon areas. 10  $\mu$ m fresh frozen spleen sections were stained for TH<sup>+</sup> sympathetic axons. TH was stained red; DNA was stained blue. Scale bar: 50 $\mu$ m. **D)** Quantitative analysis of TH<sup>+</sup> area in the spleen of control and treated animals. N = 10 spleen sections per mouse in 5 controls and 4 treated mice. Data represent means  $\pm$  SEM; two-tailed unpaired Student's t-test, \*:  $p < 0.05$ ; \*\*:  $p < 0.01$ .

### 3.4.2.2 Effect of chemical sympathectomy on physiological parameters in aged mice

To monitor the status of the treated animals, body weights and plasma cholesterol concentrations were measured. The body weight of 6-OHDA-treated mice was moderately reduced (Fig.19.A). To determine whether chemical sympathectomy affected lipids in the circulation, plasma samples were taken before sacrifice. The data showed that the levels did not reach significance (Fig.19.B). The weights of spleen, liver, heart, and gAT were determined. Relative to body weight, the percentages of the individual body weight were calculated. Similar to adult mice, the relative weights of gAT showed significant decreases in the treated animals (Fig.19.C).

## RESULTS

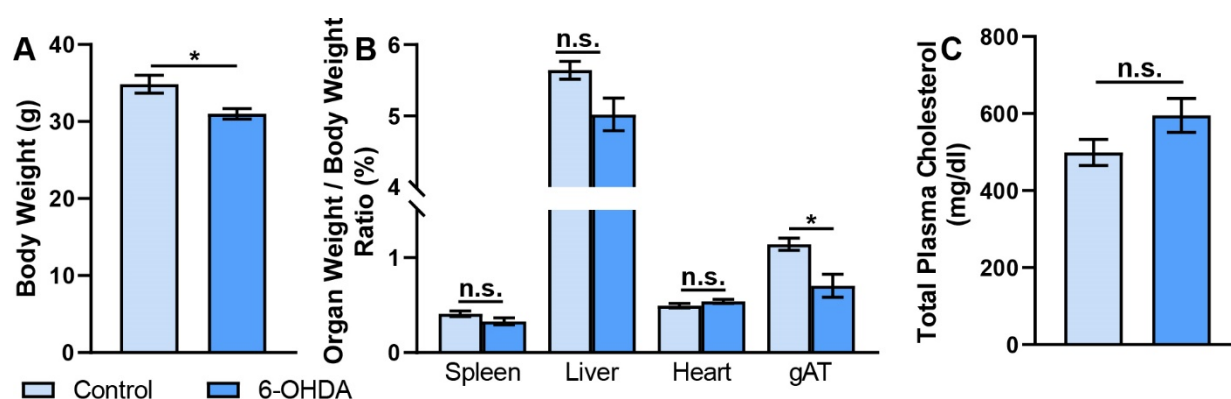


**Figure 19. Total body weight was moderately reduced, and gonadal adipose tissue weight was significantly reduced in aged mice. A)** Body weight after 4 weeks of treatment. **B)** Ratio of organ weight/body weight of spleen, liver, heart, and gAT. **C)** Total plasma cholesterol concentrations. Plasma samples were collected after 4 weeks of chemical sympathectomy. N = 5 control and 5 6-OHDA-treated mice. Data represent means ± SEM; two-tailed unpaired Student's t-test, \*:  $p < 0.05$ ; n.s.: not significant.

### 3.4.2.3 Effect of chemical sympathectomy on blood parameters in aged mice

To determine the effect of chemical sympathectomy on hematological parameters, blood of 70 weeks old *ApoE*<sup>-/-</sup> mice treated with 6-OHDA for 4 weeks was analyzed. The data did not show significant changes in the total number of leukocytes or the numbers of lymphocytes, monocytes or granulocytes, but the number of red blood cells was moderately decreased (Fig.20.A). Other components remained unchanged except for the red blood cell distribution width, which slightly increased (Fig.20.B).

## RESULTS

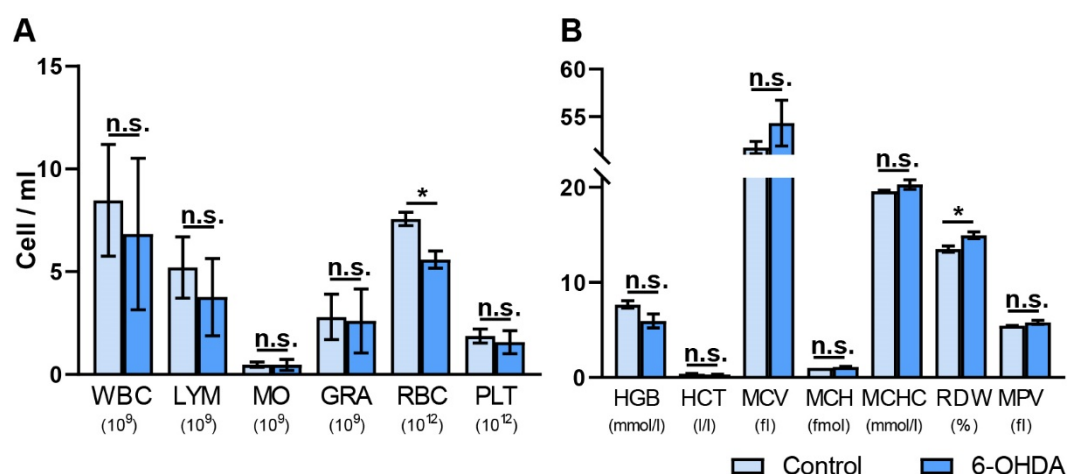


**Figure 20. No major hematological side effects with 6-OHDA treatment. A)** The number of white blood cells (WBC), numbers of lymphocytes (LYM), monocytes (MO) and granulocytes (GRA), red blood cells (RBC) and platelets (PLT) were demonstrated. Blood samples were taken through heart puncture under anesthesia. **B)** The other components of blood. Hemoglobin (HGB), hematocrit (HCT), mean corpuscular volume (MCV), mean corpuscular hemoglobin (MCH), mean corpuscular hemoglobin concentration (MCHC), red cell distribution width (RDW) and mean platelet volume (MPV) were demonstrated. N = 4 controls and 3 6-OHDA-treated mice. Data represent means  $\pm$  SEM; two-tailed unpaired Student's t-test, \*:  $p < 0.05$ , n.s.: not significant.

### 3.4.2.4 Effect of chemical sympathectomy on leukocytes in SLOs and hematopoietic progenitors in the bone marrow

To determine the effect of chemical sympathectomy on immune cells in lymphoid organs, spleen, para-aortic LNs, and blood were examined by flow cytometry using a similar gating strategy that we used for adult mice (Fig.21.A). Our data demonstrated that  $CD4^+$  Th cells among total leukocytes decreased in spleen and blood, but not in the para-aortic LNs of treated vs. control mice (Fig.21.B, C); while  $CD4^+Foxp3^+$   $T_{reg}$  cells increased in paraaortic LNs, but decreased in blood of 6-OHDA treated mice, and spleen showed tendency to increase (Fig.21.D, E). However, the percentage of  $CD11b^+CD11c^+$  myeloid cells among total leukocytes decreased in blood, but did not show any change in the treated spleen and LNs (Fig.21.F, G).

## RESULTS

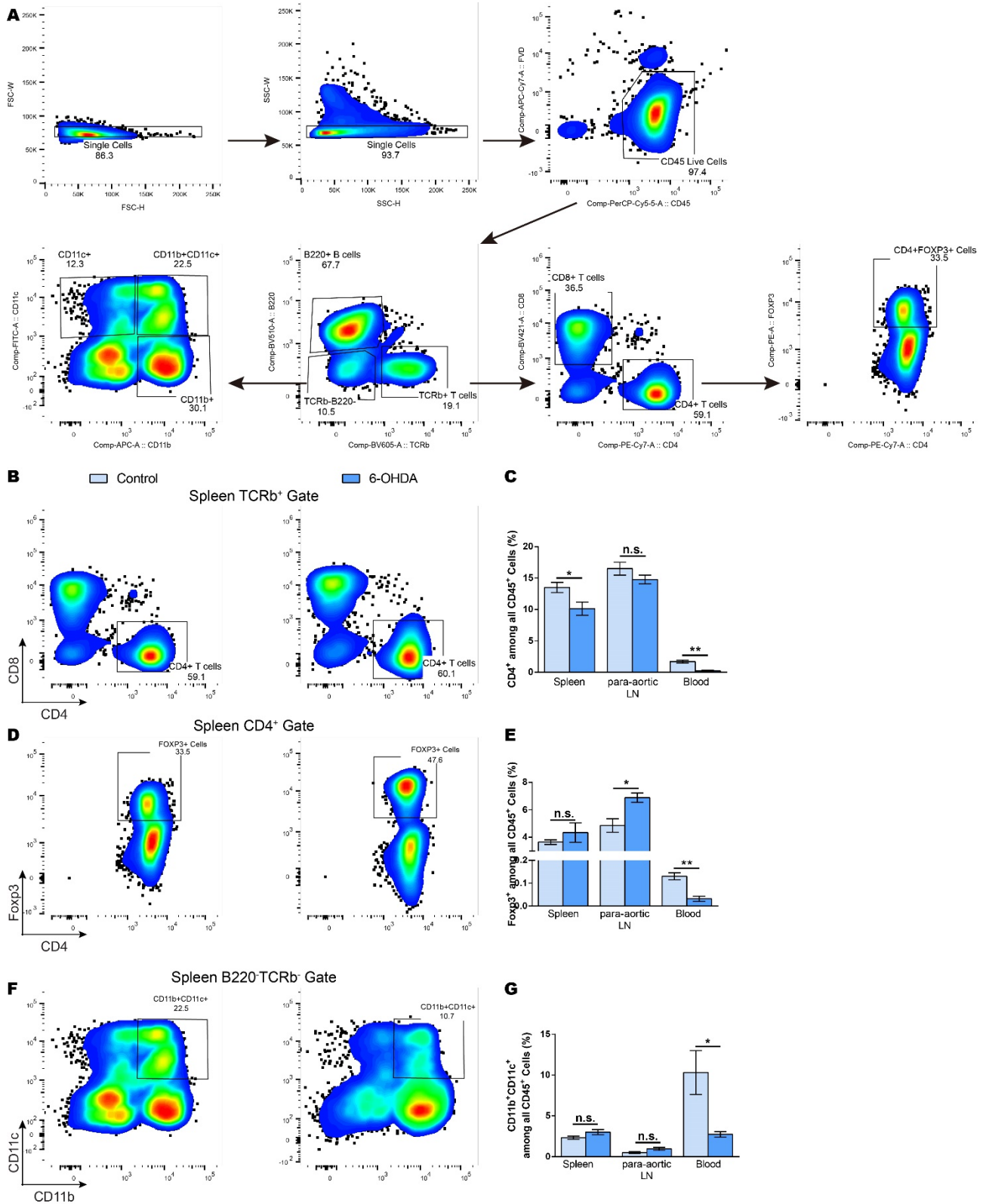


**Figure 21.** CD4<sup>+</sup> Th cells decreased in spleen, Foxp3<sup>+</sup> T<sub>reg</sub> cells increased in SLOs, but CD11b<sup>+</sup>CD11c<sup>+</sup> myeloid cells decreased in blood of sympathetic denervated aged mice. **A)** Gating strategy of FACS analysis in spleen, para-aortic LN, and blood of aged mice. **B)** Gating of CD4<sup>+</sup> Th cells. **C)** Quantification of CD4<sup>+</sup> Th cells in total CD45<sup>+</sup> leukocytes of SLOs and the circulation. **D)** Gating of Foxp3<sup>+</sup> T<sub>reg</sub> cells. **E)** Quantification of Foxp3<sup>+</sup> T<sub>reg</sub> cells in total CD45<sup>+</sup>

## RESULTS

leukocytes of SLOs and the circulation. N = 5 controls and 4 treated mice. **F)** Gating of CD11b<sup>+</sup>CD11c<sup>+</sup> DCs populations. **G)** Quantification of CD11b<sup>+</sup>CD11c<sup>+</sup> DCs in all CD45<sup>+</sup> leukocytes of SLOs and blood. Para-aortic LNs were pooled from renal LNs and lumbar LNs. N = 5 controls and 4 treated mice. Data represent means ± SEM; two-tailed unpaired Student's t-test, \*: p<0.05; \*\*: p<0.01; n.s.: not significant.

Loss of sympathetic innervation during aging increased hematopoietic stem cells (HSCs) in bone marrow in aged WT mice<sup>171,176</sup>, whereas ODHA denervation increased stem cell retention factor CXCL12 and did not alter HSCs and progenitor cells in bone marrow in young WT and *ApoE*<sup>-/-</sup> mice<sup>90,177</sup>. However, granulocyte-monocyte progenitors (GMPs) in the spleen and splenic CD11b<sup>+</sup> monocytes/macrophages/neutrophils decreased after 6-OHDA treatment<sup>175</sup>. To determine the effect of chemical sympathectomy on hematopoiesis, progenitors in bone marrow were examined by flow cytometry. Our data demonstrated that Lin<sup>-</sup>c-kit<sup>+</sup>Sca-1<sup>+</sup>CD48<sup>-</sup>CD150<sup>+</sup> HSCs were reduced in LSK cells in bone marrow, but did not show statistical difference among total lineage<sup>-</sup> cells (Fig.22.C). Likewise, Lin<sup>-</sup>c-kit<sup>+</sup>Sca1<sup>-</sup>CD34<sup>+</sup>CD16/32<sup>+</sup> GMP was reduced in LSK cells in bone marrow but did not show a statistical difference in total lineage<sup>-</sup> cells (Fig.22.E). Moreover, Lin<sup>-</sup>c-kit<sup>+</sup>Sca1<sup>-</sup>CD34<sup>+</sup>CD16/32<sup>-</sup> common myeloid progenitor (CMP) frequency among all lineage<sup>-</sup> cells was significantly reduced (Fig.22.F). Thus, our data confirmed and extended the published reports.

## RESULTS

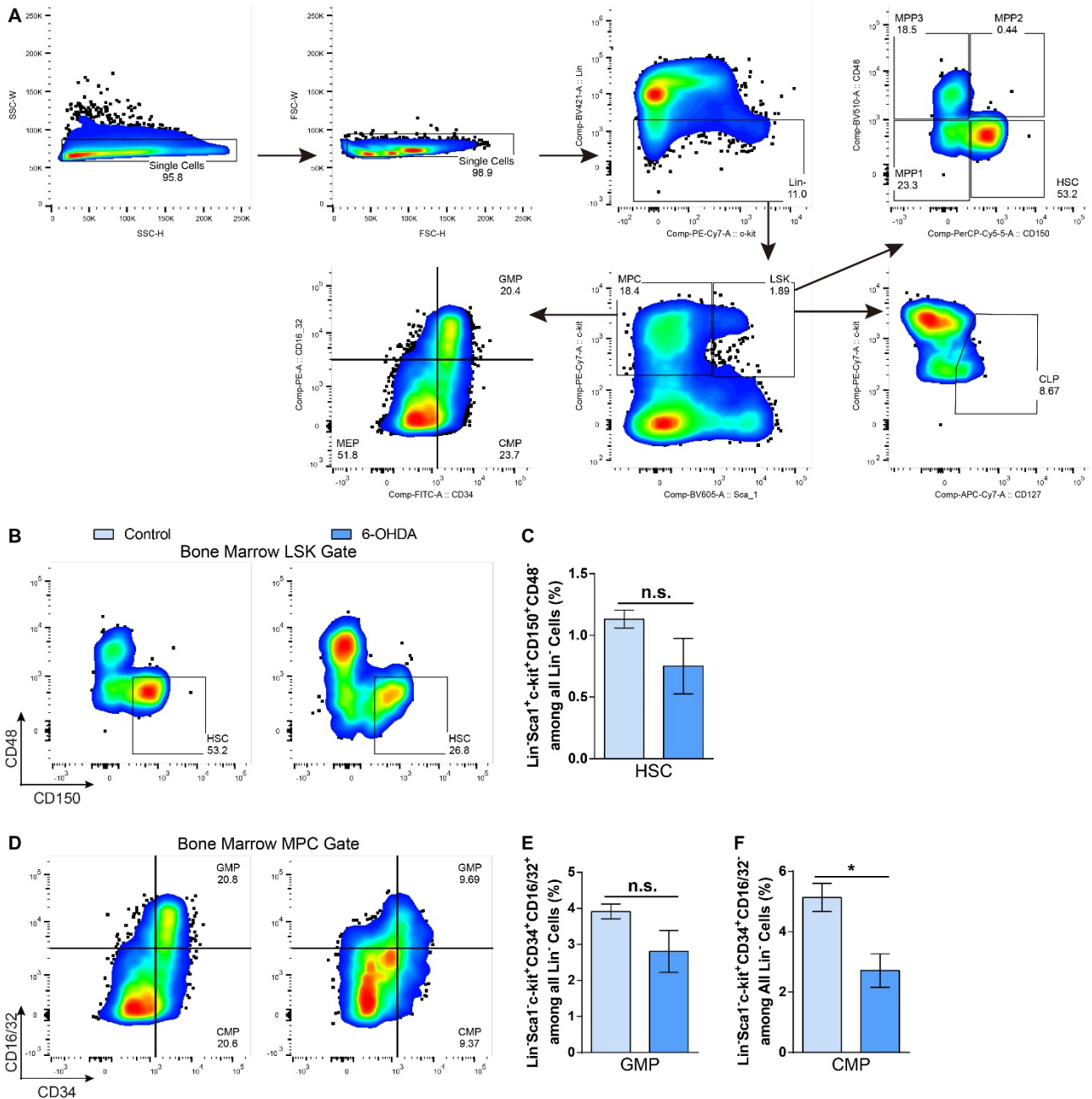


**Figure 22. HSC, GMP, and CMP decreased in bone marrow of sympathetic denervated aged mice.**

**A)** Progenitor gating strategy of FACS analysis in bone marrow of aged mice. **B)** Gating of Lin<sup>c-kit</sup><sup>+</sup>Sca1<sup>+</sup>CD48<sup>+</sup>CD150<sup>+</sup> HSCs from the Lin<sup>c-kit</sup><sup>+</sup>Sca1<sup>+</sup> (LSK) gate. **C)** Quantification of Lin<sup>c-kit</sup><sup>+</sup>Sca1<sup>+</sup>CD48<sup>+</sup>CD150<sup>+</sup> HSCs as frequency among all Lin<sup>-</sup> progenitors. N =5 control mice and 4 treated aged *ApoE*<sup>-/-</sup> mice. **D)** Gatings of Lin<sup>c-kit</sup><sup>+</sup>Sca1<sup>-</sup>CD34<sup>+</sup>CD16/32<sup>+</sup> GMPs and Lin<sup>c-kit</sup><sup>+</sup>Sca1<sup>-</sup>CD34<sup>+</sup>CD16/32<sup>-</sup> CMPs from the Lin<sup>c-kit</sup><sup>+</sup>sca1<sup>-</sup> myeloid progenitor cells (MPC) gate. **E)** Quantification of Lin<sup>c-kit</sup><sup>+</sup>Sca1<sup>-</sup>CD34<sup>+</sup>CD16/32<sup>+</sup> GMPs among all Lin<sup>-</sup> progenitors. N =5 control mice and 4 treated aged *ApoE*<sup>-/-</sup> mice. **F)** Quantification of Lin<sup>c-kit</sup><sup>+</sup>Sca1<sup>-</sup>CD34<sup>+</sup>CD16/32<sup>-</sup> CMPs in the Lin<sup>-</sup> gate of bone marrow. N =5 control mice and 4 treated aged *ApoE*<sup>-/-</sup> mice. Data represent means ± SEM; two-tailed unpaired Student's t-test, \*: p<0.05; n.s.: not significant.

## RESULTS

### 3.4.2.5 Effect of systemic sympathetic denervation on plaque and ATLO size

To determine the effect of chemical sympathectomy on ATLO and plaque structures, the abdominal aorta was sectioned and quantified. The images showed that the size of the plaque and ATLO structures were differentially affected. Whereas the size of atherosclerotic plaques was not affected during the time window of 4 weeks treatment with 6-OHDA, surprisingly, the effects of treatment on ATLOs were dramatic and occurred within the short period of time of 4 weeks (Fig.23 & 24). Both the ATLO number and size decreased, respectively, and ATLO structures were disturbed. These data strongly indicate that the SNS affects the maintenance of ATLOs in the aorta of aged mice.

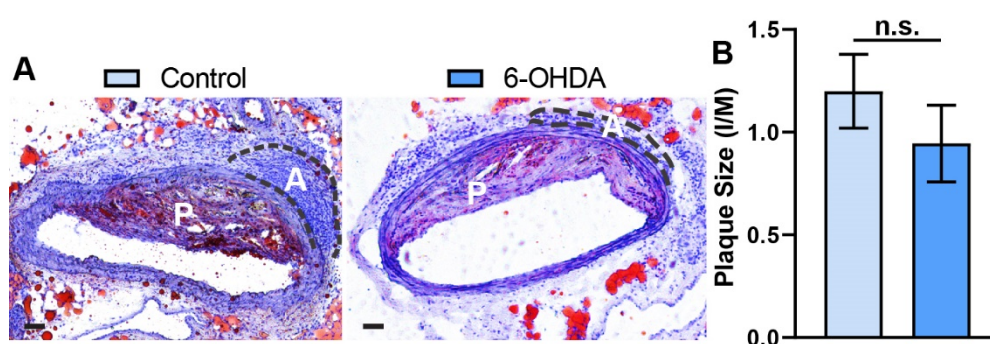


**Figure 23. Atherosclerotic plaque size was not changed in aged mice after short term 6-OHDA treatment. A)** Representative images of Oil red O/Hematoxylin (OR/H) stained abdominal aorta sections. The dotted line delineates ATLO (A), and P indicates atherosclerotic plaque. 10  $\mu$ m fresh frozen sections of the abdominal aorta were stained with OR/H. Scale bar: 50 $\mu$ m. **B)** Quantitative analysis of the plaque sizes in the abdominal aorta. Plaque size was presented as intima (I) area/media (M) area ratio. On average, 12 aorta sections per mouse were evaluated. N =5 control mice and 6 6-OHDA-treated mice. Data represent means  $\pm$  SEM; two-tailed Student's t-test, n.s.: not significant.

## RESULTS

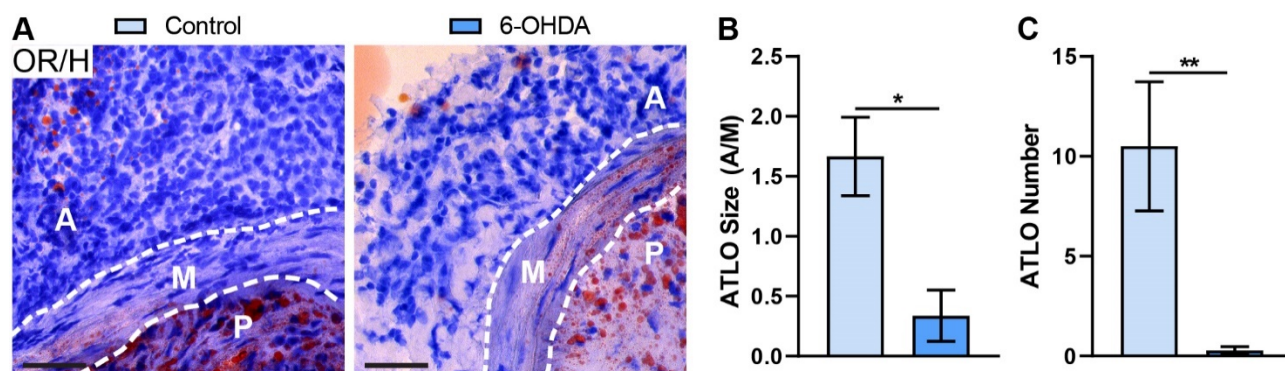


**Figure 24. ATLO size and numbers were reduced in aged mice after 6-OHDA treatment.** **A)** Representative images of OR/H stained abdominal aorta sections of control and treated mice in higher magnification. The dotted line delineates the media (M), A indicates ATLO, and P indicates atherosclerotic plaque. 10  $\mu$ m fresh frozen sections of the abdominal aorta were stained with OR/H. Scale bar: 50 $\mu$ m. **B)** Quantitative analysis of the ATLO size (A) normalized to the media (M) area. **C)** Quantitative analysis of the ATLO numbers. On average, 12 aorta sections per mouse were evaluated. N =5 control mice and 6 treated mice. Data represent means  $\pm$  SEM; two-tailed unpaired Student's t-test, \*:  $p < 0.05$ ; \*\*:  $p < 0.01$ .

### 3.4.2.6 Effect of 6-OHDA denervation on ATLO cellularity

To determine the effect of 6-OHDA treatment on the cellularity of the ATLO in more detail, sections of the abdominal aorta were stained with the combinations of CD3e/B220 and CD3e/Foxp3 antibodies. The representative images demonstrate that both the T and B cells in ATLOs were reduced in 6-OHDA-treated mice *vs.* age-matched controls to a similar extent (Fig.25.A&B). Of special interest was our observation that 6-OHDA disrupted the separate B cell versus T cell areas, which occurs in advanced stage 2 or 3 ATLOs. Moreover, quantitative data demonstrated that CD3e<sup>+</sup>Foxp3<sup>+</sup> T<sub>reg</sub> cells increased about 2-fold upon treatment (Fig.25.C).

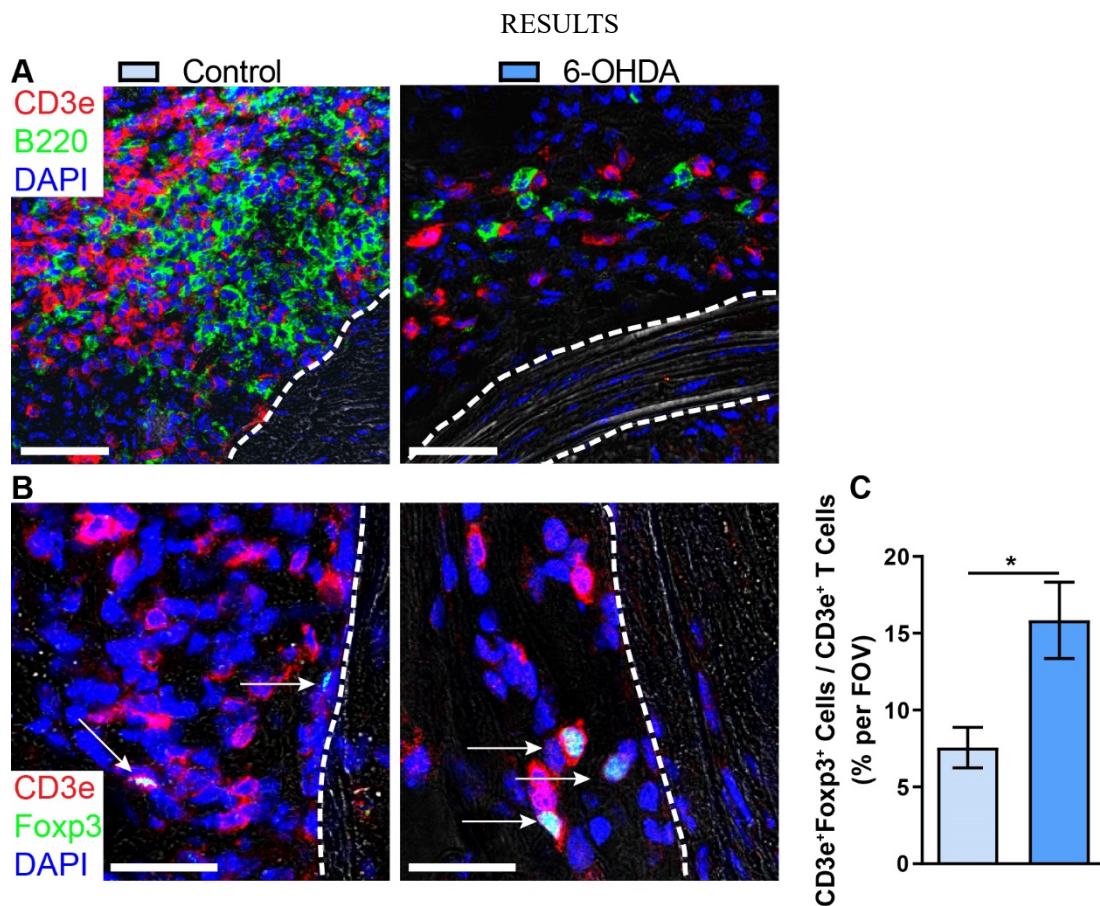


**Figure 25. Dramatic alterations of ATLO structure following 6-OHDA treatment.** **A)** Representative images of CD3e/B220 stained abdominal aorta sections. 10  $\mu$ m fresh frozen abdominal aorta sections of control and 6-OHDA-treated mice were stained for CD3e<sup>+</sup>/B220<sup>+</sup> T and B cells. CD3e was stained red; B220 was stained green; DNA was stained blue. The dotted line delineates media. Scale bar: 20  $\mu$ m. **B)** Representative images of CD3e/Foxp3 stained abdominal adventitia, showing the CD3e<sup>+</sup>Foxp3<sup>+</sup> T<sub>reg</sub> cells. 10  $\mu$ m fresh frozen abdominal aorta sections of ATLO-like structures from control and 6-OHDA-treated mice were stained for CD3e<sup>+</sup>Foxp3<sup>+</sup> T<sub>reg</sub> cells. CD3e was stained red; Foxp3 was stained green; DNA was stained blue. Scale bar: 20 $\mu$ m. **C)** Quantitative analysis of CD3e<sup>+</sup>Foxp3<sup>+</sup> T<sub>reg</sub> cell density in ATLO. The number of counted CD3e<sup>+</sup>Foxp3<sup>+</sup> cells among the CD3e<sup>+</sup> T cells in the field of view (FOV). N = 10 aorta sections per mouse in 3 control mice and 4 6-OHDA-treated mice. Two-tailed unpaired Student's t-test, \*: p<0.05.

### 3.4.2.7 Effect of chemical sympathectomy on cellularity and structures in plaques

Macrophages, SMCs, necrotic core area, fibrous cap thickness, and collagen area in abdominal aorta plaques were stained and quantified. The macrophage area in plaque was not significantly altered upon treatment (Fig.26.B), whereas plaque SMC area was significantly increased (Fig.27.B). In 6-OHDA treated mice, the necrotic core area showed a tendency of decreasing, but not significant

## RESULTS

(Fig.28.B); however, the fibrous cap thickness increased  $\sim 70\%$  of the control group (Fig.28.C). In addition, the collagen area increased significantly (Fig.29.B). Overall, the plaque vulnerability index (PVI) calculated as the ratio of the vulnerable area (necrotic core area + macrophage area) and stable fibromuscular area (collagen area + smooth muscle cell area) was markedly decreased in mice with chemical sympathectomy (Fig.29.C), suggesting that the short treatment period of 4 weeks was sufficient to induce more stable abdominal aorta plaques in aged mice.

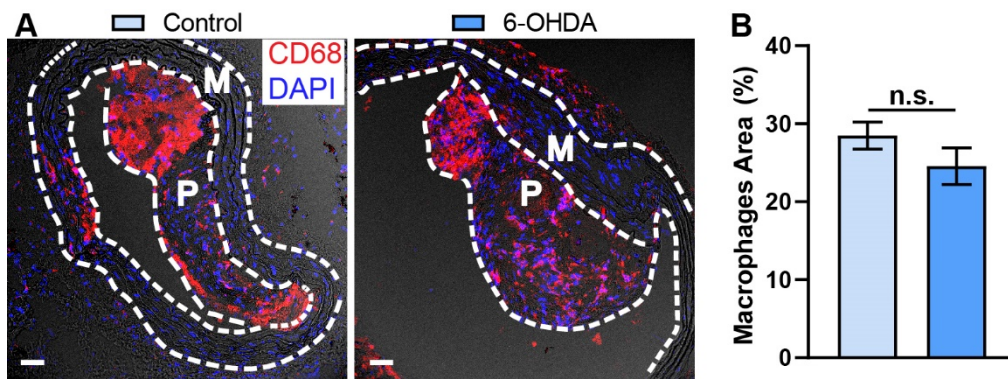


**Figure 26. No changes occurred in plaque macrophage content in 6-OHDA-treated aged mice.** **A)** Representative images of macrophage (CD68, red) staining in 10  $\mu\text{m}$  thick fresh frozen abdominal aorta sections; DNA was stained with DAPI (blue). The dotted line delineates media (M) and plaque (P). Scale bar: 100  $\mu\text{m}$ . **B)** Quantitative analysis of macrophage areas per total plaque area. On average, 8~10 sections per mouse were analyzed in 5 control mice and 4 6-OHDA-treated mice. Data represent means  $\pm$  SEM; two-tailed unpaired Student's t-test, \*:  $p < 0.05$ ; n.s.: not significant.

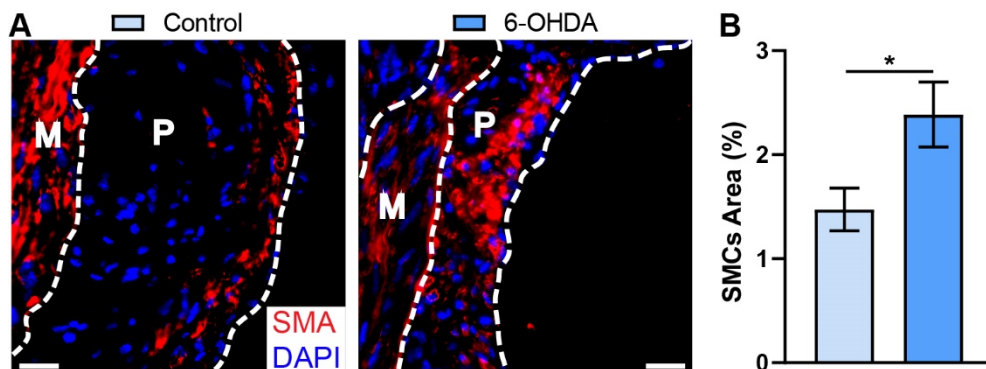


**Figure 27. Plaque SMC content increased in aged mice after 6-OHDA treatment.** **A)** Representative images of SMA (red) staining of SMCs in abdominal aorta (10  $\mu\text{m}$  frozen sections); DNA was stained with DAPI (blue). The dotted line delineates media (M) and plaque (P). Scale bar: 100  $\mu\text{m}$ . **B)** Quantitative analysis of SMC area in percent of total plaque area. On average, 10 sections per mouse,  $n = 3$  mice per group. Data represent means  $\pm$  SEM; two-tailed unpaired Student's

## RESULTS

t-test, \*:  $p < 0.05$ ; n.s.: not significant.

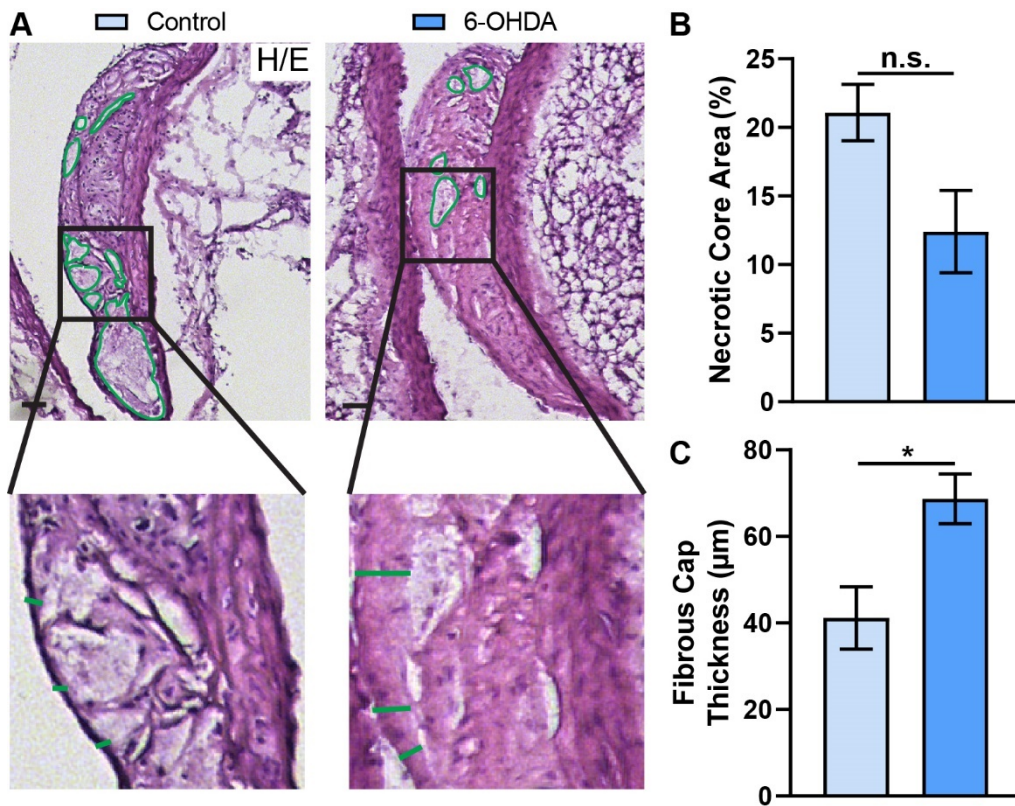
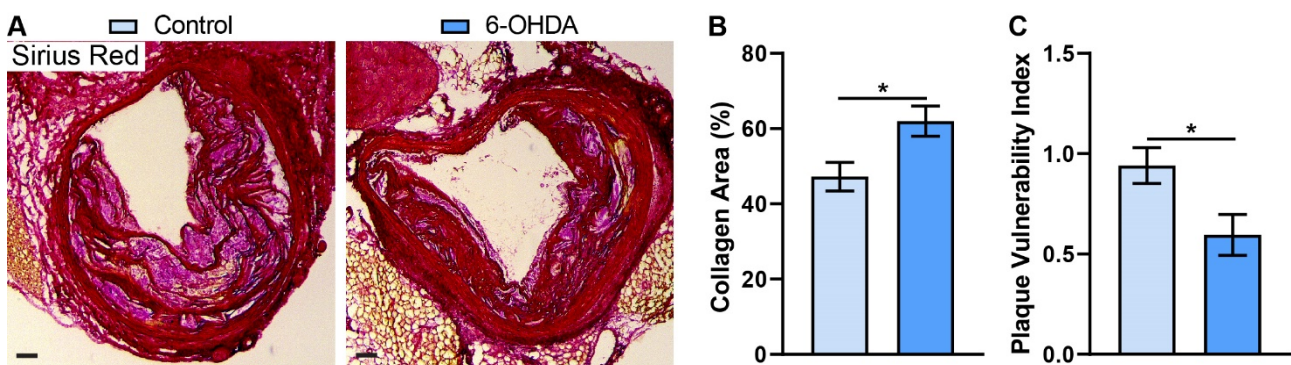


**Figure 28. Fibrous cap thickness increased, but no change in necrotic core size in plaque of aged mice in short time window of 4 weeks of 6-OHDA treatment.** **A)** Representative images of Hematoxylin/Eosin (H/E) stained abdominal aorta sections (10  $\mu\text{m}$  cryosection), showing the necrotic core areas (circles) and fibrous cap thickness (short straight lines) in plaques. Scale bar: 100  $\mu\text{m}$ . **B)** Quantitative analysis of necrotic core area in total plaque area. **C)** Quantitative analysis of fibrous cap thickness in plaques. On average, 12 aorta sections per mouse were evaluated. N = 4 control mice and 3 treated mice. Data represent means  $\pm$  SEM; two-tailed unpaired Student's t-test, \*:  $p < 0.05$ ; n.s.: not significant.



## RESULTS

**Figure 29. Collagen area in plaque increased; the PVI decreased within the short time window of 4 weeks of 6-OHDA treatment.** **A)** Representative images of Sirius red stained abdominal aorta sections (10  $\mu\text{m}$  cryosection), showing the collagen area in plaques. Scale bar: 100 $\mu\text{m}$ . **B)** Quantitative analysis of collagen areas in total plaque areas. **C)** Quantitative analysis of the plaque vulnerability index in the abdominal aorta of control and 6-OHDA-treated mice. On average, 12 aorta sections per mouse were evaluated. N = 4 control mice and 4 treated mice. Data represent means  $\pm$  SEM; two-tailed unpaired Student's t-test, \*:  $p < 0.05$ ; n.s.: not significant.

### 3.4.2.8 6-OHDA did not significantly affect TH<sup>+</sup> neurons in the CNS

Published studies demonstrated that the blood-brain barrier was compromised in *ApoE*<sup>-/-</sup> mice<sup>178</sup> raising the possibility that 6-OHDA could affect TH<sup>+</sup> neurons in the CNS. TH staining was therefore performed in the locus coeruleus (LC) area (Fig.30.A), which contained numerous TH<sup>+</sup> neurons (Fig.30.B&C). Our data demonstrated that the TH<sup>+</sup> neuron percentage per total neurons did not change (Fig.30.D). These data are in line with the previous finding that 6-OHDA selectively depletes sympathetic nerve terminals in the periphery, but not in the central nervous system<sup>179</sup>.

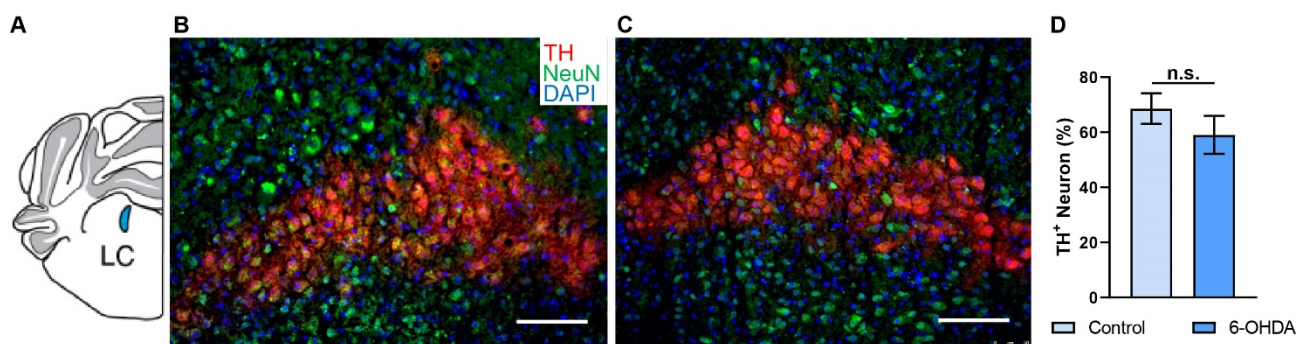


**Fig.30. 6-OHDA treatment did not affect SNS neurons in the CNS of aged mice in 6-OHDA treatment.** **A)** Schematic depiction of the LC, according to Allen's mouse brain atlas<sup>180</sup>. **B, C)** Representative images of TH (red)/NeuN (green) stained 20  $\mu\text{m}$  brain cryosections, showing the LC area. Nuclei were stained with DAPI (blue). Scale bar: 100  $\mu\text{m}$ . **D)** Quantitative analysis of TH<sup>+</sup> neurons. 3 brain sections per mouse were evaluated. N = 3 control mice and 3 6-OHDA-treated mice. Data represent means  $\pm$  SEM; two-tailed unpaired Student's t-test, n.s.: not significant.

### 3.5 Surgical sympathectomy by celiac ganglionectomy

Recently, our group demonstrated via imaging that the celiac ganglion directly projects axons to the abdominal aorta adventitia (Mohanta S. K. *et al.* 2020, *under review*). In collaboration with Profs. Carnevale and Lembo, we performed surgical ganglionectomy to study the effect of local sympathectomy on the development of atherosclerosis and ATLOs using denervation of celiac ganglia (CGX) for extended periods of time thereafter, i.e., a method that they have pioneered<sup>68</sup>. CGX was performed on *ApoE*<sup>-/-</sup> male mice at 8 months of age, subsequently maintained for 8 months, and then sacrificed for a comprehensive evaluation of atherosclerosis and the immune system (Fig.31.). Surgical experiments were performed in the laboratory of Carnevale and Lembo while I sacrificed the mice with my colleagues, collected the aortas and other tissues, and transferred them to our laboratory in Munich for further analyses (see below).

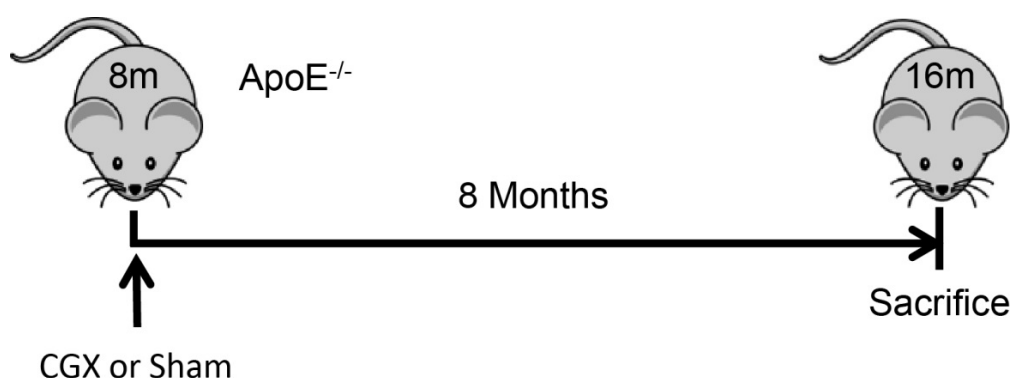


**Figure 31. Workflow of CGX in aged mice.** Surgical excision of celiac ganglia (CGX) or sham surgery was performed at the age of 8 months, and mice were sacrificed 8 months after surgery.

#### 3.5.1 Tissue NE concentration was reduced after 8 months in CGX mice

To determine the specificity of CGX in prototypical target organs of the celiac ganglion, the NE concentrations in the spleen were determined. NE concentration in the spleen of CGX mice was significantly reduced *vs.* the sham group at the end of the 8 months time window (Fig.32.). It is noteworthy that the degree of decrease in spleen NE tissue concentration did not reach the level of what was achieved by systemic 6-OHDA treatment.

## RESULTS

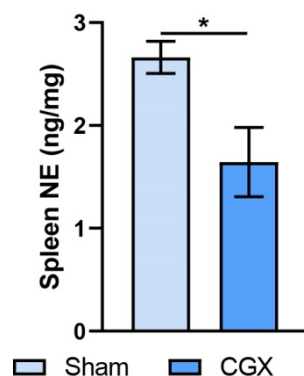


**Figure 32.** NE concentrations were reduced in the spleen upon CGX. Splenic NE concentrations in CGX and Sham groups. N = 4 sham mice and 6 CGX mice. Data represent means  $\pm$  SEM; two-tailed unpaired Student's t-test, \*:  $p < 0.05$ .

### 3.5.2 Effect of celiac ganglionectomy on physiological parameters in aged mice

To monitor the status of the treated animals, body weights were measured every two months, by our collaborators Profs. Carnevale and Lembo. The data demonstrated that the bodyweight of the mice in the CGX and control groups increased over time, but no significant difference among them (data not shown; *Mohanta S. K. et al. 2020, under review*). In addition, the body weights of the two groups were also measured before the sacrifice, and the data did not show a significant difference at the endpoint (Fig.33.A). To determine the effect of the surgical denervation on organs, the weights of spleen, heart, and kidney were determined. Based on the body weight of the animals, the ratios relative to the body weights were calculated. The normalized organ weights expressed as organ weight per body weight ratio did not show significant differences between the sham and CGX groups (Fig.33.B). To determine whether the surgical sympathectomy affected plasma lipids in the circulation, the plasma samples were taken before sacrifice. However, the analysis of total cholesterol revealed comparable levels between the two groups (Fig.33.C). Interestingly, we observed in some of these basic parameters different outcomes following chemical sympathectomy via 6-OHDA treatment or local surgical removal of the celiac ganglion.

## RESULTS

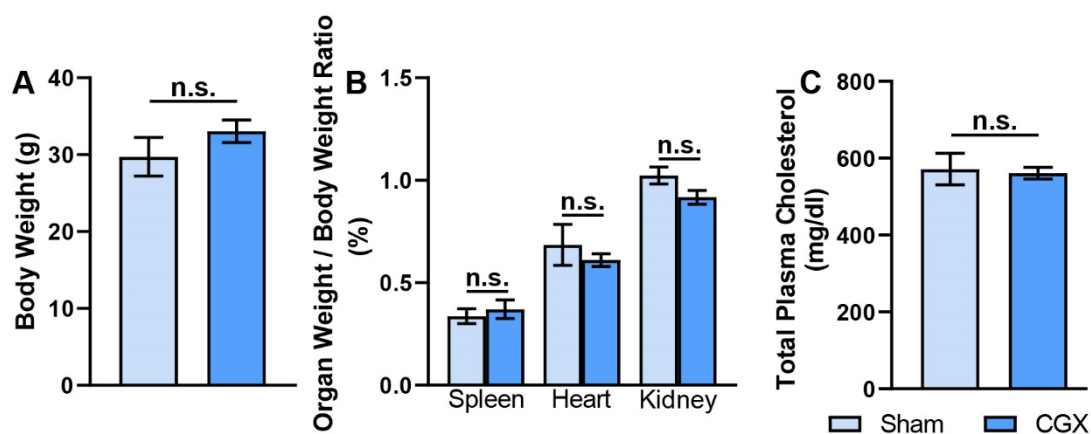


**Fig.33. Body weight, organ weights and plasma cholesterol did not change after prolonged periods following CGX.**

**A)** The body weight of the animals of the two groups was measured on the day of sacrifice i.e., after 8 months of surgery. N = 3 sham mice and 9 CGX mice. **B)** Ratios of organ weight/body weight of spleen, heart, and liver, calculated per organ and individual animal. N = 3 sham mice and 9 CGX mice. **C)** Total plasma cholesterol concentrations. N = 3 sham mice and 9 CGX mice. Data represent means  $\pm$  SEM; two-tailed unpaired Student's t-test, \*,  $p < 0.05$ ; n.s.; not significant.

### 3.5.3 Effect of CGX on immune cells in SLOs

Our data on chemical sympathectomy groups demonstrated that the  $CD11b^+CD11c^-$  myeloid cell population increased in spleen, but not in paraaortic LNs of adult and aged mice, while  $CD11b^+CD11c^+$  monocyte-derived DCs decreased in the spleen rather than in paraaortic LN of adult mice. Based on these data, we further examined the effects of SNS on the regulation of these myeloid cells. T-distributed stochastic neighbor embedding (t-SNE) is a newly developed algorithm, which gives each multi-dimensional data point a location in a two-dimensional map to achieve visualization of such data<sup>181</sup>. It had widely been used to interpret complex biological datasets by making the high-dimensional data to be easily understood. We used t-SNE analysis to determine the effect of CGX on immune cells in spleens and LNs. The t-SNE analysis of  $CD45^+$  leukocytes illustrates the finding that myeloid cells overall decreased by 60% in spleens of CGX mice (Fig.34.A), but not in the LNs of the CGX mice *vs.* age-matched sham mice (Fig.34.B).

## RESULTS

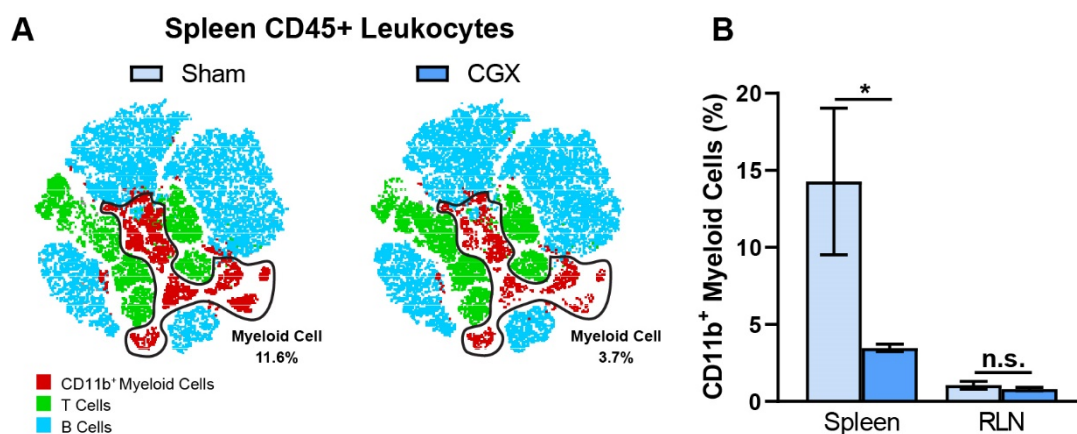


**Figure 34. Effect of CGX on immune cells in SLOs.** **A)** t-SNE analysis of the CD45<sup>+</sup> leukocytes showing the CD11b<sup>+</sup> myeloid cell populations in spleens are massively reduced, while the T cells were unchanged. **B)** Flow cytometric quantification of CD11b<sup>+</sup> myeloid cells in sham and CGX groups. N = 3 spleens of sham mice, 4 spleens of CGX mice, 4 LNs of sham mice, and 3 LNs of CGX mice. Data represent means ± SEM; two-tailed unpaired Student's t-test, \*: p < 0.05; n.s.: not significant.

### 3.5.4 Effect of local sympathetic denervation on plaque and ATLO size

To determine the effect of CGX on plaque and ATLO, we sectioned the abdominal aorta and quantified plaque sizes after the sacrifice of 8 months. Plaque sizes were significantly smaller in CGX mice versus the sham group (Fig.35.A & B). Consistent with the observation after short-term chemical sympathectomy, CGX reduced the numbers (Fig.36.B) and sizes (Fig.36.C) of ATLOs. These data support that SNS input via the celiac ganglion affects the inflammatory infiltrate of the adventitia in *ApoE*<sup>-/-</sup> mice, and in particular, in ATLOs. It should be noted, however, that the celiac ganglion gives rise to the splenic nerve and therefore, CGX, not only affected sympathetic nerves that directly innervated the adventitia but also the spleen, with possible effects on splenic myeloid cells.

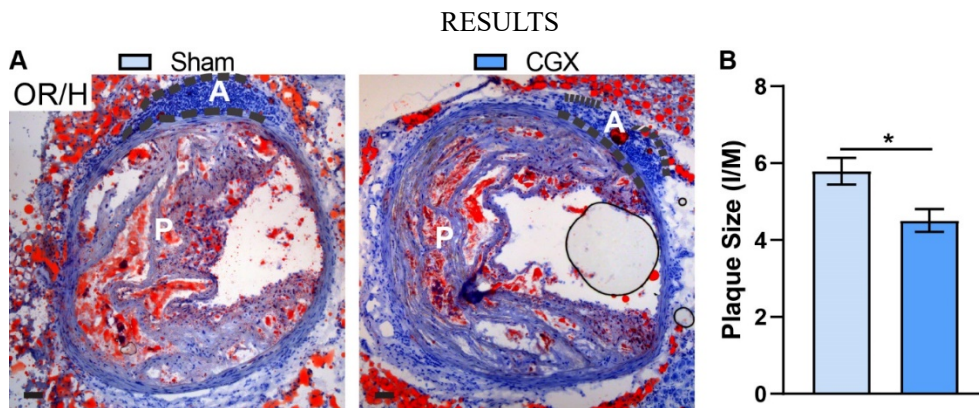


**Figure 35. Abdominal aorta plaque and ATLO size decreased following prolonged CGX.** A) Representative images of OR/H stained abdominal aorta cross-sections (10 μm cryosection) from sham and CGX mice. P indicates atherosclerotic plaque, and A indicates ATLO. Scale bar: 20μm B) Quantitative analysis of plaque sizes, calculated as intima (I) area normalized to the media (M) area. Approximately 16 serial abdominal aorta cross-sections per mouse were evaluated. N = 5 sham mice and 9 CGX mice. Data represent means ± SEM; two-tailed unpaired Student's t-test, \*: p<0.05.

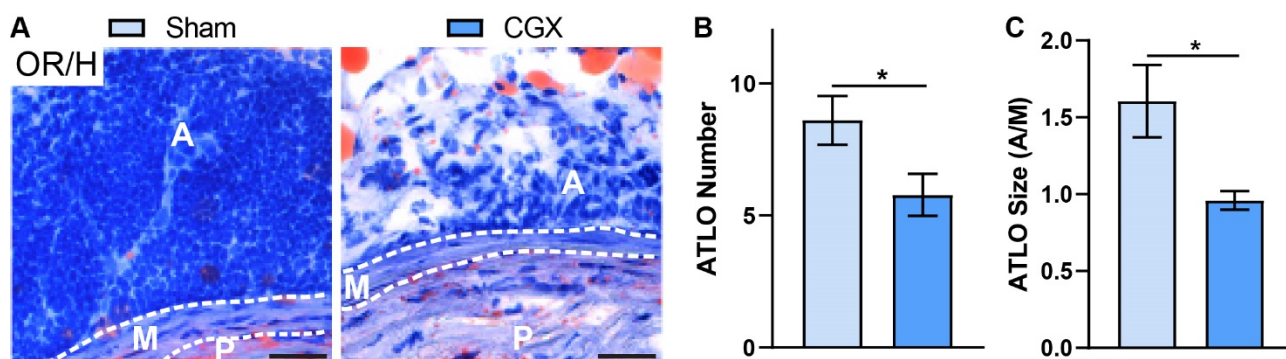


**Figure 36. ATLO number and size were reduced in aged mice after CGX treatment.** A) Representative images of OR/H stained abdominal aorta sections (10μm cryosection) from sham and CGX mice in higher magnification. The dotted line delineates media (M), P indicates atherosclerotic plaque, and A indicates ATLO. Scale bar: 50μm. B) Quantitative analysis of the ATLO numbers in the abdominal aorta. C) Quantitative analysis of the ATLO size (A) normalized to the media (M) area. On average, 16 serial abdominal aorta cross-sections per mouse were evaluated. N =5 sham mice and 9 CGX mice. Data represent means ± SEM; two-tailed unpaired Student's t-test, \*: p<0.05.

### 3.5.5 Effect of CGX on ATLO cellularity

To determine the effect of CGX on the cellularity of the ATLO in more detail, sections of the

## RESULTS

abdominal aorta were stained with the combination of CD3e/B220 antibodies. The representative images demonstrate that both the T and B cells in ATLOs were reduced in CGX mice *vs.* age-matched controls (Fig.37). Similar to the chemical sympathectomy, CGX denervation disrupted the separate B cell versus T cell areas, which occurs in advanced stages of ATLOs.

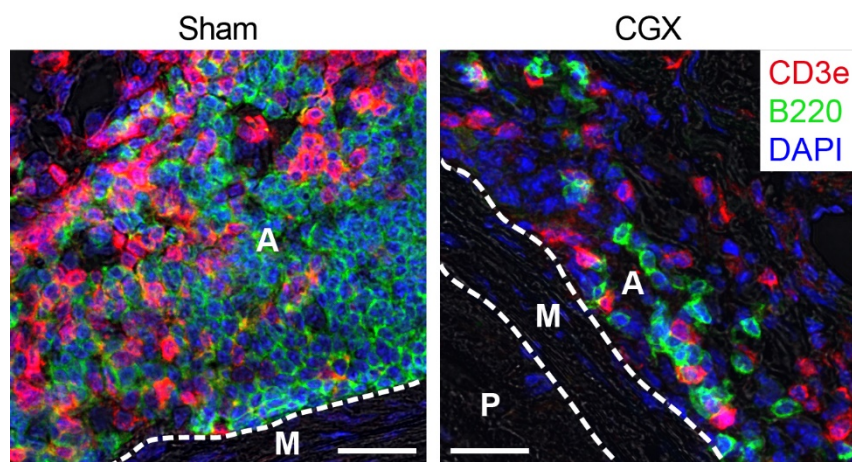


**Figure 37. Dramatic alterations of ATLO structure following CGX.** Representative images of B cell (B220, red) and T cell (CD3e, green) staining in abdominal aorta, 10  $\mu$ m fresh frozen abdominal aorta sections of sham, and CGX - treated mice were stained for CD3e<sup>+</sup>/B220<sup>+</sup> T and B cells. Dotted line delineates media (M), A indicates ATLO, and P indicates atherosclerotic plaque. Scale bar: 200  $\mu$ m.

### 3.5.6 Effect of prolonged CGX on plaque vulnerability

To assess possible changes in abdominal aorta plaque composition, immunostaining of macrophages and SMCs was performed, as well as histological analysis of collagen content, necrotic core, and fibrous cap thickness. The analyses revealed a significant decrease in the relative plaque macrophage area (Fig.38.B). However, the SMC area increased by about 2 fold (Fig.39.B). The necrotic core area was significantly reduced (Fig.40.B), while fibrous cap thickness (Fig.40.C) and the collagen plaque content were significantly increased (Fig.41.B). As a result, the plaque vulnerability index was significantly decreased (Fig.41.C), suggesting that CGX increased plaque stability in aged mice.

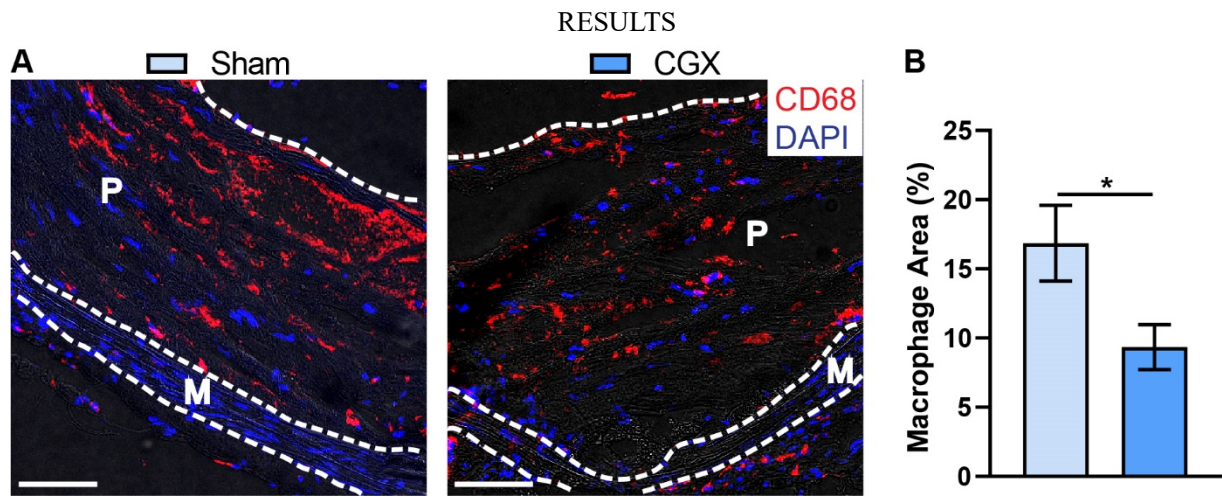


**Figure 38. Macrophage area in atherosclerotic plaque decreased following CGX.** **A)** Representative images of macrophage (CD68, red) staining in 10  $\mu$ m thick fresh frozen abdominal aorta sections; DNA was stained with DAPI (blue). The dotted line delineates media (M) and plaque (P). Scale bar: 200  $\mu$ m. **B)** Quantitative analysis of macrophage areas per total plaque area. On average, 10~16 aorta sections per mouse were analyzed in 5 sham mice and 6 CGX mice. Data represent means  $\pm$  SEM; two-tailed unpaired Student's t-test, \*:  $p < 0.05$ .

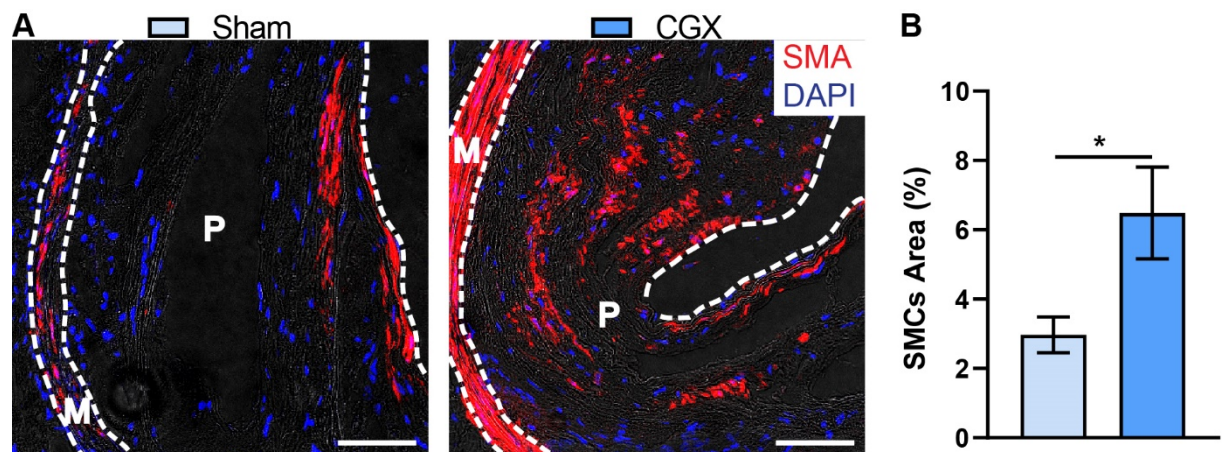


**Figure 39. SMCs area in plaque increased in aged mice after CGX.** **A)** Representative images of SMCs (SMA, red) staining in 10  $\mu$ m thick fresh frozen abdominal aorta sections; DNA was stained with DAPI (blue). The dotted line delineates media (M) and plaque (P). Scale bar: 200  $\mu$ m. **B)** Quantitative analysis of SMC areas per total plaque area. On average, 10~16 sections per mouse were analyzed in 5 sham mice and 6 CGX mice. Data represent means  $\pm$  SEM; two-tailed unpaired Student's t-test, \*:  $p < 0.05$ .

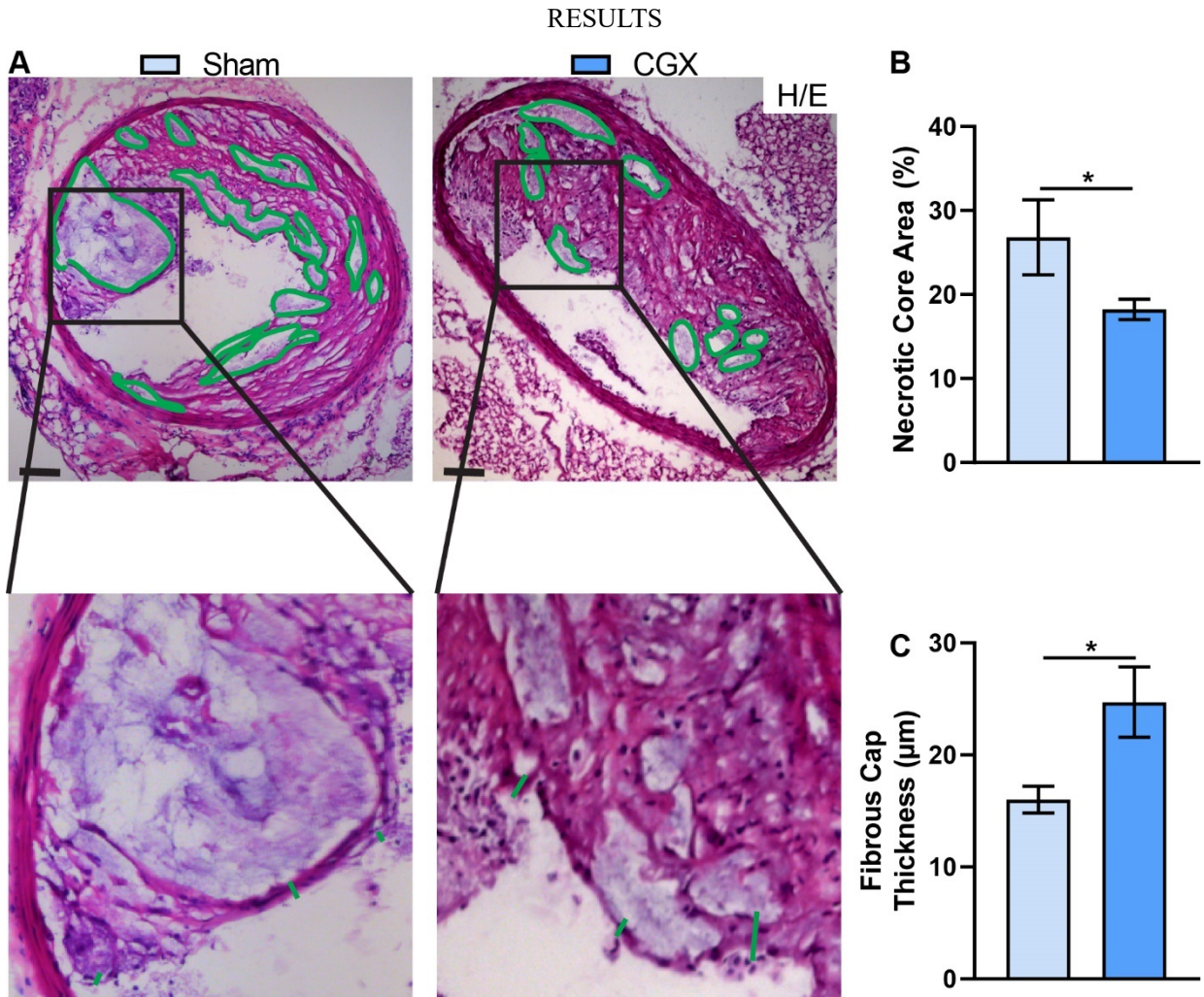


**Figure 40. Necrotic core area decreased, and fibrous cap thickness increased following CGX.** A) Representative images of H/E stained abdominal aorta sections (10 µm cryosection), showing the necrotic core (circles) and fibrous cap (short straight lines) in plaques. Scale bar: 20µm. B) Quantitative analysis of necrotic core area in total plaque area. C) Quantitative analysis of fibrous cap thickness in plaques. On average, 12 ~ 16 aorta sections per mouse were evaluated. N = 5 sham mice and 6 CGX mice. Data represent means ± SEM; two-tailed unpaired Student's t-test, \*:  $p < 0.05$ .

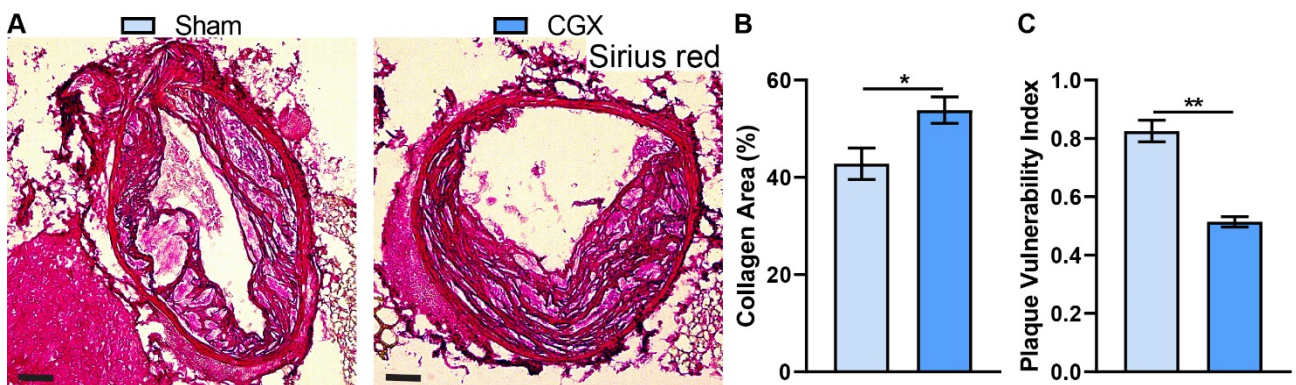


**Figure 41. Collagen areas increased, and the PVI decreased in aged mice upon CGX.** A) Representative images of

## RESULTS

Sirius red stained abdominal aorta sections (10  $\mu\text{m}$  cryosection), showing the collagen areas in plaques. Scale bar: 50 $\mu\text{m}$ .

**B)** Quantitative analysis of the collagen area in total plaque areas. **C)** Quantitative analysis of the PVI in abdominal aorta of sham and CGX mice. On average, 12 ~ 16 aorta sections per mouse were evaluated. N = 5 sham mice and 6 CGX mice.

Data represent means  $\pm$  SEM; two-tailed unpaired Student's t-test, \*:  $p < 0.05$ ; \*\*:  $p < 0.01$ .

## 4. DISCUSSION

Data described above support the conclusion that the SNS engages in a tripartite model, in which it bidirectionally interacts with both the immune system and the diseased arterial wall in a highly territorialized way: The neurotransmitter NE is selectively up-regulated in the adventitia of atherosclerotic aorta segments; TH<sup>+</sup> axon density specifically increases in atherosclerotic adventitia segments reaching maximal levels in ATLOs; multiple genes regulating axon neogenesis and other neuroimmune mediators exclusively increase in atherosclerotic adventitia segments whereas axon repellants decrease; both chemical and surgical SNS denervation by 6-OHDA and CGX, respectively, disrupt ATLO structure and size; plaque vulnerability decreases by both systemic chemical and surgical CG denervation, respectively, in aged *ApoE*<sup>-/-</sup> mice; and most importantly, the SNS affects atherosclerosis progression via the CG and possibly via one of its major nerves, i.e., the splenic nerve. When taken together, our analyses support a concept of neuroimmune cardiovascular interfaces in the healthy artery and that these interfaces undergo major restructuring events in those adventitia segments that are burdened by atherosclerosis. Adventitial neuroimmune cardiovascular interfaces establish biological platforms that allow the efferent SNS to affect the immune system and *vice versa* enables the immune system to alert the peripheral SNS. The discovery of such an unexpected novel crosstalk may provide a host of novel opportunities to develop new therapeutic strategies to treat atherosclerosis, by interfering with the regulatory role of the SNS in atherosclerotic plaque progression and stability (Fig.40 & Table 9).

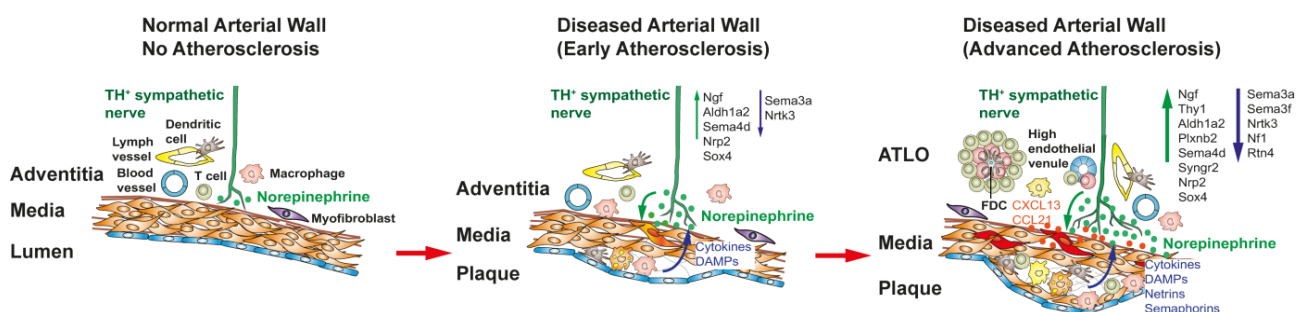


**Figure 40.** The adventitia of diseased artery segments is a biological platform for the interaction of the SNS with both the immune system and the cardiovascular system. Left panel: The adventitia is innervated by the SNS in normal arteries; middle panel: tyrosine hydroxylase positive axons begin to increase (axon neogenesis) and release

## DISCUSSION

norepinephrine in response to plaque formation in the intima; right panel: ATLOs in the adventitia interact with the SNS and the arterial wall in advanced atherosclerosis; green arrow up in middle and right panels: genes involved in axon neogenesis; blue arrow down in middle and right panels: genes involved in inhibition (axon repellants) and guidance of axons. Abbreviations: FDC, follicular dendritic cell; danger-associated molecular patterns, damage-associated molecular patterns; Ngf, nerve growth factor; Aldh1a2, aldehyde dehydrogenase 1 family member A2; Sema4d, semaphorin 4D; Plxnb2, plexin B2; Syngn2, synaptogyrin 2; Nrp2, neuropilin 2; Sox4, SRY-box transcription factor 4; Nrtk3, neurotrophic receptor tyrosine kinase 3; Nf1, Neurofibromin 1; Rtn4, reticulon 4.

Approach	Effects on Plaque	Effects on ATLO
<b>4 weeks chemical sympathectomy</b>	<div style="display: flex; justify-content: space-between;"> <div style="text-align: center;"> <span style="color: green;">↓</span> Vulnerability                 </div> <div style="text-align: center;"> <span style="color: red;">↑</span> SMC Collagen Fibrous cap                 </div> </div>	<div style="display: flex; justify-content: space-between;"> <div style="text-align: center;"> <span style="color: green;">↓</span> ATLO number ATLO size T/B cell                 </div> <div style="text-align: center;"> <span style="color: red;">↑</span> Treg                 </div> </div>
<b>8 months celiac ganglionectomy</b>	<div style="display: flex; justify-content: space-between;"> <div style="text-align: center;"> <span style="color: green;">↓</span> Plaque size Macrophage Necrotic core Vulnerability                 </div> <div style="text-align: center;"> <span style="color: red;">↑</span> SMC Collagen Fibrous cap                 </div> </div>	<div style="text-align: center;"> <span style="color: green;">↓</span> ATLO number ATLO size T/B cell                 </div>

**Table 9. Effects of SNS denervation in atherosclerosis and ATLO.** Four weeks of chemical sympathectomy reduced the number of T<sub>reg</sub> cells in ATLOs of aged *ApoE*<sup>-/-</sup> mice. Eight months after CGX, the plaque macrophage area is reduced, as are the necrotic core area and the plaque size. The plaque vulnerability index is decreased, and the SMC area, collagen area, and the fibrous cap thickness are all increased; moreover, the ATLO number and size and the lymphocyte numbers in ATLOs decreased after both chemical and surgical sympathectomy.

### 4.1 Territoriality of the arterial SNS innervation in atherosclerosis

To understand neuroimmune crosstalk in atherosclerosis, it was important to define the anatomy of SNS innervation in arterial wall laminae. It is well established that the SNS uses the adventitia medium-sized or large-sized arteries as its main conduit to reach its targets, indicating strict regulatory mechanisms of axon network formation in both physiology and disease<sup>182,183</sup>. Axon guidance is regulated by a balance of axon neogenesis-stimulating genes and axon repellants, resulting in a well-controlled SNS network. Our results show that nerve axons from perivascular sympathetic ganglia and nerves extend into the adventitia but not the media of the normal WT aorta. The SNS is restricted to the lamina adventitia, while the lamina media, as well as lamina intima of the arterial wall, is devoid

## DISCUSSION

of any TH<sup>+</sup> sympathetic axons, although few axons were detected in the media/adventitia border (Fig.7 & 8). Earlier studies of our group showed that adventitia axon density gradually increases along the aortic tree in healthy WT mice (Mohanta S. K. et al. 2020, under review). We further observed that sympathetic axon density was higher in the abdominal aorta adventitia segment of aged WT mice compared to the aortic root (Fig.7 & 8). Interestingly, NE tissue concentrations increased in blood and arteries during aging in WT mice (Fig.6). In the diseased aorta, we show a further marked increase in adventitia sympathetic innervations preferentially in the aortic root and abdominal aorta segments afflicted with atherosclerosis (Fig.7 & 8). These results were consistent with the idea that atherosclerosis affects the PNS innervation pattern, including its growth and guidance<sup>184-186</sup>. When taken together, these results support the conclusion that the SNS in the arterial wall adventitia undergoes restructuring depending on age and atherosclerotic plaque burden in a highly territorialized fashion<sup>88</sup>.

Furthermore, earlier studies from our lab have shown that in advanced atherosclerosis, the adventitia in the abdominal aorta of aged *ApoE*<sup>-/-</sup> mice was inflamed to form ATLOs<sup>25,45</sup>. ATLOs contain all innate and adaptive immune cells that can be found in SLOs. These immune cells also produce neurotransmitters, neuroendocrine hormones, neuropeptides, and axon guidance molecules<sup>53,56,101,103,129,153,187</sup>. Interestingly, some of these neuronal mediators, such as ephrins and semaphorins, were shown to play potential roles in atherogenesis though none of these studies showed any direct connections with the disease<sup>140,153,154,188-191</sup>. In this study, we observed an ATLO-associated increase in axon density during atherosclerosis progression within the abdominal aorta (Fig.8). Adventitia axon density was more pronounced in atherosclerotic aorta segments with ATLOs when compared to plaque-free *ApoE*<sup>-/-</sup> aorta segments or WT abdominal aorta segments (Fig.8, data not shown), likely reflecting that ATLOs neogenesis promotes atherosclerosis-dependent axon sprouting in the diseased abdominal aorta. These results corroborate our LCM-based microarray analyses (see below). We did not observe TH<sup>+</sup> axons in the adventitia that crossed the ATLO-media border, indicating that axon neogenesis is limited to ATLOs. Multiple lines of evidence reported here support the conclusion that the SNS is locally affected by atherosclerosis and its adjacent inflammatory infiltrates in the adventitia: NE levels selectively increase in adventitia segments that are burdened by atherosclerosis. These data require attention for several reasons: They raise the question of the source of NE in the diseased adventitia segments. Two possible sources should be considered: i. The

## DISCUSSION

SNS axon endings are well known to produce NE, and these data are strongly supported by my findings of TH<sup>+</sup> axon endings in the adventitia; ii. several immune cell lineages and their subtypes have recently been demonstrated to express TH and therefore are likely producers of neurotransmitters, including NE in the adventitia<sup>175</sup>. Cells that have been shown to express TH, i.e., the key enzyme of catecholamine formation, are B cells and macrophages, but T cells are also expressing the enzyme<sup>173</sup>. These data indicate that most likely, there are two independent sources of NE in the inflamed adventitia, particularly in ATLOs: axon endings and immune cells. Irrespective of its source, NE and other catecholamines have a variety of biological effects on the immune system both locally and systemically<sup>91</sup>. In general, catecholamines are stress hormones acting on the immune system in the bone marrow, secondary lymphoid organs such as lymph nodes and spleen<sup>104,175</sup>. Moreover, they affect a number of other cells, including arterial wall cells such as SMCs and endothelial cells to exert not only effects on the vascular tone but also a variety of proinflammatory functions all being considered to be proatherogenic<sup>60,86</sup>. Therefore, catecholamines can be viewed as proinflammatory in many diseases, including cancer<sup>192</sup> and atherosclerosis<sup>90</sup>. Furthermore, FACS analyses of adventitial immune cells also obtained in our group have demonstrated that various types of immune cells express several adrenergic  $\beta$  receptor subtypes, including ADR $\beta$ 2 (*Mohanta S. K. et al. 2020, under review*). However, we observed that there is a differential expression of the three major adrenergic  $\beta$  receptors 1,2,3. In earlier studies, the AD $\beta$ R2 in adventitia innate lymphocytes has been identified as a regulator of atherosclerosis<sup>35</sup>. Certainly, the role and differential expression of AD $\beta$ R subtypes by distinct immune cell subsets in the diseased arterial wall remains to be studied in more detail in the future. Yet, as immune cells directly interact with axon endings of the SNS in the adventitia, we propose that major types of crosstalk may occur in the diseased aorta adventitia, including autocrine adrenergic receptor activation in immune cells and release of NE from axon endings of the SNS.

### 4.2 Site of neuronal responses in the aorta

We observed that SNS axons dramatically increase in adventitia segments of aged *ApoE*<sup>-/-</sup> mice that are affected by atherosclerosis, particularly the segments with ATLOs (Fig.8) and that these newly formed axons are likely to participate in the neuroimmune cardiovascular crosstalk. Other data in our

## DISCUSSION

group demonstrate that the aberrant axons of the SNS also undergo restructuring by the formation of newly formed small diameter axon networks (Mohanta S. K. *et al.* 2020, *under review*). These data lead us to discuss several questions: i) how does atherosclerosis influence adventitia innervations, and ii) how do ATLOs promote axon sprouting in the diseased aorta? Comparison of nervous system gene expression in total aortas of WT versus *ApoE*<sup>-/-</sup> mice during aging revealed a dramatic shift in neuronal gene expression profiles that are involved in the maintenance and development of the NS, particularly at 32 wk and 78 wk *ApoE*<sup>-/-</sup> mice (Fig.9; supplement Table S1). The mining of differential gene expression profiles in diseased whole aortas during aging yielded important candidates of neuroimmune crosstalk including GO terms *nervous system development* (bex1; brain expressed gene; interleukin 6; brain-derived growth factor; nerve growth factor, VCAM1), *autonomic nervous system development* (purinergic receptor P2X, ligand-gated ion channel 4; unc-5, netrin receptor C neurotrophin, neuron navigator 2 which was markedly down-regulated), *sympathetic nervous system development* (a series of semaphorins; neuropilin 2), *regulation of axon guidance* (CXCL12; semaphorins). Each of these genes plays important roles in the PNS, and many of them are mediators of neuroimmune cardiovascular crosstalk, while some of them are genes that can be expressed by neuronal cells and by *bona fide* arterial wall cells such as endothelial cells and SMCs<sup>130,185,186</sup>. For example, neuropilin 2 guides axon growth during nervous system development<sup>156</sup>; neurotrophin 3 supports growth, differentiation, and survival of new neurons in the PNS and CNS<sup>158,159</sup>; semaphorins regulate axon guidance and NS development as well as influence cardiovascular and immune functions<sup>155,185,186</sup>. These data indicated that age-dependent changes in axon growth and guidance factors occur in WT and *ApoE*<sup>-/-</sup> mice (Fig.9; supplement Table S1). These data were particularly pronounced when aorta transcriptomes of laser capture microdissection-derived laminae were mined: When we inspected the transcriptomes of diseased adventitia segments with ATLOs versus other arterial tissue compartments in the normal or diseased aorta, we observed significant up-regulation of multiple SNS genes responsible for axon growth, guidance, and maturation in ATLOs including genes in GO terms *nervous system development*, *neuron projection development*, *axons*, and *regulation of axon guidance* (Fig.10; supplement Table S2). Adventitia segments afflicted with atherosclerotic plaques showed much higher expression of mRNAs coding for Sema4D (semaphorin 4D), multiple other semaphorins, and plxnB2 (plexin B2) when compared to their plaque-free segments, and adventitia segments with ATLOs were the highest among all tissues studied. Semaphorins and plexins are well-established mediators of axon neogenesis<sup>160-162</sup>. In the NS,

## DISCUSSION

CXCL12 is required for neuronal development<sup>193</sup>, migration<sup>194</sup>, axon branching<sup>195,196</sup>, and Sema4D controls axon guidance in hippocampal neurons<sup>197,198</sup>. These results support our morphological evidence on enhanced adventitial sympathetic innervations in *ApoE*<sup>-/-</sup> aorta segments afflicted with plaques and ATLOs. When the laser capture microdissection-based gene expression data are considered, many of the aging-related genes were specifically up- or down-regulated in the adventitial layer of the arterial wall. Importantly, many of the axon pathfinding genes were downregulated in adult and aged *ApoE*<sup>-/-</sup> aorta, which coincides with plaque formation and axon neogenesis. It is plausible that inflammatory signals from intimal plaque activates adventitial sympathetic axons to release NE. According to this scenario, NE would modulate medial SMC phenotypes<sup>199</sup> and would attract leukocytes in the adventitia<sup>200</sup>. ATLO immune cells release axon growth and guidance molecules, including NGF, semaphorins to initiate axon neogenesis<sup>129,201-203</sup> in a feed-back loop (Fig. 40). In addition, ATLOs protect atherosclerosis progression under distinct experimental conditions<sup>27</sup>.

It is further tempting to suggest that the neuronal responses in the normal and diseased aorta might be organized by adventitia and/or ATLOs to participate in arterial wall homeostasis. These data also support the notion that atherosclerosis induces the neuronal responses in the diseased aorta during aging. In addition, our bidirectional neuroimmune crosstalk hypothesis is based on the fact that highly expressed ATLO-specific neuronal transcript such as *Aldh1a1*, *Cxcl12*, *Sema4D*, and *Plxn2* were shown in other models to have pleiotropic roles in the development and maintenance of SLOs<sup>129,204-207</sup>. Moreover, *Raldh1*-expressing nerve axons were found to be increased in ATLOs (data not shown), which were reported to initiate SLO formation during embryogenesis via retinoic acid<sup>208</sup>. Further studies are required to understand the biological network of differentially regulated gene products in the aged diseased arterial wall and how they relate to atherosclerosis pathogenesis. Single-cell transcriptome analyses of the diseased aorta will help to identify and quantify transcripts coding for enzymes involved in NE biosynthesis in immune cell subtypes in the inflamed aorta adventitia and in particular in ATLOs in addition to TH<sup>+</sup> SNS axon endings as reported here. These studies are currently being performed in our group. To fully understand the effects of the SNS on the diseased arterial wall, such studies need to analyze other cells involved in atherosclerosis, i.e., SMCs and endothelial cells as well.

### 4.3 Immunometabolic effects of SNS denervation

Another aspect of the current data requires consideration: 6-OHDA specifically and systemically denervates the SNS<sup>73,90</sup>. It has been shown to affect stress-induced inflammatory responses in myocardial infarction<sup>88</sup> apparently via a bone marrow-derived myeloid axis that involves the spleen reservoir of myeloid cells. Using 6-OHDA, we confirmed a series of previously reported effects of chemical SNS denervation, including effects of the drug on the bone marrow, secondary lymphoid organs, and the circulation<sup>74,91,173,175</sup>. In addition, we observed that 6-OHDA had a major effect on the gonadal white adipose tissue in adult mice that has not previously been reported. In view of the impacts of the SNS in regulating metabolism in adipose tissue (we did not observe apparent decreases in the visceral white adipose tissue of the peritoneum), it will be important to investigate the effects of 6-OHDA on energy metabolism and brown adipose tissue metabolism including body temperature using single-cell transcriptome analyses of both immune cells and adipocytes. Since a multitude of effects of 6-OHDA on the immune system were evident, we reasoned, however, that the drug is not well suited to study its effect on atherosclerosis progression in long-term experiments: given the many effects of 6-OHDA on multiple immune cell subtypes at different locations of the immune system including the bone marrow, data would be very difficult to interpret regarding specific actions on atherosclerosis progression. For this purpose, we examined the effect of surgical SNS denervation in long-term CGX studies on atherosclerosis in collaboration with our collaborators Profs. Carnevale and Lembo at IRCCS Neuromed, Pozzilli, Italy. These studies allowed us to compare the systemic effects of 6-OHDA on adventitial immunity with that of local SNS denervation using CGX.

### 4.4 Sympathetic denervation prevents athero-progression

Earlier, members of our group used tissue clearing approaches to demonstrate that the celiac ganglion directly innervates the abdominal aorta adventitia (*Mohanta S. K. et al. 2020, under review*). In parallel studies, our colleagues in Italy performed CGX to selectively deplete the celiac ganglion, which is a major peripheral SNS ganglion innervating the abdominal aorta. We had the opportunity to examine the acute (4 weeks of time window) effects of 6-OHDA on aorta immunity in *ApoE*<sup>-/-</sup> mice during aging and compare these effects with that of long-term CGX within a time window of 8 months after surgery. Surprisingly, 6-OHDA (within a period of 2 weeks) leads to rapid collapse and

## DISCUSSION

disintegration of structures of ATLOs, including the disappearance of separate B cell and T cell areas, reduction of ATLO sizes and an increase in adventitial T<sub>reg</sub> cells. In view of previous data of our group that the turnover of naïve T cells is rapid in ATLOs, these data indicate a rapid effect of the SNS on arterial wall immunity. It is likely that the effect of 6-OHDA is specifically due to an effect of the SNS on arterial wall inflammation for the following reasons: i. similar changes could be observed in CGX mice 8 months after surgery, including a disruption of the ATLO structure; and ii. importantly, similar to 6-OHDA, CGX reduced several critical parameters of plaque instability.

A major finding of the CGX-denervation analyses was the observation that 8 months after CGX, atherosclerotic plaques were significantly smaller, with increased plaque stability (as was ATLO size and number). These data of selective surgically removing a major SNS ganglion which innervates the abdominal aorta adventitia resulting in atherosclerosis attenuation provide a new paradigm of atherosclerosis research: They provide for the first time evidence in an experimental mouse model that the SNS directly affects disease progression through its action on the adventitia and/or spleen. These data may open the possibility to develop new therapeutic targets, including approaches that have been developed in the recently exploding area of bioelectronic medicine to interfere with electrical signals in the NS to treat peripheral inflammatory diseases<sup>209</sup>.

### 4.5 Outlook

This thesis proposes a new concept of adventitial neuroimmune cardiovascular interfaces, allowing the efferent SNS to affect the immune system and *vice versa*. We conclude that the aortic adventitia of WT mice is innervated by sympathetic axons connecting the arterial wall to the perivascular sympathetic ganglia that connect the PNS and the CNS; that atherosclerosis-dependent adventitial inflammation enhances the expression of neurotrophic molecules to trigger axon sprouting in a localized and segmental manner; and that long term local sympathetic denervation attenuates atherosclerosis, halts ATLO neogenesis and increases plaque stability. Data in this thesis also provide evidence that the SNS undergoes restructuring during atherosclerosis. However, many questions remain to be addressed, including the following: i) how does atherosclerosis influence arterial innervation in other hyperlipidemic mouse models, including *Ldlr*<sup>-/-</sup> mice? ii) What are the

## DISCUSSION

mechanisms of interactions between immune cells and axons in ATLO? Which receptors and signaling molecules are involved? iii) Finally, what is the impact of arterial denervation on vascular function? Do changes of arterial tone in response to systemic or abdominal aorta denervation contribute in part to the observed changes in atherosclerotic plaque progression and ATLO numbers?

## 5. SUMMARY

The SNS engages in multilevel and multifactorial crosstalk with the immune system and the cardiovascular system in aged atherosclerosis-burdened mice. NE is selectively up-regulated in the adventitia of atherosclerotic aorta segments; TH<sup>+</sup> axon density specifically increases in atherosclerotic adventitia segments reaching maximal levels in ATLOs; genes regulating axon neogenesis and other neuroimmune mediators increase in atherosclerotic adventitia segments whereas axon repellants decrease; chemical and surgical SNS denervation by 6-OHDA and CGX, respectively, disrupt ATLO structure and sizes; plaque vulnerability decreases by systemic chemical or surgical celiac ganglia denervation; and most importantly, the SNS affects atherosclerosis progression via the celiac ganglia and possibly via the splenic nerve. When taken together, my analyses support a concept of neuroimmune cardiovascular interfaces that are pronounced and highly developed in those adventitia segments that are burdened by atherosclerosis. Adventitial neuroimmune cardiovascular interfaces establish biological platforms that allow the efferent SNS to affect the immune system and *vice versa*, allow the immune system to affect the peripheral SNS, restructure it, and which are associated with the emergence of a potentially vicious cycle of disease development during aging. These data provide a host of unexpected opportunities to develop new strategies to treat atherosclerosis by interfering with the apparently detrimental and direct role of the SNS in atherosclerosis progression and plaque vulnerability.

## 6. ZUSAMMENFASSUNG

Das sympathische Nervensystem (SNS) interagiert auf verschiedenen Ebenen mit dem Immunsystem und dem kardiovaskulären System von alten hyperlipidämischen Mäusen mit fortgeschrittener Atherosklerose. Die Gewebekonzentrationen von Adrenalin sind selektiv in Adventitiaabschnitten erhöht, die von Atherosklerose betroffen sind; die Dichte von Tyroxinhydroxylase exprimierenden Nervenaxone nimmt in erkrankten Adventitiaabschnitten deutlich zu mit maximalen Werten in ATLOs; Gene, die in die Regulation der Neubildung von Nervenaxonen involviert sind und andere Mediatoren, die die Interaktion des Immunsystems und dem Nervensystem regulieren, werden selektiv in Adventitiaabschnitten exprimiert, die Atherosklerose in der Intima zeigen; die pharmakologische Denervierung durch 6-OHDA oder die chirurgische Entfernung des Ganglion Coeliacum führt zu einem Kollaps der ATLO Struktur; die Plaquevulnerabilität wird durch 6-OHDA oder die chirurgische Intervention reduziert. Die chirurgische Intervention in das sympathische Nervensystem führt zu einer Abschwächung der Atheroskleroseprogression. Zusammenfassend zeigen die Ergebnisse, dass die Interaktion des Sympathischen Nervensystems, des Immunsystems und das kardiovaskulären Systems in der Adventitia biologische Plattformen darstellen, um die Krankheitsentwicklung zu beeinflussen. Aus diesen Ergebnissen ergeben sich zahllose bisher unbekannte Optionen für neue Therapiestrategien der Atherosklerose.

## 7. REFERENCES

- 1 Medzhitov, R. Origin and physiological roles of inflammation. *Nature* **454**, 428-435, (2008).
- 2 Nathan, C. & Ding, A. Nonresolving inflammation. *Cell* **140**, 871-882, (2010).
- 3 Dinarello, C. A. Anti-inflammatory Agents: Present and Future. *Cell* **140**, 935-950, (2010).
- 4 Mensah, G. A., Roth, G. A. & Fuster, V. The Global Burden of Cardiovascular Diseases and Risk Factors: 2020 and Beyond. *J Am Coll Cardiol* **74**, 2529-2532, (2019).
- 5 Fuster, V. Global burden of cardiovascular disease: time to implement feasible strategies and to monitor results. *Journal of the American College of Cardiology* **64**, 520-522, (2014).
- 6 Libby, P., Ridker, P. M. & Hansson, G. K. Progress and challenges in translating the biology of atherosclerosis. *Nature* **473**, 317-325, (2011).
- 7 Libby, P. Inflammation in atherosclerosis. *Arteriosclerosis, thrombosis, and vascular biology* **32**, 2045-2051, (2012).
- 8 Libby, P., Lichtman, A. H. & Hansson, G. K. Immune effector mechanisms implicated in atherosclerosis: from mice to humans. *Immunity* **38**, 1092-1104, (2013).
- 9 Glass, C. K. & Witztum, J. L. Atherosclerosis. the road ahead. *Cell* **104**, 503-516, (2001).
- 10 Mallika, V., Goswami, B. & Rajappa, M. Atherosclerosis pathophysiology and the role of novel risk factors: a clinicobiochemical perspective. *Angiology* **58**, 513-522, (2007).
- 11 Benjamin, E. J. *et al.* Heart Disease and Stroke Statistics-2017 Update: A Report From the American Heart Association. *Circulation* **135**, e146-e603, (2017).
- 12 Hansson, G. K. Inflammation, atherosclerosis, and coronary artery disease. *The New England journal of medicine* **352**, 1685-1695, (2005).
- 13 Libby, P. *et al.* Atherosclerosis. *Nat Rev Dis Primers* **5**, 56, (2019).
- 14 Hu, D., Yin, C., Luo, S., Habenicht, A. J. R. & Mohanta, S. K. Vascular Smooth Muscle Cells Contribute to Atherosclerosis Immunity. *Front Immunol* **10**, 1101, (2019).
- 15 Paulin, N. *et al.* Double-Strand DNA Sensing Aim2 Inflammasome Regulates Atherosclerotic Plaque Vulnerability. *Circulation* **138**, 321-323, (2018).
- 16 Hansson, G. K., Libby, P. & Tabas, I. Inflammation and plaque vulnerability. *Journal of internal medicine* **278**, 483-493, (2015).
- 17 Silvestre-Roig, C. *et al.* Atherosclerotic plaque destabilization: mechanisms, models, and therapeutic strategies. *Circulation research* **114**, 214-226, (2014).
- 18 Virmani, R. *et al.* Atherosclerotic plaque progression and vulnerability to rupture: angiogenesis as a source of intraplaque hemorrhage. *Arteriosclerosis, thrombosis, and vascular biology* **25**, 2054-2061, (2005).
- 19 Weih, F., Grabner, R., Hu, D., Beer, M. & Habenicht, A. J. Control of dichotomic innate and adaptive immune responses by artery tertiary lymphoid organs in atherosclerosis. *Frontiers in physiology* **3**, 226, (2012).
- 20 Hartwig, H. *et al.* Atherosclerotic Plaque Destabilization in Mice: A Comparative Study. *PLoS One* **10**, e0141019, (2015).
- 21 Wang, J. C. & Bennett, M. Aging and atherosclerosis: mechanisms, functional consequences, and potential therapeutics for cellular senescence. *Circulation research* **111**, 245-259, (2012).
- 22 Walter, M. Interrelationships among HDL metabolism, aging, and atherosclerosis. *Arteriosclerosis, thrombosis, and vascular biology* **29**, 1244-1250, (2009).
- 23 Ferrari, A. U., Radaelli, A. & Centola, M. Invited review: aging and the cardiovascular system. *J Appl Physiol (1985)* **95**, 2591-2597, (2003).
- 24 Bolton, E. & Rajkumar, C. The ageing cardiovascular system. *Reviews in Clinical Gerontology* **21**, 99-109,

## REFERENCES

- (2011).
- 25 Moos, M. P. *et al.* The lamina adventitia is the major site of immune cell accumulation in standard chow-fed apolipoprotein E-deficient mice. *Arteriosclerosis, thrombosis, and vascular biology* **25**, 2386-2391, (2005).
- 26 Mohanta, S. K. *et al.* Artery tertiary lymphoid organs contribute to innate and adaptive immune responses in advanced mouse atherosclerosis. *Circulation research* **114**, 1772-1787, (2014).
- 27 Hu, D. *et al.* Artery Tertiary Lymphoid Organs Control Aorta Immunity and Protect against Atherosclerosis via Vascular Smooth Muscle Cell Lymphotoxin beta Receptors. *Immunity* **42**, 1100-1115, (2015).
- 28 Srikakulapu, P. *et al.* Artery Tertiary Lymphoid Organs Control Multilayered Territorialized Atherosclerosis B-Cell Responses in Aged ApoE<sup>-/-</sup> Mice. *Arteriosclerosis, thrombosis, and vascular biology* **36**, 1174-1185, (2016).
- 29 Getz, G. S. & Reardon, C. A. Animal models of atherosclerosis. *Arteriosclerosis, thrombosis, and vascular biology* **32**, 1104-1115, (2012).
- 30 Getz, G. S. & Reardon, C. A. Diet and murine atherosclerosis. *Arteriosclerosis, thrombosis, and vascular biology* **26**, 242-249, (2006).
- 31 Ishibashi, S., Goldstein, J. L., Brown, M. S., Herz, J. & Burns, D. K. Massive xanthomatosis and atherosclerosis in cholesterol-fed low density lipoprotein receptor-negative mice. *J Clin Invest* **93**, 1885-1893, (1994).
- 32 Ma, Y. *et al.* Hyperlipidemia and atherosclerotic lesion development in Ldlr-deficient mice on a long-term high-fat diet. *PLoS One* **7**, e35835, (2012).
- 33 Centa, M. *et al.* Acute Loss of Apolipoprotein E Triggers an Autoimmune Response That Accelerates Atherosclerosis. *Arteriosclerosis, thrombosis, and vascular biology* **38**, e145-e158, (2018).
- 34 Bjorklund, M. M. *et al.* Induction of atherosclerosis in mice and hamsters without germline genetic engineering. *Circulation research* **114**, 1684-1689, (2014).
- 35 Newland, S. A. *et al.* Type-2 innate lymphoid cells control the development of atherosclerosis in mice. *Nature communications* **8**, 15781, (2017).
- 36 Hansson, G. K., Libby, P., Schonbeck, U. & Yan, Z. Q. Innate and adaptive immunity in the pathogenesis of atherosclerosis. *Circulation research* **91**, 281-291, (2002).
- 37 Murphy, Kenneth M. & Weaver, Casey. *Janeway's Immunobiology*. 9th Edition edn, 924 (W. W. Norton & Company, 2016).
- 38 Andersson, J., Libby, P. & Hansson, G. K. Adaptive immunity and atherosclerosis. *Clinical immunology* **134**, 33-46, (2010).
- 39 Ketelhuth, D. F. & Hansson, G. K. Adaptive Response of T and B Cells in Atherosclerosis. *Circulation research* **118**, 668-678, (2016).
- 40 Ait-Oufella, H. *et al.* Natural regulatory T cells control the development of atherosclerosis in mice. *Nature medicine* **12**, 178-180, (2006).
- 41 Roozendaal, R. & Mebius, R. E. Stromal cell-immune cell interactions. *Annual review of immunology* **29**, 23-43, (2011).
- 42 Zhao, L. *et al.* The 5-lipoxygenase pathway promotes pathogenesis of hyperlipidemia-dependent aortic aneurysm. *Nature medicine* **10**, 966-973, (2004).
- 43 Houtkamp, M. A., de Boer, O. J., van der Loos, C. M., van der Wal, A. C. & Becker, A. E. Adventitial infiltrates associated with advanced atherosclerotic plaques: structural organization suggests generation of local humoral immune responses. *The Journal of pathology* **193**, 263-269, (2001).
- 44 Lotzer, K. *et al.* Mouse aorta smooth muscle cells differentiate into lymphoid tissue organizer-like cells on combined tumor necrosis factor receptor-1/lymphotoxin beta-receptor NF-kappaB signaling. *Arteriosclerosis, thrombosis, and vascular biology* **30**, 395-402, (2010).
- 45 Grabner, R. *et al.* Lymphotoxin beta receptor signaling promotes tertiary lymphoid organogenesis in the aorta adventitia of aged ApoE<sup>-/-</sup> mice. *The Journal of experimental medicine* **206**, 233-248, (2009).
- 46 Mohanta, S., Yin, C., Weber, C., Hu, D. & Habenicht, A. J. Aorta Atherosclerosis Lesion Analysis in

## REFERENCES

- Hyperlipidemic Mice. *Bio-protocol* **6**, (2016).
- 47 Yin, C., Mohanta, S. K., Srikakulapu, P., Weber, C. & Habenicht, A. J. Artery Tertiary Lymphoid Organs: Powerhouses of Atherosclerosis Immunity. *Front Immunol* **7**, 387, (2016).
- 48 Yoo, B. B. & Mazmanian, S. K. The Enteric Network: Interactions between the Immune and Nervous Systems of the Gut. *Immunity* **46**, 910-926, (2017).
- 49 Schuenke M, Schulte E & U, Schumacher. *Thieme Atlas of Anatomy, Head and Neuroanatomy*. (Thieme, 2010).
- 50 Schuenke M, Schulte E & U, Schumacher. *Thieme Atlas of Anatomy, Neck and Internal Organs*. (Thieme, 2010).
- 51 Betts, J. Gordon *et al. Human Anatomy and Physiology*. (OpenStax College, 2013).
- 52 Tracey, K. J. Reflex control of immunity. *Nature reviews. Immunology* **9**, 418-428, (2009).
- 53 Sternberg, E. M. Neural regulation of innate immunity: a coordinated nonspecific host response to pathogens. *Nature reviews. Immunology* **6**, 318-328, (2006).
- 54 Tracey, K. J. The inflammatory reflex. *Nature* **420**, 853-859, (2002).
- 55 Storkebaum, E. & Carmeliet, P. Paracrine control of vascular innervation in health and disease. *Acta physiologica* **203**, 61-86, (2011).
- 56 Andersson, U. & Tracey, K. J. Reflex principles of immunological homeostasis. *Annual review of immunology* **30**, 313-335, (2012).
- 57 Straub, R. H. *et al.* Anti-inflammatory role of sympathetic nerves in chronic intestinal inflammation. *Gut* **57**, 911-921, (2008).
- 58 Kin, N. W. & Sanders, V. M. It takes nerve to tell T and B cells what to do. *Journal of leukocyte biology* **79**, 1093-1104, (2006).
- 59 del Rey, A. & Besedovsky, H. O. Sympathetic nervous system-immune interactions in autoimmune lymphoproliferative diseases. *Neuroimmunomodulation* **15**, 29-36, (2008).
- 60 Capellino, S. *et al.* Catecholamine-producing cells in the synovial tissue during arthritis: modulation of sympathetic neurotransmitters as new therapeutic target. *Annals of the rheumatic diseases* **69**, 1853-1860, (2010).
- 61 Harle, P., Mobius, D., Carr, D. J., Scholmerich, J. & Straub, R. H. An opposing time-dependent immunomodulating effect of the sympathetic nervous system conferred by altering the cytokine profile in the local lymph nodes and spleen of mice with type II collagen-induced arthritis. *Arthritis and rheumatism* **52**, 1305-1313, (2005).
- 62 Nance, D. M. & Sanders, V. M. Autonomic innervation and regulation of the immune system (1987-2007). *Brain, behavior, and immunity* **21**, 736-745, (2007).
- 63 Katayama, Y. *et al.* Signals from the sympathetic nervous system regulate hematopoietic stem cell egress from bone marrow. *Cell* **124**, 407-421, (2006).
- 64 Felten, D. L., Felten, S. Y., Carlson, S. L., Olschowka, J. A. & Livnat, S. Noradrenergic and peptidergic innervation of lymphoid tissue. *Journal of immunology* **135**, 755s-765s, (1985).
- 65 Watson C, Paxinos G & L, Puelles. *The Mouse Nervous System*. (Academic Press, 2012).
- 66 Nance, D. M., Hopkins, D. A. & Bieger, D. Re-investigation of the innervation of the thymus gland in mice and rats. *Brain, behavior, and immunity* **1**, 134-147, (1987).
- 67 Carnevale, D. *et al.* A cholinergic-sympathetic pathway primes immunity in hypertension and mediates brain-to-spleen communication. *Nature communications* **7**, 13035, (2016).
- 68 Carnevale, D. *et al.* The angiogenic factor PlGF mediates a neuroimmune interaction in the spleen to allow the onset of hypertension. *Immunity* **41**, 737-752, (2014).
- 69 Kooijman, S. *et al.* Splenic autonomic denervation increases inflammatory status but does not aggravate atherosclerotic lesion development. *American journal of physiology. Heart and circulatory physiology* **309**, H646-654, (2015).
- 70 Rosas-Ballina, M. *et al.* Splenic nerve is required for cholinergic antiinflammatory pathway control of TNF in endotoxemia. *Proceedings of the National Academy of Sciences of the United States of America* **105**, 11008-

## REFERENCES

- 11013, (2008).
- 71 Kurkowski, R., Kummer, W. & Heym, C. Substance P-immunoreactive nerve fibers in tracheobronchial lymph nodes of the guinea pig: origin, ultrastructure and coexistence with other peptides. *Peptides* **11**, 13-20, (1990).
- 72 Shepherd, A. J., Beresford, L. J., Bell, E. B. & Miyan, J. A. Mobilisation of specific T cells from lymph nodes in contact sensitivity requires substance P. *Journal of neuroimmunology* **164**, 115-123, (2005).
- 73 Straub, R. H., Wiest, R., Strauch, U. G., Harle, P. & Scholmerich, J. The role of the sympathetic nervous system in intestinal inflammation. *Gut* **55**, 1640-1649, (2006).
- 74 Chiu, I. M. *et al.* Bacteria activate sensory neurons that modulate pain and inflammation. *Nature* **501**, 52-57, (2013).
- 75 Baral, P. *et al.* Nociceptor sensory neurons suppress neutrophil and gammadelta T cell responses in bacterial lung infections and lethal pneumonia. *Nature medicine* **24**, 417-426, (2018).
- 76 Callahan, T. A., Moynihan, J. A. & Piekut, D. T. Central nervous system activation following peripheral chemical sympathectomy: implications for neural-immune interactions. *Brain, behavior, and immunity* **12**, 230-241, (1998).
- 77 Zhou, X. *et al.* Effect of the sonic hedgehog receptor smoothed on the survival and function of dopaminergic neurons. *Experimental neurology* **283**, 235-245, (2016).
- 78 Szpunar, M. J., Belcher, E. K., Dawes, R. P. & Madden, K. S. Sympathetic innervation, norepinephrine content, and norepinephrine turnover in orthotopic and spontaneous models of breast cancer. *Brain, behavior, and immunity* **53**, 223-233, (2016).
- 79 Janig, W. Sympathetic nervous system and inflammation: a conceptual view. *Autonomic neuroscience : basic & clinical* **182**, 4-14, (2014).
- 80 Orhan, Arslan. *Neuroanatomical Basis of Clinical Neurology*. (CRC Press, 2015).
- 81 Zaglia, T. & Mongillo, M. Cardiac sympathetic innervation, from a different point of (re)view. *The Journal of physiology* **595**, 3919-3930, (2017).
- 82 Kolmus, K., Tavernier, J. & Gerlo, S. beta2-Adrenergic receptors in immunity and inflammation: stressing NF-kappaB. *Brain, behavior, and immunity* **45**, 297-310, (2015).
- 83 Meltzer, J. C. *et al.* Stress-induced suppression of in vivo splenic cytokine production in the rat by neural and hormonal mechanisms. *Brain, behavior, and immunity* **18**, 262-273, (2004).
- 84 Ziegler, M. G., Lake, C. R. & Kopin, I. J. Plasma noradrenaline increases with age. *Nature* **261**, 333-335, (1976).
- 85 Luff, S. E. Development of neuromuscular junctions on small mesenteric arteries of the rat. *Journal of neurocytology* **28**, 47-62, (1999).
- 86 Heidt, T. *et al.* Chronic variable stress activates hematopoietic stem cells. *Nature medicine* **20**, 754-758, (2014).
- 87 Courties, G. *et al.* Ischemic stroke activates hematopoietic bone marrow stem cells. *Circulation research* **116**, 407-417, (2015).
- 88 Sager, H. B. *et al.* RNAi targeting multiple cell adhesion molecules reduces immune cell recruitment and vascular inflammation after myocardial infarction. *Science translational medicine* **8**, 342ra380, (2016).
- 89 Wirth, T. *et al.* The sympathetic nervous system modulates CD4(+)Foxp3(+) regulatory T cells via noradrenaline-dependent apoptosis in a murine model of lymphoproliferative disease. *Brain, behavior, and immunity* **38**, 100-110, (2014).
- 90 Dutta, P. *et al.* Myocardial infarction accelerates atherosclerosis. *Nature* **487**, 325-329, (2012).
- 91 Ebbinghaus, M., Gajda, M., Boettger, M. K., Schaible, H. G. & Brauer, R. The anti-inflammatory effects of sympathectomy in murine antigen-induced arthritis are associated with a reduction of Th1 and Th17 responses. *Annals of the rheumatic diseases* **71**, 253-261, (2012).
- 92 Rakhshan, K. *et al.* Evaluation of Chronic Physical and Psychological Stress Induction on Cardiac Ischemia / Reperfusion Injuries in Isolated Male Rat Heart: The Role of Sympathetic Nervous System. *Acta Med Iran* **53**, 482-490, (2015).

## REFERENCES

- 93 Klatt, S. *et al.* Peripheral elimination of the sympathetic nervous system stimulates immunocyte retention in lymph nodes and ameliorates collagen type II arthritis. *Brain, behavior, and immunity* **54**, 201-210, (2016).
- 94 Suzuki, K., Hayano, Y., Nakai, A., Furuta, F. & Noda, M. Adrenergic control of the adaptive immune response by diurnal lymphocyte recirculation through lymph nodes. *The Journal of experimental medicine* **213**, 2567-2574, (2016).
- 95 Ebbinghaus, M. *et al.* Interleukin-17A is involved in mechanical hyperalgesia but not in the severity of murine antigen-induced arthritis. *Scientific reports* **7**, 10334, (2017).
- 96 Padro, C. J. & Sanders, V. M. Neuroendocrine regulation of inflammation. *Seminars in immunology* **26**, 357-368, (2014).
- 97 Brodde, O. E. & Michel, M. C. Adrenergic and muscarinic receptors in the human heart. *Pharmacological reviews* **51**, 651-690, (1999).
- 98 Cannavo, A. & Koch, W. J. Targeting beta3-Adrenergic Receptors in the Heart: Selective Agonism and beta-Blockade. *Journal of cardiovascular pharmacology* **69**, 71-78, (2017).
- 99 Kenney, M. J. & Ganta, C. K. Autonomic nervous system and immune system interactions. *Compr Physiol* **4**, 1177-1200, (2014).
- 100 Steinman, L. Elaborate interactions between the immune and nervous systems. *Nature immunology* **5**, 575-581, (2004).
- 101 Dantzer, R., O'Connor, J. C., Freund, G. G., Johnson, R. W. & Kelley, K. W. From inflammation to sickness and depression: when the immune system subjugates the brain. *Nature reviews. Neuroscience* **9**, 46-56, (2008).
- 102 Thayer, J. F. & Sternberg, E. M. Neural aspects of immunomodulation: focus on the vagus nerve. *Brain, behavior, and immunity* **24**, 1223-1228, (2010).
- 103 Bellinger, D. L. *et al.* Sympathetic modulation of immunity: relevance to disease. *Cellular immunology* **252**, 27-56, (2008).
- 104 Mignini, F., Streccioni, V. & Amenta, F. Autonomic innervation of immune organs and neuroimmune modulation. *Auton Autacoid Pharmacol* **23**, 1-25, (2003).
- 105 Elenkov, I. J., Wilder, R. L., Chrousos, G. P. & Vizi, E. S. The sympathetic nerve--an integrative interface between two supersystems: the brain and the immune system. *Pharmacological reviews* **52**, 595-638, (2000).
- 106 Shi, P. *et al.* Brain microglial cytokines in neurogenic hypertension. *Hypertension* **56**, 297-303, (2010).
- 107 Kang, Y. M. *et al.* Brain nuclear factor-kappa B activation contributes to neurohumoral excitation in angiotensin II-induced hypertension. *Cardiovasc Res* **82**, 503-512, (2009).
- 108 Young, C. N. *et al.* ER stress in the brain subfornical organ mediates angiotensin-dependent hypertension. *J Clin Invest* **122**, 3960-3964, (2012).
- 109 Nohr, D., Michel, S., Fink, T. & Weihe, E. Pro-enkephalin opioid peptides are abundant in porcine and bovine splenic nerves, but absent from nerves of rat, mouse, hamster, and guinea-pig spleen. *Cell and tissue research* **281**, 143-152, (1995).
- 110 Flierl, M. A. *et al.* Phagocyte-derived catecholamines enhance acute inflammatory injury. *Nature* **449**, 721-725, (2007).
- 111 Nguyen, K. D. *et al.* Alternatively activated macrophages produce catecholamines to sustain adaptive thermogenesis. *Nature* **480**, 104-108, (2011).
- 112 Rosas-Ballina, M. *et al.* Acetylcholine-synthesizing T cells relay neural signals in a vagus nerve circuit. *Science* **334**, 98-101, (2011).
- 113 Reardon, C. *et al.* Lymphocyte-derived ACh regulates local innate but not adaptive immunity. *Proceedings of the National Academy of Sciences of the United States of America* **110**, 1410-1415, (2013).
- 114 Olofsson, P. S., Rosas-Ballina, M., Levine, Y. A. & Tracey, K. J. Rethinking inflammation: neural circuits in the regulation of immunity. *Immunol Rev* **248**, 188-204, (2012).
- 115 Scheiermann, C. *et al.* Adrenergic nerves govern circadian leukocyte recruitment to tissues. *Immunity* **37**, 290-

## REFERENCES

- 301, (2012).
- 116 Mina-Osorio, P. *et al.* Neural signaling in the spleen controls B-cell responses to blood-borne antigen. *Mol Med* **18**, 618-627, (2012).
- 117 Schmidt, P., Holsboer, F. & Spengler, D. Beta(2)-adrenergic receptors potentiate glucocorticoid receptor transactivation via G protein beta gamma-subunits and the phosphoinositide 3-kinase pathway. *Mol Endocrinol* **15**, 553-564, (2001).
- 118 Zhang, Z. H. *et al.* EP(3) receptors mediate PGE(2)-induced hypothalamic paraventricular nucleus excitation and sympathetic activation. *American journal of physiology. Heart and circulatory physiology* **301**, H1559-1569, (2011).
- 119 Yu, Y. *et al.* Brain perivascular macrophages and the sympathetic response to inflammation in rats after myocardial infarction. *Hypertension* **55**, 652-659, (2010).
- 120 Oka, T. Prostaglandin E2 as a mediator of fever: the role of prostaglandin E (EP) receptors. *Front Biosci* **9**, 3046-3057, (2004).
- 121 Ootsuka, Y., Blessing, W. W., Steiner, A. A. & Romanovsky, A. A. Fever response to intravenous prostaglandin E2 is mediated by the brain but does not require afferent vagal signaling. *Am J Physiol Regul Integr Comp Physiol* **294**, R1294-1303, (2008).
- 122 Fu, L. W. & Longhurst, J. C. Interleukin-1beta sensitizes abdominal visceral afferents of cats to ischaemia and histamine. *The Journal of physiology* **521 Pt 1**, 249-260, (1999).
- 123 Shi, Z. *et al.* Inflammatory cytokines in paraventricular nucleus modulate sympathetic activity and cardiac sympathetic afferent reflex in rats. *Acta physiologica* **203**, 289-297, (2011).
- 124 Zhang, Z. H., Wei, S. G., Francis, J. & Felder, R. B. Cardiovascular and renal sympathetic activation by blood-borne TNF-alpha in rat: the role of central prostaglandins. *Am J Physiol Regul Integr Comp Physiol* **284**, R916-927, (2003).
- 125 Kenney, M. J. Frequency characteristics of sympathetic nerve discharge in anesthetized rats. *Am J Physiol* **267**, R830-840, (1994).
- 126 Straub, R. H., Rauch, L., Fassold, A., Lowin, T. & Pongratz, G. Neuronally released sympathetic neurotransmitters stimulate splenic interferon-gamma secretion from T cells in early type II collagen-induced arthritis. *Arthritis and rheumatism* **58**, 3450-3460, (2008).
- 127 Kannan-Hayashi, Y. *et al.* Neuritogenic effects of T cell-derived IL-3 on mouse splenic sympathetic neurons in vivo. *Journal of immunology* **180**, 4227-4234, (2008).
- 128 Lorton, D. *et al.* Changes in the density and distribution of sympathetic nerves in spleens from Lewis rats with adjuvant-induced arthritis suggest that an injury and sprouting response occurs. *J Comp Neurol* **489**, 260-273, (2005).
- 129 Kerschensteiner, M., Meinl, E. & Hohlfeld, R. Neuro-immune crosstalk in CNS diseases. *Neuroscience* **158**, 1122-1132, (2009).
- 130 Eichmann, A. & Brunet, I. Arterial innervation in development and disease. *Science translational medicine* **6**, 252ps259, (2014).
- 131 Mukouyama, Y. S., Gerber, H. P., Ferrara, N., Gu, C. & Anderson, D. J. Peripheral nerve-derived VEGF promotes arterial differentiation via neuropilin 1-mediated positive feedback. *Development* **132**, 941-952, (2005).
- 132 Brunet, I. *et al.* Netrin-1 controls sympathetic arterial innervation. *J Clin Invest* **124**, 3230-3240, (2014).
- 133 Amiya, E., Watanabe, M. & Komuro, I. The Relationship between Vascular Function and the Autonomic Nervous System. *Annals of vascular diseases* **7**, 109-119, (2014).
- 134 Wallin, B. G. & Charkoudian, N. Sympathetic neural control of integrated cardiovascular function: insights from measurement of human sympathetic nerve activity. *Muscle & nerve* **36**, 595-614, (2007).
- 135 Joyner, M. J., Charkoudian, N. & Wallin, B. G. A sympathetic view of the sympathetic nervous system and human blood pressure regulation. *Experimental physiology* **93**, 715-724, (2008).

## REFERENCES

- 136 Fink, G. D. Arthur C. Corcoran Memorial Lecture. Sympathetic activity, vascular capacitance, and long-term regulation of arterial pressure. *Hypertension* **53**, 307-312, (2009).
- 137 Gordan, R., Gwathmey, J. K. & Xie, L. H. Autonomic and endocrine control of cardiovascular function. *World journal of cardiology* **7**, 204-214, (2015).
- 138 Bruno, R. M. *et al.* Sympathetic regulation of vascular function in health and disease. *Frontiers in physiology* **3**, 284, (2012).
- 139 Libby, P. & Hansson, G. K. Inflammation and immunity in diseases of the arterial tree: players and layers. *Circulation research* **116**, 307-311, (2015).
- 140 Bot, I. *et al.* The neuropeptide substance P mediates adventitial mast cell activation and induces intraplaque hemorrhage in advanced atherosclerosis. *Circulation research* **106**, 89-92, (2010).
- 141 Aggarwal, M., Zhang, J. & Mori, S. Magnetic resonance imaging-based mouse brain atlas and its applications. *Methods in molecular biology* **711**, 251-270, (2011).
- 142 Marques, N. F., Massari, C. M. & Tasca, C. I. Guanosine Protects Striatal Slices Against 6-OHDA-Induced Oxidative Damage, Mitochondrial Dysfunction, and ATP Depletion. *Neurotoxicity research* **35**, 475-483, (2019).
- 143 Daugherty, A. & Rateri, D. L. Development of experimental designs for atherosclerosis studies in mice. *Methods* **36**, 129-138, (2005).
- 144 Potteaux, S. *et al.* Suppressed monocyte recruitment drives macrophage removal from atherosclerotic plaques of ApoE<sup>-/-</sup> mice during disease regression. *J Clin Invest* **121**, 2025-2036, (2011).
- 145 Bianchini, M. *et al.* PD-L1 expression on nonclassical monocytes reveals their origin and immunoregulatory function. *Sci Immunol* **4**, (2019).
- 146 Maaten, L & Hinton, G. Visualizing data using t-SNE. *J MACH LEARN RES* **9**, 2579-2605, (2008).
- 147 Beer, M. *et al.* Laser-capture microdissection of hyperlipidemic/ApoE(-)/(-) mouse aorta atherosclerosis. *Methods in molecular biology* **755**, 417-428, (2011).
- 148 Gentleman, R. C. *et al.* Bioconductor: open software development for computational biology and bioinformatics. *Genome biology* **5**, R80, (2004).
- 149 Bolstad, B. M., Irizarry, R. A., Astrand, M. & Speed, T. P. A comparison of normalization methods for high density oligonucleotide array data based on variance and bias. *Bioinformatics* **19**, 185-193, (2003).
- 150 Goldstein, D. S. *et al.* Age-dependence of hypertensive-normotensive differences in plasma norepinephrine. *Hypertension* **5**, 100-104, (1983).
- 151 Pak, C. H. Plasma adrenaline and noradrenaline concentrations of the spontaneously hypertensive rat. *Japanese heart journal* **22**, 987-995, (1981).
- 152 Yin, C. *et al.* ApoE attenuates unresolvable inflammation by complex formation with activated C1q. *Nature medicine* **25**, 496-506, (2019).
- 153 Wanschel, A. *et al.* Neuroimmune guidance cue Semaphorin 3E is expressed in atherosclerotic plaques and regulates macrophage retention. *Arteriosclerosis, thrombosis, and vascular biology* **33**, 886-893, (2013).
- 154 Yukawa, K. *et al.* Deletion of Sema4D gene reduces intimal neovascularization and plaque growth in apolipoprotein E-deficient mice. *International journal of molecular medicine* **26**, 39-44, (2010).
- 155 Yazdani, U. & Terman, J. R. The semaphorins. *Genome biology* **7**, 211, (2006).
- 156 Takahashi, T., Nakamura, F., Jin, Z., Kalb, R. G. & Strittmatter, S. M. Semaphorins A and E act as antagonists of neuropilin-1 and agonists of neuropilin-2 receptors. *Nature neuroscience* **1**, 487-493, (1998).
- 157 Pook, C., Ahrens, J. M. & Claggett-Dame, M. Expression pattern of Nav2 in the murine CNS with development. *Gene expression patterns : GEP* **35**, 119099, (2020).
- 158 Bates, B. *et al.* Neurotrophin-3 is required for proper cerebellar development. *Nature neuroscience* **2**, 115-117, (1999).
- 159 Farinas, I., Jones, K. R., Backus, C., Wang, X. Y. & Reichardt, L. F. Severe sensory and sympathetic deficits in mice lacking neurotrophin-3. *Nature* **369**, 658-661, (1994).

## REFERENCES

- 160 Orr, B. O., Fetter, R. D. & Davis, G. W. Retrograde semaphorin-plexin signalling drives homeostatic synaptic plasticity. *Nature* **550**, 109-113, (2017).
- 161 Paldy, E. *et al.* Semaphorin 4C Plexin-B2 signaling in peripheral sensory neurons is pronociceptive in a model of inflammatory pain. *Nature communications* **8**, 176, (2017).
- 162 Chen, Y., Soong, J., Mohanty, S., Xu, L. & Scott, G. The neural guidance receptor Plexin C1 delays melanoma progression. *Oncogene* **32**, 4941-4949, (2013).
- 163 Park, T. I. *et al.* Cultured pericytes from human brain show phenotypic and functional differences associated with differential CD90 expression. *Scientific reports* **6**, 26587, (2016).
- 164 GrandPre, T., Nakamura, F., Vartanian, T. & Strittmatter, S. M. Identification of the Nogo inhibitor of axon regeneration as a Reticulon protein. *Nature* **403**, 439-444, (2000).
- 165 Vogel, K. S., Brannan, C. I., Jenkins, N. A., Copeland, N. G. & Parada, L. F. Loss of neurofibromin results in neurotrophin-independent survival of embryonic sensory and sympathetic neurons. *Cell* **82**, 733-742, (1995).
- 166 Lifton, R. P., Gharavi, A. G. & Geller, D. S. Molecular mechanisms of human hypertension. *Cell* **104**, 545-556, (2001).
- 167 Imai, J. *et al.* Cold exposure suppresses serum adiponectin levels through sympathetic nerve activation in mice. *Obesity* **14**, 1132-1141, (2006).
- 168 Horvathova, L. *et al.* Chemical sympathectomy increases neutrophil-to-lymphocyte ratio in tumor-bearing rats but does not influence cancer progression. *Journal of neuroimmunology* **278**, 255-261, (2015).
- 169 Furlan, A. *et al.* Visceral motor neuron diversity delineates a cellular basis for nipple- and pilo-erection muscle control. *Nature neuroscience* **19**, 1331-1340, (2016).
- 170 Miles, K., Chelmicka-Schorr, E., Atweh, S., Otten, G. & Arnason, B. G. Sympathetic ablation alters lymphocyte membrane properties. *Journal of immunology* **135**, 797s-801s, (1985).
- 171 Maryanovich, M. *et al.* Adrenergic nerve degeneration in bone marrow drives aging of the hematopoietic stem cell niche. *Nature medicine* **24**, 782-791, (2018).
- 172 Irwin, M. R. & Cole, S. W. Reciprocal regulation of the neural and innate immune systems. *Nature reviews. Immunology* **11**, 625-632, (2011).
- 173 Swirski, F. K. & Nahrendorf, M. Leukocyte behavior in atherosclerosis, myocardial infarction, and heart failure. *Science* **339**, 161-166, (2013).
- 174 Glatzel, M., Heppner, F. L., Albers, K. M. & Aguzzi, A. Sympathetic innervation of lymphoreticular organs is rate limiting for prion neuroinvasion. *Neuron* **31**, 25-34, (2001).
- 175 Vasamsetti, S. B. *et al.* Sympathetic Neuronal Activation Triggers Myeloid Progenitor Proliferation and Differentiation. *Immunity* **49**, 93-106 e107, (2018).
- 176 Sudo, K., Ema, H., Morita, Y. & Nakauchi, H. Age-associated characteristics of murine hematopoietic stem cells. *The Journal of experimental medicine* **192**, 1273-1280, (2000).
- 177 Lucas, D. *et al.* Chemotherapy-induced bone marrow nerve injury impairs hematopoietic regeneration. *Nature medicine* **19**, 695-703, (2013).
- 178 Duvernoy, H. M. & Risold, P. Y. The circumventricular organs: an atlas of comparative anatomy and vascularization. *Brain research reviews* **56**, 119-147, (2007).
- 179 Perino, A. *et al.* Combined inhibition of PI3Kbeta and PI3Kgamma reduces fat mass by enhancing alpha-MSH-dependent sympathetic drive. *Science signaling* **7**, ra110, (2014).
- 180 Paxinos, G. & Franklin, K. B. J. . *The Mouse Brain in Stereotaxic Coordinates*. 3rd Edition edn, 256 (Academic Press, 2008).
- 181 Hinton, Laurens van der Maaten AND Geoffrey. Visualizing Data using t-SNE. *Journal of Machine Learning Research* **9**, 2579-2605, (2008).
- 182 de Juan, A. *et al.* Artery-Associated Sympathetic Innervation Drives Rhythmic Vascular Inflammation of Arteries and Veins. *Circulation* **140**, 1100-1114, (2019).

## REFERENCES

- 183 Dolezel, S., Gerova, M., Gero, J., Sladek, T. & Vasku, J. Adrenergic innervation of the coronary arteries and the myocardium. *Acta Anat (Basel)* **100**, 306-316, (1978).
- 184 Mukouyama, Y. S., Shin, D., Britsch, S., Taniguchi, M. & Anderson, D. J. Sensory nerves determine the pattern of arterial differentiation and blood vessel branching in the skin. *Cell* **109**, 693-705, (2002).
- 185 Glebova, N. O. & Ginty, D. D. Growth and survival signals controlling sympathetic nervous system development. *Annual review of neuroscience* **28**, 191-222, (2005).
- 186 Nam, J. *et al.* Coronary veins determine the pattern of sympathetic innervation in the developing heart. *Development* **140**, 1475-1485, (2013).
- 187 Straub, R. H., Bijlsma, J. W., Masi, A. & Cutolo, M. Role of neuroendocrine and neuroimmune mechanisms in chronic inflammatory rheumatic diseases-The 10-year update. *Seminars in arthritis and rheumatism*, (2013).
- 188 Sheikine, Y. *et al.* Activation of VPAC1 receptors aggravates early atherosclerosis in hypercholesterolemic apolipoprotein E-deficient mice. *Biochemical and biophysical research communications* **402**, 471-476, (2010).
- 189 van Gils, J. M. *et al.* The neuroimmune guidance cue netrin-1 promotes atherosclerosis by inhibiting the emigration of macrophages from plaques. *Nature immunology* **13**, 136-143, (2012).
- 190 Randolph, G. J. & Gautier, E. L. Emerging roles of neural guidance molecules in atherosclerosis: sorting out the complexity. *Arteriosclerosis, thrombosis, and vascular biology* **33**, 882-883, (2013).
- 191 Funk, S. D. & Orr, A. W. Ephs and ephrins resurface in inflammation, immunity, and atherosclerosis. *Pharmacological research : the official journal of the Italian Pharmacological Society* **67**, 42-52, (2013).
- 192 Renz, B. W. *et al.* beta2 Adrenergic-Neurotrophin Feedforward Loop Promotes Pancreatic Cancer. *Cancer cell* **34**, 863-867, (2018).
- 193 Li, G. *et al.* Regional distribution of cortical interneurons and development of inhibitory tone are regulated by Cxcl12/Cxcr4 signaling. *The Journal of neuroscience : the official journal of the Society for Neuroscience* **28**, 1085-1098, (2008).
- 194 Stumm, R. & Holtt, V. CXC chemokine receptor 4 regulates neuronal migration and axonal pathfinding in the developing nervous system: implications for neuronal regeneration in the adult brain. *Journal of molecular endocrinology* **38**, 377-382, (2007).
- 195 Pujol, F., Kitabgi, P. & Boudin, H. The chemokine SDF-1 differentially regulates axonal elongation and branching in hippocampal neurons. *Journal of cell science* **118**, 1071-1080, (2005).
- 196 Ohshima, Y. *et al.* Regulation of axonal elongation and pathfinding from the entorhinal cortex to the dentate gyrus in the hippocampus by the chemokine stromal cell-derived factor 1 alpha. *The Journal of neuroscience : the official journal of the Society for Neuroscience* **28**, 8344-8353, (2008).
- 197 Huber, A. B., Kolodkin, A. L., Ginty, D. D. & Cloutier, J. F. Signaling at the growth cone: ligand-receptor complexes and the control of axon growth and guidance. *Annual review of neuroscience* **26**, 509-563, (2003).
- 198 Oinuma, I., Ishikawa, Y., Katoh, H. & Negishi, M. The Semaphorin 4D receptor Plexin-B1 is a GTPase activating protein for R-Ras. *Science* **305**, 862-865, (2004).
- 199 Damon, D. H. Vascular-dependent effects of elevated glucose on postganglionic sympathetic neurons. *American journal of physiology. Heart and circulatory physiology* **300**, H1386-1392, (2011).
- 200 Straub, R. H. *et al.* Neurotransmitters of the sympathetic nerve terminal are powerful chemoattractants for monocytes. *Journal of leukocyte biology* **67**, 553-558, (2000).
- 201 Kerschensteiner, M., Stadelmann, C., Dechant, G., Wekerle, H. & Hohlfeld, R. Neurotrophic cross-talk between the nervous and immune systems: implications for neurological diseases. *Annals of neurology* **53**, 292-304, (2003).
- 202 Hohlfeld, R., Kerschensteiner, M. & Meinl, E. Dual role of inflammation in CNS disease. *Neurology* **68**, S58-63; discussion S91-56, (2007).
- 203 Andersson, U. & Tracey, K. J. Neural reflexes in inflammation and immunity. *The Journal of experimental medicine* **209**, 1057-1068, (2012).

## REFERENCES

- 204 van de Pavert, S. A. & Mebius, R. E. New insights into the development of lymphoid tissues. *Nature reviews. Immunology* **10**, 664-674, (2010).
- 205 Schmid, M. C. *et al.* Combined blockade of integrin- $\alpha 4\beta 1$  plus cytokines SDF-1 $\alpha$  or IL-1 $\beta$  potently inhibits tumor inflammation and growth. *Cancer research* **71**, 6965-6975, (2011).
- 206 Shi, W. *et al.* The class IV semaphorin CD100 plays nonredundant roles in the immune system: defective B and T cell activation in CD100-deficient mice. *Immunity* **13**, 633-642, (2000).
- 207 Yu, D. *et al.* Axon growth and guidance genes identify T-dependent germinal centre B cells. *Immunology and cell biology* **86**, 3-14, (2008).
- 208 van de Pavert, S. A. *et al.* Chemokine CXCL13 is essential for lymph node initiation and is induced by retinoic acid and neuronal stimulation. *Nature immunology* **10**, 1193-1199, (2009).
- 209 Terrando, Valentin A. Pavlov and Niccolò. *Neuro-Immune Interactions in Inflammation and Autoimmunity*. (Frontiers Media SA, 2018).

## 8. ACKNOWLEDGEMENTS

First, I would like to express my gratitude towards my supervisor, Univ.-Prof. Dr. rer. nat. Sabine Steffens for the opportunity to pursue my PhD work. I especially appreciate her kind understanding and support during my work. Secondly, I extend many thanks and appreciations to my colleague Dr. Sarajo Mohanta, an experienced researcher, for his intensive supervision, training, time for discussion, theoretical and practical support, constructive criticism and patience. In addition, I would like to express my thanks to Prof. Dr. med. Andreas J R Habenicht for his support, timely advice and crucial comments. I deeply appreciate his kind understanding, moral support, constant encouragement, helpful suggestions and ideas for improvements of my project. Without supervision, encouragement and constructive advice of all my colleagues, this thesis would not have been possible.

It was a great pleasure to work with a cheerful and friendly group of colleagues, and I would like to thank them for their help. During the past years, I have been advised and aided by Dr. Changjun Yin, his helpful advice, and encouragement. I would also like to acknowledge Ting Sun, Shu Lu and Chuankai Zhang for their support during my experiments; I am very thankful to Shu Lu for his help with FACS work. I also thank the mouse caretakers in the mouse facility ZVH.

I am particularly grateful to my wife Zhe Ma and my family and their trust and support. I would never have been able to make this journey of my doctoral study without Zhe's help, support and encouragement.

Last but not least, I would like to take this opportunity to express my immense gratitude to all the past and present members of the Habenicht lab who have given their invaluable support and assistance. Additionally, I would like to thank the China Scholarship Council (CSC) for the funding during my Doctoral studies.

## 9. SUPPLEMENT

**Table S1. Probe sets of abdominal aorta up and down-regulated transcripts in WT and *ApoE*<sup>-/-</sup> adventitia during aging.**

Differential expression of probe sets was determined as described in Material and Methods for Nervous System related Gene Ontology terms: **A.** nervous system development (GO: 0007399), **B.** autonomic nervous system development (GO: 0048483), **C.** sympathetic nervous system development (GO: 0048485), **D.** axon (GO: 0030424), **E.** regulation of axon guidance (GO: 1902667). Further data are displayed as heat maps in Fig. 9. Probe sets are ordered according to fold change between aorta from 78 weeks old *ApoE*<sup>-/-</sup> mice versus 6 weeks old WT mice. Gene symbols and gene names are indicated for ease of reading. Columns of the mean value for each gene show signal intensity without normalization.

### A. Nervous system development (GO: 0007399)

Affymetrix Probe set ID	Gene Symbol	Gene Name	Entrez Gene ID	Mean	Mean	Mean	Mean	Mean	Mean	Fold change <i>ApoE</i> <sup>-/-</sup> aorta 78 weeks vs. 6 weeks	p ANOVA
				WT aorta 6 weeks	WT aorta 32 weeks	WT aorta 78 weeks	<i>ApoE</i> <sup>-/-</sup> aorta 6 weeks	<i>ApoE</i> <sup>-/-</sup> aorta 32 weeks	<i>ApoE</i> <sup>-/-</sup> aorta 78 weeks		
1448595_a_at	Bex1	brain expressed gene 1	19716	66	41	55	50	1511	2221	44.48	0.000006
1436312_at	Ikzf1	IKAROS family zinc finger 1	22778	40	43	212	35	338	948	27.12	0.000004
1440878_at	Runx1	runt related transcription factor 1	12394	14	74	21	21	216	523	24.72	0.0005
1450297_at	Il6	interleukin 6	16193	21	10	57	21	290	523	24.46	0.0001
1451715_at	Mafb	v-maf musculoaponeurotic fibrosarcoma oncogene family, protein B (avian)	16658	15	15	102	16	192	372	23.94	0.00004
1418126_at	Ccl5	chemokine (C-C motif) ligand 5	20304	24	73	420	67	406	1222	18.28	0.009
1437540_at	Mcoln3	mucolipin 3	171166	26	9	18	26	287	468	18.26	0.0002

SUPPLEMENT

Affymetrix Probe set ID	Gene Symbol	Gene Name	Entrez Gene ID	Mean	Mean	Mean	Mean	Mean	Mean	Fold change	p ANOVA
				WT aorta 6 weeks	WT aorta 32 weeks	WT aorta 78 weeks	<i>ApoE</i> <sup>-/-</sup> aorta 6 weeks	<i>ApoE</i> <sup>-/-</sup> aorta 32 weeks	<i>ApoE</i> <sup>-/-</sup> aorta 78 weeks	<i>ApoE</i> <sup>-/-</sup> aorta 78 weeks vs. 6 weeks	
1448710_at	Cxcr4	chemokine (C-X-C motif) receptor 4	12767	80	112	107	77	529	1120	14.50	0.00001
1422864_at	Runx1	runt related transcription factor 1	12394	32	22	35	23	162	289	12.44	0.0007
1427682_a_at	Egr2	early growth response 2	13654	23	75	125	39	203	395	10.20	0.0008
1420380_at	Ccl2	chemokine (C-C motif) ligand 2	20296	99	49	126	95	414	915	9.65	0.0001
1424727_at	Ccr5	chemokine (C-C motif) receptor 5	12774	106	121	172	113	704	959	8.46	0.00002
1425548_a_at	Lst1	leukocyte specific transcript 1	16988	105	154	402	155	440	1266	8.14	0.00005
1451716_at	Mafb	v-maf musculoaponeurotic fibrosarcoma oncogene family, protein B (avian)	16658	333	458	367	317	1256	2418	7.62	0.000002
1421186_at	Ccr2	chemokine (C-C motif) receptor 2	12772	154	154	132	130	619	939	7.21	0.00003
1459850_x_at	Glrb	glycine receptor, beta subunit	14658	10	52	233	82	120	582	7.13	0.00008
1422789_at	Aldh1a2	aldehyde dehydrogenase family 1, subfamily A2	19378	129	153	190	89	410	604	6.81	0.003
1435349_at	Nrp2	neuropilin 2	18187	144	221	258	172	631	1151	6.70	0.000004
1420715_a_at	Pparg	peroxisome proliferator activated receptor gamma	19016	29	476	171	60	375	400	6.65	0.002
1435190_at	Chl1	cell adhesion molecule with homology to L1CAM	12661	94	82	109	75	200	449	5.99	0.0005
1418939_at	Hlx	H2.0-like homeobox	15284	96	177	76	73	232	436	5.99	0.009
1419675_at	Ngf	nerve growth factor	18049	96	124	154	81	284	480	5.92	0.0002
1429055_at	4930506M07Rik	RIKEN cDNA 4930506M07 gene	71653	151	242	229	146	492	829	5.67	0.0000009
1434920_a_at	Ev1	Ena-vasodilator stimulated phosphoprotein	14026	401	319	244	361	1291	1927	5.34	0.000003
1434653_at	Ptk2b	PTK2 protein tyrosine kinase 2 beta	19229	261	463	424	263	748	1346	5.12	0.000001
1419156_at	Sox4	SRY-box containing gene 4	20677	45	29	24	52	139	266	5.07	0.002
1448424_at	Frzb	frizzled-related protein	20378	506	369	489	454	1836	2240	4.93	0.000003
1416658_at	Frzb	frizzled-related protein	20378	1100	1421	1480	1239	4409	6059	4.89	0.000001

SUPPLEMENT

Affymetrix Probe set ID	Gene Symbol	Gene Name	Entrez Gene ID	Mean	Mean	Mean	Mean	Mean	Mean	Fold change	p ANOVA
				WT aorta 6 weeks	WT aorta 32 weeks	WT aorta 78 weeks	<i>ApoE</i> <sup>-/-</sup> aorta 6 weeks	<i>ApoE</i> <sup>-/-</sup> aorta 32 weeks	<i>ApoE</i> <sup>-/-</sup> aorta 78 weeks	<i>ApoE</i> <sup>-/-</sup> aorta 78 weeks vs. 6 weeks	
1422865_at	Runx1	runt related transcription factor 1	12394	89	117	181	101	255	487	4.84	0.000004
1425546_a_at	Trf	transferrin	22041	639	1302	813	496	2340	2368	4.78	0.0002
1419754_at	Myo5a	myosin VA	17918	220	271	225	234	836	1112	4.76	0.000002
1455678_at	Sema4b	sema domain, immunoglobulin domain (Ig), transmembrane domain (TM) and short cytoplasmic domain, (semaphorin) 4B	20352	85	190	229	85	222	401	4.69	0.0003
1433471_at	Tcf7	transcription factor 7, T-cell specific	21414	53	91	158	76	117	356	4.67	0.002
1422259_a_at	Ccr5	chemokine (C-C motif) receptor 5	12774	60	72	104	57	206	266	4.64	0.0001
1422046_at	Itgam	integrin alpha M	16409	128	116	120	118	435	542	4.60	0.00004
1417574_at	Cxcl12	chemokine (C-X-C motif) ligand 12	20315	577	562	615	474	1216	2174	4.58	0.00001
1427683_at	Egr2	early growth response 2	13654	116	167	305	129	304	582	4.52	0.00004
1431320_a_at	Myo5a	myosin VA	17918	242	253	283	248	618	1092	4.40	0.00006
1455745_at	Cln8	ceroid-lipofuscinosis, neuronal 8	26889	98	39	150	92	119	397	4.33	0.01
1421187_at	Ccr2	chemokine (C-C motif) receptor 2	12772	59	71	18	57	218	244	4.27	0.0001
1439902_at	C5ar1	complement component 5a receptor 1	12273	128	130	163	108	287	460	4.24	0.00007
1417378_at	Cadm1	cell adhesion molecule 1	54725	353	320	421	290	608	1230	4.24	0.000009
1451318_a_at	Lyn	Yamaguchi sarcoma viral (v-yes-1) oncogene homolog	17096	462	582	644	492	947	2046	4.16	0.0004
1434069_at	Prex1	phosphatidylinositol-3,4,5-trisphosphate-dependent Rac exchange factor 1	277360	329	307	310	286	624	1159	4.06	0.00001
1434447_at	Met	met proto-oncogene	17295	104	240	130	88	282	347	3.97	0.007
1420980_at	Pak1	p21 protein (Cdc42/Rac)-activated kinase 1	18479	206	351	527	184	452	714	3.88	0.0002
1450106_a_at	Evl	Ena-vasodilator stimulated phosphoprotein	14026	204	102	102	167	472	644	3.85	0.00001
1425598_a_at	Lyn	Yamaguchi sarcoma viral (v-yes-1) oncogene homolog	17096	289	305	374	285	703	1086	3.81	0.00002
1420653_at	Tgfb1	transforming growth factor, beta 1	21803	516	538	551	440	1292	1670	3.79	0.0000008

SUPPLEMENT

Affymetrix Probe set ID	Gene Symbol	Gene Name	Entrez Gene ID	Mean	Mean	Mean	Mean	Mean	Mean	Fold change	p ANOVA
				WT aorta 6 weeks	WT aorta 32 weeks	WT aorta 78 weeks	<i>ApoE</i> <sup>-/-</sup> aorta 6 weeks	<i>ApoE</i> <sup>-/-</sup> aorta 32 weeks	<i>ApoE</i> <sup>-/-</sup> aorta 78 weeks	<i>ApoE</i> <sup>-/-</sup> aorta 78 weeks vs. 6 weeks	
1436205_at	Nfasc	neurofascin	269116	115	213	425	121	331	448	3.71	0.0001
1420824_at	Sema4d	sema domain, immunoglobulin domain (Ig), transmembrane domain (TM) and short cytoplasmic domain, (semaphorin) 4D	20354	442	582	773	550	1135	2039	3.71	0.00002
1436659_at	Dclk1	doublecortin-like kinase 1	13175	489	280	341	231	543	850	3.68	0.00007
1450070_s_at	Pak1	p21 protein (Cdc42/Rac)-activated kinase 1	18479	121	221	345	128	285	461	3.59	0.00002
1434376_at	Cd44	CD44 antigen	12505	1791	1902	1898	1744	4193	5926	3.40	0.000002
1434028_at	Arnt2	aryl hydrocarbon receptor nuclear translocator 2	11864	122	76	123	92	125	306	3.33	0.0004
1417376_a_at	Cadm1	cell adhesion molecule 1	54725	233	253	273	241	443	802	3.33	0.00004
1419717_at	Sema3e	sema domain, immunoglobulin domain (Ig), short basic domain, secreted, (semaphorin) 3E	20349	45	246	371	49	223	161	3.31	0.00008
1452534_a_at	Hmgb2	high mobility group box 2	97165	241	207	303	190	313	618	3.25	0.003
1417377_at	Cadm1	cell adhesion molecule 1	54725	70	106	76	97	176	303	3.13	0.03
1422286_a_at	Tgif1	TGFB-induced factor homeobox 1	21815	202	310	281	230	397	713	3.11	0.00001
1448110_at	Sema4a	sema domain, immunoglobulin domain (Ig), transmembrane domain (TM) and short cytoplasmic domain, (semaphorin) 4A	20351	125	336	187	117	357	358	3.05	0.002
1423135_at	Thy1	thymus cell antigen 1, theta	21838	627	1056	1441	602	1257	1828	3.04	0.00006
1426528_at	Nrp2	neuropilin 2	18187	374	498	438	366	711	1099	3.01	0.0001
1436329_at	Egr3	early growth response 3	13655	185	349	793	270	575	811	3.01	0.00002
1419296_at	Arhgap4	Rho GTPase activating protein 4	171207	98	128	194	112	189	335	2.98	0.002
1451596_a_at	Sphk1	sphingosine kinase 1	20698	244	221	377	250	360	741	2.96	0.00002
1417275_at	Mal	myelin and lymphocyte protein, T-cell differentiation protein	17153	137	222	231	132	305	391	2.96	0.005
1435277_x_at	Nme1	non-metastatic cells 1, protein (NM23A) expressed in	18102	601	729	835	612	940	1797	2.94	0.0002
1450718_at	Sh2b2	SH2B adaptor protein 2	23921	63	262	99	80	234	233	2.92	0.001

SUPPLEMENT

Affymetrix Probe set ID	Gene Symbol	Gene Name	Entrez Gene ID	Mean	Mean	Mean	Mean	Mean	Mean	Fold change	p ANOVA
				WT aorta 6 weeks	WT aorta 32 weeks	WT aorta 78 weeks	<i>ApoE</i> <sup>-/-</sup> aorta 6 weeks	<i>ApoE</i> <sup>-/-</sup> aorta 32 weeks	<i>ApoE</i> <sup>-/-</sup> aorta 78 weeks	<i>ApoE</i> <sup>-/-</sup> aorta 78 weeks vs. 6 weeks	
1423760_at	Cd44	CD44 antigen	12505	1662	1238	1431	1711	3226	4914	2.87	0.00001
1428142_at	Etv5	ets variant gene 5	104156	196	328	548	227	537	647	2.86	0.000001
1436051_at	Myo5a	myosin VA	17918	576	563	492	535	998	1526	2.85	0.000007
1421188_at	Ccr2	chemokine (C-C motif) receptor 2	12772	167	187	236	166	349	465	2.81	0.0002
1421385_a_at	Myo7a	myosin VIIA	17921	228	269	272	241	408	673	2.79	0.00003
1438767_at	Osm	oncostatin M	18413	163	165	212	132	206	365	2.77	0.01
1422190_at	C5ar1	complement component 5a receptor 1	12273	195	215	240	175	354	473	2.71	0.003
1424271_at	Dclk1	doublecortin-like kinase 1	13175	292	165	234	212	323	565	2.66	0.0002
1437313_x_at	Hmgb2	high mobility group box 2	97165	346	344	347	274	557	714	2.61	0.004
1423319_at	Hhex	hematopoietically expressed homeobox	15242	379	409	524	346	644	902	2.61	0.0001
1420992_at	Ankrd1	ankyrin repeat domain 1 (cardiac muscle)	107765	360	408	520	408	418	1054	2.58	0.001
1435172_at	Eomes	comesodermin homolog ( <i>Xenopus laevis</i> )	13813	87	83	131	84	79	209	2.49	0.02
1449024_a_at	Hexa	hexosaminidase A	15211	3981	4203	4253	3815	6526	9294	2.44	0.000001
1434222_at	Sipa111	signal-induced proliferation-associated 1 like 1	217692	323	423	492	281	437	682	2.43	0.007
1424110_a_at	Nme1	non-metastatic cells 1, protein (NM23A) expressed in	18102	985	921	1138	860	1215	2081	2.42	0.00001
1437341_x_at	Cnp	2',3'-cyclic nucleotide 3' phosphodiesterase	12799	549	1181	1058	646	1392	1561	2.42	0.00005
1456722_at	Chrdl1	chordin-like 1	83453	321	865	1330	243	893	586	2.42	0.00002
1420979_at	Pak1	p21 protein (Cdc42/Rac)-activated kinase 1	18479	117	153	183	151	188	365	2.41	0.0002
1460180_at	Hexb	hexosaminidase B	15212	2074	1861	1956	2155	3581	5176	2.40	0.000005
1456200_at	Ipmk	inositol polyphosphate multikinase	69718	143	158	211	134	227	321	2.39	0.02
1443086_at	Alcam	activated leukocyte cell adhesion molecule	11658	132	94	114	110	183	263	2.38	0.003
1418872_at	Abcb1b	ATP-binding cassette, sub-family B (MDR/TAP), member 1B	18669	296	463	365	244	637	582	2.38	0.03
1428393_at	Nrn1	neuritin 1	68404	477	526	619	424	808	983	2.32	0.0004

SUPPLEMENT

Affymetrix Probe set ID	Gene Symbol	Gene Name	Entrez Gene ID	Mean	Mean	Mean	Mean	Mean	Mean	Fold change	p ANOVA
				WT aorta 6 weeks	WT aorta 32 weeks	WT aorta 78 weeks	<i>ApoE</i> <sup>-/-</sup> aorta 6 weeks	<i>ApoE</i> <sup>-/-</sup> aorta 32 weeks	<i>ApoE</i> <sup>-/-</sup> aorta 78 weeks	<i>ApoE</i> <sup>-/-</sup> aorta 78 weeks vs. 6 weeks	
1455664_at	Rtn4rl1	reticulon 4 receptor-like 1	237847	133	204	427	140	271	319	2.27	0.0004
1452014_a_at	Igf1	insulin-like growth factor 1	16000	1344	786	740	1302	1591	2903	2.23	0.00007
1431619_a_at	Dtnbp1	dystrobrevin binding protein 1	94245	606	702	737	566	907	1258	2.22	0.0002
1451435_at	Cux1	cut-like homeobox 1	13047	555	875	1049	728	1068	1618	2.22	0.00003
1417073_a_at	Qk	quaking	19317	754	1094	772	790	1532	1755	2.22	0.00001
1424988_at	Mylip	myosin regulatory light chain interacting protein	218203	1745	2337	2721	2229	3751	4924	2.21	0.000006
1425536_at	Stx3	syntaxin 3	20908	726	546	694	525	780	1156	2.20	0.00002
1433532_a_at	Mbp	myelin basic protein	17196	199	406	286	170	516	373	2.20	0.0005
1459866_x_at	Cyfp1	cytoplasmic FMR1 interacting protein 1	20430	2214	1931	4813	2570	2430	5622	2.19	0.003
1434768_at	Tpp1	tripeptidyl peptidase I	12751	602	1005	777	677	1428	1443	2.13	0.0001
1417627_a_at	Limk1	LIM-domain containing, protein kinase	16885	172	228	202	165	299	343	2.08	0.005
1448823_at	Cxcl12	chemokine (C-X-C motif) ligand 12	20315	5885	5864	6394	5182	8384	10772	2.08	0.000007
1450148_at	Mcoln3	mucolipin 3	171166	126	148	159	118	236	245	2.07	0.006
1451031_at	Sfrp4	secreted frizzled-related protein 4	20379	3168	3328	3227	3125	4790	6466	2.07	0.00006
1450020_at	Cx3cr1	chemokine (C-X3-C) receptor 1	13051	104	116	64	146	283	302	2.06	0.0003
1440885_at	Evl	Ena-vasodilator stimulated phosphoprotein	14026	280	281	310	280	349	578	2.06	0.0002
1438934_x_at	Sema4a	sema domain, immunoglobulin domain (Ig), transmembrane domain (TM) and short cytoplasmic domain, (semaphorin) 4A	20351	279	620	406	326	749	662	2.03	0.0001
1458276_x_at	Cit	citron	12704	527	625	736	586	814	1185	2.02	0.0002
1437467_at	Alcam	activated leukocyte cell adhesion molecule	11658	1218	853	801	1161	1573	2332	2.01	0.00001
1420991_at	Ankrd1	ankyrin repeat domain 1 (cardiac muscle)	107765	393	368	562	463	354	916	1.98	0.0008
1456873_at	Clic5	chloride intracellular channel 5	224796	253	465	378	199	416	388	1.95	0.002
1452483_a_at	Cd44	CD44 antigen	12505	362	174	68	354	614	673	1.90	0.0001

SUPPLEMENT

Affymetrix Probe set ID	Gene Symbol	Gene Name	Entrez Gene ID	Mean	Mean	Mean	Mean	Mean	Mean	Fold change	p ANOVA
				WT aorta 6 weeks	WT aorta 32 weeks	WT aorta 78 weeks	<i>ApoE</i> <sup>-/-</sup> aorta 6 weeks	<i>ApoE</i> <sup>-/-</sup> aorta 32 weeks	<i>ApoE</i> <sup>-/-</sup> aorta 78 weeks	<i>ApoE</i> <sup>-/-</sup> aorta 78 weeks vs. 6 weeks	
1448028_at	Tbc1d24	TBC1 domain family, member 24	224617	245	360	313	237	481	450	1.90	0.0002
1448789_at	Aldh1a3	aldehyde dehydrogenase family 1, subfamily A3	56847	214	338	347	199	408	375	1.88	0.001
1454714_x_at	Phgdh	3-phosphoglycerate dehydrogenase	236539	672	347	513	511	401	930	1.82	0.00004
1433575_at	Sox4	SRY-box containing gene 4	20677	1496	1042	950	1407	2361	2518	1.79	0.0005
1450723_at	Isl1	ISL1 transcription factor, LIM/homeodomain	16392	263	345	497	169	404	302	1.79	0.0002
1450722_at	Nup50	nucleoporin 50	18141	394	263	276	362	405	641	1.77	0.01
1455422_x_at	Sept4	septin 4	18952	184	346	341	197	401	345	1.75	0.007
1424950_at	Sox9	SRY-box containing gene 9	20682	72	134	46	113	313	192	1.71	0.0008
1434201_at	Chrdl1	chordin-like 1	83453	532	736	1039	350	782	591	1.69	0.002
1421267_a_at	Cited2	Cbp/p300-interacting transactivator, with Glu/Asp-rich carboxy-terminal domain, 2	17684	539	282	377	381	284	635	1.67	0.01
1437347_at	Ednrb	endothelin receptor type B	13618	604	655	708	488	1040	812	1.66	0.04
1439505_at	Clic5	chloride intracellular channel 5	224796	161	350	237	141	320	232	1.65	0.003
1427844_a_at	Cebpb	CCAAT/enhancer binding protein (C/EBP), beta	12608	525	607	345	459	607	739	1.61	0.02
1434298_at	Zeb2	zinc finger E-box binding homeobox 2	24136	585	781	619	542	1106	873	1.61	0.002
1417706_at	Naglu	alpha-N-acetylglucosaminidase (Sanfilippo disease IIIB)	27419	795	663	570	757	881	1210	1.60	0.003
1419519_at	Igf1	insulin-like growth factor 1	16000	1239	830	842	1231	1164	1823	1.48	0.002
1416041_at	Sgk1	serum/glucocorticoid regulated kinase 1	20393	4259	2102	2122	2774	3162	4106	1.48	0.003
1448610_a_at	Sod2	superoxide dismutase 2, mitochondrial	20656	2162	4794	2950	2349	4920	3410	1.45	0.00005
1448260_at	Uchl1	ubiquitin carboxy-terminal hydrolase L1	22223	921	1386	2253	1093	1256	1577	1.44	0.001
1431292_a_at	Twf2	twinfilin, actin-binding protein, homolog 2 (Drosophila)	23999	311	331	170	266	334	381	1.43	0.008
1420705_at	Foxb1	forkhead box B1	64290	106	81	213	108	80	154	1.43	0.01
1452968_at	Cthrc1	collagen triple helix repeat containing 1	68588	532	173	171	375	514	531	1.42	0.00001

SUPPLEMENT

Affymetrix Probe set ID	Gene Symbol	Gene Name	Entrez Gene ID	Mean	Mean	Mean	Mean	Mean	Mean	Fold change	p ANOVA
				WT aorta 6 weeks	WT aorta 32 weeks	WT aorta 78 weeks	<i>ApoE</i> <sup>-/-</sup> aorta 6 weeks	<i>ApoE</i> <sup>-/-</sup> aorta 32 weeks	<i>ApoE</i> <sup>-/-</sup> aorta 78 weeks	<i>ApoE</i> <sup>-/-</sup> aorta 78 weeks vs. 6 weeks	
1440847_at	Mtss1	metastasis suppressor 1	211401	232	198	167	270	256	380	1.41	0.002
1419380_at	Zfp423	zinc finger protein 423	94187	342	436	384	171	334	237	1.39	0.01
1437466_at	Alcam	activated leukocyte cell adhesion molecule	11658	1174	896	721	1080	1307	1484	1.37	0.0005
1455287_at	Cdk6	cyclin-dependent kinase 6	12571	1570	828	752	1241	1062	1691	1.36	0.0008
1418824_at	Arf6	ADP-ribosylation factor 6	11845	104	201	59	74	137	98	1.33	0.004
1437270_a_at	Clefl	cardiotrophin-like cytokine factor 1	56708	122	162	123	194	244	248	1.28	0.001
1426300_at	Alcam	activated leukocyte cell adhesion molecule	11658	837	704	452	853	812	1083	1.27	0.0003
1435293_at	Adam22	a disintegrin and metallopeptidase domain 22	11496	188	320	465	205	304	258	1.26	0.0009
1439364_a_at	Mmp2	matrix metallopeptidase 2	17390	3914	2827	2177	3996	3443	4990	1.25	0.0002
1449281_at	Nrtn	neurturin	18188	798	1222	1747	897	950	1097	1.22	0.002
1436334_at	Synj1	synaptojanin 1	104015	306	248	175	344	389	411	1.20	0.004
1416136_at	Mmp2	matrix metallopeptidase 2	17390	5328	3177	2750	5567	4910	6603	1.19	0.000007
1416544_at	Ezh2	enhancer of zeste homolog 2 (Drosophila)	14056	388	231	178	362	334	424	1.17	0.0003
1422168_a_at	Bdnf	brain derived neurotrophic factor	12064	379	154	134	211	196	244	1.16	0.01
1426301_at	Alcam	activated leukocyte cell adhesion molecule	11658	1020	869	430	1033	1316	1191	1.15	0.00005
1429590_at	Tacc1	transforming, acidic coiled-coil containing protein 1	320165	642	400	985	786	457	902	1.15	0.0001
1438166_x_at	Ndufs4	NADH dehydrogenase (ubiquinone) Fe-S protein 4	17993	240	491	382	281	370	311	1.11	0.0003
1424945_at	Chrdl1	chordin-like 1	83453	113	293	176	123	226	127	1.03	0.03
1426413_at	Neurod1	neurogenic differentiation 1	18012	129	154	261	162	169	166	1.02	0.02
1422054_a_at	Skil	SKI-like	20482	246	101	121	163	127	166	1.02	0.006
1418815_at	Cdh2	cadherin 2	12558	290	241	136	332	384	337	1.01	0.0001
1443857_at	Hook3	hook homolog 3 (Drosophila)	320191	206	174	80	161	182	155	-1.03	0.007
1456487_at	Adcy1	adenylate cyclase 1	432530	268	258	597	169	163	159	-1.06	0.0003

SUPPLEMENT

Affymetrix Probe set ID	Gene Symbol	Gene Name	Entrez Gene ID	Mean	Mean	Mean	Mean	Mean	Mean	Fold change	p ANOVA
				WT aorta 6 weeks	WT aorta 32 weeks	WT aorta 78 weeks	<i>ApoE</i> <sup>-/-</sup> aorta 6 weeks	<i>ApoE</i> <sup>-/-</sup> aorta 32 weeks	<i>ApoE</i> <sup>-/-</sup> aorta 78 weeks	<i>ApoE</i> <sup>-/-</sup> aorta 78 weeks vs. 6 weeks	
1456344_at	Tnc	tenascin C	21923	629	178	202	583	237	540	-1.08	0.0007
1424114_s_at	Lamb1	laminin B1	16777	538	636	261	540	661	492	-1.10	0.02
1416774_at	Wee1	WEE 1 homolog 1 (S. pombe)	22390	290	100	82	157	112	137	-1.15	0.01
1419988_at	Map3k7	mitogen-activated protein kinase kinase kinase 7	26409	315	258	126	237	304	204	-1.17	0.009
1450923_at	Tgfb2	transforming growth factor, beta 2	21808	1865	763	913	1661	846	1372	-1.21	0.00002
1426873_s_at	Jup	junction plakoglobin	16480	549	887	616	536	1012	438	-1.22	0.01
1423136_at	Fgfl	fibroblast growth factor 1	14164	1327	1623	3023	1506	1479	1194	-1.26	0.0004
1424113_at	Lamb1	laminin B1	16777	238	253	78	240	302	189	-1.27	0.01
1436475_at	Nr2f2	nuclear receptor subfamily 2, group F, member 2	11819	457	720	910	552	624	421	-1.31	0.001
1423250_a_at	Tgfb2	transforming growth factor, beta 2	21808	1242	785	543	952	797	724	-1.31	0.002
1448395_at	Sfrp1	secreted frizzled-related protein 1	20377	1584	999	626	1162	1758	870	-1.33	0.0003
1448181_at	Klf15	Kruppel-like factor 15	66277	763	795	754	497	452	369	-1.35	0.01
1437401_at	Igf1	insulin-like growth factor 1	16000	3422	1365	1164	3131	1932	2309	-1.36	0.00001
1451229_at	Hdac11	histone deacetylase 11	232232	358	503	669	373	473	274	-1.36	0.001
1433888_at	Atp2b2	ATPase, Ca <sup>++</sup> transporting, plasma membrane 2	11941	184	246	187	166	238	119	-1.40	0.03
1420946_at	Atrx	alpha thalassemia/mental retardation syndrome X-linked homolog (human)	22589	339	121	192	292	173	208	-1.40	0.0002
1434413_at	Igf1	insulin-like growth factor 1	16000	5137	2144	1819	4645	2785	3305	-1.41	0.000002
1420375_at	Kif3a	kinesin family member 3A	16568	880	427	407	698	599	474	-1.47	0.001
1424801_at	Enah	enabled homolog (Drosophila)	13800	4220	5157	6251	4372	3675	2948	-1.48	0.000007
1416081_at	Smad1	MAD homolog 1 (Drosophila)	17125	422	266	160	386	270	258	-1.50	0.006
1427256_at	Vcan	versican	13003	4054	3298	4216	3156	2766	2102	-1.50	0.0001
1427086_at	Slit3	slit homolog 3 (Drosophila)	20564	3299	3281	4585	3368	3146	2243	-1.50	0.0002

SUPPLEMENT

Affymetrix Probe set ID	Gene Symbol	Gene Name	Entrez Gene ID	Mean	Mean	Mean	Mean	Mean	Mean	Fold change	p ANOVA
				WT aorta 6 weeks	WT aorta 32 weeks	WT aorta 78 weeks	<i>ApoE</i> <sup>-/-</sup> aorta 6 weeks	<i>ApoE</i> <sup>-/-</sup> aorta 32 weeks	<i>ApoE</i> <sup>-/-</sup> aorta 78 weeks	<i>ApoE</i> <sup>-/-</sup> aorta 78 weeks vs. 6 weeks	
1422553_at	Pten	phosphatase and tensin homolog	19211	1496	1011	617	1534	1229	973	-1.58	0.006
1421907_at	Med1	mediator complex subunit 1	19014	1092	681	497	1138	844	722	-1.58	0.05
1458492_x_at	Ntm	neurotrimin	235106	274	111	166	270	84	171	-1.58	0.007
1444240_at	Shank1	SH3/ankyrin domain gene 1	243961	377	214	162	282	209	177	-1.59	0.0004
1420416_at	Sema3a	sema domain, immunoglobulin domain (Ig), short basic domain, secreted, (semaphorin) 3A	20346	592	635	742	571	371	353	-1.62	0.0007
1449522_at	Unc5c	unc-5 homolog C ( <i>C. elegans</i> )	22253	1347	1626	1830	1126	1257	695	-1.62	0.00003
1416594_at	Sfrp1	secreted frizzled-related protein 1	20377	476	46	81	379	384	230	-1.64	0.000007
1420508_at	Sema3f	sema domain, immunoglobulin domain (Ig), short basic domain, secreted, (semaphorin) 3F	20350	612	478	695	562	440	339	-1.66	0.009
1428816_a_at	Gata2	GATA binding protein 2	14461	317	363	391	301	360	176	-1.71	0.007
1450869_at	Fgf1	fibroblast growth factor 1	14164	1018	1045	1341	1104	810	644	-1.71	0.002
1418572_x_at	Tnfrsf12a	tumor necrosis factor receptor superfamily, member 12a	27279	4018	1875	1871	2661	1230	1534	-1.73	0.001
1425940_a_at	Ssbp3	single-stranded DNA binding protein 3	72475	719	852	350	679	798	389	-1.75	0.00009
1421624_a_at	Enah	enabled homolog ( <i>Drosophila</i> )	13800	655	503	706	521	380	293	-1.78	0.00002
1436326_at	Rora	RAR-related orphan receptor alpha	19883	1392	760	671	1244	696	699	-1.78	0.000008
1418534_at	Fzd2	frizzled homolog 2 ( <i>Drosophila</i> )	57265	1454	1890	2149	1830	1602	1021	-1.79	0.002
1436962_at	Prdm6	PR domain containing 6	225518	1150	1382	1488	1267	1097	703	-1.80	0.0004
1420867_at	Tmed2	transmembrane emp24 domain trafficking protein 2	56334	4283	2576	2103	4101	2231	2275	-1.80	0.0003
1424034_at	Rora	RAR-related orphan receptor alpha	19883	2711	1328	1522	2238	1085	1240	-1.80	0.000007
1437312_at	Bmpr1b	bone morphogenetic protein receptor, type 1B	12167	793	878	772	646	485	356	-1.82	0.00008
1419638_at	Efnb2	ephrin B2	13642	1432	1271	913	1071	1162	576	-1.86	0.0005
1423260_at	Id4	inhibitor of DNA binding 4	15904	1324	835	1462	1167	626	628	-1.86	0.0003

SUPPLEMENT

Affymetrix Probe set ID	Gene Symbol	Gene Name	Entrez Gene ID	Mean	Mean	Mean	Mean	Mean	Mean	Fold change	p ANOVA
				WT aorta 6 weeks	WT aorta 32 weeks	WT aorta 78 weeks	<i>ApoE</i> <sup>-/-</sup> aorta 6 weeks	<i>ApoE</i> <sup>-/-</sup> aorta 32 weeks	<i>ApoE</i> <sup>-/-</sup> aorta 78 weeks	<i>ApoE</i> <sup>-/-</sup> aorta 78 weeks vs. 6 weeks	
1418690_at	Ptprz1	protein tyrosine phosphatase, receptor type Z, polypeptide 1	19283	342	326	409	325	286	174	-1.87	0.01
1450040_at	Timp2	tissue inhibitor of metalloproteinase 2	21858	4561	3836	2257	4847	4523	2578	-1.88	0.000003
1455188_at	Ephb1	Eph receptor B1	270190	416	222	152	277	142	147	-1.89	0.0009
1418525_at	Pcm1	pericentriolar material 1	18536	478	528	248	467	498	238	-1.96	0.0004
1434572_at	Hdac9	histone deacetylase 9	79221	1063	818	854	827	532	419	-1.98	0.0001
1437497_a_at	Hsp90aa1	heat shock protein 90, alpha (cytosolic), class A member 1	15519	5723	2848	2686	4499	2669	2264	-1.99	0.0005
1423201_at	Ncor1	nuclear receptor co-repressor 1	20185	1470	1205	688	1381	1386	690	-2.00	0.002
1427489_at	Itga8	integrin alpha 8	241226	13018	11974	11136	12649	10626	6308	-2.01	0.00004
1460647_a_at	Nr2f6	nuclear receptor subfamily 2, group F, member 6	13864	548	268	250	589	280	292	-2.01	0.0006
1423503_at	Jam3	junction adhesion molecule 3	83964	1694	1509	1630	1718	1241	853	-2.01	0.00002
1451109_a_at	Nedd4	neural precursor cell expressed, developmentally down-regulated 4	17999	8225	6612	5788	8615	6658	4257	-2.02	0.000002
1449549_at	Efnb2	ephrin B2	13642	375	201	119	295	244	145	-2.03	0.002
1418533_s_at	Fzd2	frizzled homolog 2 (Drosophila)	57265	1179	1358	1420	1520	1179	745	-2.04	0.001
1426864_a_at	Ncam1	neural cell adhesion molecule 1	17967	5818	5284	6280	5493	4292	2691	-2.04	0.0009
1433716_x_at	Gfra2	glial cell line derived neurotrophic factor family receptor alpha 2	14586	391	406	407	410	263	199	-2.05	0.0006
1449865_at	Sema3a	sema domain, immunoglobulin domain (Ig), short basic domain, secreted, (semaphorin) 3A	20346	309	247	260	222	152	108	-2.05	0.0003
1423341_at	Cspg4	chondroitin sulfate proteoglycan 4	121021	2867	3151	3031	3480	2631	1691	-2.06	0.0004
1416513_at	Lamb2	laminin, beta 2	16779	2960	2931	2397	3051	2454	1472	-2.07	0.0009
1455377_at	Ttl7	tubulin tyrosine ligase-like family, member 7	70892	1065	1212	1244	1119	796	538	-2.08	0.00001
1424893_at	Ndel1	nuclear distribution gene E-like homolog 1 (A. nidulans)	83431	589	345	258	562	383	269	-2.09	0.0006
1429021_at	Epha4	Eph receptor A4	13838	285	252	191	281	263	134	-2.10	0.002
1426565_at	Igf1r	insulin-like growth factor I receptor	16001	855	656	557	894	689	425	-2.11	0.00004

SUPPLEMENT

Affymetrix Probe set ID	Gene Symbol	Gene Name	Entrez Gene ID	Mean	Mean	Mean	Mean	Mean	Mean	Fold change	p ANOVA
				WT aorta 6 weeks	WT aorta 32 weeks	WT aorta 78 weeks	<i>ApoE</i> <sup>-/-</sup> aorta 6 weeks	<i>ApoE</i> <sup>-/-</sup> aorta 32 weeks	<i>ApoE</i> <sup>-/-</sup> aorta 78 weeks	<i>ApoE</i> <sup>-/-</sup> aorta 78 weeks vs. 6 weeks	
1424035_at	Rora	RAR-related orphan receptor alpha	19883	289	153	146	329	133	156	-2.11	0.0008
1453103_at	Ablim1	actin-binding LIM protein 1	226251	792	461	382	680	551	323	-2.11	0.001
1421889_a_at	Aplp2	amyloid beta (A4) precursor-like protein 2	11804	7353	6298	5048	7604	6126	3587	-2.12	0.000003
1425511_at	Mark1	MAP/microtubule affinity-regulating kinase 1	226778	1032	681	697	1004	585	473	-2.12	0.002
1434788_at	Fzd3	frizzled homolog 3 (Drosophila)	14365	340	236	236	278	208	131	-2.12	0.0006
1427433_s_at	Hoxa3	homeobox A3	15400	832	1458	1118	1077	952	507	-2.13	0.004
1439163_at	Zbtb16	zinc finger and BTB domain containing 16	235320	4351	2731	1642	2374	1436	1113	-2.13	0.003
1426086_a_at	Fmr1	fragile X mental retardation syndrome 1 homolog	14265	310	177	173	262	139	123	-2.14	0.008
1448507_at	Efhd1	EF hand domain containing 1	98363	7289	8109	9155	7989	6499	3717	-2.15	0.0002
1455165_at	Rora	RAR-related orphan receptor alpha	19883	1506	1025	992	1296	785	602	-2.15	0.0003
1453734_at	Atrx	alpha thalassemia/mental retardation syndrome X-linked homolog (human)	22589	1169	1154	711	1256	1062	582	-2.16	0.00008
1418532_at	Fzd2	frizzled homolog 2 (Drosophila)	57265	987	1111	1082	1452	843	673	-2.16	0.003
1418876_at	Foxd1	forkhead box D1	15229	128	211	207	170	219	79	-2.16	0.0003
1429591_at	Tacc1	transforming, acidic coiled-coil containing protein 1	320165	304	259	141	355	261	164	-2.17	0.0002
1415877_at	Dpysl3	dihydropyrimidinase-like 3	22240	1396	989	1066	1613	1105	742	-2.17	0.01
1420583_a_at	Rora	RAR-related orphan receptor alpha	19883	2192	981	1052	1729	829	794	-2.18	0.00001
1422399_a_at	Rab23	RAB23, member RAS oncogene family	19335	521	290	206	440	289	202	-2.18	0.006
1416484_at	Ttc3	tetratricopeptide repeat domain 3	22129	660	268	328	548	296	250	-2.19	0.0004
1435933_at	Scn2a1	sodium channel, voltage-gated, type II, alpha 1	110876	447	462	580	585	392	266	-2.20	0.003
1425491_at	Bmpr1a	bone morphogenetic protein receptor, type 1A	12166	1823	1470	1341	1657	1225	752	-2.20	0.000001
1448662_at	Fzd6	frizzled homolog 6 (Drosophila)	14368	396	250	225	414	288	187	-2.21	0.001

SUPPLEMENT

Affymetrix Probe set ID	Gene Symbol	Gene Name	Entrez Gene ID	Mean	Mean	Mean	Mean	Mean	Mean	Fold change	p ANOVA
				WT aorta 6 weeks	WT aorta 32 weeks	WT aorta 78 weeks	<i>ApoE</i> <sup>-/-</sup> aorta 6 weeks	<i>ApoE</i> <sup>-/-</sup> aorta 32 weeks	<i>ApoE</i> <sup>-/-</sup> aorta 78 weeks	<i>ApoE</i> <sup>-/-</sup> aorta 78 weeks vs. 6 weeks	
1425840_a_at	Sema3f	sema domain, immunoglobulin domain (Ig), short basic domain, secreted, (semaphorin) 3F	20350	1159	829	701	1090	946	494	-2.21	0.005
1436917_s_at	Gpsm1	G-protein signalling modulator 1 (AGS3-like, C. elegans)	67839	498	636	511	687	546	310	-2.22	0.002
1425745_a_at	Tacc2	transforming, acidic coiled-coil containing protein 2	57752	5102	5051	5910	5301	3972	2393	-2.22	0.0009
1421105_at	Jag1	jagged 1	16449	418	399	208	413	343	185	-2.23	0.001
1435382_at	Ndn	necdin	17984	2585	2248	2023	2687	2385	1192	-2.25	0.000003
1433825_at	Ntrk3	neurotrophic tyrosine kinase, receptor, type 3	18213	2815	3219	2805	3246	2590	1433	-2.26	0.00001
1456398_at	Tug1	taurine upregulated gene 1	544752	1135	660	536	1093	909	479	-2.28	0.0001
1416168_at	Serpinf1	serine (or cysteine) peptidase inhibitor, clade F, member 1	20317	9990	7808	6654	9590	7008	4163	-2.30	0.0000009
1419356_at	Klf7	Kruppel-like factor 7 (ubiquitous)	93691	791	730	543	1009	720	437	-2.31	0.02
1425911_a_at	Fgfr1	fibroblast growth factor receptor 1	14182	2689	2462	1520	2733	2404	1179	-2.32	0.00008
1434917_at	Cobl	cordon-bleu	12808	698	431	535	635	387	274	-2.32	0.0005
1429459_at	Sema3d	sema domain, immunoglobulin domain (Ig), short basic domain, secreted, (semaphorin) 3D	108151	1876	2526	2559	2190	2061	941	-2.33	0.00002
1449416_at	Fzd4	frizzled homolog 4 (Drosophila)	14366	155	197	60	170	133	73	-2.33	0.0001
1417307_at	Dmd	dystrophin, muscular dystrophy	13405	3103	3461	3449	3440	2644	1467	-2.35	0.0001
1428967_at	Igf1r	insulin-like growth factor I receptor	16001	571	494	387	594	476	253	-2.35	0.001
1428948_at	Kenma1	potassium large conductance calcium-activated channel, subfamily M, alpha member 1	16531	1313	1673	1494	1674	1297	711	-2.36	0.0004
1437673_at	Wnt5a	wingless-related MMTV integration site 5A	22418	246	284	183	201	226	85	-2.37	0.003
1429308_at	Prdm16	PR domain containing 16	70673	1061	1059	1212	1350	973	568	-2.38	0.003
1427646_a_at	Arhgef2	rho/rac guanine nucleotide exchange factor (GEF) 2	16800	707	443	469	802	425	336	-2.39	0.01
1422872_at	Bmpr1b	bone morphogenetic protein receptor, type 1B	12167	284	214	97	201	174	84	-2.41	0.002

SUPPLEMENT

Affymetrix Probe set ID	Gene Symbol	Gene Name	Entrez Gene ID	Mean	Mean	Mean	Mean	Mean	Mean	Fold change	p ANOVA
				WT aorta 6 weeks	WT aorta 32 weeks	WT aorta 78 weeks	<i>ApoE</i> <sup>-/-</sup> aorta 6 weeks	<i>ApoE</i> <sup>-/-</sup> aorta 32 weeks	<i>ApoE</i> <sup>-/-</sup> aorta 78 weeks	<i>ApoE</i> <sup>-/-</sup> aorta 78 weeks vs. 6 weeks	
1426057_a_at	Epha3	Eph receptor A3	13837	354	175	106	275	185	114	-2.41	0.00002
1420948_s_at	Atrx	alpha thalassemia/mental retardation syndrome X-linked homolog (human)	22589	909	593	427	852	586	351	-2.42	0.000006
1421028_a_at	Mef2c	myocyte enhancer factor 2C	17260	1504	712	697	1362	767	561	-2.43	0.00005
1451758_at	Lamc3	laminin gamma 3	23928	660	609	738	782	547	322	-2.43	0.0003
1456862_at	Six4	sine oculis-related homeobox 4 homolog (Drosophila)	20474	297	233	130	260	191	107	-2.43	0.0002
1423259_at	Id4	inhibitor of DNA binding 4	15904	2223	1799	2564	2286	1425	935	-2.45	0.0001
1418467_at	Smardc3	SWI/SNF related, matrix associated, actin dependent regulator of chromatin, subfamily d, member 3	66993	3088	2973	3145	3357	2028	1365	-2.46	0.0002
1419302_at	Heyl	hairy/enhancer-of-split related with YRPW motif-like	56198	2146	3375	3364	3282	2862	1332	-2.46	0.002
1420893_a_at	Tgfr1	transforming growth factor, beta receptor I	21812	500	241	176	395	282	160	-2.47	0.002
1456072_at	Ppp1r9a	protein phosphatase 1, regulatory (inhibitor) subunit 9A	243725	572	559	542	620	434	251	-2.47	0.004
1425987_a_at	Kcnma1	potassium large conductance calcium-activated channel, subfamily M, alpha member 1	16531	869	718	649	1004	538	406	-2.48	0.0002
1448665_at	Dmd	dystrophin, muscular dystrophy	13405	3866	4810	3735	4342	3542	1754	-2.48	0.0005
1435857_s_at	Aplp1	amyloid beta (A4) precursor-like protein 1	11803	1201	1062	913	1482	888	598	-2.48	0.00008
1418106_at	Hey2	hairy/enhancer-of-split related with YRPW motif 2	15214	1458	1593	1187	1741	1431	697	-2.50	0.002
1442223_at	Enah	enabled homolog (Drosophila)	13800	2649	1163	1426	2010	803	803	-2.50	0.0003
1421042_at	Arhgef2	rho/rac guanine nucleotide exchange factor (GEF) 2	16800	1304	849	791	1487	796	594	-2.50	0.0007
1419874_x_at	Zbtb16	zinc finger and BTB domain containing 16	235320	6278	3341	1805	1960	1297	780	-2.51	0.002
1433571_at	Serinc5	serine incorporator 5	218442	794	889	562	818	743	325	-2.52	0.000004
1425575_at	Epha3	Eph receptor A3	13837	1622	1172	800	1599	964	625	-2.56	0.0001
1442623_at	Mef2a	myocyte enhancer factor 2A	17258	485	334	264	559	360	217	-2.57	0.006

SUPPLEMENT

Affymetrix Probe set ID	Gene Symbol	Gene Name	Entrez Gene ID	Mean	Mean	Mean	Mean	Mean	Mean	Fold change	p ANOVA
				WT aorta 6 weeks	WT aorta 32 weeks	WT aorta 78 weeks	<i>ApoE</i> <sup>-/-</sup> aorta 6 weeks	<i>ApoE</i> <sup>-/-</sup> aorta 32 weeks	<i>ApoE</i> <sup>-/-</sup> aorta 78 weeks	<i>ApoE</i> <sup>-/-</sup> aorta 78 weeks vs. 6 weeks	
1423671_at	Dner	delta/notch-like EGF-related receptor	227325	323	165	139	247	143	96	-2.57	0.00009
1435383_x_at	Ndn	necdin	17984	2452	2158	1894	2563	2106	993	-2.58	0.00001
1429348_at	Sema3c	sema domain, immunoglobulin domain (Ig), short basic domain, secreted, (semaphorin) 3C	20348	5840	4811	4881	5391	3746	2088	-2.58	0.00001
1440037_at	Pbx1	pre B-cell leukemia transcription factor 1	18514	1840	1511	984	2209	1537	854	-2.59	0.0005
1429870_at	Tnik	TRAF2 and NCK interacting kinase	665113	481	278	285	449	281	171	-2.63	0.001
1434776_at	Sema5a	sema domain, seven thrombospondin repeats (type 1 and type 1-like), transmembrane domain (TM) and short cytoplasmic domain, (semaphorin) 5A	20356	1173	1042	923	1225	893	465	-2.64	0.00005
1425071_s_at	Ntrk3	neurotrophic tyrosine kinase, receptor, type 3	18213	1353	1313	1101	1485	1088	562	-2.64	0.00002
1455792_x_at	Ndn	necdin	17984	1755	1284	1276	1795	1136	672	-2.67	0.0000008
1448695_at	Prki	protein kinase C, iota	18759	341	254	228	358	176	133	-2.68	0.0008
1422863_s_at	Pdlim5	PDZ and LIM domain 5	56376	3167	1691	1849	3366	1639	1254	-2.69	0.000008
1422329_a_at	Ntrk3	neurotrophic tyrosine kinase, receptor, type 3	18213	444	460	378	557	350	207	-2.69	0.001
1422862_at	Pdlim5	PDZ and LIM domain 5	56376	1326	526	692	1270	512	472	-2.69	0.001
1421276_a_at	Dst	dystonin	13518	2715	2134	2214	2977	1577	1095	-2.72	0.00001
1425594_at	Lamc3	laminin gamma 3	23928	813	623	783	829	528	302	-2.75	0.0001
1453148_at	Sema3d	sema domain, immunoglobulin domain (Ig), short basic domain, secreted, (semaphorin) 3D	108151	486	368	333	414	354	151	-2.75	0.0005
1423885_at	Lamc1	laminin, gamma 1	226519	3172	2150	1557	3542	2064	1289	-2.75	0.000003
1440870_at	Prdm16	PR domain containing 16	70673	3472	3400	2883	3750	2950	1362	-2.75	0.0006
1450928_at	Id4	inhibitor of DNA binding 4	15904	1805	1460	1906	1864	1282	675	-2.76	0.0008
1420894_at	Tgfr1	transforming growth factor, beta receptor I	21812	728	397	262	618	485	221	-2.79	0.0003

SUPPLEMENT

Affymetrix Probe set ID	Gene Symbol	Gene Name	Entrez Gene ID	Mean	Mean	Mean	Mean	Mean	Mean	Fold change	p ANOVA
				WT aorta 6 weeks	WT aorta 32 weeks	WT aorta 78 weeks	<i>ApoE</i> <sup>-/-</sup> aorta 6 weeks	<i>ApoE</i> <sup>-/-</sup> aorta 32 weeks	<i>ApoE</i> <sup>-/-</sup> aorta 78 weeks	<i>ApoE</i> <sup>-/-</sup> aorta 78 weeks vs. 6 weeks	
1425574_at	Epha3	Eph receptor A3	13837	550	193	247	534	236	189	-2.82	0.00004
1455256_at	Tnik	TRAF2 and NCK interacting kinase	665113	894	747	720	946	526	335	-2.82	0.000003
1420847_a_at	Fgfr2	fibroblast growth factor receptor 2	14183	1774	1326	1323	1872	962	658	-2.84	0.000001
1439753_x_at	Six4	sine oculis-related homeobox 4 homolog (Drosophila)	20474	337	251	107	265	151	93	-2.86	0.001
1458129_at	Rora	RAR-related orphan receptor alpha	19883	783	531	348	754	409	262	-2.87	0.000007
1419592_at	Unc5c	unc-5 homolog C (C. elegans)	22253	899	521	732	739	391	256	-2.89	0.000002
1450839_at	D0H4S114	DNA segment, human D4S114	27528	2835	976	1037	2379	1041	820	-2.90	0.00004
1420518_a_at	Igsf9	immunoglobulin superfamily, member 9	93842	648	634	643	921	509	317	-2.90	0.002
1437422_at	Sema5a	sema domain, seven thrombospondin repeats (type 1 and type 1-like), transmembrane domain (TM) and short cytoplasmic domain, (semaphorin) 5A	20356	1698	981	693	1562	940	534	-2.93	0.001
1427019_at	Ptprz1	protein tyrosine phosphatase, receptor type Z, polypeptide 1	19283	3136	3922	3540	3893	3168	1327	-2.93	0.00002
1421027_a_at	Mef2c	myocyte enhancer factor 2C	17260	2673	1597	972	2514	1694	854	-2.94	0.00002
1438886_at	Heyl	hairy/enhancer-of-split related with YRPW motif-like	56198	1213	1722	1813	1831	1479	606	-3.02	0.005
1422861_s_at	Pdlim5	PDZ and LIM domain 5	56376	1520	574	587	1358	499	448	-3.03	0.000007
1436736_x_at	D0H4S114	DNA segment, human D4S114	27528	4527	1701	1559	3896	1847	1285	-3.03	0.00009
1415923_at	Ndn	necdin	17984	2186	1652	1489	2317	1765	764	-3.03	0.000003
1449876_at	Prkg1	protein kinase, cGMP-dependent, type I	19091	522	270	273	534	314	172	-3.10	0.02
1460292_a_at	Smarca1	SWI/SNF related, matrix associated, actin dependent regulator of chromatin, subfamily a, member 1	93761	532	258	229	478	225	154	-3.10	0.000009
1420816_at	Ywhag	tyrosine 3-monooxygenase/tryptophan 5-monooxygenase activation protein, gamma polypeptide	22628	282	232	24	242	210	77	-3.12	0.00007
1452284_at	Ptprz1	protein tyrosine phosphatase, receptor type Z, polypeptide 1	19283	5834	6396	6604	6978	4095	2212	-3.15	0.0002

SUPPLEMENT

Affymetrix Probe set ID	Gene Symbol	Gene Name	Entrez Gene ID	Mean	Mean	Mean	Mean	Mean	Mean	Fold change	p ANOVA
				WT aorta 6 weeks	WT aorta 32 weeks	WT aorta 78 weeks	<i>ApoE</i> <sup>-/-</sup> aorta 6 weeks	<i>ApoE</i> <sup>-/-</sup> aorta 32 weeks	<i>ApoE</i> <sup>-/-</sup> aorta 78 weeks	<i>ApoE</i> <sup>-/-</sup> aorta 78 weeks vs. 6 weeks	
1450944_at	Cspg4	chondroitin sulfate proteoglycan 4	121021	2950	2322	2043	3391	1949	1074	-3.16	0.0003
1427280_at	Scn2a1	sodium channel, voltage-gated, type II, alpha 1	110876	405	391	294	526	320	165	-3.19	0.001
1434802_s_at	Ntf3	neurotrophin 3	18205	1438	1549	1601	1608	1120	505	-3.19	0.0001
1420924_at	Timp2	tissue inhibitor of metalloproteinase 2	21858	4447	2888	1116	4616	3785	1443	-3.20	0.000001
1421413_a_at	Pdlim5	PDZ and LIM domain 5	56376	1083	385	357	952	358	297	-3.21	0.00001
1459211_at	Gli2	GLI-Kruppel family member GLI2	14633	626	825	781	942	651	293	-3.22	0.0006
1436791_at	Wnt5a	wingless-related MMTV integration site 5A	22418	706	850	713	786	717	241	-3.26	0.00002
1450786_x_at	Pdlim5	PDZ and LIM domain 5	56376	3095	1273	1382	2923	1191	895	-3.27	0.0000009
1416504_at	Ulk1	Unc-51 like kinase 1 (C. elegans)	22241	331	259	149	310	231	94	-3.29	0.02
1421955_a_at	Nedd4	neural precursor cell expressed, developmentally down-regulated 4	17999	4175	2268	1932	4365	2670	1326	-3.29	0.000001
1439556_at	Ncam1	neural cell adhesion molecule 1	17967	840	957	1281	1242	644	374	-3.32	0.004
1421239_at	Il6st	interleukin 6 signal transducer	16195	1217	641	455	1220	907	366	-3.33	0.00001
1425444_a_at	Tgfr2	transforming growth factor, beta receptor II	21813	389	251	90	474	366	140	-3.39	0.0008
1451022_at	Lrp6	low density lipoprotein receptor-related protein 6	16974	207	120	45	199	131	58	-3.46	0.0002
1415900_a_at	Kit	kit oncogene	16590	224	229	153	266	226	74	-3.58	0.03
1430309_at	Nipbl	Nipped-B homolog (Drosophila)	71175	555	342	115	493	442	131	-3.78	0.006
1425070_at	Ntrk3	neurotrophic tyrosine kinase, receptor, type 3	18213	432	387	283	506	358	133	-3.79	0.002
1426865_a_at	Ncam1	neural cell adhesion molecule 1	17967	4525	3020	2488	4655	2914	1221	-3.81	0.00001
1450803_at	Ntf3	neurotrophin 3	18205	1538	1352	1448	1623	1055	421	-3.86	0.0001
1420696_at	Sema3c	sema domain, immunoglobulin domain (Ig), short basic domain, secreted, (semaphorin) 3C	20348	1722	945	955	1502	729	389	-3.86	0.0000004
1421306_a_at	Hdac9	histone deacetylase 9	79221	305	172	99	215	135	54	-3.94	0.0005
1453724_a_at	Serpinf1	serine (or cysteine) peptidase inhibitor, clade F, member 1	20317	5890	3518	3372	5656	2741	1400	-4.04	0.0000001

SUPPLEMENT

Affymetrix Probe set ID	Gene Symbol	Gene Name	Entrez Gene ID	Mean	Mean	Mean	Mean	Mean	Mean	Fold change	p ANOVA
				WT aorta 6 weeks	WT aorta 32 weeks	WT aorta 78 weeks	<i>ApoE</i> <sup>-/-</sup> aorta 6 weeks	<i>ApoE</i> <sup>-/-</sup> aorta 32 weeks	<i>ApoE</i> <sup>-/-</sup> aorta 78 weeks	<i>ApoE</i> <sup>-/-</sup> aorta 78 weeks vs. 6 weeks	
1432344_a_at	Aplp2	amyloid beta (A4) precursor-like protein 2	11804	4061	2836	1879	4704	2582	1163	-4.05	0.000009
1460305_at	Itga3	integrin alpha 3	16400	702	715	415	747	569	184	-4.05	0.002
1422014_at	Foxp2	forkhead box P2	114142	402	281	164	414	238	101	-4.09	0.0002
1427688_a_at	Ptprs	protein tyrosine phosphatase, receptor type, S	19280	213	90	64	211	124	51	-4.11	0.03
1421850_at	Mtap1b	microtubule-associated protein 1B	17755	321	179	106	278	160	67	-4.14	0.005
1426179_a_at	Twsg1	twisted gastrulation homolog 1 (Drosophila)	65960	1585	840	684	1549	918	373	-4.15	0.00006
1421832_at	Twsg1	twisted gastrulation homolog 1 (Drosophila)	65960	4431	2685	2017	4815	2345	1154	-4.17	0.0000009
1450437_a_at	Ncam1	neural cell adhesion molecule 1	17967	633	313	183	560	291	127	-4.40	0.0003
1442467_at	Nav2	neuron navigator 2	78286	256	224	391	668	223	146	-4.57	0.004
1439713_at	Itga1	integrin alpha 1	109700	410	304	118	425	278	92	-4.61	0.0002
1440970_at	Kalrn	kalirin, RhoGEF kinase	545156	393	365	487	325	275	70	-4.65	0.002
1427771_x_at	Itgb1	integrin beta 1 (fibronectin receptor beta)	16412	1680	2297	732	2442	1692	505	-4.83	0.001
1451550_at	Ephb3	Eph receptor B3	13845	655	344	323	633	328	130	-4.86	0.006
1449548_at	Efnb2	ephrin B2	13642	626	323	205	479	304	97	-4.93	0.0006
1448818_at	Wnt5a	wingless-related MMTV integration site 5A	22418	653	606	253	721	519	140	-5.14	0.000008
1441057_at	Myh10	myosin, heavy polypeptide 10, non-muscle	77579	233	220	105	293	218	57	-5.16	0.002
1443315_at	Dmd	dystrophin, muscular dystrophy	13405	623	553	418	811	338	146	-5.55	0.00007
1421851_at	Mtap1b	microtubule-associated protein 1B	17755	2988	1811	1372	2899	1315	505	-5.74	0.000005
1450397_at	Mtap1b	microtubule-associated protein 1B	17755	439	236	98	416	256	67	-6.20	0.01
1424848_at	Kcnma1	potassium large conductance calcium-activated channel, subfamily M, alpha member 1	16531	198	143	95	211	133	29	-7.20	0.005
1421426_at	Hhip	Hedgehog-interacting protein	15245	616	323	306	592	238	82	-7.26	0.000004
1455277_at	Hhip	Hedgehog-interacting protein	15245	1020	806	831	1058	605	135	-7.86	0.00002

SUPPLEMENT

1450043_at	Fzd7	frizzled homolog 7 (Drosophila)	14369	233	108	68	207	105	24	-8.51	0.0008
1456379_x_at	Dner	delta/notch-like EGF-related receptor	227325	429	105	86	281	116	33	-8.55	0.00004
1438083_at	Hhip	Hedgehog-interacting protein	15245	525	362	217	639	306	50	-12.81	0.00001
1425426_a_at	Mef2a	myocyte enhancer factor 2A	17258	361	123	58	300	202	23	-13.03	0.00009
1431162_a_at	Enah	enabled homolog (Drosophila)	13800	321	104	108	260	80	14	-19.06	0.0001
1437933_at	Hhip	Hedgehog-interacting protein	15245	1160	928	476	1468	666	54	-26.96	0.000002

**B. Autonomic nervous system development (GO: 0048483)**

Affymetrix Probe set ID	Gene Symbol	Gene Name	Entrez Gene ID	Mean	Mean	Mean	Mean	Mean	Mean	Fold change	p ANOVA
				WT aorta 6 weeks	WT aorta 32 weeks	WT aorta 78 weeks	<i>ApoE</i> <sup>-/-</sup> aorta 6 weeks	<i>ApoE</i> <sup>-/-</sup> aorta 32 weeks	<i>ApoE</i> <sup>-/-</sup> aorta 78 weeks	<i>ApoE</i> <sup>-/-</sup> aorta 78 weeks vs. 6 weeks	
1427682_a_at	Egr2	early growth response 2	13654	23	75	125	39	203	395	10.2	0.0008
1435349_at	Nrp2	neuropilin 2	18187	144	221	258	172	631	1151	6.70	0.000004
1448162_at	Vcam1	vascular cell adhesion molecule 1	22329	1927	2139	2776	1455	7397	8838	6.07	0.0000001
1418939_at	Hlx	H2.0-like homeobox	15284	96	177	76	73	232	436	5.99	0.009
1451314_a_at	Vcam1	vascular cell adhesion molecule 1	22329	902	949	1671	857	3474	5052	5.89	0.000001
1419156_at	Sox4	SRY (sex determining region Y)-box 4	20677	45	29	24	52	139	266	5.07	0.002
1456778_at	Nrp2	neuropilin 2	18187	177	400	352	199	748	912	4.59	0.00001
1415989_at	Vcam1	vascular cell adhesion molecule 1	22329	1174	1182	1475	1035	3424	4723	4.56	0.0000004
1427683_at	Egr2	early growth response 2	13654	116	167	305	129	304	582	4.52	0.00004
1426528_at	Nrp2	neuropilin 2	18187	374	498	438	366	711	1099	3.01	0.0001
1433575_at	Sox4	SRY (sex determining region Y)-box 4	20677	1496	1042	950	1407	2361	2518	1.79	0.0005
1437347_at	Ednrb	endothelin receptor type B	13618	604	655	708	488	1040	812	1.66	0.04

SUPPLEMENT

Affymetrix Probe set ID	Gene Symbol	Gene Name	Entrez Gene ID	Mean	Mean	Mean	Mean	Mean	Mean	Fold change	p ANOVA
				WT aorta 6 weeks	WT aorta 32 weeks	WT aorta 78 weeks	<i>ApoE</i> <sup>-/-</sup> aorta 6 weeks	<i>ApoE</i> <sup>-/-</sup> aorta 32 weeks	<i>ApoE</i> <sup>-/-</sup> aorta 78 weeks	<i>ApoE</i> <sup>-/-</sup> aorta 78 weeks vs. 6 weeks	
1420416_at	Sema3a	sema domain, immunoglobulin domain (Ig), short basic domain, secreted, (semaphorin) 3A	20346	592	635	742	571	371	353	-1.62	0.0007
1420508_at	Sema3f	sema domain, immunoglobulin domain (Ig), short basic domain, secreted, (semaphorin) 3F	20350	612	478	695	562	440	339	-1.66	0.009
1449865_at	Sema3a	sema domain, immunoglobulin domain (Ig), short basic domain, secreted, (semaphorin) 3A	20346	309	247	260	222	152	108	-2.05	0.0003
1434788_at	Fzd3	frizzled class receptor 3	14365	340	236	236	278	208	131	-2.12	0.0006
1425840_a_at	Sema3f	sema domain, immunoglobulin domain (Ig), short basic domain, secreted, (semaphorin) 3F	20350	1159	829	701	1090	946	494	-2.21	0.005
1444706_at	Nav2	neuron navigator 2	78286	498	427	270	526	428	185	-2.84	0.003
1434802_s_at	Ntf3	neurotrophin 3	18205	1438	1549	1601	1608	1120	505	-3.19	0.0001
1450803_at	Ntf3	neurotrophin 3	18205	1538	1352	1448	1623	1055	421	-3.86	0.0001
1443968_at	Adarb1	adenosine deaminase, RNA-specific, B1	110532	661	471	231	803	428	202	-3.98	0.0002
1442467_at	Nav2	neuron navigator 2	78286	256	224	391	668	223	146	-4.57	0.004

C. Sympathetic nervous system development (GO: 0048485)

Affymetrix Probe set ID	Gene Symbol	Gene Name	Entrez Gene ID	Mean	Mean	Mean	Mean	Mean	Mean	Fold change	p ANOVA
				WT aorta 6 weeks	WT aorta 32 weeks	WT aorta 78 weeks	<i>ApoE</i> <sup>-/-</sup> aorta 6 weeks	<i>ApoE</i> <sup>-/-</sup> aorta 32 weeks	<i>ApoE</i> <sup>-/-</sup> aorta 78 weeks	<i>ApoE</i> <sup>-/-</sup> aorta 78 weeks vs. 6 weeks	
1435349_at	Nrp2	neuropilin 2	18187	144	221	258	172	631	1151	6.70	0.000004

SUPPLEMENT

Affymetrix Probe set ID	Gene Symbol	Gene Name	Entrez Gene ID	Mean	Mean	Mean	Mean	Mean	Mean	Fold change	p ANOVA
				WT aorta 6 weeks	WT aorta 32 weeks	WT aorta 78 weeks	<i>ApoE</i> <sup>-/-</sup> aorta 6 weeks	<i>ApoE</i> <sup>-/-</sup> aorta 32 weeks	<i>ApoE</i> <sup>-/-</sup> aorta 78 weeks	<i>ApoE</i> <sup>-/-</sup> aorta 78 weeks vs. 6 weeks	
1419156_at	Sox4	SRY (sex determining region Y)-box 4	20677	45	29	24	52	139	266	5.07	0.002
1456778_at	Nrp2	neuropilin 2	18187	177	400	352	199	748	912	4.59	0.00001
1426528_at	Nrp2	neuropilin 2	18187	374	498	438	366	711	1099	3.01	0.0001
1433575_at	Sox4	SRY (sex determining region Y)-box 4	20677	1496	1042	950	1407	2361	2518	1.79	0.0005
1420416_at	Sema3a	sema domain, immunoglobulin domain (Ig), short basic domain, secreted, (semaphorin) 3A	20346	592	635	742	571	371	353	-1.62	0.0007
1420508_at	Sema3f	sema domain, immunoglobulin domain (Ig), short basic domain, secreted, (semaphorin) 3F	20350	612	478	695	562	440	339	-1.66	0.009
1449865_at	Sema3a	sema domain, immunoglobulin domain (Ig), short basic domain, secreted, (semaphorin) 3A	20346	309	247	260	222	152	108	-2.05	0.0003
1434788_at	Fzd3	frizzled class receptor 3	14365	340	236	236	278	208	131	-2.12	0.0006
1425840_a_at	Sema3f	sema domain, immunoglobulin domain (Ig), short basic domain, secreted, (semaphorin) 3F	20350	1159	829	701	1090	946	494	-2.21	0.005

**D. Axon (GO: 0030424)**

Affymetrix Probe set ID	Gene Symbol	Gene Name	Entrez Gene ID	Mean	Mean	Mean	Mean	Mean	Mean	Fold change	p ANOVA
				WT aorta 6 weeks	WT aorta 32 weeks	WT aorta 78 weeks	<i>ApoE</i> <sup>-/-</sup> aorta 6 weeks	<i>ApoE</i> <sup>-/-</sup> aorta 32 weeks	<i>ApoE</i> <sup>-/-</sup> aorta 78 weeks	<i>ApoE</i> <sup>-/-</sup> aorta 78 weeks vs. 6 weeks	
1423478_at	Prkcb	protein kinase C, beta	18751	16	30	23	23	185	358	15.24	0.00005
1448710_at	Cxcr4	chemokine (C-X-C motif) receptor 4	12767	80	112	107	77	529	1120	14.5	0.00001

SUPPLEMENT

Affymetrix Probe set ID	Gene Symbol	Gene Name	Entrez Gene ID	Mean	Mean	Mean	Mean	Mean	Mean	Fold change	p ANOVA
				WT aorta 6 weeks	WT aorta 32 weeks	WT aorta 78 weeks	<i>ApoE</i> <sup>-/-</sup> aorta 6 weeks	<i>ApoE</i> <sup>-/-</sup> aorta 32 weeks	<i>ApoE</i> <sup>-/-</sup> aorta 78 weeks	<i>ApoE</i> <sup>-/-</sup> aorta 78 weeks vs. 6 weeks	
1455269_a_at	Coro1a	coronin, actin binding protein 1A	12721	169	336	625	275	1527	3332	12.12	0.00001
1416246_a_at	Coro1a	coronin, actin binding protein 1A	12721	334	325	498	336	1586	3943	11.75	0.00001
1419127_at	Npy	neuropeptide Y	109648	108	319	439	119	643	1319	11.11	0.005
1420380_at	Ccl2	chemokine (C-C motif) ligand 2	20296	99	49	126	95	414	915	9.65	0.0001
1424471_at	Rapgef3	Rap guanine nucleotide exchange factor (GEF) 3	223864	48	79	109	30	179	247	8.20	0.007
1460419_a_at	Prkcb	protein kinase C, beta	18751	250	359	588	265	1076	2126	8.01	0.000002
1417788_at	Sncg	synuclein, gamma	20618	439	893	1492	340	1742	2668	7.85	0.000002
1435349_at	Nrp2	neuropilin 2	18187	144	221	258	172	631	1151	6.70	0.000004
1419675_at	Ngf	nerve growth factor	18049	96	124	154	81	284	480	5.92	0.0002
1450731_s_at	Tnfrsf21	tumor necrosis factor receptor superfamily, member 21	94185	139	239	322	135	462	774	5.75	0.00005
1429055_at	Shtn1	shootin 1	71653	151	242	229	146	492	829	5.67	0.0000009
1424942_a_at	Myc	myelocytomatosis oncogene	17869	145	158	147	90	250	500	5.53	0.0004
1434653_at	Ptk2b	PTK2 protein tyrosine kinase 2 beta	19229	261	463	424	263	748	1346	5.12	0.000001
1418099_at	Tnfrsf1b	tumor necrosis factor receptor superfamily, member 1b	21938	300	400	416	308	986	1555	5.05	0.000006
1419754_at	Myo5a	myosin VA	17918	220	271	225	234	836	1112	4.76	0.000002
1416956_at	Kcnab2	potassium voltage-gated channel, shaker-related subfamily, beta member 2	16498	55	104	109	89	245	420	4.74	0.01
1427038_at	Penk	preproenkephalin	18619	426	738	1575	396	1376	1826	4.61	0.000007
1456778_at	Nrp2	neuropilin 2	18187	177	400	352	199	748	912	4.59	0.00001
1431320_a_at	Myo5a	myosin VA	17918	242	253	283	248	618	1092	4.40	0.00006
1450027_at	Sdc3	syndecan 3	20970	682	646	963	681	1884	3001	4.40	0.0000001
1417378_at	Cadm1	cell adhesion molecule 1	54725	353	320	421	290	608	1230	4.24	0.000009

SUPPLEMENT

Affymetrix Probe set ID	Gene Symbol	Gene Name	Entrez Gene ID	Mean	Mean	Mean	Mean	Mean	Mean	Fold change	p ANOVA
				WT aorta 6 weeks	WT aorta 32 weeks	WT aorta 78 weeks	<i>ApoE</i> <sup>-/-</sup> aorta 6 weeks	<i>ApoE</i> <sup>-/-</sup> aorta 32 weeks	<i>ApoE</i> <sup>-/-</sup> aorta 78 weeks	<i>ApoE</i> <sup>-/-</sup> aorta 78 weeks vs. 6 weeks	
1434069_at	Prex1	phosphatidylinositol-3,4,5-trisphosphate-dependent Rac exchange factor 1	277360	329	307	310	286	624	1159	4.06	0.00001
1420980_at	Pak1	p21 (RAC1) activated kinase 1	18479	206	351	527	184	452	714	3.88	0.0002
1440802_at	Clasp2	CLIP associating protein 2	76499	80	60	195	60	65	228	3.80	0.0001
1420653_at	Tgfb1	transforming growth factor, beta 1	21803	516	538	551	440	1292	1670	3.79	0.0000008
1436205_at	Nfasc	neurofascin	269116	115	213	425	121	331	448	3.71	0.0001
1450070_s_at	Pak1	p21 (RAC1) activated kinase 1	18479	121	221	345	128	285	461	3.59	0.00002
1439662_at	Homer1	homer scaffolding protein 1	26556	101	190	47	61	194	216	3.54	0.02
1449473_s_at	Cd40	CD40 antigen	21939	84	45	100	68	145	230	3.39	0.03
1417376_a_at	Cadm1	cell adhesion molecule 1	54725	233	253	273	241	443	802	3.33	0.00004
1417870_x_at	Ctsz	cathepsin Z	64138	2419	2069	2395	2250	4491	7458	3.31	0.000004
1416882_at	Rgs10	regulator of G-protein signalling 10	67865	904	825	1195	831	1420	2749	3.31	0.00002
1425525_a_at	P2rx4	purinergic receptor P2X, ligand-gated ion channel 4	18438	981	1075	1000	992	2007	3273	3.30	0.000005
1452202_at	Pde2a	phosphodiesterase 2A, cGMP-stimulated	207728	132	257	146	97	229	315	3.24	0.002
1417869_s_at	Ctsz	cathepsin Z	64138	1722	2299	1558	1723	4678	5493	3.19	0.00002
1450970_at	Got1	glutamic-oxaloacetic transaminase 1, soluble	14718	316	334	392	278	478	879	3.16	0.00001
1417377_at	Cadm1	cell adhesion molecule 1	54725	70	106	76	97	176	303	3.13	0.03
1423135_at	Thy1	thymus cell antigen 1, theta	21838	627	1056	1441	602	1257	1828	3.04	0.00006
1426528_at	Nrp2	neuropilin 2	18187	374	498	438	366	711	1099	3.01	0.0001
1419296_at	Arhgap4	Rho GTPase activating protein 4	171207	98	128	194	112	189	335	2.98	0.002
1451596_a_at	Sphk1	sphingosine kinase 1	20698	244	221	377	250	360	741	2.96	0.00002
1451461_a_at	Aldoc	aldolase C, fructose-bisphosphate	11676	126	87	166	81	126	236	2.91	0.003
1436051_at	Myo5a	myosin VA	17918	576	563	492	535	998	1526	2.85	0.000007

SUPPLEMENT

Affymetrix Probe set ID	Gene Symbol	Gene Name	Entrez Gene ID	Mean	Mean	Mean	Mean	Mean	Mean	Fold change	p ANOVA
				WT aorta 6 weeks	WT aorta 32 weeks	WT aorta 78 weeks	<i>ApoE</i> <sup>-/-</sup> aorta 6 weeks	<i>ApoE</i> <sup>-/-</sup> aorta 32 weeks	<i>ApoE</i> <sup>-/-</sup> aorta 78 weeks	<i>ApoE</i> <sup>-/-</sup> aorta 78 weeks vs. 6 weeks	
1436482_a_at	Sdc3	syndecan 3	20970	142	143	248	206	465	583	2.83	0.000005
1440481_at	Stat1	signal transducer and activator of transcription 1	20846	104	104	103	117	165	316	2.71	0.002
1452527_a_at	P2rx4	purinergic receptor P2X, ligand-gated ion channel 4	18438	795	656	705	788	1380	2060	2.62	0.00002
1460365_a_at	Dnm1	dynamamin 1	13429	360	488	540	351	619	915	2.60	0.0003
1420915_at	Stat1	signal transducer and activator of transcription 1	20846	300	422	402	313	628	778	2.49	0.00002
1436958_x_at	Tpm3	tropomyosin 3, gamma	59069	1979	1809	2504	1784	2952	4300	2.41	0.00001
1420979_at	Pak1	p21 (RAC1) activated kinase 1	18479	117	153	183	151	188	365	2.41	0.0002
1443086_at	Alcam	activated leukocyte cell adhesion molecule	11658	132	94	114	110	183	263	2.38	0.003
1437302_at	Adrb2	adrenergic receptor, beta 2	11555	177	216	102	100	244	233	2.32	0.02
1447707_s_at	Pde2a	phosphodiesterase 2A, cGMP-stimulated	207728	449	827	783	473	891	1092	2.31	0.0001
1431619_a_at	Dtnbp1	dystrobrevin binding protein 1	94245	606	702	737	566	907	1258	2.22	0.0002
1425536_at	Stx3	syntaxin 3	20908	726	546	694	525	780	1156	2.20	0.00002
1433532_a_at	Mbp	myelin basic protein	17196	199	406	286	170	516	373	2.20	0.0005
1417868_a_at	Ctsz	cathepsin Z	64138	5736	5108	5096	4892	8001	10740	2.20	0.00003
1424470_a_at	Rapgef3	Rap guanine nucleotide exchange factor (GEF) 3	223864	331	405	457	280	487	612	2.19	0.002
1459866_x_at	Cyfp1	cytoplasmic FMR1 interacting protein 1	20430	2214	1931	4813	2570	2430	5622	2.19	0.003
1418701_at	Comt	catechol-O-methyltransferase	12846	365	543	655	378	654	819	2.17	0.001
1416531_at	Gsto1	glutathione S-transferase omega 1	14873	1050	1347	1262	1054	1423	2257	2.14	0.0007
1450033_a_at	Stat1	signal transducer and activator of transcription 1	20846	462	539	381	447	740	951	2.12	0.0008
1448564_at	Cib1	calcium and integrin binding 1 (calmyrin)	23991	634	676	740	622	957	1300	2.09	0.002
1417627_a_at	Limk1	LIM-domain containing, protein kinase	16885	172	228	202	165	299	343	2.08	0.005
1444089_at	Sptbn1	spectrin beta, non-erythrocytic 1	20742	369	360	441	417	549	868	2.08	0.00002
1418829_a_at	Eno2	enolase 2, gamma neuronal	13807	196	295	276	201	357	415	2.07	0.0002

SUPPLEMENT

Affymetrix Probe set ID	Gene Symbol	Gene Name	Entrez Gene ID	Mean	Mean	Mean	Mean	Mean	Mean	Fold change	p ANOVA
				WT aorta 6 weeks	WT aorta 32 weeks	WT aorta 78 weeks	<i>ApoE</i> <sup>-/-</sup> aorta 6 weeks	<i>ApoE</i> <sup>-/-</sup> aorta 32 weeks	<i>ApoE</i> <sup>-/-</sup> aorta 78 weeks	<i>ApoE</i> <sup>-/-</sup> aorta 78 weeks vs. 6 weeks	
1426475_at	Hmbs	hydroxymethylbilane synthase	15288	292	401	439	312	504	637	2.04	0.002
1436930_x_at	Hmbs	hydroxymethylbilane synthase	15288	265	265	397	278	386	564	2.03	0.005
1416514_a_at	Fscn1	fascin actin-bundling protein 1	14086	639	483	355	708	1135	1424	2.01	0.0003
1437467_at	Alcam	activated leukocyte cell adhesion molecule	11658	1218	853	801	1161	1573	2332	2.01	0.00001
1450468_at	Myoc	myocilin	17926	219	361	481	191	426	374	1.96	0.002
1460415_a_at	Cd40	CD40 antigen	21939	95	54	83	119	130	222	1.88	0.01
1428104_at	Tpx2	TPX2, microtubule-associated	72119	192	118	95	112	209	198	1.77	0.005
1435495_at	Adora1	adenosine A1 receptor	11539	149	258	96	89	185	158	1.77	0.004
1436037_at	Itga4	integrin alpha 4	16401	583	457	457	585	753	1018	1.74	0.002
1441248_at	Clcn3	chloride channel, voltage-sensitive 3	12725	133	79	240	167	115	249	1.49	0.005
1448260_at	Uchl1	ubiquitin carboxy-terminal hydrolase L1	22223	921	1386	2253	1093	1256	1577	1.44	0.001
1431292_a_at	Twf2	twinfilin actin binding protein 2	23999	311	331	170	266	334	381	1.43	0.008
1437466_at	Alcam	activated leukocyte cell adhesion molecule	11658	1174	896	721	1080	1307	1484	1.37	0.0005
1448280_at	Syp	synaptophysin	20977	132	270	250	150	227	203	1.35	0.01
1427567_a_at	Tpm3	tropomyosin 3, gamma	59069	1164	720	702	1098	1349	1470	1.34	0.00002
1426300_at	Alcam	activated leukocyte cell adhesion molecule	11658	837	704	452	853	812	1083	1.27	0.0003
1435293_at	Adam22	a disintegrin and metallopeptidase domain 22	11496	188	320	465	205	304	258	1.26	0.0009
1449281_at	Nrtn	neurturin	18188	798	1222	1747	897	950	1097	1.22	0.002
1422168_a_at	Bdnf	brain derived neurotrophic factor	12064	379	154	134	211	196	244	1.16	0.01
1426301_at	Alcam	activated leukocyte cell adhesion molecule	11658	1020	869	430	1033	1316	1191	1.15	0.00005
1456741_s_at	Gpm6a	glycoprotein m6a	234267	321	375	691	339	405	372	1.10	0.005
1416936_at	Aatk	apoptosis-associated tyrosine kinase	11302	183	256	405	222	288	238	1.07	0.001
1437064_at	Ar	androgen receptor	11835	496	815	1038	657	700	592	-1.11	0.001

SUPPLEMENT

Affymetrix Probe set ID	Gene Symbol	Gene Name	Entrez Gene ID	Mean	Mean	Mean	Mean	Mean	Mean	Fold change	p ANOVA
				WT aorta 6 weeks	WT aorta 32 weeks	WT aorta 78 weeks	<i>ApoE</i> <sup>-/-</sup> aorta 6 weeks	<i>ApoE</i> <sup>-/-</sup> aorta 32 weeks	<i>ApoE</i> <sup>-/-</sup> aorta 78 weeks	<i>ApoE</i> <sup>-/-</sup> aorta 78 weeks vs. 6 weeks	
1417319_at	Nectin3	nectin cell adhesion molecule 3	58998	242	192	118	204	171	170	-1.2	0.006
1450923_at	Tgfb2	transforming growth factor, beta 2	21808	1865	763	913	1661	846	1372	-1.21	0.00002
1423250_a_at	Tgfb2	transforming growth factor, beta 2	21808	1242	785	543	952	797	724	-1.31	0.002
1420375_at	Kif3a	kinesin family member 3A	16568	880	427	407	698	599	474	-1.47	0.001
1460214_at	Pcp4	Purkinje cell protein 4	18546	178	200	303	147	184	96	-1.53	0.001
1425270_at	Kif1b	kinesin family member 1B	16561	446	260	160	355	267	226	-1.57	0.0003
1458492_x_at	Ntm	neurotrimin	235106	274	111	166	270	84	171	-1.58	0.007
1436819_at	Sept6	septin 6	56526	411	539	598	456	460	286	-1.6	0.0003
1420416_at	Sema3a	sema domain, immunoglobulin domain (Ig), short basic domain, secreted, (semaphorin) 3A	20346	592	635	742	571	371	353	-1.62	0.0007
1449522_at	Unc5c	unc-5 netrin receptor C	22253	1347	1626	1830	1126	1257	695	-1.62	0.00003
1433600_at	Adra2a	adrenergic receptor, alpha 2a	11551	514	662	743	565	691	344	-1.64	0.005
1420472_at	Mtpn	myotrophin	14489	1844	1008	761	1637	1166	915	-1.79	0.00004
1455779_at	Map1a	microtubule-associated protein 1 A	17754	667	856	1039	817	703	455	-1.8	0.001
1418690_at	Ptprz1	protein tyrosine phosphatase, receptor type Z, polypeptide 1	19283	342	326	409	325	286	174	-1.87	0.01
1450040_at	Timp2	tissue inhibitor of metalloproteinase 2	21858	4561	3836	2257	4847	4523	2578	-1.88	0.000003
1455188_at	Ephb1	Eph receptor B1	270190	416	222	152	277	142	147	-1.89	0.0009
1436043_at	Scn7a	sodium channel, voltage-gated, type VII, alpha	20272	824	1112	671	989	1056	524	-1.89	0.0001
1423331_a_at	Nectin3	nectin cell adhesion molecule 3	58998	798	487	362	703	494	355	-1.98	0.00003
1437497_a_at	Hsp90aa1	heat shock protein 90, alpha (cytosolic), class A member 1	15519	5723	2848	2686	4499	2669	2264	-1.99	0.0005
1436876_at	Rgs7bp	regulator of G-protein signalling 7 binding protein	52882	1395	1561	1446	1411	1562	697	-2.02	0.00007
1459457_at	Camk2d	calcium/calmodulin-dependent protein kinase II, delta	108058	781	570	418	816	545	401	-2.04	0.001
1426864_a_at	Ncam1	neural cell adhesion molecule 1	17967	5818	5284	6280	5493	4292	2691	-2.04	0.0009

SUPPLEMENT

Affymetrix Probe set ID	Gene Symbol	Gene Name	Entrez Gene ID	Mean	Mean	Mean	Mean	Mean	Mean	Fold change	p ANOVA
				WT aorta 6 weeks	WT aorta 32 weeks	WT aorta 78 weeks	<i>ApoE</i> <sup>-/-</sup> aorta 6 weeks	<i>ApoE</i> <sup>-/-</sup> aorta 32 weeks	<i>ApoE</i> <sup>-/-</sup> aorta 78 weeks	<i>ApoE</i> <sup>-/-</sup> aorta 78 weeks vs. 6 weeks	
1449865_at	Sema3a	sema domain, immunoglobulin domain (Ig), short basic domain, secreted, (semaphorin) 3A	20346	309	247	260	222	152	108	-2.05	0.0003
1432004_a_at	Dnm2	dynamain 2	13430	392	371	174	429	440	208	-2.07	0.00008
1450038_s_at	Usp9x	ubiquitin specific peptidase 9, X chromosome	22284	602	551	524	735	457	354	-2.08	0.006
1419256_at	Sptbn1	spectrin beta, non-erythrocytic 1	20742	1848	1034	1192	1997	1043	960	-2.08	0.00003
1424893_at	Ndel1	nudE neurodevelopment protein 1 like 1	83431	589	345	258	562	383	269	-2.09	0.0006
1452379_at	Auts2	autism susceptibility candidate 2	319974	398	364	179	331	255	158	-2.09	0.006
1429021_at	Epha4	Eph receptor A4	13838	285	252	191	281	263	134	-2.1	0.002
1457139_at	Auts2	autism susceptibility candidate 2	319974	3168	2656	2496	3522	2293	1676	-2.1	0.004
1426565_at	Igf1r	insulin-like growth factor I receptor	16001	855	656	557	894	689	425	-2.11	0.00004
1434788_at	Fzd3	frizzled class receptor 3	14365	340	236	236	278	208	131	-2.12	0.0006
1426086_a_at	Fmr1	fragile X mental retardation 1	14265	310	177	173	262	139	123	-2.14	0.008
1427495_at	Scn7a	sodium channel, voltage-gated, type VII, alpha	20272	317	406	219	385	317	179	-2.15	0.0005
1460286_at	Sept6	septin 6	56526	208	240	236	260	178	121	-2.15	0.004
1415877_at	Dpysl3	dihydropyrimidinase-like 3	22240	1396	989	1066	1613	1105	742	-2.17	0.01
1423872_a_at	Dag1	dystroglycan 1	13138	1787	1488	1041	2019	1467	926	-2.18	0.0005
1434766_at	Prkaa2	protein kinase, AMP-activated, alpha 2 catalytic subunit	108079	979	1180	867	982	830	448	-2.19	0.00004
1435933_at	Scn2a	sodium channel, voltage-gated, type II, alpha	110876	447	462	580	585	392	266	-2.2	0.003
1418497_at	Fgf13	fibroblast growth factor 13	14168	1336	1516	1982	1500	1170	678	-2.21	0.00007
1427293_a_at	Auts2	autism susceptibility candidate 2	319974	535	351	201	468	318	210	-2.22	0.009
1425292_at	Dtna	dystrobrevin alpha	13527	745	384	270	468	297	208	-2.25	0.00008
1433825_at	Ntrk3	neurotrophic tyrosine kinase, receptor, type 3	18213	2815	3219	2805	3246	2590	1433	-2.26	0.00001
1437390_x_at	Stx1a	syntaxin 1A (brain)	20907	2144	2174	1812	2304	1827	1008	-2.28	0.00004

SUPPLEMENT

Affymetrix Probe set ID	Gene Symbol	Gene Name	Entrez Gene ID	Mean	Mean	Mean	Mean	Mean	Mean	Fold change	p ANOVA
				WT aorta 6 weeks	WT aorta 32 weeks	WT aorta 78 weeks	<i>ApoE</i> <sup>-/-</sup> aorta 6 weeks	<i>ApoE</i> <sup>-/-</sup> aorta 32 weeks	<i>ApoE</i> <sup>-/-</sup> aorta 78 weeks	<i>ApoE</i> <sup>-/-</sup> aorta 78 weeks vs. 6 weeks	
1416168_at	Serpinf1	serine (or cysteine) peptidase inhibitor, clade F, member 1	20317	9990	7808	6654	9590	7008	4163	-2.3	0.000009
1434917_at	Cobl	cordons-bleu WH2 repeat	12808	698	431	535	635	387	274	-2.32	0.0005
1428967_at	Igf1r	insulin-like growth factor I receptor	16001	571	494	387	594	476	253	-2.35	0.001
1433504_at	Pygb	brain glycogen phosphorylase	110078	2663	2588	3256	2997	2770	1273	-2.35	0.0001
1428948_at	Kcnma1	potassium large conductance calcium-activated channel, subfamily M, 16531 alpha member 1	1313	1673	1494	1674	1297	711	711	-2.36	0.0004
1450384_at	Bace1	beta-site APP cleaving enzyme 1	23821	646	484	315	716	484	304	-2.36	0.0005
1424398_at	Dhx36	DEAH (Asp-Glu-Ala-His) box polypeptide 36	72162	1099	832	305	975	944	413	-2.36	0.0001
1458534_at	Rgs7bp	regulator of G-protein signalling 7 binding protein	52882	491	461	651	493	349	208	-2.37	0.00002
1438680_at	Auts2	autism susceptibility candidate 2	319974	3299	2291	2458	3970	1826	1654	-2.4	0.00003
1423221_at	Tubb4a	tubulin, beta 4A class IVA	22153	1339	1400	884	1627	1253	670	-2.43	0.0004
1441507_at	Sptbn1	spectrin beta, non-erythrocytic 1	20742	639	537	336	783	564	320	-2.45	0.00007
1448541_at	Klc1	kinesin light chain 1	16593	682	412	303	673	442	274	-2.46	0.0002
1448468_a_at	Kcnab1	potassium voltage-gated channel, shaker-related subfamily, beta member 1	16497	5653	5003	5882	5456	3743	2217	-2.46	0.00002
1439527_at	Pgr	progesterone receptor	18667	1070	1270	1283	1023	564	415	-2.46	0.0002
1456131_x_at	Dag1	dystroglycan 1	13138	1930	1503	1015	2194	1497	889	-2.47	0.0004
1437967_at	Ccdc141	coiled-coil domain containing 141	545428	787	564	576	530	462	215	-2.47	0.0003
1456072_at	Ppp1r9a	protein phosphatase 1, regulatory subunit 9A	243725	572	559	542	620	434	251	-2.47	0.004
1425987_a_at	Kcnma1	potassium large conductance calcium-activated channel, subfamily M, 16531 alpha member 1	869	718	649	1004	538	406	406	-2.48	0.0002
1427569_a_at	Utrn	utrophin	22288	1009	880	682	985	673	392	-2.51	0.0002
1429463_at	Prkaa2	protein kinase, AMP-activated, alpha 2 catalytic subunit	108079	1407	1460	827	1475	1117	580	-2.54	0.0005

SUPPLEMENT

Affymetrix Probe set ID	Gene Symbol	Gene Name	Entrez Gene ID	Mean	Mean	Mean	Mean	Mean	Mean	Fold change	p ANOVA
				WT aorta 6 weeks	WT aorta 32 weeks	WT aorta 78 weeks	<i>ApoE</i> <sup>-/-</sup> aorta 6 weeks	<i>ApoE</i> <sup>-/-</sup> aorta 32 weeks	<i>ApoE</i> <sup>-/-</sup> aorta 78 weeks	<i>ApoE</i> <sup>-/-</sup> aorta 78 weeks vs. 6 weeks	
1456069_at	Dtna	dystrobrevin alpha	13527	792	393	280	510	261	198	-2.58	0.00002
1431973_at	Sept6	septin 6	56526	216	231	334	234	115	90	-2.6	0.009
1425071_s_at	Ntrk3	neurotrophic tyrosine kinase, receptor, type 3	18213	1353	1313	1101	1485	1088	562	-2.64	0.00002
1437559_at	Rgs7bp	regulator of G-protein signalling 7 binding protein	52882	841	957	658	931	892	351	-2.65	0.000009
1454729_at	Tmem108	transmembrane protein 108	81907	246	193	158	345	172	129	-2.67	0.001
1450439_at	Hcfc1	host cell factor C1	15161	378	249	201	398	254	149	-2.67	0.01
1422329_a_at	Ntrk3	neurotrophic tyrosine kinase, receptor, type 3	18213	444	460	378	557	350	207	-2.69	0.001
1421276_a_at	Dst	dystonin	13518	2715	2134	2214	2977	1577	1095	-2.72	0.00001
1426066_a_at	Dtna	dystrobrevin alpha	13527	435	343	359	463	323	164	-2.82	0.00004
1448366_at	Stx1a	syntaxin 1A (brain)	20907	603	579	500	677	411	239	-2.83	0.00005
1429768_at	Dtna	dystrobrevin alpha	13527	1176	1275	984	1264	864	437	-2.89	0.0002
1419592_at	Unc5c	unc-5 netrin receptor C	22253	899	521	732	739	391	256	-2.89	0.000002
1420518_a_at	Igsf9	immunoglobulin superfamily, member 9	93842	648	634	643	921	509	317	-2.9	0.002
1427019_at	Ptprz1	protein tyrosine phosphatase, receptor type Z, polypeptide 1	19283	3136	3922	3540	3893	3168	1327	-2.93	0.00002
1421471_at	Npy1r	neuropeptide Y receptor Y1	18166	1628	1362	1385	1301	828	434	-3	0.00009
1450462_at	Crhr2	corticotropin releasing hormone receptor 2	12922	221	256	193	293	209	97	-3.02	0.0006
1455886_at	Cbl	Casitas B-lineage lymphoma	12402	268	191	60	223	236	72	-3.09	0.007
1450037_at	Usp9x	ubiquitin specific peptidase 9, X chromosome	22284	470	480	247	568	439	182	-3.12	0.001
1452284_at	Ptprz1	protein tyrosine phosphatase, receptor type Z, polypeptide 1	19283	5834	6396	6604	6978	4095	2212	-3.15	0.0002
1427280_at	Scn2a	sodium channel, voltage-gated, type II, alpha	110876	405	391	294	526	320	165	-3.19	0.001
1434802_s_at	Ntf3	neurotrophin 3	18205	1438	1549	1601	1608	1120	505	-3.19	0.0001
1420924_at	Timp2	tissue inhibitor of metalloproteinase 2	21858	4447	2888	1116	4616	3785	1443	-3.2	0.000001
1416504_at	Ulk1	unc-51 like kinase 1	22241	331	259	149	310	231	94	-3.29	0.02

SUPPLEMENT

Affymetrix Probe set ID	Gene Symbol	Gene Name	Entrez Gene ID	Mean	Mean	Mean	Mean	Mean	Mean	Fold change	p ANOVA
				WT aorta 6 weeks	WT aorta 32 weeks	WT aorta 78 weeks	<i>ApoE</i> <sup>-/-</sup> aorta 6 weeks	<i>ApoE</i> <sup>-/-</sup> aorta 32 weeks	<i>ApoE</i> <sup>-/-</sup> aorta 78 weeks	<i>ApoE</i> <sup>-/-</sup> aorta 78 weeks vs. 6 weeks	
1429946_at	Ccdc141	coiled-coil domain containing 141	545428	384	95	125	330	127	100	-3.29	0.00005
1439556_at	Ncam1	neural cell adhesion molecule 1	17967	840	957	1281	1242	644	374	-3.32	0.004
1419223_a_at	Dtna	dystrobrevin alpha	13527	778	568	466	766	439	205	-3.74	0.000004
1425070_at	Ntrk3	neurotrophic tyrosine kinase, receptor, type 3	18213	432	387	283	506	358	133	-3.79	0.002
1426865_a_at	Ncam1	neural cell adhesion molecule 1	17967	4525	3020	2488	4655	2914	1221	-3.81	0.00001
1450803_at	Ntf3	neurotrophin 3	18205	1538	1352	1448	1623	1055	421	-3.86	0.0001
1456329_at	Prtg	protogenin	235472	173	161	99	230	116	59	-3.88	0.005
1418430_at	Kif5b	kinesin family member 5B	16573	2416	1642	741	2530	1690	636	-3.98	0.0001
1453724_a_at	Serpinf1	serine (or cysteine) peptidase inhibitor, clade F, member 1	20317	5890	3518	3372	5656	2741	1400	-4.04	0.0000001
1460305_at	Itga3	integrin alpha 3	16400	702	715	415	747	569	184	-4.05	0.002
1421850_at	Map1b	microtubule-associated protein 1B	17755	321	179	106	278	160	67	-4.14	0.005
1454043_a_at	Kcnab1	potassium voltage-gated channel, shaker-related subfamily, beta member 1	16497	2379	1571	1474	2214	1077	512	-4.33	0.0000003
1450437_a_at	Ncam1	neural cell adhesion molecule 1	17967	633	313	183	560	291	127	-4.4	0.0003
1441057_at	Myh10	myosin, heavy polypeptide 10, non-muscle	77579	233	220	105	293	218	57	-5.16	0.002
1418431_at	Kif5b	kinesin family member 5B	16573	565	266	138	528	333	102	-5.2	0.0003
1421851_at	Map1b	microtubule-associated protein 1B	17755	2988	1811	1372	2899	1315	505	-5.74	0.000005
1450397_at	Map1b	microtubule-associated protein 1B	17755	439	236	98	416	256	67	-6.2	0.01
1424848_at	Kcnma1	potassium large conductance calcium-activated channel, subfamily M, 16531 alpha member 1	198	143	95	211	133	29	29	-7.2	0.005

**E. Regulation of axon guidance (GO: 1902667)**

SUPPLEMENT

Affymetrix Probe set ID	Gene Symbol	Gene Name	Entrez Gene ID	Mean	Mean	Mean	Mean	Mean	Mean	Fold change	p ANOVA
				WT aorta 6 weeks	WT aorta 32 weeks	WT aorta 78 weeks	<i>ApoE</i> <sup>-/-</sup> aorta 6 weeks	<i>ApoE</i> <sup>-/-</sup> aorta 32 weeks	<i>ApoE</i> <sup>-/-</sup> aorta 78 weeks	<i>ApoE</i> <sup>-/-</sup> aorta 78 weeks vs. 6 weeks	
1455678_at	Sema4b	sema domain, immunoglobulin domain (Ig), transmembrane domain (TM) and short cytoplasmic domain, (semaphorin) 4B	20352	85	190	229	85	222	401	4.69	0.0003
1417574_at	Cxcl12	chemokine (C-X-C motif) ligand 12	20315	577	562	615	474	1216	2174	4.58	0.00001
1420824_at	Sema4d	sema domain, immunoglobulin domain (Ig), transmembrane domain (TM) and short cytoplasmic domain, (semaphorin) 4D	20354	442	582	773	550	1135	2039	3.71	0.00002
1419717_at	Sema3e	sema domain, immunoglobulin domain (Ig), short basic domain, secreted, (semaphorin) 3E	20349	45	246	371	49	223	161	3.31	0.00008
1448110_at	Sema4a	sema domain, immunoglobulin domain (Ig), transmembrane domain (TM) and short cytoplasmic domain, (semaphorin) 4A	20351	125	336	187	117	357	358	3.05	0.002
1448823_at	Cxcl12	chemokine (C-X-C motif) ligand 12	20315	5885	5864	6394	5182	8384	10772	2.08	0.000007
1438934_x_at	Sema4a	sema domain, immunoglobulin domain (Ig), transmembrane domain (TM) and short cytoplasmic domain, (semaphorin) 4A	20351	279	620	406	326	749	662	2.03	0.0001
1420416_at	Sema3a	sema domain, immunoglobulin domain (Ig), short basic domain, secreted, (semaphorin) 3A	20346	592	635	742	571	371	353	-1.62	0.0007
1420508_at	Sema3f	sema domain, immunoglobulin domain (Ig), short basic domain, secreted, (semaphorin) 3F	20350	612	478	695	562	440	339	-1.66	0.009
1449865_at	Sema3a	sema domain, immunoglobulin domain (Ig), short basic domain, secreted, (semaphorin) 3A	20346	309	247	260	222	152	108	-2.05	0.0003
1425840_a_at	Sema3f	sema domain, immunoglobulin domain (Ig), short basic domain, secreted, (semaphorin) 3F	20350	1159	829	701	1090	946	494	-2.21	0.005
1429459_at	Sema3d	sema domain, immunoglobulin domain (Ig), short basic domain, secreted, (semaphorin) 3D	108151	1876	2526	2559	2190	2061	941	-2.33	0.00002
1437673_at	Wnt5a	wingless-type MMTV integration site family, member 5A	22418	246	284	183	201	226	85	-2.37	0.003

SUPPLEMENT

Affymetrix Probe set ID	Gene Symbol	Gene Name	Entrez Gene ID	Mean	Mean	Mean	Mean	Mean	Mean	Fold change	p ANOVA
				WT aorta 6 weeks	WT aorta 32 weeks	WT aorta 78 weeks	<i>ApoE</i> <sup>-/-</sup> aorta 6 weeks	<i>ApoE</i> <sup>-/-</sup> aorta 32 weeks	<i>ApoE</i> <sup>-/-</sup> aorta 78 weeks	<i>ApoE</i> <sup>-/-</sup> aorta 78 weeks vs. 6 weeks	
1429348_at	Sema3c	sema domain, immunoglobulin domain (Ig), short basic domain, secreted, (semaphorin) 3C	20348	5840	4811	4881	5391	3746	2088	-2.58	0.00001
1434776_at	Sema5a	sema domain, seven thrombospondin repeats (type 1 and type 1-like), transmembrane domain (TM) and short cytoplasmic domain, (semaphorin) 5A	20356	1173	1042	923	1225	893	465	-2.64	0.00005
1453148_at	Sema3d	sema domain, immunoglobulin domain (Ig), short basic domain, secreted, (semaphorin) 3D	108151	486	368	333	414	354	151	-2.75	0.0005
1437422_at	Sema5a	sema domain, seven thrombospondin repeats (type 1 and type 1-like), transmembrane domain (TM) and short cytoplasmic domain, (semaphorin) 5A	20356	1698	981	693	1562	940	534	-2.93	0.001
1436791_at	Wnt5a	wingless-type MMTV integration site family, member 5A	22418	706	850	713	786	717	241	-3.26	0.00002
1420696_at	Sema3c	sema domain, immunoglobulin domain (Ig), short basic domain, secreted, (semaphorin) 3C	20348	1722	945	955	1502	729	389	-3.86	0.0000004
1448818_at	Wnt5a	wingless-type MMTV integration site family, member 5A	22418	653	606	253	721	519	140	-5.14	0.000008

**Table S2. Probe sets of up and down regulated genes in WT and *ApoE*<sup>-/-</sup> aorta adventitia.**

Differential expression of probe sets was determined as described in Material and Methods for Nervous System related Gene Ontology terms: **A.** nervous system development (GO: 0007399), **B.** axon (GO: 0030424), **C.** neuron projection development (GO: 0031175), **D.** regulation of neuron projection development (GO: 0010975), **E.** regulation of axon guidance (GO: 1902667). Further data are displayed as heat maps in Fig. 10. Probe sets are ordered according to fold change between between ATLO *versus* *ApoE*<sup>-/-</sup> adventitia no plaque. Gene symbols and gene names are indicated for ease of reading. Columns of the mean value for each gene show signal intensity without normalization.

SUPPLEMENT

**A. Nervous system development (GO: 0007399)**

Affymetrix Probe set ID	Gene Symbol	Gene Name	Entrez Gene ID	Mean Mean WT adventitia	Mean ApoE <sup>-/-</sup> adventitia no plaque	Mean ApoE <sup>-/-</sup> adventitia ATLO	Fold Change	p ANOVA
1420994_at	B3gnt5	UDP-GlcNAc:betaGal beta-1,3-N-acetylglucosaminyltransferase 5	108105	181	56	422	7.47	0.01
1448710_at	Cxcr4	chemokine (C-X-C motif) receptor 4	12767	173	108	679	6.28	0.0006
1418126_at	Ccl5	chemokine (C-C motif) ligand 5	20304	365	370	2237	6.05	0.0005
1421186_at	Ccr2	chemokine (C-C motif) receptor 2	12772	199	276	1663	6.03	0.0004
1416034_at	Cd24a	CD24a antigen	12484	789	219	1319	6.03	0.03
1417795_at	Chl1	cell adhesion molecule with homology to L1CAM	12661	91	70	410	5.89	0.003
1437313_x_at	Hmgb2	high mobility group box 2	97165	206	137	673	4.90	0.03
1425548_a_at	Lst1	leukocyte specific transcript 1	16988	299	324	1456	4.49	0.0006
1448182_a_at	Cd24a	CD24a antigen	12484	2015	885	3938	4.45	0.02
1437270_a_at	Cclf1	cardiotrophin-like cytokine factor 1	56708	73	65	278	4.26	0.002
1423760_at	Cd44	CD44 antigen	12505	973	709	2965	4.18	0.0009
1437502_x_at	Cd24a	CD24a antigen	12484	734	528	2209	4.18	0.007
1433471_at	Tcf7	transcription factor 7, T-cell specific	21414	63	127	496	3.90	0.007
1451031_at	Sfrp4	secreted frizzled-related protein 4	20379	1995	1856	7019	3.78	0.0008
1434920_a_at	Evl	Ena-vasodilator stimulated phosphoprotein	14026	241	258	922	3.57	0.006
1424727_at	Ccr5	chemokine (C-C motif) receptor 5	12774	203	243	867	3.57	0.0002
1439377_x_at	Cdc20	cell division cycle 20 homolog (S. cerevisiae)	107995	199	138	488	3.53	0.05
1448823_at	Cxcl12	chemokine (C-X-C motif) ligand 12	20315	5201	4107	14034	3.42	0.0006
1419296_at	Arhgap4	Rho GTPase activating protein 4	171207	114	114	387	3.38	0.002
1416136_at	Mmp2	matrix metalloproteinase 2	17390	1350	1003	3223	3.21	0.001
1422571_at	Thbs2	thrombospondin 2	21826	133	83	262	3.17	0.006
1451318_a_at	Lyn	Yamaguchi sarcoma viral (v-yes-1) oncogene homolog	17096	898	815	2503	3.07	0.002

SUPPLEMENT

Affymetrix Probe set ID	Gene Symbol	Gene Name	Entrez Gene ID	Mean Mean WT adventitia no plaque	Mean ApoE <sup>-/-</sup> adventitia	Mean ApoE <sup>-/-</sup> adventitia ATLO	Fold Change	p ANOVA
1426392_a_at	Actr3	ARP3 actin-related protein 3 homolog (yeast)	74117	1572	2277	6934	3.05	0.002
1420380_at	Ccl2	chemokine (C-C motif) ligand 2	20296	97	93	277	2.99	0.02
1450020_at	Cx3cr1	chemokine (C-X3-C) receptor 1	13051	111	120	358	2.98	0.01
1417399_at	Gas6	growth arrest specific 6	14456	3662	2195	6547	2.98	0.001
1435172_at	Eomes	comesodermin homolog (Xenopus laevis)	13813	114	88	260	2.96	0.04
1437874_s_at	Hexb	hexosaminidase B	15212	2147	1450	4123	2.84	0.0002
1425598_a_at	Lyn	Yamaguchi sarcoma viral (v-yes-1) oncogene homolog	17096	250	147	418	2.84	0.04
1460180_at	Hexb	hexosaminidase B	15212	805	619	1749	2.82	0.004
1427464_s_at	Hspa5	heat shock protein 5	14828	2559	2061	5766	2.80	0.01
1419221_a_at	Rgs14	regulator of G-protein signaling 14	51791	378	220	592	2.70	0.003
1422789_at	Aldh1a2	aldehyde dehydrogenase family 1, subfamily A2	19378	33	137	364	2.66	0.003
1451716_at	Mafb	v-maf musculoaponeurotic fibrosarcoma oncogene family, protein B (avian)	16658	263	203	534	2.62	0.01
1420979_at	Pak1	p21 protein (Cdc42/Rac)-activated kinase 1	18479	92	85	220	2.59	0.007
1421188_at	Ccr2	chemokine (C-C motif) receptor 2	12772	142	224	578	2.58	0.001
1420824_at	Sema4d	sema domain, immunoglobulin domain (Ig), transmembrane domain (TM) and short cytoplasmic domain, (semaphorin) 4D	20354	346	351	905	2.58	0.001
1424271_at	Dclk1	doublecortin-like kinase 1	13175	241	155	398	2.58	0.01
1434968_a_at	Actr3	ARP3 actin-related protein 3 homolog (yeast)	74117	3293	2952	7470	2.53	0.0003
1416064_a_at	Hspa5	heat shock protein 5	14828	9764	5738	13652	2.38	0.01
1452051_at	Actr3	ARP3 actin-related protein 3 homolog (yeast)	74117	2427	2081	4932	2.37	0.0004
1416683_at	Plxnb2	plexin B2	140570	892	575	1346	2.34	0.01
1452870_at	Apaf1	apoptotic peptidase activating factor 1	11783	322	235	533	2.26	0.005
1423135_at	Thy1	thymus cell antigen 1, theta	21838	1210	1017	2298	2.26	0.006
1421141_a_at	Foxp1	forkhead box P1	108655	149	87	194	2.24	0.03

SUPPLEMENT

Affymetrix Probe set ID	Gene Symbol	Gene Name	Entrez Gene ID	Mean Mean WT adventitia no plaque	Mean ApoE <sup>-/-</sup> adventitia	Mean ApoE <sup>-/-</sup> adventitia ATLO	Fold Change	p ANOVA
1450663_at	Thbs2	thrombospondin 2	21826	204	136	303	2.22	0.0006
1450106_a_at	Ev1	Ena-vasodilator stimulated phosphoprotein	14026	98	123	267	2.17	0.01
1434312_at	Arf6	ADP-ribosylation factor 6	11845	462	539	1155	2.14	0.01
1415849_s_at	Stmn1	stathmin 1	16765	1019	545	1160	2.13	0.05
1420895_at	Tgfr1	transforming growth factor, beta receptor I	21812	1033	860	1823	2.12	0.0005
1426247_at	Stk24	serine/threonine kinase 24 (STE20 homolog, yeast)	223255	284	281	594	2.11	0.002
1421205_at	Atm	ataxia telangiectasia mutated homolog (human)	11920	203	149	311	2.09	0.05
1415961_at	Itm2c	integral membrane protein 2C	64294	3233	2407	5024	2.09	0.01
1439440_x_at	Twf2	twinfilin, actin-binding protein, homolog 2 (Drosophila)	23999	465	836	1743	2.08	0.0002
1434653_at	Ptk2b	PTK2 protein tyrosine kinase 2 beta	19229	211	345	718	2.08	0.0005
1449278_at	Eif2ak3	eukaryotic translation initiation factor 2 alpha kinase 3	13666	512	335	693	2.07	0.0007
1449018_at	Pfn1	profilin 1	18643	1301	964	1989	2.06	0.02
1431394_a_at	Lrrk2	leucine-rich repeat kinase 2	66725	342	219	451	2.06	0.007
1437341_x_at	Cnp	2',3'-cyclic nucleotide 3' phosphodiesterase	12799	2606	2006	4120	2.05	0.004
1426983_at	Fnbp1	formin binding protein 1	14269	549	417	854	2.05	0.0007
1419754_at	Myo5a	myosin VA	17918	241	258	525	2.03	0.006
1439364_a_at	Mmp2	matrix metalloproteinase 2	17390	1244	1404	2789	1.99	0.003
1421142_s_at	Foxp1	forkhead box P1	108655	369	167	324	1.94	0.007
1426301_at	Alcam	activated leukocyte cell adhesion molecule	11658	141	209	395	1.89	0.03
1426300_at	Alcam	activated leukocyte cell adhesion molecule	11658	152	175	327	1.87	0.02
1426587_a_at	Stat3	signal transducer and activator of transcription 3	20848	692	909	1647	1.81	0.005
1417440_at	Arid1a	AT rich interactive domain 1A (SWI-like)	93760	224	306	541	1.77	0.004
1417574_at	Cxcl12	chemokine (C-X-C motif) ligand 12	20315	929	1295	2254	1.74	0.001
1435176_a_at	Id2	inhibitor of DNA binding 2	15902	1279	1571	2611	1.66	0.003

SUPPLEMENT

Affymetrix Probe set ID	Gene Symbol	Gene Name	Entrez Gene ID	Mean Mean WT adventitia no plaque	Mean ApoE <sup>-/-</sup> adventitia	Mean ApoE <sup>-/-</sup> adventitia ATLO	Fold Change	p ANOVA
1431292_a_at	Twf2	twinfilin, actin-binding protein, homolog 2 (Drosophila)	23999	161	216	341	1.58	0.009
1424089_a_at	Tcf4	transcription factor 4	21413	531	781	1124	1.44	0.0006
1417627_a_at	Limk1	LIM-domain containing, protein kinase	16885	147	244	303	1.24	0.02
1425492_at	Bmpr1a	bone morphogenetic protein receptor, type 1A	12166	1146	564	677	1.20	0.001
1422912_at	Bmp4	bone morphogenetic protein 4	12159	679	315	363	1.15	0.003
1426645_at	Hsp90aa1	heat shock protein 90, alpha (cytosolic), class A member 1	15519	2856	1044	1175	1.13	0.02
1425315_at	Dock7	dedicator of cytokinesis 7	67299	97	208	228	1.10	0.003
1426805_at	Smarca4	SWI/SNF related, matrix associated, actin dependent regulator of chromatin, subfamily a, member 4	20586	92	226	221	-1.02	0.003
1417304_at	Chrd	chordin	12667	234	130	117	-1.11	0.02
1460251_at	Fas	Fas (TNF receptor superfamily member 6)	14102	194	493	416	-1.19	0.008
1423893_x_at	Apbb1	amyloid beta (A4) precursor protein-binding, family B, member 1	11785	559	315	263	-1.2	0.01
1454803_a_at	Hdac11	histone deacetylase 11	232232	578	321	250	-1.28	0.01
1421955_a_at	Neddd4	neural precursor cell expressed, developmentally down-regulated 4	17999	520	262	197	-1.33	0.02
1438067_at	Nfl	neurofibromatosis 1	18015	255	169	126	-1.35	0.002
1416855_at	Gas1	growth arrest specific 1	14451	4395	2200	1609	-1.37	0.003
1455422_x_at	Sept4	septin 4	18952	224	492	339	-1.45	0.02
1416077_at	Adm	adrenomedullin	11535	414	250	168	-1.49	0.03
1451630_at	Ttl	tubulin tyrosine ligase	69737	407	257	171	-1.5	0.02
1438093_x_at	Dbi	diazepam binding inhibitor	13167	3372	8997	5992	-1.5	0.002
1436791_at	Wnt5a	wingless-related MMTV integration site 5A	22418	274	220	130	-1.68	0.02
1432372_a_at	Spr	sepiapterin reductase	20751	451	378	224	-1.69	0.02
1455792_x_at	Ndn	necdin	17984	1896	1540	904	-1.7	0.03
1438143_s_at	Atxn2	ataxin 2	20239	811	1651	937	-1.76	0.006

SUPPLEMENT

Affymetrix Probe set ID	Gene Symbol	Gene Name	Entrez Gene ID	Mean Mean WT adventitia no plaque	Mean Mean <i>ApoE</i> <sup>-/-</sup> adventitia ATLO	Mean Mean <i>ApoE</i> <sup>-/-</sup> adventitia ATLO	Fold Change	p ANOVA
1419301_at	Fzd4	frizzled homolog 4 (Drosophila)	14366	1285	1168	619	-1.89	0.01
1421116_a_at	Rtn4	reticulon 4	68585	1981	1673	886	-1.89	0.003
1455976_x_at	Dbi	diazepam binding inhibitor	13167	21059	25870	12697	-2.04	0.002
1427207_s_at	Afg3l2	AFG3(ATPase family gene 3)-like 2 (yeast)	69597	790	1202	575	-2.09	0.01
1426770_at	Pex5	peroxisomal biogenesis factor 5	19305	296	376	176	-2.14	0.0007
1449389_at	Tal1	T-cell acute lymphocytic leukemia 1	21349	224	287	134	-2.14	0.01
1417437_at	Xrcc6	X-ray repair complementing defective repair in Chinese hamster cells 6	14375	415	642	293	-2.19	0.03
1448154_at	Ndrg2	N-myc downstream regulated gene 2	29811	1708	1877	852	-2.2	0.001
1448601_s_at	Msx1	homeobox, msh-like 1	17701	569	411	185	-2.23	0.004
1420909_at	Vegfa	vascular endothelial growth factor A	22339	579	833	365	-2.28	0.007
1418700_at	Lias	lipoic acid synthetase	79464	618	757	331	-2.29	0.0005
1421889_a_at	Aplp2	amyloid beta (A4) precursor-like protein 2	11804	1809	1580	687	-2.3	0.003
1452031_at	Slc1a3	solute carrier family 1 (glial high affinity glutamate transporter), member 3	20512	631	790	339	-2.33	0.009
1424114_s_at	Lamb1	laminin B1	16777	988	1852	787	-2.35	0.03
1422471_at	Pex13	peroxisomal biogenesis factor 13	72129	2404	2414	1023	-2.36	0.0004
1421888_x_at	Aplp2	amyloid beta (A4) precursor-like protein 2	11804	419	553	233	-2.37	0.005
1422541_at	Ptprm	protein tyrosine phosphatase, receptor type, M	19274	821	889	371	-2.4	0.0006
1424113_at	Lamb1	laminin B1	16777	194	544	227	-2.4	0.007
1449214_a_at	Opa1	optic atrophy 1 homolog (human)	74143	191	411	171	-2.41	0.009
1417456_at	Gnpat	glyceronephosphate O-acyltransferase	14712	1537	1493	615	-2.43	0.001
1460653_at	Atxn2	ataxin 2	20239	317	385	157	-2.45	0.002
1428179_at	Ndufv2	NADH dehydrogenase (ubiquinone) flavoprotein 2	72900	4751	6134	2502	-2.45	0.003
1427206_at	Afg3l2	AFG3(ATPase family gene 3)-like 2 (yeast)	69597	372	566	228	-2.48	0.003
1448610_a_at	Sod2	superoxide dismutase 2, mitochondrial	20656	7304	10047	4007	-2.51	0.01

SUPPLEMENT

Affymetrix Probe set ID	Gene Symbol	Gene Name	Entrez Gene ID	Mean Mean WT adventitia no plaque	Mean ApoE <sup>-/-</sup> adventitia	Mean ApoE <sup>-/-</sup> adventitia ATLO	Fold Change	p ANOVA
1426688_at	Sdha	succinate dehydrogenase complex, subunit A, flavoprotein (Fp)	66945	6709	7056	2802	-2.52	0.0004
1452692_a_at	Ndufv2	NADH dehydrogenase (ubiquinone) flavoprotein 2	72900	8706	11959	4710	-2.54	0.004
1419457_at	Rgnef	Rho-guanine nucleotide exchange factor	110596	406	519	202	-2.57	0.005
1422432_at	Dbi	diazepam binding inhibitor	13167	13218	17922	6882	-2.6	0.0006
1426340_at	Slc1a3	solute carrier family 1 (glial high affinity glutamate transporter), member 3	20512	668	895	332	-2.7	0.003
1423260_at	Id4	inhibitor of DNA binding 4	15904	700	546	197	-2.77	0.001
1419107_at	Ophn1	oligophrenin 1	94190	223	416	147	-2.83	0.005
1423259_at	Id4	inhibitor of DNA binding 4	15904	465	420	148	-2.84	0.005
1449379_at	Kdr	kinase insert domain protein receptor	16542	922	1344	460	-2.92	0.0003
1426689_s_at	Sdha	succinate dehydrogenase complex, subunit A, flavoprotein (Fp)	66945	5287	7847	2625	-2.99	0.0006
1417193_at	Sod2	superoxide dismutase 2, mitochondrial	20656	4093	4932	1631	-3.02	0.004
1448959_at	Ndufs4	NADH dehydrogenase (ubiquinone) Fe-S protein 4	17993	1670	2617	849	-3.08	0.001
1418472_at	Aspa	aspartoacylase	11484	1180	1324	425	-3.11	0.001
1438159_x_at	Ndufv2	NADH dehydrogenase (ubiquinone) flavoprotein 2	72900	5369	8751	2790	-3.14	0.005
1438166_x_at	Ndufs4	NADH dehydrogenase (ubiquinone) Fe-S protein 4	17993	640	1051	332	-3.16	0.009
1416665_at	Coq7	demethyl-Q 7	12850	1221	1672	518	-3.23	0.001
1427677_a_at	Sox6	SRY-box containing gene 6	20679	314	329	99	-3.32	0.0008
1450718_at	Sh2b2	SH2B adaptor protein 2	23921	312	781	232	-3.36	0.005
1450928_at	Id4	inhibitor of DNA binding 4	15904	742	990	251	-3.94	0.005
1420715_a_at	Pparg	peroxisome proliferator activated receptor gamma	19016	1214	2486	541	-4.59	0.002

**B. Axon (GO: 0030424)**

SUPPLEMENT

Affymetrix Probe set ID	Gene Symbol	Gene Name	Entrez Gene ID	Mean Mean WT adventitia no plaque	Mean ApoE <sup>-/-</sup> adventitia	Mean ApoE <sup>-/-</sup> adventiti a ATLO	Fold Change	p ANOVA
1415857_at	Emb	embigin	13723	246	33	698	21.2	0.002
1416246_a_at	Coro1a	coronin, actin binding protein 1A	12721	586	614	4470	7.28	0.001
1455269_a_at	Coro1a	coronin, actin binding protein 1A	12721	729	1006	6703	6.66	0.0005
1448710_at	Cxcr4	chemokine (C-X-C motif) receptor 4	12767	173	108	679	6.28	0.0006
1416956_at	Kcnab2	potassium voltage-gated channel, shaker-related subfamily, beta member 2	16498	103	80	327	4.09	0.0007
1449473_s_at	Cd40	CD40 antigen	21939	82	106	366	3.47	0.002
1419296_at	Arhgap4	Rho GTPase activating protein 4	171207	114	114	387	3.38	0.002
1460419_a_at	Prkcb	protein kinase C, beta	18751	558	515	1600	3.11	0.001
1448950_at	Il1r1	interleukin 1 receptor, type I	16177	304	400	1241	3.10	0.001
1420380_at	Ccl2	chemokine (C-C motif) ligand 2	20296	97	93	277	2.99	0.02
1415856_at	Emb	embigin	13723	357	250	730	2.92	0.004
1455796_x_at	Olfm1	olfactomedin 1	56177	236	232	674	2.90	0.03
1424181_at	Sept6	septin 6	56526	246	152	410	2.69	0.006
1420979_at	Pak1	p21 (RAC1) activated kinase 1	18479	92	85	220	2.59	0.007
1418099_at	Tnfrsf1b	tumor necrosis factor receptor superfamily, member 1b	21938	249	293	744	2.54	0.0005
1416882_at	Rgs10	regulator of G-protein signalling 10	67865	666	498	1262	2.53	0.005
1423478_at	Prkcb	protein kinase C, beta	18751	128	169	405	2.39	0.007
1417379_at	Iqgap1	IQ motif containing GTPase activating protein 1	29875	1088	837	2001	2.39	0.005
1423135_at	Thy1	thymus cell antigen 1, theta	21838	1210	1017	2298	2.26	0.006
1421917_at	Pdgfra	platelet derived growth factor receptor, alpha polypeptide	18595	2511	1052	2377	2.26	0.006
1416759_at	Mical1	microtubule associated monooxygenase, calponin and LIM domain containing 1	171580	195	209	469	2.25	0.006
1415903_at	Slc38a1	solute carrier family 38, member 1	105727	355	247	540	2.19	0.009
1436958_x_at	Tpm3	tropomyosin 3, gamma	59069	2270	2037	4370	2.15	0.001
1439440_x_at	Twf2	twinfilin actin binding protein 2	23999	465	836	1743	2.08	0.0002

SUPPLEMENT

Affymetrix Probe set ID	Gene Symbol	Gene Name	Entrez Gene ID	Mean Mean WT adventitia no plaque	Mean Mean <i>ApoE</i> <sup>-/-</sup> adventitia a ATLO	Mean Mean <i>ApoE</i> <sup>-/-</sup> adventiti a ATLO	Fold Change	p ANOVA
1434653_at	Ptk2b	PTK2 protein tyrosine kinase 2 beta	19229	211	345	718	2.08	0.0005
1431394_a_at	Lrrk2	leucine-rich repeat kinase 2	66725	342	219	451	2.06	0.007
1450033_a_at	Stat1	signal transducer and activator of transcription 1	20846	577	396	806	2.04	0.03
1419754_at	Myo5a	myosin VA	17918	241	258	525	2.03	0.006
1450027_at	Sdc3	syndecan 3	20970	499	538	1074	2.00	0.001
1426301_at	Alcam	activated leukocyte cell adhesion molecule	11658	141	209	395	1.89	0.03
1451992_at	Grk2	G protein-coupled receptor kinase 2	110355	286	337	634	1.88	0.0004
1426300_at	Alcam	activated leukocyte cell adhesion molecule	11658	152	175	327	1.87	0.02
1420622_a_at	Hspa8	heat shock protein 8	15481	2008	4254	7834	1.84	0.002
1416514_a_at	Fscn1	fascin actin-bundling protein 1	14086	696	1277	2268	1.78	0.003
1427260_a_at	Tpm3	tropomyosin 3, gamma	59069	2558	2975	5173	1.74	0.008
1448279_at	Arpc3	actin related protein 2/3 complex, subunit 3	56378	2398	2856	4949	1.73	0.002
1431292_a_at	Twf2	twinfilin actin binding protein 2	23999	161	216	341	1.58	0.009
1417869_s_at	Ctsz	cathepsin Z	64138	1441	2202	3160	1.43	0.0005
1417627_a_at	Limk1	LIM-domain containing, protein kinase	16885	147	244	303	1.24	0.02
1435884_at	Itsn1	intersectin 1 (SH3 domain protein 1A)	16443	305	514	630	1.23	0.02
1426645_at	Hsp90aa1	heat shock protein 90, alpha (cytosolic), class A member 1	15519	2856	1044	1175	1.13	0.02
1423893_x_at	Apbb1	amyloid beta (A4) precursor protein-binding, family B, member 1	11785	559	315	263	1.20	0.01
1438067_at	Nfl	neurofibromin 1	18015	255	169	126	1.35	0.002
1416936_at	Aatk	apoptosis-associated tyrosine kinase	11302	375	248	176	1.41	0.03
1451200_at	Kif1b	kinesin family member 1B	16561	1062	797	472	1.69	0.006
1436930_x_at	Hmbs	hydroxymethylbilane synthase	15288	346	791	443	1.78	0.005
1421116_a_at	Rtn4	reticulon 4	68585	1981	1673	886	1.89	0.003
1450468_at	Myoc	myocilin	17926	493	184	96	1.92	0.003

SUPPLEMENT

Affymetrix Probe set ID	Gene Symbol	Gene Name	Entrez Gene ID	Mean WT adventitia no plaque	Mean <i>ApoE</i> <sup>-/-</sup> adventitia	Mean <i>ApoE</i> <sup>-/-</sup> adventiti a ATLO	Fold Change	p ANOVA
1449183_at	Comt	catechol-O-methyltransferase	12846	3957	3057	1530	2.00	0.005
1416203_at	Aqp1	aquaporin 1	11826	2374	2250	1117	2.01	0.006
1428835_at	Myh14	myosin, heavy polypeptide 14	71960	335	400	196	2.04	0.007
1456036_x_at	Gsto1	glutathione S-transferase omega 1	14873	1871	3391	1659	2.04	0.0007
1436945_x_at	Stim1	stromal interaction molecule 1	20866	326	678	311	2.18	0.0006
1449097_at	Txnrd2	thioredoxin reductase 2	26462	225	462	188	2.45	0.002
1419107_at	Ophn1	oligophrenin 1	94190	223	416	147	2.83	0.005
1426785_s_at	Mgll	monoglyceride lipase	23945	4158	6890	2338	2.95	0.004
1450391_a_at	Mgll	monoglyceride lipase	23945	2951	4634	1549	2.99	0.004
1426235_a_at	Glul	glutamate-ammonia ligase (glutamine synthetase)	14645	1762	2441	813	3.00	0.001
1453836_a_at	Mgll	monoglyceride lipase	23945	1691	2149	690	3.12	0.002
1425534_at	Stau2	staufen double-stranded RNA binding protein 2	29819	235	319	99	3.23	0.001
1455961_at	Mme	membrane metallo endopeptidase	17380	904	1246	350	3.56	0.0007
1415984_at	Acadm	acyl-Coenzyme A dehydrogenase, medium chain	11364	12039	12144	3085	3.94	0.0008

**C. Neuron projection development (GO: 0031175)**

Affymetrix Probe set ID	Gene Symbol	Gene Name	Entrez Gene ID	Mean WT adventitia no plaque	Mean <i>ApoE</i> <sup>-/-</sup> adventitia	Mean <i>ApoE</i> <sup>-/-</sup> adventiti a ATLO	Fold Change	p ANOVA
1415857_at	Emb	embigin	13723	250	34	696	20.68	0.002
1448710_at	Cxcr4	chemokine (C-X-C motif) receptor 4	12767	176	111	677	6.12	0.0006
1450757_at	Cdh11	cadherin 11	12552	531	194	1144	5.91	0.0004

SUPPLEMENT

Affymetrix Probe set ID	Gene Symbol	Gene Name	Entrez Gene ID	Mean Mean WT adventitia no plaque	Mean Mean <i>ApoE</i> <sup>-/-</sup> adventitia	Mean Mean <i>ApoE</i> <sup>-/-</sup> adventiti a ATLO	Fold Change	p ANOVA
1416034_at	Cd24a	CD24a antigen	12484	787	223	1310	5.89	0.03
1455332_x_at	Fcgr2b	Fc receptor, IgG, low affinity IIb	14130	470	384	2239	5.83	0.0002
1417795_at	Ch11	cell adhesion molecule L1-like	12661	93	71	414	5.79	0.003
1417620_at	Rac2	Rac family small GTPase 2	19354	550	374	2077	5.56	0.002
1451941_a_at	Fcgr2b	Fc receptor, IgG, low affinity IIb	14130	616	351	1765	5.03	0.0009
1422105_at	Cd3e	CD3 antigen, epsilon polypeptide	12501	53	66	329	4.97	0.02
1435477_s_at	Fcgr2b	Fc receptor, IgG, low affinity IIb	14130	1277	1053	5197	4.93	0.0003
1448756_at	S100a9	S100 calcium binding protein A9 (calgranulin B)	20202	75	168	751	4.47	0.05
1448182_a_at	Cd24a	CD24a antigen	12484	1990	881	3934	4.46	0.02
1425548_a_at	Lst1	leukocyte specific transcript 1	16988	304	329	1438	4.38	0.0006
1423760_at	Cd44	CD44 antigen	12505	966	707	2925	4.14	0.0009
1437502_x_at	Cd24a	CD24a antigen	12484	734	530	2180	4.11	0.007
1435476_a_at	Fcgr2b	Fc receptor, IgG, low affinity IIb	14130	1563	952	3610	3.79	0.0003
1448823_at	Cxcl12	chemokine (C-X-C motif) ligand 12	20315	5242	4093	15383	3.76	0.0005
1428112_at	Manf	mesencephalic astrocyte-derived neurotrophic factor	74840	1423	1177	4297	3.65	0.009
1434920_a_at	Evl	Ena-vasodilator stimulated phosphoprotein	14026	245	262	916	3.49	0.006
1424727_at	Ccr5	chemokine (C-C motif) receptor 5	12774	207	247	862	3.48	0.0002
1439377_x_at	Cdc20	cell division cycle 20	107995	202	142	490	3.46	0.05
1450905_at	Plxnc1	plexin C1	54712	133	125	421	3.37	0.003
1419296_at	Arhgap4	Rho GTPase activating protein 4	171207	117	117	390	3.34	0.002
1416136_at	Mmp2	matrix metalloproteinase 2	17390	1334	995	3187	3.20	0.001
1426392_a_at	Actr3	ARP3 actin-related protein 3	74117	1554	2244	7131	3.18	0.001
1438115_a_at	Slc9a3r1	solute carrier family 9 (sodium/hydrogen exchanger), member 3 regulator 1	26941	573	324	966	2.98	0.002
1427464_s_at	Hspa5	heat shock protein 5	14828	2542	2032	5846	2.88	0.01

SUPPLEMENT

Affymetrix Probe set ID	Gene Symbol	Gene Name	Entrez Gene ID	Mean Mean WT adventitia no plaque	Mean ApoE <sup>-/-</sup> adventitia	Mean ApoE <sup>-/-</sup> adventiti a ATLO	Fold Change	p ANOVA
1415856_at	Emb	embigin	13723	361	254	727	2.86	0.004
1455796_x_at	Olfm1	olfactomedin 1	56177	240	236	673	2.85	0.03
1427746_x_at	H2-K1	histocompatibility 2, K1, K region	14972	2590	3208	9009	2.81	0.007
1419033_at	Stk26	serine/threonine kinase 26	70415	145	132	366	2.78	0.02
1433741_at	Cd38	CD38 antigen	12494	782	576	1560	2.71	0.001
1434968_a_at	Actr3	ARP3 actin-related protein 3	74117	3254	2911	7730	2.66	0.0003
1438116_x_at	Slc9a3r1	solute carrier family 9 (sodium/hydrogen exchanger), member 3 regulator 1	26941	642	449	1169	2.60	0.001
1420979_at	Pak1	p21 (RAC1) activated kinase 1	18479	94	87	224	2.58	0.007
1423213_at	Plxnc1	plexin C1	54712	289	260	670	2.57	0.02
1416064_a_at	Hspa5	heat shock protein 5	14828	10376	5824	14936	2.56	0.02
1460555_at	Ripor2	RHO family interacting cell polarization regulator 2	193385	244	281	718	2.56	0.006
1424271_at	Dclk1	doublecortin-like kinase 1	13175	245	158	402	2.54	0.01
1420824_at	Sema4d	sema domain, immunoglobulin domain (Ig), transmembrane domain (TM) and short cytoplasmic domain, (semaphorin) 4D	20354	350	355	898	2.53	0.001
1452050_at	Camk1d	calcium/calmodulin-dependent protein kinase ID	227541	170	182	448	2.46	0.006
1452051_at	Actr3	ARP3 actin-related protein 3	74117	2390	2050	4951	2.42	0.0004
1417379_at	Iqgap1	IQ motif containing GTPase activating protein 1	29875	1078	832	1972	2.37	0.005
1416683_at	Plxnb2	plexin B2	140570	886	576	1331	2.31	0.01
1452587_at	Actr2	ARP2 actin-related protein 2	66713	2897	1833	4127	2.25	0.001
1423135_at	Thy1	thymus cell antigen 1, theta	21838	1198	1009	2267	2.25	0.006
1421141_a_at	Foxp1	forkhead box P1	108655	152	89	198	2.23	0.03
1421858_at	Adam17	a disintegrin and metallopeptidase domain 17	11491	558	468	1020	2.18	0.001
1450106_a_at	Evl	Ena-vasodilator stimulated phosphoprotein	14026	100	126	271	2.16	0.01
1415961_at	Itm2c	integral membrane protein 2C	64294	3191	2373	5053	2.13	0.01

SUPPLEMENT

Affymetrix Probe set ID	Gene Symbol	Gene Name	Entrez Gene ID	Mean Mean WT adventitia no plaque	Mean ApoE <sup>-/-</sup> adventitia	Mean ApoE <sup>-/-</sup> adventiti a ATLO	Fold Change	p ANOVA
1452410_a_at	Fes	feline sarcoma oncogene	14159	148	154	329	2.13	0.002
1449315_at	Tenm3	teneurin transmembrane protein 3	23965	166	97	206	2.12	0.01
1434312_at	Arf6	ADP-ribosylation factor 6	11845	465	541	1144	2.12	0.01
1419873_s_at	Csflr	colony stimulating factor 1 receptor	12978	2473	2512	5285	2.10	0.007
1415849_s_at	Stmn1	stathmin 1	16765	1011	546	1148	2.10	0.05
1426247_at	Stk24	serine/threonine kinase 24	223255	289	286	594	2.08	0.002
1437341_x_at	Cnp	2',3'-cyclic nucleotide 3' phosphodiesterase	12799	2570	1977	4104	2.08	0.005
1417676_a_at	Ptpro	protein tyrosine phosphatase, receptor type, O	19277	295	207	428	2.07	0.03
1439440_x_at	Twf2	twinfilin actin binding protein 2	23999	468	831	1720	2.07	0.0002
1434653_at	Ptk2b	PTK2 protein tyrosine kinase 2 beta	19229	215	350	716	2.04	0.0005
1431394_a_at	Lrrk2	leucine-rich repeat kinase 2	66725	346	223	454	2.03	0.007
1428103_at	Adam10	a disintegrin and metallopeptidase domain 10	11487	1623	1760	3527	2.00	0.002
1439364_a_at	Mmp2	matrix metallopeptidase 2	17390	1231	1387	2752	1.98	0.003
1421142_s_at	Foxp1	forkhead box P1	108655	373	171	329	1.92	0.007
1426301_at	Alcam	activated leukocyte cell adhesion molecule	11658	144	213	399	1.88	0.03
1426300_at	Alcam	activated leukocyte cell adhesion molecule	11658	156	179	332	1.85	0.02
1417574_at	Cxcl12	chemokine (C-X-C motif) ligand 12	20315	923	1280	2221	1.73	0.001
1431292_a_at	Twf2	twinfilin actin binding protein 2	23999	164	220	345	1.57	0.009
1450170_x_at	H2-D1	histocompatibility 2, D region locus 1	14964	77	232	347	1.50	0.001
1417869_s_at	Ctsz	cathepsin Z	64138	1425	2170	3119	1.44	0.0005
1455978_a_at	Matn2	matrilin 2	17181	914	1411	1903	1.35	0.01
1432466_a_at	ApoE	apolipoprotein E	11816	15735	99	130	1.31	0.0002
1417627_a_at	Limk1	LIM-domain containing, protein kinase	16885	150	248	307	1.24	0.02
1435884_at	Itsn1	intersectin 1 (SH3 domain protein 1A)	16443	310	516	630	1.22	0.02

SUPPLEMENT

Affymetrix Probe set ID	Gene Symbol	Gene Name	Entrez Gene ID	Mean Mean WT adventitia no plaque	Mean ApoE <sup>-/-</sup> adventitia	Mean ApoE <sup>-/-</sup> adventiti a ATLO	Fold Change	p ANOVA
1438506_s_at	Abi1	abl-interactor 1	11308	177	393	465	1.18	0.002
1417937_at	Dact1	dishevelled-binding antagonist of beta-catenin 1	59036	1064	490	577	1.18	0.01
1422912_at	Bmp4	bone morphogenetic protein 4	12159	678	319	367	1.15	0.003
1426645_at	Hsp90aa1	heat shock protein 90, alpha (cytosolic), class A member 1	15519	2832	1035	1164	1.12	0.02
1425315_at	Dock7	dedicator of cytokinesis 7	67299	99	212	232	1.09	0.003
1448050_s_at	Map4k4	mitogen-activated protein kinase kinase kinase 4	26921	179	342	365	1.06	0.03
1460251_at	Fas	Fas (TNF receptor superfamily member 6)	14102	198	495	419	1.18	0.008
1423893_x_at	Apbb1	amyloid beta (A4) precursor protein-binding, family B, member 1	11785	560	319	268	1.19	0.01
1421955_a_at	Nedd4	neural precursor cell expressed, developmentally down-regulated 4	17999	522	266	201	1.33	0.03
1438067_at	Nf1	neurofibromin 1	18015	259	173	128	1.35	0.002
1416855_at	Gas1	growth arrest specific 1	14451	4400	2169	1588	1.37	0.004
1416936_at	Aatk	apoptosis-associated tyrosine kinase	11302	379	252	180	1.40	0.03
1416077_at	Adm	adrenomedullin	11535	417	254	171	1.49	0.03
1451630_at	Ttl	tubulin tyrosine ligase	69737	411	261	175	1.49	0.02
1436791_at	Wnt5a	wingless-type MMTV integration site family, member 5A	22418	279	224	133	1.68	0.02
1455792_x_at	Ndn	necdin	17984	1872	1521	898	1.69	0.03
1437992_x_at	Gja1	gap junction protein, alpha 1	14609	5453	4558	2678	1.70	0.04
1438143_s_at	Atxn2	ataxin 2	20239	807	1630	930	1.75	0.006
1419301_at	Fzd4	frizzled class receptor 4	14366	1271	1156	619	1.87	0.01
1421116_a_at	Rtn4	reticulon 4	68585	1952	1652	880	1.88	0.003
1435537_at	Ptprd	protein tyrosine phosphatase, receptor type, D	19266	1086	842	443	1.90	0.004
1450468_at	Myoc	myocilin	17926	495	188	98	1.91	0.003
1451411_at	Gprc5b	G protein-coupled receptor, family C, group 5, member B	64297	245	315	153	2.07	0.003
1427207_s_at	Afg3l2	AFG3-like AAA ATPase 2	69597	786	1191	575	2.07	0.01

SUPPLEMENT

Affymetrix Probe set ID	Gene Symbol	Gene Name	Entrez Gene ID	Mean Mean WT adventitia no plaque	Mean ApoE <sup>-/-</sup> adventitia	Mean ApoE <sup>-/-</sup> adventiti a ATLO	Fold Change	p ANOVA
1422673_at	Prkd1	protein kinase D1	18760	463	512	247	2.08	0.006
1426773_at	Mfn1	mitofusin 1	67414	288	362	170	2.13	0.001
1421999_at	Tshr	thyroid stimulating hormone receptor	22095	227	276	124	2.22	0.001
1420909_at	Vegfa	vascular endothelial growth factor A	22339	580	828	370	2.24	0.007
1419247_at	Rgs2	regulator of G-protein signaling 2	19735	1376	2335	1031	2.26	0.02
1424114_s_at	Lamb1	laminin B1	16777	981	1827	784	2.33	0.03
1422541_at	Ptpm	protein tyrosine phosphatase, receptor type, M	19274	816	883	375	2.35	0.0006
1424113_at	Lamb1	laminin B1	16777	198	546	231	2.37	0.008
1449214_a_at	Opa1	OPA1, mitochondrial dynamin like GTPase	74143	195	414	174	2.38	0.009
1460653_at	Atxn2	ataxin 2	20239	321	389	161	2.42	0.002
1427206_at	Afg3l2	AFG3-like AAA ATPase 2	69597	377	567	232	2.44	0.003
1425321_a_at	Clmn	calmin	94040	215	235	93	2.53	0.007
1419457_at	Arhgef28	Rho guanine nucleotide exchange factor (GEF) 28	110596	410	521	205	2.54	0.006
1419107_at	Ophn1	oligophrenin 1	94190	227	419	150	2.79	0.005
1449379_at	Kdr	kinase insert domain protein receptor	16542	915	1329	462	2.87	0.0003
1450391_a_at	Mgll	monoglyceride lipase	23945	2911	4631	1530	3.03	0.004
1426785_s_at	Mgll	monoglyceride lipase	23945	4136	7080	2307	3.07	0.003
1453836_a_at	Mgll	monoglyceride lipase	23945	1669	2118	688	3.08	0.002
1425534_at	Stau2	staufen double-stranded RNA binding protein 2	29819	240	323	101	3.20	0.001
1420545_a_at	Chn1	chimerin 1	108699	215	221	64	3.46	0.006
1434465_x_at	Vldlr	very low density lipoprotein receptor	22359	1604	3380	977	3.46	0.001
1417900_a_at	Vldlr	very low density lipoprotein receptor	22359	506	972	223	4.36	0.0002

SUPPLEMENT

**D. Regulation of neuron projection development (GO: 0010975)**

Affymetrix Probe set ID	Gene Symbol	Gene Name	Entrez Gene ID	Mean Mean WT adventitia no plaque	Mean Mean <i>ApoE</i> <sup>-/-</sup> adventitia a ATLO	Mean Mean <i>ApoE</i> <sup>-/-</sup> adventiti a ATLO	Fold Change	p ANOVA
1448710_at	Cxcr4	chemokine (C-X-C motif) receptor 4	12767	173	108	679	6.28	0.0006
1416034_at	Cd24a	CD24a antigen	12484	789	219	1319	6.03	0.03
1448756_at	S100a9	S100 calcium binding protein A9 (calgranulin B)	20202	74	165	753	4.56	0.05
1448182_a_at	Cd24a	CD24a antigen	12484	2015	885	3938	4.45	0.02
1437502_x_at	Cd24a	CD24a antigen	12484	734	528	2209	4.18	0.007
1424727_at	Ccr5	chemokine (C-C motif) receptor 5	12774	203	243	867	3.57	0.0002
1439377_x_at	Cdc20	cell division cycle 20	107995	199	138	488	3.53	0.05
1450905_at	Plxnc1	plexin C1	54712	130	122	418	3.42	0.003
1448823_at	Cxcl12	chemokine (C-X-C motif) ligand 12	20315	5201	4107	14034	3.42	0.0006
1419296_at	Arhgap4	Rho GTPase activating protein 4	171207	114	114	387	3.38	0.002
1426392_a_at	Actr3	ARP3 actin-related protein 3	74117	1572	2277	6934	3.05	0.002
1455796_x_at	Olfm1	olfactomedin 1	56177	236	232	674	2.9	0.03
1427464_s_at	Hspa5	heat shock protein 5	14828	2559	2061	5766	2.8	0.01
1433741_at	Cd38	CD38 antigen	12494	785	575	1581	2.75	0.001
1427746_x_at	H2-K1	histocompatibility 2, K1, K region	14972	2625	3220	8602	2.67	0.007
1423213_at	Plxnc1	plexin C1	54712	285	256	671	2.62	0.02
1420979_at	Pak1	p21 (RAC1) activated kinase 1	18479	92	85	220	2.59	0.007
1420824_at	Sema4d	sema domain, immunoglobulin domain (Ig), transmembrane domain (TM) and short cytoplasmic domain, (semaphorin) 4D	20354	346	351	905	2.58	0.001
1434968_a_at	Actr3	ARP3 actin-related protein 3	74117	3293	2952	7470	2.53	0.0003
1452050_at	Camk1d	calcium/calmodulin-dependent protein kinase ID	227541	166	179	445	2.49	0.006
1417379_at	Iqgap1	IQ motif containing GTPase activating protein 1	29875	1088	837	2001	2.39	0.005

SUPPLEMENT

Affymetrix Probe set ID	Gene Symbol	Gene Name	Entrez Gene ID	Mean Mean WT adventitia no plaque	Mean Mean <i>ApoE</i> <sup>-/-</sup> adventitia a ATLO	Fold Change	p ANOVA	
1416064_a_at	Hspa5	heat shock protein 5	14828	9764	5738	13652	2.38	0.01
1452051_at	Actr3	ARP3 actin-related protein 3	74117	2427	2081	4932	2.37	0.0004
1416683_at	Plxnb2	plexin B2	140570	892	575	1346	2.34	0.01
1423135_at	Thy1	thymus cell antigen 1, theta	21838	1210	1017	2298	2.26	0.006
1452587_at	Actr2	ARP2 actin-related protein 2	66713	2936	1858	4150	2.23	0.001
1421858_at	Adam17	a disintegrin and metallopeptidase domain 17	11491	557	465	1029	2.21	0.001
1452410_a_at	Fes	feline sarcoma oncogene	14159	145	151	324	2.15	0.002
1434312_at	Arf6	ADP-ribosylation factor 6	11845	462	539	1155	2.14	0.01
1449315_at	Tenm3	teneurin transmembrane protein 3	23965	163	95	202	2.12	0.01
1426247_at	Stk24	serine/threonine kinase 24	223255	284	281	594	2.11	0.002
1416006_at	Mdk	midkine	17242	270	172	362	2.1	0.03
1415961_at	Itm2c	integral membrane protein 2C	64294	3233	2407	5024	2.09	0.01
1439440_x_at	Twf2	twinfilin actin binding protein 2	23999	465	836	1743	2.08	0.0002
1434653_at	Ptk2b	PTK2 protein tyrosine kinase 2 beta	19229	211	345	718	2.08	0.0005
1431394_a_at	Lrrk2	leucine-rich repeat kinase 2	66725	342	219	451	2.06	0.007
1428103_at	Adam10	a disintegrin and metallopeptidase domain 10	11487	1643	1784	3559	1.99	0.002
1417574_at	Cxcl12	chemokine (C-X-C motif) ligand 12	20315	929	1295	2254	1.74	0.001
1431292_a_at	Twf2	twinfilin actin binding protein 2	23999	161	216	341	1.58	0.009
1450170_x_at	H2-D1	histocompatibility 2, D region locus 1	14964	75	228	343	1.51	0.002
1417869_s_at	Ctsz	cathepsin Z	64138	1441	2202	3160	1.43	0.0005
1432466_a_at	ApoE	apolipoprotein E	11816	14332	96	127	1.31	0.0002
1417627_a_at	Limk1	LIM-domain containing, protein kinase	16885	147	244	303	1.24	0.02
1435884_at	Itsn1	intersectin 1 (SH3 domain protein 1A)	16443	305	514	630	1.23	0.02
1422912_at	Bmp4	bone morphogenetic protein 4	12159	679	315	363	1.15	0.003

SUPPLEMENT

Affymetrix Probe set ID	Gene Symbol	Gene Name	Entrez Gene ID	Mean Mean WT adventitia no plaque	Mean ApoE <sup>-/-</sup> adventitia	Mean ApoE <sup>-/-</sup> adventiti a ATLO	Fold Change	p ANOVA
1448050_s_at	Map4k4	mitogen-activated protein kinase kinase kinase 4	26921	176	338	360	1.07	0.03
1423893_x_at	Apbb1	amyloid beta (A4) precursor protein-binding, family B, member 1	11785	559	315	263	1.2	0.01
1421955_a_at	Nedd4	neural precursor cell expressed, developmentally down-regulated 4	17999	520	262	197	1.33	0.02
1422444_at	Itga6	integrin alpha 6	16403	275	634	473	1.34	0.04
1438067_at	Nf1	neurofibromin 1	18015	255	169	126	1.35	0.002
1416936_at	Aatk	apoptosis-associated tyrosine kinase	11302	375	248	176	1.41	0.03
1451630_at	Ttl	tubulin tyrosine ligase	69737	407	257	171	1.5	0.02
1436791_at	Wnt5a	wingless-type MMTV integration site family, member 5A	22418	274	220	130	1.68	0.02
1419301_at	Fzd4	frizzled class receptor 4	14366	1285	1168	619	1.89	0.01
1421116_a_at	Rtn4	reticulon 4	68585	1981	1673	886	1.89	0.003
1435537_at	Ptprd	protein tyrosine phosphatase, receptor type, D	19266	1096	847	440	1.93	0.004
1451411_at	Gprc5b	G protein-coupled receptor, family C, group 5, member B	64297	240	311	149	2.08	0.003
1422673_at	Prkd1	protein kinase D1	18760	460	510	242	2.11	0.006
1426773_at	Mfn1	mitofusin 1	67414	283	358	167	2.15	0.001
1419247_at	Rgs2	regulator of G-protein signaling 2	19735	1393	2367	1040	2.28	0.02
1420909_at	Vegfa	vascular endothelial growth factor A	22339	579	833	365	2.28	0.007
1449214_a_at	Opa1	OPA1, mitochondrial dynamin like GTPase	74143	191	411	171	2.41	0.009
1426785_s_at	Mgll	monoglyceride lipase	23945	4158	6890	2338	2.95	0.004
1450391_a_at	Mgll	monoglyceride lipase	23945	2951	4634	1549	2.99	0.004
1453836_a_at	Mgll	monoglyceride lipase	23945	1691	2149	690	3.12	0.002
1425534_at	Stau2	staufen double-stranded RNA binding protein 2	29819	235	319	99	3.23	0.001
1434465_x_at	Vldlr	very low density lipoprotein receptor	22359	1625	3416	984	3.47	0.001
1420545_a_at	Chn1	chimerin 1	108699	211	217	62	3.48	0.006
1417900_a_at	Vldlr	very low density lipoprotein receptor	22359	504	980	219	4.48	0.0002

SUPPLEMENT

**E. Regulation of axon guidance (GO: 1902667)**

Affymetrix Probe set ID	Gene Symbol	Gene Name	Entrez Gene ID	Mean WT adventitia	Mean <i>ApoE</i> <sup>-/-</sup> adventitia no plaque	Mean <i>ApoE</i> <sup>-/-</sup> adventiti a ATLO	Fold Change	p ANOVA
1448823_at	Cxcl12	chemokine (C-X-C motif) ligand 12	20315	5201	4107	14034	3.42	0.0006
1420824_at	Sema4d	sema domain, immunoglobulin domain (Ig), transmembrane domain (TM) and short cytoplasmic domain, (semaphorin) 4D	20354	346	351	905	2.58	0.001
1417574_at	Cxcl12	chemokine (C-X-C motif) ligand 12	20315	929	1295	2254	1.74	0.001
1436791_at	Wnt5a	wingless-type MMTV integration site family, member 5A	22418	274	220	130	1.68	0.02
1420909_at	Vegfa	vascular endothelial growth factor A	22339	579	833	365	2.28	0.007